On the Integration of Calcite Scale Management and Operational Optimisation of CCUS in Pre-Salt Carbonate Reservoirs

Hydra Walesca de Lima Rodrigues

Submitted for the degree of Doctor of Philosophy in Petroleum Engineering

Heriot-Watt University

School of Energy, Geoscience, Infrastructure and Society

Institute of GeoEnergy Engineering

Edinburgh, UK

July 2021

ABSTRACT

In this thesis, we describe a simulation-based reactive transport workflow to optimise Carbon Capture Utilization and Storage (CCUS) in carbonate reservoirs. Although CCUS may play a crucial role in reducing greenhouse gas emissions, it does not come short of challenges. Here we focus on three of them: i) the economics, ii) carbon footprint and iii) inorganic scale, the latter being crucial when carbon dioxide (CO_2) water-alternating-gas (WAG) is performed in reactive carbonate rocks. Our objective is to integrate reservoir engineering calculations, cash flow projections, carbon accounting and production chemistry to support field operational decisions. The analysis is made in the context of the Brazilian Pre-salt oilfields that have been pioneering deep-water CO_2 utilization for Enhanced Oil Recovery (EOR) to avoid flaring.

We used well-established optimisation techniques - statistical sampling and evolutionary algorithms - to identify CO_2-EOR strategies with the highest potential to co-optimise profitability and CO_2 storage, without triggering calcite deposition to the point of permanent jeopardy of production wells and facilities. Based on the production brine chemistry and flow rate forecasts, we assessed calcite scale risk and designed damage prevention strategies with the lowest cost of scale inhibitor "squeeze" treatment deployment. The methodology is presented through synthetic sector models and then applied to a field case for validation. We used deterministic models, but the impact of geological uncertainties on the outcomes is demonstrated using a set of representative models of the field case.

The optimized CCUS strategies showed the potential to enhance profitability and offset operational emissions through adjustments of well operations, with limited additional investment. In addition, the mineral scaling assessment revealed how applying WAG schemes in carbonate reservoirs with considerable initial CO_2 content will result in a lower calcite deposition risk compared to waterflooding.

The proposed workflow provides valuable insights into the simulation and optimisation of CCUS projects with high calcite scaling risk. Its application demonstrated the importance of an integrated analysis that seeks to improve economic returns in a sustainable manner, with reduced production damage caused by CO_2 speciation.

ACKNOWLEDGEMENTS

When I think back on the ups and downs of undertaking the work presented in this thesis, two quotes come to mind. The first one, attributed to Sir Winston Churchill, was much needed to keep me going, whether a simulation wasn't running, or a paragraph wasn't flowing: "*Success is going from failure to failure without losing your enthusiasm*". The power of incremental steps is at the core of progress - be it scientific, economical, or personal - and it was palpable to me throughout this journey.

The second one was a Will Durant's succinct capture of an Aristotelian idea: "*We are what we repeatedly do. Excellence, then, is not an act, but a habit*", Pursuing this Ph.D. has been a means to discovering deep embedded habits - that needed to be either rewired or nourished – and to cultivating new ones. Certainly, one of the most challenging yet rewarding experiences of my life. A humbling path towards crafting a fulfilling career that hopefully contributes to the improvement of the community at large.

Nevertheless, this was not, by any stretch of the imagination, a solo pursuit. I always had an amazing support network, and I will attempt to thank them all here.

My deepest gratitude goes to my mom, who worked tirelessly to raise me on her own. She did the hardest job in the world with no training, no compensation, no breaks. Even through adversity, she made sure I grew up with a strong sense that education, grit, and moral values were my only ticket to a better life. I am forever in her debt.

My gratitude extends to the family members that were pivotal during my upbringing. My aunt Gorete for supporting my primary education and being a safe harbour of kindness and generosity. My uncles, Tim and Sim, who act as the cool older brothers I've never had. My uncle Amancio for the support and providing us with a place to live.

My wholehearted appreciation goes to the man that stole my heart, Sacha. Your patience and companionship made this bumpy ride smoother. Your thoughtful honest feedback and example inspired me to deliver my best. Your presence gave colour to lockdown days. Rest assured, your love and support are embedded in every word of this manuscript.

A huge thank you also goes to all my friends in Brazil and in Edinburgh (Vitória, Rafaelle, Ismênia, Ken, Bentivi, Rafaella, Hanna, the Zouk Edinburgh crew, to mention a few), who brought tremendous joy to my life and were understanding of my absence when the research demanded most of my energy.

Throughout my academic life, I have always felt so lucky to have the most brilliant and encouraging mentors I could have hoped for. During my time at UFC, Prof. Bruno Prata took me under his wings, truly believing that I could accomplish more than I could imagine. He guided me in so many levels – academic, intellectual, professional, and emotional – not only with words of wisdom and encouragement but specially through his example. His conscientiousness, his moral compass, and his relentless pursuit of knowledge have been a great source of inspiration.

I am also deeply thankful for the support from Prof. Célio Loureiro and Prof. Mardônio Lucena during the uncertain times prior to securing my Ph.D. position, which gave me the means to go across the pond. Additionally, the help from the now professors Pedro Felipe and Hugo Peixoto was pivotal during my M.Sc. studies, and I thank them for it.

As a Ph.D. researcher, I had the privilege to have prof. Eric Mackay and Dr. Daniel Arnold as my supervisors. I could not have envisioned having better mentors. I am profoundly grateful for their technical insights that were fundamental to the work in this thesis and, above all, for their guidance and support combined with sincere trust that I was capable of achieving whatever the challenge was, even (specially) when I doubted myself.

Eric - to say that you will always be a role model to me is an understatement. From the first e-mail interactions, when I was in Brazil struggling to get a scholarship, all the way to the finishing line, when I was juggling writing-up and job hunting, your attitude has been filled with care and respect, and a genuine desire to help. Clayton M. Christensen once wrote: "*The metric by which God will assess my life isn't dollars but the individual people whose lives I've touched*". I think that, consciously or not, you use the same metric to measure your success in life. It is my impression that you live as if every day your sole purpose was to help individuals around you became better people. Thank you for showing me how to live with integrity and humility, never forgetting to add humour whenever possible.

Dan - more than the brilliant (sometimes intimidating) ideas for this Ph.D. project and communication advice, you have been an inspiration with your constant growth mindset and sheer dedication to everything you set your mind to.

I also would like to thank the researchers who contributed to the work presented here with thoughtful feedback or co-authoring papers, namely Dr. Oscar Vazquez, Vahid Azari, prof. Ken Sorbie, Dr. Mike Singleton, and the FAST JIP sponsors. Special thanks go to Dr. Duarte Silva, who tailored a version of his scale prediction code to the needs of this research and

who was also part of the group of friends that made my days in Edinburgh even more enjoyable. On that note, I would like to thank all my colleagues in the FAST group, students and staff, for creating such a welcoming atmosphere. Heather O'Hara, for making everything happen with efficiency and care. The now doctors, Alsu Valiakhmetova, Mohamed Arab, Khosro Jarrahian, Xu Wang, and 'a linda' Suzanny Paiva, for their caring friendship. Dr. Ayrton Ribeiro for his friendship and invaluable assistance particularly at the beginning of this journey. Dr. Lorraine Boak, who's friendship I discovered later, but I am so glad I have got to know her better – such a strong role model and considerate soul. Dr. Alex Graham, for the laughs in the corridors and the words of encouragement towards the end of this endeavour. It has been an honour to work alongside these brilliant yet humble people from diverse backgrounds.

I sincerely appreciate the financial support of the Conselho Nacional de Desenvolvimento Científico e Tecnológico (CNPq), Petrogal Brasil S.A., and Energi Simulation, which made this work possible. Computer Modelling Group (CMG™) is thanked for granting access to their software package and providing technical support whenever needed.

I also appreciate the support network at Heriot-Watt University, which enabled this work to be carried out: the IT Support team (Mamel, Graeme and Alan Brown), the EGIS PGR student support (Susan and Debbie), Peter Scott for the immigration advice, among other administrative staff.

Last but not least, I would like to thank Prof. Dennis Schiozer and Dr. Babak Jafarizadeh for devoting their time and attention to read through this thesis and for engaging in thoughtful discussion with me during my viva. Your inputs were much appreciated.

Research Thesis Submission

Please note this form should be bound into the submitted thesis.

Name:	Hydra Walesca de Lima Rodrigues		
School:	School of Energy, Geoscience, Infrastructure and Society (EGIS)		
Version: *(i.e. First, Resubmission, Final)*	Final	Degree Sought:	Ph.D. in Petroleum Engineering

Declaration

In accordance with the appropriate regulations I hereby submit my thesis and I declare that:

The thesis embodies the results of my own work and has been composed by myself

Where appropriate, I have made acknowledgement of the work of others

The thesis is the correct version for submission and is the same version as any electronic versions submitted*.

My thesis for the award referred to, deposited in the Heriot-Watt University Library, should be made available for loan or photocopying and be available via the Institutional Repository, subject to such conditions as the Librarian may require

I understand that as a student of the University I am required to abide by the Regulations of the University and to conform to its discipline.

I confirm that the thesis has been verified against plagiarism via an approved plagiarism detection application e.g. Turnitin.

ONLY for submissions including published works

Please note you are only required to complete the Inclusion of Published Works Form (page 2) if your thesis contains published works)

Where the thesis contains published outputs under Regulation 6 (9.1.2) or Regulation 43 (9) these are accompanied by a critical review which accurately describes my contribution to the research and, for multi-author outputs, a signed declaration indicating the contribution of each author (complete)

Inclusion of published outputs under Regulation 6 (9.1.2) or Regulation 43 (9) shall not constitute plagiarism.

* *Please note that it is the responsibility of the candidate to ensure that the correct version of the thesis is submitted.*

Signature of Candidate:	Hydra Rodrigues	Date:	09/07/2021

Submission

Submitted By *(name in capitals):*	HYDRA WALESCA DE LIMA RODRIGUES
Signature of Individual Submitting:	Hydra Rodrigues
Date Submitted:	09/07/2021

For Completion in the Student Service Centre (SSC)

Limited Access	Requested	Yes		No		Approved	Yes		No	
E-thesis Submitted (mandatory for final theses)										
Received in the SSC by *(name in capitals):*						Date:				

TABLE OF CONTENTS

LISTS OF FIGURES

LISTS OF TABLES

LIST OF PUBLICATIONS BY THE CANDIDATE

Rodrigues, H. W. L., Mackay, E. J., Arnold, D. Multi-objective Optimisation of CO_2 Recycling Operations for CCUS in Pre-Salt Carbonate Reservoirs. Paper under review - International Journal of Greenhouse Gas Control. Presented (oral) at the 15th International Conference on Greenhouse Gas Control Technologies (GHGT-15), Virtual, March 2021. DOI: 10.2139/ssrn.3811515.

Azari, V., **Rodrigues**, H. W. L., Suieshova, A., Vazquez, O., Mackay, E. Long-term Strategy Optimisation of Scale Squeeze Treatment in a Carbonate Reservoir Under CO_2-WAG (Water-Alternating-Gas) Injection. Paper under review - SPE Journal. Presented (by 1st author) at the SPE International Oilfield Chemistry Conference, Virtual, April 2021.

Rodrigues, H., Mackay, E. J., Arnold, D. Economic Optimisation and Calcite Scale Management of CO_2-EOR (Enhanced Oil Recovery) in Carbonate Reservoirs. Paper presented (oral) at the SPE International Oilfield Scale Conference and Exhibition, Virtual, June 2020 (preparing for peer-review). DOI: https://doi.org/10.2118/200678-MS.

Rodrigues, H., Mackay, E. J., Arnold, D. Optimisation of CO_2-WAG and Calcite Scale Management in Pre-Salt Carbonate Reservoirs. Paper presented (oral) at Offshore Technology Conference Brasil, Rio de Janeiro, Brazil, October 2019 (preparing for peer-review). DOI: https://doi.org/10.4043/29823-MS.

Rodrigues, H., Mackay, E. J., Arnold, D. Impact of WAG Design on Calcite Scaling Risk in Coupled CO_2-EOR and Storage Projects in Carbonate Reservoirs. Paper presented (poster) at the SPE Reservoir Simulation Conference, Galveston, Texas, USA, April 2019 (preparing for peer-review). DOI: https://doi.org/10.2118/193882-MS.

Rodrigues, H., Chauvachata, P., Vazquez O. Mackay, E. J. Technical Evaluation and Comparison of EOR strategies: Polymer versus CO_2 Flooding. Paper presented (oral) at the Oil Field Chemistry Symposium, Geilo, Norway, March 2019.

Rodrigues, H., Mackay, E. J., Arnold, D. Impact of CO_2-WAG Design Optimisation on Coupled CO_2-EOR and Storage Projects in Carbonate Reservoirs. Extended abstract presented (oral) at the Fifth CO_2 Geological Storage Workshop, Utrecht, Netherlands, Nov 2018. DOI: https://doi.org/10.3997/2214-4609.201802994.

Rodrigues, H. W. L., Prata, B. A., Bonates, T. O. Integrated Optimisation Model for Location and Sizing of Offshore Platforms and Location of Oil Wells. Journal of Petroleum Science and Engineering, Volume 145, 2016, Pages 734-741, ISSN 0920-4105. DOI: https://doi.org/10.1016/j.petrol.2016.07.002.

NOMENCLATURE

A_β	reactive surface area of mineral β.
BET	Brunauer–Emmett–Teller
BHP	bottomhole pressure
BIC	binary interaction coefficients
BOE	barrel of oil equivalent
BPS	Brazilian Pre-salt
CAPEX	capital expenditure
CCUS	Carbon Capture Utilization and Storage
CF	carbon footprint
CGI	continuous gas injection
CIC	CO_2 injection concentration
CSE	carbon storage efficiency
CSM	carbon storage mass
DECE	Designed Exploration and Controlled Evolution
EOR	Enhanced Oil Recovery
EOS	equation of state
EWT	extended well test
FPSO	Floating Production Storage and Offloading
GHG	greenhouse gas
GOR	gas oil ratio
GUR	gross utilization ratio
HCPV	hydrocarbon pore volume
IR	injection rate
K_{sp}	Mineral solubility product.
kv/kh	Vertical to horizontal permeability ratio.

LNG	liquefied natural gas
LPG	liquefied petroleum gas
LSWAG	low salinity seawater water alternating gas
MIC	minimum inhibitor concentration
MMP	minimum miscibility pressure
NG	natural gas
NGPP	natural gas processing plant
NPV	net present value
OGIP	original gas in place
OOIP	original oil in place
OPEX	operational expenditure
PAG	polymer alternating gas
PSO	particle swarm optimisation
PV	pore volume
PVT	pressure-volume-temperature
RSM	response surface methodology
r_β	kinetic rate constant of mineral β.
S_g	gas saturation.
SHSS	solvent half-slug size
S_w	Water saturation.
SI	scale inhibitor
SR	saturation ratio
SRU	sulphate removal unit
TC	trace component
TST	transition state theory
V_{MT}	volume of main treatment (squeeze)
V_{OF}	volume of overflush (squeeze)

WAG	water alternating gas
WF	waterflooding
WR	WAG ratio
WTW	wells-to-wheels

UNITS CONVERSION

Units	Equivalent Units
1 MMBtu =	1.06×10^{9} J
1 BOE =	6.12×10^{9} J
1 US barrel (bbl) =	1.59×10^{-1} m^3

Chapter 1 - Introduction

1.1. Problem Statement

Scientific evidence indicates that anthropogenic greenhouse gas (GHG) emissions are the leading cause of climate change (bp, 2020). A consensus hence emerged that the world's energy systems need a rapid unprecedented transition, and that the oil and gas (O&G) industry have a big role to play. First, because the sector ultimately accounts for 42% of global emissions, with two-thirds from upstream operations (McKinsey, 2020). Second, because the O&G industry is best placed to deploy one of the key technologies for reaching net-zero targets: carbon capture, utilization, and storage (CCUS) (IEA, 2020a).

Currently, the main CCUS category is carbon dioxide (CO_2) injection in oilfield reservoirs for Enhanced Oil Recovery (EOR) (Ringrose, 2020), a mature technology that has been commercially implemented by the O&G industry in multiple countries over decades. The additional oil recovered by miscible and pressure maintenance effects brings extra income that finances the CO_2 capture and storage. In CO_2-EOR, a portion of the injected CO_2 remains underground and the CO_2 that returns to the surface is captured and reinjected for permanent CO_2 storage (IEA, 2019a).

Following this rationale, CO_2 has been reinjected into deep-sea oil reservoirs in the Brazilian Pre-salt (BPS) region to improve oil productivity and safely dispose of a GHG that would otherwise be emitted. The Santos Basin project is pioneering commercial large-scale CCUS in deep-waters, with a CO_2 capture capacity of 3 Mtpa (million metric tonnes per annum) (IEA, 2020a). The CO_2 comes from the associated gas, which can contain from 1% to 79% m/m of CO_2 in the Santos Basin, with a median concentration of approximately 15% (d'Almeida et al., 2018).

CO_2-EOR is a promising recovery method for the supergiant BPS oilfields. Some key characteristics make these reservoirs apt for miscible displacement techniques: high initial reservoir pressure (depths from 5 to 6.5 km); moderate temperature (60 to 70 °C); light to moderate crude oil (28 to 32 °API); preliminary studies showing high residual oil saturation after waterflooding; and high gas oil ratio (GOR), ranging from 200 to 400 sm^3/sm^3 (da Costa Fraga et al., 2015).

Although geographical isolation - some 300 km from the shore - currently restricts anthropogenic CO_2 transportation to the BPS fields, the Santos Basin demonstration project

can act as a catalyst for commercial-scale CCUS, playing a strategic role in promoting a lower-carbon economy. Whilst avoiding gas flaring and venting, it can also create the infrastructure, prove the technology, and enable future CCS hubs. For example, it may be possible to reuse existing natural gas pipelines for the transport of captured CO_2 onshore to the BPS fields, after decommissioning or if natural gas export becomes uneconomical. The repurposing of these pipelines could prevent substantial decommissioning costs and would require only a fraction (1 to 10%) of the investment of building a new one (IEA, 2020a).

Water Alternating Gas (WAG) in Carbonate Reservoirs

The main BPS reservoirs are fractured microbial and chemical carbonates with pronounced heterogeneity, which can cripple the efficiency of CO_2-EOR (Salomão et al., 2015). At high concentrations, CO_2 is highly mobile and flows preferentially through high permeability paths or top layers (gravity segregation), resulting in poor oil sweep. To alleviate this problem, CO_2 can be intercalated with slugs of a lower mobility fluid such as water in a Water-Alternating-Gas (WAG) manner.

WAG has been widely used in the O&G industry to tackle early breakthrough of low viscosity injected fluids such as CO_2 and improve sweep efficiency. However, the reactive nature of the BPS carbonate reservoirs poses a threat to flow assurance when CO_2-WAG is applied due to CO_2-brine-rock interactions. Injected CO_2 can react with ions present in the brine and minerals in the porous medium, causing severe inorganic scale issues in production systems.

In this work we will focus on calcium carbonate ($CaCO_3$) in the form of calcite scale. Its general principle is that, when CO_2 is injected at high pressures, part of it speciates in the aqueous phase, reducing the pH of the brine and, consequently, increasing calcite solubility. The BPS carbonate rocks are likely to suffer intense dissolution in high pressure zones, since they are mainly composed of limestone (calcite and aragonite) and dolomite ($CaMg(CO_3)_2$), superimposed by sealing layers of anhydrite ($CaSO_4$) and halite (NaCl). This dissolution may jeopardize injection wellbore integrity. When the brine approaches the production wells and it experiences large pressure drops, the CO_2 evolves from solution, raising the pH of the brine. Due to a greater availability of calcium and bicarbonate ions, the solubility of calcite reduces, and deposition may occur, plugging the pores around production wells and the tubing downstream.

It is, therefore, desirable to delay CO_2 breakthrough and, ideally, ensure its permanent geological storage. Improving the geological storage of CO_2 recycled for EOR purposes represents an opportunity not only to increase oil productivity and mitigate the carbon footprint of current oilfield projects, but also to prevent flow assurance hazards (inorganic scale, wax, asphaltenes and hydrates) and corrosion issues (Pizarro and Branco, 2012). Although these flow assurance challenges all may affect the operability of production wells, the focus of this thesis will be on the calcite scale risk faced by operators. It is in their best interest to determine CCUS design parameters, specifically CO_2-WAG, that balance out the project's profitability, scaling risk and CO_2 emissions.

Several studies looked at optimising aspects of CO_2- EOR, carbon storage, and scaling separately (Silva, 2017, Ribeiro, 2017, McCoy, 2008), but only a few searched for synergies and trade-offs between pairs of objectives (Ettehadtavakkol, 2013, Ghomian, 2008, Gundogan, 2011) and none have attempted their complete integration. To the best of our knowledge, this is the first study assessing the economic, environmental, and operational viability (regarding mineral scale) of CCUS projects in the Pre-salt region, bridging some of the gaps amongst these three key aspects.

1.2. Objectives and Methods

In this work we use reservoir modelling and simulation tools to investigate the optimisation of CCUS projects in a specific context: when the injection supply is restricted to the basin's native CO_2 and when there is considerable risk of carbonate scaling issues. The objective was to develop a methodology that combined reactive transport and optimisation tools using reservoir models (synthetic sector and high-fidelity), focusing on the following questions:

- How to model and design CCUS field operations to improve profitability and give a safe destination to CO_2 contaminant from associated gas?
- What is the potential of CO_2-EOR to reduce CO_2 emissions, considering the entire value chain and limited CO_2 supply?
- How to assess and prevent calcite scale hazards in carbonate reservoirs with significant initial CO_2 content using numerical simulation?

We integrated reservoir engineering calculations with the following bespoke forecast models to support field operational decisions:

- *cash flow projections* that described the relationship between subsurface behaviour, wells, and surface facilities with the economic response.
- *carbon lifecycle analysis* that quantified emissions for the hydrocarbons' entire value chain.
- *production chemistry model* subdivided in two parts: (1) reactive transport simulations at the reservoir and surface levels to assess calcite scaling risk, and (2) design of optimised scale prevention strategies for production wells.

The complete data set of these models (alongside results of the 'CO_2 Recycle' study of Chapter 6) are available online (DOI: 10.17861/e267dcd5-3046-4a7f-9190-299764197bfd). The proposed methodology provides insights into how to recycle CO_2 in an offshore oilfield for better economics and lower carbon footprint, considering calcite mineral deposition risk. Although tailored to the Brazilian Pre-salt characteristics, we believe the knowledge and methods addressed can be easily adapted to coupled CO_2-EOR and carbon storage projects where mineral scale poses a threat to flow assurance. Ultimately, the workflow integrates critical challenges that are interconnected yet often addressed independently and it can be applied to support the complex decision-making process of CCUS design operations in carbonate reservoirs.

1.3. Outline of the Dissertation

In this chapter we have outlined the context that motivated the development of this body of work, as well as indicated what was set out to be achieved, and how. The remaining chapters are organized as follows.

Chapter 2 contextualizes the study within the relevant literature and provides the background for the modelling assumptions and approaches chosen for this study. We discuss the state-of-the-art in CCUS field operational optimisation and CO_2-brine-reservoir rock interactions, covering the studies that most influenced our research decisions.

Chapter 3 is an account of the research methodology, where we discuss what was included in our models to integrate multiphase miscible displacement with geochemical reactions. We detail the three forecast models we developed – economic, carbon emissions, and scaling risk and management. We also show the sensitivity analysis that improved our understanding of the system modelled, namely: compositional hydrocarbon model lumping, mineral kinetic parameters, and inclusion of hysteresis.

The fourth chapter applies the methodology to pilot studies - two-well box models – to validate it with a reduced computational expense. We investigate the implications of changes in the workflow (objective functions, operational strategy type, and optimisation variables).

In Chapter 5 we upgrade the simulations to the field-scale, applying the workflow to CCUS operations in a hypothetical BPS field, aiming at minimising carbon footprint of the project whilst improving its economics and calcite scale management using multi-objective optimisation. We demonstrate the impact of including geochemistry calculations in larger models and the geological uncertainties in our forecasts.

Finally, Chapter 6 summarizes the conclusions of this study and the recommendations for future work in the scope of CCUS operations in reactive carbonate reservoirs.

Chapter 2– Literature Review and Conceptual Framework

In this chapter we expand on the matters mentioned in Chapter 1 that motivated this work. We also outline the most recent developments in production optimisation of coupled CO_2-EOR and storage and how these studies influenced the present one.

2.1. CO_2-EOR as a CCUS Technology

Enhanced Oil Recovery (EOR) involves the injection of fluids not normally present in petroleum reservoirs with the goal of increasing ultimate oil recovery (Lake et al., 2014). The choice and design of these processes for a particular reservoir takes a variety of factors into account: oil type, saturation distributions, reservoir rock/fluids interactions, formation heterogeneities, physical state resulting from past operations (primary and secondary recovery), and availability of injection fluids (Green and Willhite, 1998).

Many studies have focused on EOR as a tertiary recovery method, but EOR is not restricted to a specific period of the reservoir's production life. Tertiary recovery is simply any recovery method applied after primary recovery (natural drive mechanisms) and secondary recovery (pressure maintenance via water or gas injection). Nevertheless, CO_2-EOR has been applied early in Brazilian Pre-salt Santos Basin oilfields due to the necessity of utilising the significant native CO_2 produced alongside the oil as soon as it is available (Pizarro and Branco, 2012).

2.1.1. Why CO_2 for EOR?

CO_2 has a unique behaviour compared to other injection gases: in the supercritical state, it has the density of a liquid but the viscosity of a gas. Injection of CO_2 at miscible conditions alters the properties of the hydrocarbon phase, making it less viscous and more mobile. CO_2 acts as a solvent, *vaporizing* intermediate-weight oil components into the gas phase and, at the same time, *condensing* itself into the oil phase. Additionally, CO_2 can reach residual or non-swept oil that remained in the reservoir after conventional recovery methods by reducing capillary forces, which promotes a better microscopic displacement.

Below a certain pressure, known as Minimum Miscible Pressure (MMP), CO_2 flooding will be immiscible, a condition that yields inferior oil recovery factors and it is more commonly applied in heavy oil reservoirs (Delfani et al., 2008). According to Stalkup (1983), average reservoir pressure must be ideally above MMP at the displacing solvent front for miscible displacement to occur, otherwise, mechanisms intrinsic to miscible processes such as oil

swelling, viscosity reduction by solvent dissolution in oil and vaporization of hydrocarbons will be compromised. Fortunately, CO_2 achieves miscibility with reservoir oils at lower pressures than other common injection gases (e.g., nitrogen and hydrocarbon associated gas).

However, the mobility ratio between CO_2 and the displaced oil bank is usually unfavourable due to the low viscosity of the former (Stalkup, 1983). To overcome the issue, a strategic injection of alternative slugs of water and CO_2 can be adopted, as part of a WAG injection method, aiming to stabilize the front and promote a more uniform volumetric sweep, especially in heterogeneous reservoirs. Most of the scenarios investigated in this thesis are CO_2-WAG schemes due to the heterogeneity intrinsic of the carbonate rocks in the BPS, and the limited availability of CO_2 for injection.

2.1.2. The CO_2-EOR Potential to Mitigate Greenhouse Gas Emissions

CO_2-EOR presents an opportunity to cover the costs of the CO_2 sequestration by producing incremental oil. Its application can reverse the productivity decline of mature fields and produce hydrocarbons with a lower carbon footprint.

With a successful track record since the 1970s and 166 projects fully operating in 2017 (IEA, 2019b), CO_2-EOR is a well-established technology and the technical risks well known. Even with uncertainties around costs and technical complexities (mostly related to capturing and transporting the CO_2 from industrial systems), CCUS is actionable today and can mitigate greenhouse gas (GHG) emissions as other technologies develop and become economically feasible (Friedmann et al., 2019). In contrast, exclusive CCS is pure cost and does not create value on its own without regulatory framework, such as tax incentives or the imposition of a carbon price.

The CO_2-EOR potential to deliver climate benefits can only be fully realized with quantitative life-cycle assessment that considers the specific characteristics of the project and the oil and gas market dynamics (IEA, 2020a). The next section is a brief discussion on quantifying carbon emissions for our applications.

2.2. Considerations on Carbon Emissions

2.2.1. Carbon Accounting

To remain relevant in the energy transition and beyond, O&G companies must carefully consider the carbon emissions profile of their processes and their total environmental footprint, using this information as an additional criterion to optimise business decisions.

At the time of writing, net-zero commitments have pledged to eliminate more than 20% of global oil and gas emissions by 2050, and CCUS is expected to play a crucial role (IEA, 2020a). The coverage of these commitments varies, with some companies targeting only their own operational emissions (Scope 1), while others include indirect emissions from external energy suppliers (Scope 2), and from the use of the hydrocarbon products sold (Scope 3). The three categories are from the Greenhouse Gas (GHG) Protocol, a widely used carbon-accounting tool (WRI and WBCSD, 2021). But compartmentalizing CO_2 emissions into these boxes is not as straightforward as one may think.

For example, for a solely oil and natural gas exploration and production company X, the scope 3 emissions from refining their produced hydrocarbons are the scope 1 emissions of refinery Y. The emissions from combustion of that oil as a finished product are scope 3 emissions for the producer of the oil, the refiner, and the seller, simultaneously. If an electricity producer uses natural gas from company X to generate power, then sells the electricity to company X, the emissions from the natural gas combustion may be the electricity producer's scope 1, *and* company X's scope 2 *and* scope 3. Thus, double counting is likely to occur throughout the value chain.

There is a risk, however, of no organization claiming certain emissions using the rationale that they are someone else's scope 1, until is down to the individual level, when the consumer may be directly charged a carbon tax based on the total carbon footprint of the activity or product they are purchasing. The World Bank advises against this scenario, since consumers and even refinery operators have limited influence over decisions taken at the point of extraction (World Bank, 2017). Another possibility is that energy source companies embrace scope 1, 2 and 3 emissions, paying a carbon tax based on their operations and on what will be done with their products. Then, they would pass on the costs down the supply chain accordingly. Purchasing natural gas for a combustion turbine would possibly cost more than buying it to produce hydrogen for fertilizer production, for example.

The merits of the nomenclature used in carbon accounting and how it will affect carbon taxing is beyond the realm of this text. Suffice to say that the concepts of scope 1, 2 and 3 seem sensible under specific circumstances, ideally when a company operates a single large asset, or is a highly integrated oil and gas corporation.

In short, it is essential that companies reliably quantify at least their direct emissions at the granular, asset- and process-level. The focus should not be only on reporting past emissions, but also on forecasting future ones and drawing plans to reduce them. Even where there is no carbon pricing regulation yet, O&G companies can apply a cost to their future carbon emissions to quantify their impact on the project economics. The same reservoir simulation models that aid investments decisions can help on these predictions, with a certain degree of uncertainties that needs to be considered.

2.2.2. Gas Utilization and Flaring in the BPS

Most emissions in exploration and production (E&P) activities are associated with the venting, flaring, and fugitive emissions of natural gas, and most flaring that occurs today is routine flaring, the kind that can be avoided when planned well in advance (IEA, 2020b).

Flaring is the combustion of natural gas during oil and gas exploration, production, and processing operations. Flaring is regulated and permitted for safety reasons during activities such as well completion, routine and nonroutine maintenance, or other unplanned events and emergency shutdowns (Kah, 2020). It can be also used to control and reduce emissions of volatile gases from hydrocarbon storage tanks, and to avoid the releasing of gases into the atmosphere – e.g., where there is insufficient infrastructure to gather and transport the gas for sale. Even when there is infrastructure in place, flaring is likely to occur when a well starts flowing since its high initial pressure and rates may overwhelm the surface facilities.

The decision of avoiding flaring in the BPS operations was made early at the project planning stage, which allowed for the provision of the necessary infrastructure to monetize the gas (separators, compressors, pipelines) (ANP et al., 2020). As the giant reserves had a high associate GOR, simply flaring all that gas was neither economical nor environmentally acceptable.

Membrane separation was the technology of choice to remove the CO_2 from the produced hydrocarbon gas and fulfil the specification of no more than 3% vol/vol of CO_2 in the export

sales gas. The capture process is based on polymeric or inorganic membranes that let the CO_2 pass through but retain the other gas components. The facilities in the Santos Basin Floating Production Storage and Offloading (FPSO) vessels are the only large-scale membrane-based capture plants in the world (IEA, 2020a). They are suitable to the typical space-restricted BPS FPSO due to their compact nature (Rochedo et al., 2016).

The purified natural gas (NG), mainly methane, is sold and/or used in the platform to generate electricity or aid production (gas-lifting). But there was still the question of the CO_2-rich gas stream, to which the answer of most operators was to use it for CO_2-EOR. According to da Costa Fraga et al. (2015), CO_2-WAG in the BPS is more of a reservoir management strategy than an EOR one, due to the low availability of CO_2. They argue that a WAG ratio of 1 would only be achieved if all the produced gas were reinjected. This happens occasionally - when produced gas volumes exceed the membrane module capacity, the extra gas is reinjected directly into the reservoir with the CO_2-rich gas stream to avoid complete flaring (Rochedo et al., 2016).

In this thesis, we engaged in finding out whether these decisions were sensible, and how to find optimised ways of using the excess CO_2-rich gas (and even part of the sales gas) to improve oil recovery and reduce flaring emissions. Carbon emissions counting was, therefore, essential for this analysis.

In Chapter 3, the reader will see a description of how we quantified CCUS emissions for a barrel of oil produced. Flaring was the key part of E&P emissions since it is the optimisable term. The following assumptions were made based on local flaring guidelines:

- During Extended Well Test (EWT) in the BPS, all produced gas is flared since the gas export capabilities have not yet been installed. Additionally, the regulations limit the flaring to a maximum of 500,000 sm^3/d, and the cumulative volume flared within the first 90 days of production cannot exceed 7.5×10^7 sm^3.
- After the exploration period, the operator can flare up to 3% of the monthly produced gas volumes without legal implications, for security or planned well testing only (ANP, 2000).
- Flaring beyond that level is met with a penalty, which we are assuming is USD 40 per metric tonne of CO_2 emitted (Galp, 2018).

Although assuming perfect combustion, we acknowledge that flaring emissions depend not only on the volume of gas but also on the combustion *efficiency* of the flare. Inefficient

flares generate more methane emissions, which has a global warming potential 28 to 36 times higher than of the CO_2 over 100 years (EPA, 2020). According to the IEA (2020b), more than 99% of the natural gas can be fully combusted when flaring occurs in optimal conditions, but in reality these conditions are rare.

2.3. Challenges in CCUS Operational Optimisation

Many factors influence the design of a coupled CO_2-EOR and storage project in deep-water carbonate reservoirs. The displacement alone can be highly complex because of aspects such as channelling caused by stratification, segregated flow caused by buoyancy effects, crossflow between strata, permeability changes caused by dissolution/precipitation of rock, trapping of oil and gas by mobile water, relative permeability hysteresis, to name a few (Stalkup, 1983). Reservoir modelling studies can play a crucial role in shedding some light on the optimal application of miscible flooding schemes, by incorporating at least a few of the many phenomena happening in the subsurface.

2.3.1. Operational Optimisation Techniques

Production optimisation during CO_2-EOR consists of adjusting parameters the operator can control to improve reservoir performance. Surface and downhole variables are normally considered: injection and production rates or bottomhole pressures, injected fluids type and composition, injection temperature. However, systematically optimising large field operations can be a time-consuming task, especially considering physical and financial uncertainties and technical constraints (Chen, 2012). The production strategy possibilities can be endless, so reservoir engineers traditionally opt for field best practices (e.g., voidage balance) and/or simulation-based optimisation techniques.

The general procedure of an optimisation algorithm consists of finding the combination of design variable values that results in the best objective function(s) value(s) (minimum or maximum), while satisfying the system's constraints. In the context of this work, although there is synergy between CO_2-EOR and CO_2 storage aspects when molecules of CO_2 occupy pore space previously filled with oil, their objectives are not completely aligned. From a pure EOR perspective, optimised operating conditions would require the lowest volume of CO_2 to recover a barrel of oil, while from a CO_2 storage point of view, the main goal is to bury as much CO_2 as possible underground. When scaling risk is also a reality, delaying water breakthrough becomes essential, which would also benefit the financial objective.

The optimisation problem becomes one of finding that 'sweet spot' that balances out these aspects.

Such a multi-criteria (multi-objective) problem often has no single optimal solution, but instead a set of solutions defined as Pareto optimal solutions (Talbi, 2009). They represent a compromise between conflicting objectives, where no objective can be improved without harming the other(s). Then, the best overall solution can be identified based on the decision-maker's judgment and other criteria, such as ease of implementation, safety, other flow assurance consequences, etc.

There are many optimisation algorithms that can be applied for reservoir engineering problems and the choice of the most suitable one is down to the nature of the problem (its formulation, the number of design variables, the linearity and continuity of the functions, the computational resources available, among other factors). An in-depth review of optimisation techniques can be found elsewhere (Venter, 2010, Abraham and Goldberg, 2005). Here we briefly discuss the applicability of heuristic algorithms, specifically meta-heuristics, which have been effectively used in large complex nonlinear problems and were the chosen method in this thesis. Figure 2.1 shows where these algorithms sit on the realm of optimisation methods.

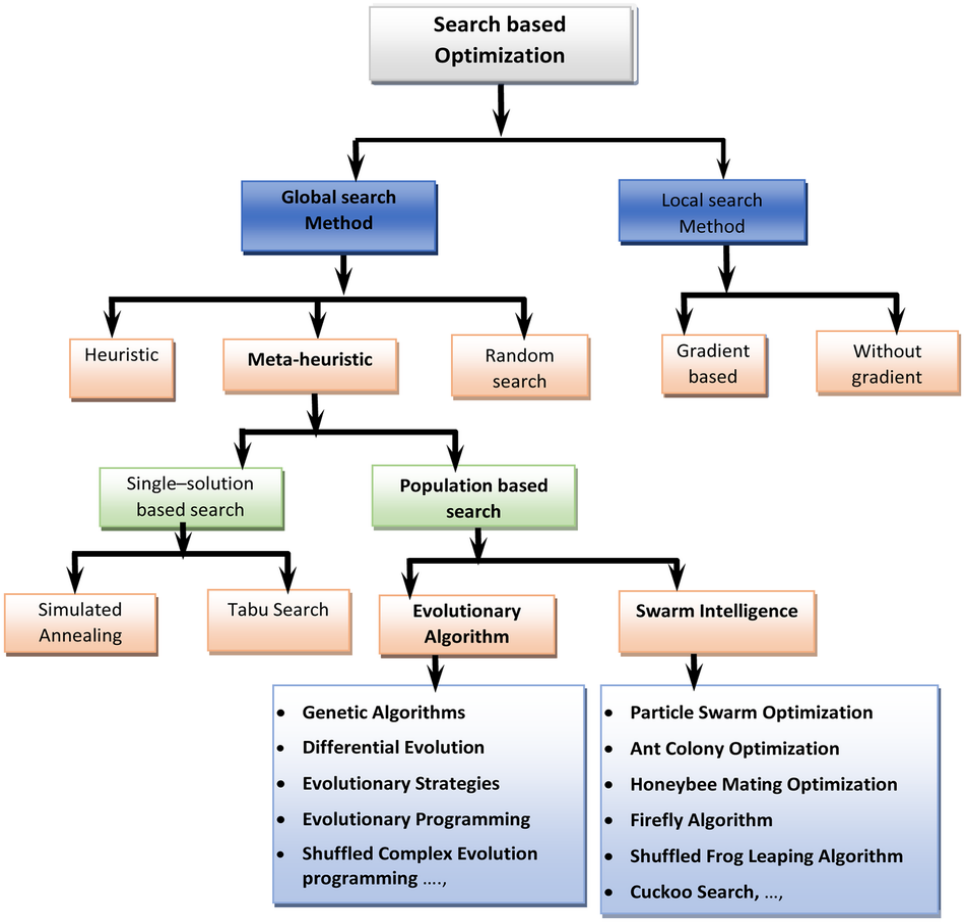

Figure 2.1 Taxonomy of optimisation methods. Source: Janga Reddy and Nagesh Kumar (2020).

Although heuristic algorithms often scale efficiently to large problems, they do not guarantee optimality nor feasibility, simply seeking better solutions that may or may not be close to the global optimum. To avoid local optima entrapment, meta-heuristics are regularly used, searching further than the predefined neighbourhood. Many of these meta-heuristic methods are based on biological behaviours. In essence, they all move from a starting point towards a better solution by following logical rules (heuristic) (Grond et al., 2012). The process is carried out until the algorithm is not able to find a better solution, in this case, a better operational strategy.

In our single-objective optimisation studies, we applied CMOST AI Designed Exploration Controlled Evolution (DECE), which is CMG™'s proprietary two-stage iterative optimisation process (CMG, 2020a). In the first stage (exploration), Latin Hypercube sampling and Tabu search techniques are applied to independently select values from the range of input variables to create new experiments (simulation runs). In the second stage (controlled evolution), the simulation results obtained in the previous stage are statistically analysed to improve the next generation's solution quality, moving towards better values of the objective function. To avoid local maxima or minima entrapment, rejected candidate values

are periodically checked and they can be recalled for the next stage (CMG, 2020a), although there is no guarantee that a global optimal will be found. The DECE optimisation method has been successfully applied in several real-world reservoir simulation studies to solve history matching and optimisation problems (CMG, 2020a).

Our multi-objective optimisation problems were tackled using Particle Swarm Optimisation (PSO), one of the most well-known population-based stochastic optimisation techniques, inspired by the social behaviour of bird flocking, fish schooling, and ant colonies (Eberhart and Kennedy, 1995). In PSO, the system starts with a population of random solutions. The particles iteratively evaluate their candidate solutions and remember the location of their best success so far, making this information available to their neighbours and learning where to go. This information guides the motion of the particles through the search space, and the generations usually converges towards better solutions compared to the starting point.

2.3.2. Numerical Studies in CO_2-EOR and Storage

Research into CCUS projects' optimisation has gained pace in recent years especially since climate imperatives have been pushing forward CO_2-EOR technologies. Many of these studies were based on proxy models, since running high-fidelity reservoir models several times can be numerically far too expensive.

Ghomian et al. (2008) investigated the impact of controllable (WAG ratio, CO_2 slug size) and non-controllable parameters (Dykstra-Parsons coefficient, horizontal and vertical correlation length, and hysteresis) in coupled CO_2-EOR and storage performance using proxy models generated by response surface methodology (RSM). In this method, a subset of experiments is statistically selected from many possible combinations, deriving a simplified mathematical relationship between input variables and outcomes from a few flow simulations. They reported a 75% reduction in computational load and good agreement with their flow simulation studies. Ampomah et al. (2017) also applied a design of experiment approach to optimise oil recovery and storage during CO_2-EOR. They used a Latin hypercube sampling algorithm to build a surrogate model that reduced computational time. They reported the proxy model was close to their full-field confirmation (less than 2% difference). However, Schiozer et al. (2019) argue that proxy models are likely over-simplified and may not capture the complexity of the physics-based reservoir models, let alone of the subsurface itself.

Ettehadtavakkol et al. (2014) optimised CO_2-EOR-storage performance in a sandstone and a carbonate reservoir. They simulated 90 designs for each reservoir model, but it is unclear how the variables' domains were sampled to generate those designs. In their model, the net benefit of CO_2 storage was negative, as CO_2 capture cost was 80 USD/tCO_2 and the storage tax credit was just 40 USD/tCO_2. The only way to turn a profit was through the extra revenue from incremental hydrocarbon recovery, so it was no surprise when a trade-off between the economic and CO_2 storage objectives was observed. The negative economic effects were more pronounced in the heterogeneous carbonate reservoir.

In a more recent study, Li et al. (2018) demonstrated the improved economic outcomes of optimising not only the conventional WAG variables (half-cycle lengths, injection rates and bottomhole pressure of producers), but also the length of primary, secondary and tertiary recovery across the field life. They used CMG™ CMOST AI DECE algorithm to maximise the NPV of the project deployed in a sector reservoir model. This is a similar approach to our own in this thesis, although we expanded it to consider environmentally driven objectives, with single- and multi-objective studies.

Another important study that contribute to our understanding of the problem was a doctoral thesis in CO_2-EOR and storage optimisation under uncertainties (Ettehadtavakkol, 2013). In one of the main studies, the author optimised three operational variables - gas injection rate, flood duration, and WAG ratio – for simultaneous WAG schemes considering three main outcomes: average oil production per well, net CO_2 utilization ratio (amount of CO_2 stored per incremental barrel of oil produced), and CO_2 recycle ratio (ratio between CO_2 production rate and fresh CO_2 injection rate). The field development schedule, number of wells, CO_2 separation plant size, and compression power were a consequence of the three variables optimised. It was observed that increasing the CO_2 injection rate accelerated the project's deployment, which anticipated cash flows and improved the economics. The author also concluded that applying high WAG ratios constrained the CO_2 storage capacity.

2.3.3. WAG Optimisation Variables

WAG ratio is considered an important parameter in WAG process designs and it is defined as the ratio between water injected volume and gas injected volume in each cycle at reservoir conditions. A WAG ratio of 1 is normally applied in the field, although its value depends on the availability of gas to be injected and injection wells capacity (Belazreg et

al., 2019). Ettehadtavakkol (2013) says that typical ranges vary from zero to five, while Huang and Holm (1988) argue that values can range from 0.5 to four.

The solvent (CO_2) half-slug size is often considered in optimisation studies and is reported in injected pore volumes (PV) or hydrocarbon pore volumes (HCPV). Hadlow (1992) states that normally a volume of CO_2 from 1% to 4% of a HCPV is injected followed by water until the desired WAG ratio is achieved. Chen et al. (1984) argue that calculated minimum solvent slug-size is in the order of 1% to 5% of the original HCPV, although field experience suggests that successful projects require slug sizes much larger than that. Another study shows that the alternation frequencies vary from 0.1% to 2% of a PV for each fluid (Huang and Holm, 1988). The cumulative volume of CO_2 injected into the reservoir throughout the project's life is called ultimate or total CO_2 slug size.

2.4. Calcite Scaling Risk in the Presence of CO_2

The importance of mineral dissolution and precipitation in production systems due to the injection of CO_2 has long been recognized (Jin et al., 2016). The way CO_2-EOR operational strategies influence flow assurance is crucial information that can support the decision-making process of selecting a project's design. Having a geochemistry model embedded in the reservoir simulation calculations can help operators understand the complex interactions happening as each barrel of injected fluid travels throughout the porous medium, encountering formation water, reactive rock, and hydrocarbon phases. The output data of these simulations, more specifically ion compositions and flow rate distributions in time for each production well, can be used to predict how much scale deposition (in our case, calcite) will occur and where in the production system, so a scale management plan can be drawn up.

The path from the production wellbore to the surface facilities is crucial since it is where produced fluids suffer the most significant pressure drops, causing CO_2 to be released to the gaseous phase, raising the brine's pH, which increases the availability of calcium and bicarbonate ions and reduces the solubility of calcite, resulting in its precipitation.

2.4.1. The Calcium Carbonate System

In the context of alternating injection of CO_2–rich gas and low sulphate seawater in the Brazilian Pre-salt carbonate reservoirs, calcium carbonate in the form of calcite is perhaps the most significant mineral to be considered on an inorganic scale management study.

Indeed, calcite is the most abundant carbonate mineral in deep-sea sedimentary rocks (Morse and Arvidson, 2002). In the BPS carbonate reservoirs, anhydrite ($CaSO_4$) can also pose a significant risk when seawater is injected, but according to numerical studies performed by André et al. (2015), calcite dissolution will have a bigger impact on porosity than anhydrite precipitation, if both are happening simultaneously. Additionally, sulphate scale is greatly reduced in the BPS with seawater desulphation plants installed in the FPSOs. Hence, we assumed that the geochemistry of this system can be described by the carbonic acid system equilibria as follows. Reservoir rock composition is considered as 80% calcite, based on BPS fields reported rock compositions (Yasuda et al., 2013).

When CO_2 dissolves in water, gaseous $CO_{2(g)}$ becomes aqueous $CO_{2(aq)}$, and some of it combines with water molecules to form carbonic acid, H_2CO_3 - a planar triangular CO_3^{2-} ion complexed with two protons (H^+). However, most $CO_{2(aq)}$ stays in solution as a hydrated linear $CO_{2(aq)}$ molecule. For simplicity, the two species are added as H_2CO_3*, which deprotonates to produce bicarbonate, HCO_3^-. Combining these steps results in reaction (2.1):

$$CO_{2(g)} \leftrightarrow CO_{2(aq)}$$

$$CO_{2(aq)} + H_2O \leftrightarrow H_2CO_3^*$$

$$H_2CO_3^* \leftrightarrow H^+ + HCO_3^-$$

$$CO_{2(g)} + H_2O \leftrightarrow H^+ + HCO_3^- \qquad log\ K_{eq}(331.9\ \mathrm{K}) = -6.32 \qquad (2.1)$$

Where K_{eq} is the chemical equilibrium constant for this aqueous phase chemical equilibrium reaction, obtained from the GEM™ database and considered as a function of temperature. Bicarbonate can deprotonate to yield carbonate, CO_3^{2-} or, depending on the pH, H^+ can associate with carbonate ions from calcite to form bicarbonate. Both ways are represented by equation (2.2):

$$HCO_3^- \leftrightarrow H^+ + CO_3^{2-} \qquad log\ K_{eq}(331.9\ \mathrm{K}) = -10.21 \qquad (2.2)$$

Finally, we need to include the water self-ionization and the dissolution/precipitation of $CaCO_3$ in the form of mineral calcite:

$$H_2O \leftrightarrow OH^- + H^+ \qquad log\ K_{eq}(331.9\ \mathrm{K}) = -13.04 \qquad (2.3)$$

$$CaCO_{3(s)} \leftrightarrow Ca^{2+} + CO_3^{2-} \qquad log\ K_{sp}(298.15\ \mathrm{K}) = -8.48 \qquad (2.4)$$

Where K_{sp} is the solubility product for the rate-dependent calcite dissolution/precipitation reaction, also a function of temperature only. Adding reactions (2.1), (2.2) and (2.4) gives us the overall fundamental equation that shows how CO_2 speciation affects calcite dissolution/precipitation - an increase in CO_2 concentration results in dissolution of $CaCO_3$, while removal of CO_2 causes calcite to precipitate:

$$CO_{2(g)} + H_2O + CaCO_{3(s)} \leftrightarrow Ca^{2+} + 2HCO_3^- \quad (2.5)$$

Mineral dissolution and precipitation reactions cause changes in reservoir petrophysical properties (porosity and permeability), so in our simulations, porosity alterations were quantified based on the molar quantities of calcite varying at each timestep. The classical Kozeny-Carman power law model (Carman, 1956) was then used to estimate permeability changes as a function of the porosity variations.

It is important to consider the simulator's limitations regarding integration of multiphase behaviour with geochemical reactions; they normally compromise in one aspect over another. For instance, the compositional simulator used in this study requires the identification of independent reactions for the system, while these reactions can take place, or not, depending on brine composition (Venkatraman et al., 2017). The next section is a discussion of one of the biggest sources of uncertainty in geochemistry modelling – the mineral reaction kinetics.

2.4.2. Calcite Reaction Kinetics

Reactions between chemical components in the aqueous phase are fast in comparison to mineral dissolution/precipitation reactions (CMG, 2020b). Hence, in the commercial reservoir simulator used in this work (GEM™), intra-aqueous reactions are represented as chemical-equilibrium whereas mineral reactions are represented as rate-dependent. The chemical equilibrium constants, K_{eq}, are from well-established models (Appelo and Postma, 2004), but for mineral reactions, the simulator requires input data from the user: rate constant (k_β) and reactive surface area (A_β). They are key to the empirical kinetic expression that dictates the pace of dissolution and precipitation of minerals (Bethke, 1996):

$$r_\beta = k_\beta A_\beta \left(1 - \frac{Q_\beta}{K_{eq,\beta}}\right) \quad (2.6)$$

where r_β is the reaction rate for mineral β (mol/m^3/s), k_β is the rate constant (mol/m^2/s), A_β is the reactive surface area (m^2/m^3), $K_{eq,\beta}$ is the chemical equilibrium constant of mineral reaction β, and Q_β is the activity product of mineral reaction β.

The ratio $Q_\beta/K_{eq,\beta}$ represents the saturation state of the system or saturation ratio (SR), which is the distance of solution from the equilibrium state of the mineral reaction. For the calcite mineral reaction represented by equation (2.4), SR can be written as:

$$SR = \frac{a_{Ca^{2+}} a_{CO_3^{2-}}}{K_{sp}^{CaCO_3}} \tag{2.7}$$

Where a_i represents the activity of ion i (Ca^{2+} and CO_3^{2-} respectively). The following conditions apply:

- $SR < 1$: the system is undersaturated; no precipitation occurs.
- $SR = 1$: the system is in equilibrium.
- $SR > 1$: the system is supersaturated; precipitation may occur.

Equation (2.6) is a particular case of the general Transition State Theory (TST) based kinetic rate law, obtained by assuming a linear relationship between r_β and SR and disregarding other aqueous species that potentially accelerate or limit r_β. These assumptions are consistent with far-from-equilibrium conditions (Anabaraonye et al., 2019), which hold true where rapid changes occur in the subsurface - around injection wells and production systems. Deep within the reservoir, as the flow rates are generally low, thermodynamic equilibrium is normally reached, so mineral reaction kinetics can be omitted without jeopardizing prediction accuracy (instantaneous equilibrium assumption) (Mackay, 2003). Near-equilibrium dissolution rates are highly non-linear (Subhas et al., 2015), so an exponent should be determined for the degree of saturation term, fitted through experimental data.

For CO_2-water systems, the dissolution of calcite has been commonly described with three parallel reactions related to three regimes (Plummer et al., 1978):

$$CaCO_{3(s)} + H^+ \overset{k_1}{\leftrightarrow} Ca^{2+} + HCO_3^- \tag{2.8}$$

$$CaCO_{3(s)} + H_2CO_3^* \overset{k_2}{\leftrightarrow} Ca^{2+} + 2HCO_3^- \tag{2.9}$$

$$CaCO_{3(s)} \overset{k_3}{\leftrightarrow} Ca^{2+} + CO_3^{2-} \tag{2.10}$$

The rate of reaction (2.8) dominates under acidic conditions (pH < 3.5), it is transport-controlled, and it depends on the pH only. The rate of reaction (2.9) depends on both pH and the CO_2 partial pressure, and it is surface-controlled, while the rate of reaction (2.10) prevails under 'neutral' pH conditions (pH > 5.5), and it is considerably influenced by the precipitation reaction.

The rate dependence on pH is illustrated in Figure 2.2. In regime 1, dissolution is so fast that the diffusion of species between the bulk of the solution and the boundary layer is the limiting factor. In contrast, in regime 2, transport is fast compared to the rate of surface reaction, making the dissolution rate more dependent upon the brine composition and CO_2 partial pressure (Brantley, 2008).

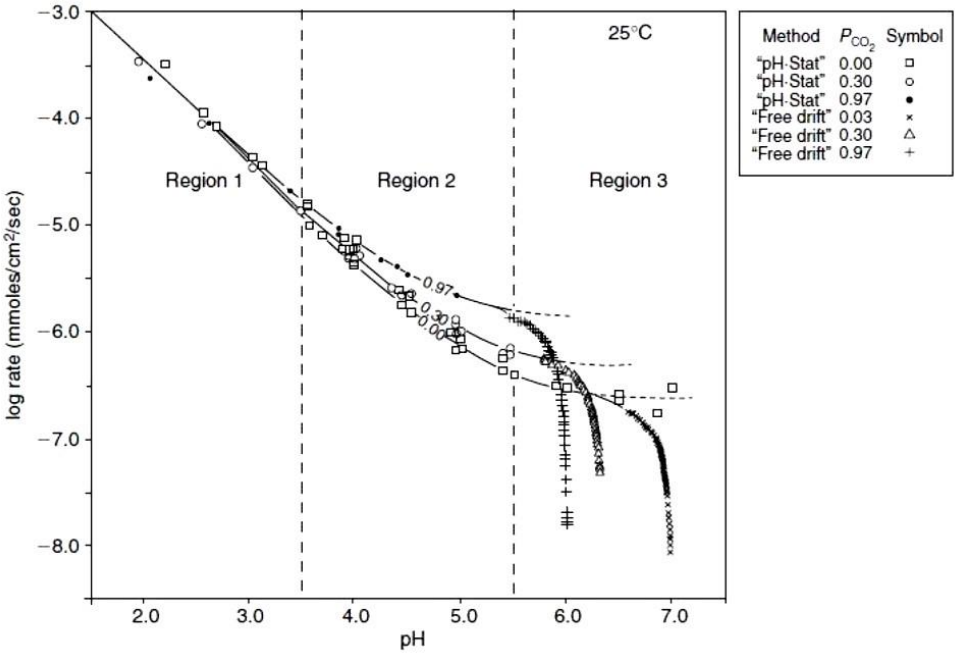

Figure 2.2 Calcite dissolution rates measured at 298.15 K as a function of pH and CO_2 partial pressure. Source: Appelo and Postma (2004).

The overall calcite rate r_β is the summation of the rates of all three parallel reactions. Substituting in equation (2.6) we obtain:

$$r_\beta = A_\beta\left(k_1 a_{H^+} + k_2 a_{H_2CO_3^*} + k_3\right)\left(1 - \frac{Q_\beta}{K_{eq,\beta}}\right) \tag{2.11}$$

where k_1, k_2, and k_3 are rate constants and a_i refers to the activity of the relevant species.

GEM™ has the general TST kinetic rate law implemented, but it does not allow for the dependence of the mineral reaction rate on the chemical components. The rate constant k_β in GEM™ is only dependent on temperature, according to the Arrhenius equation:

$$k_\beta(T) = k_\beta(T^{ref}) exp\left[-\frac{E_a}{R}\left(\frac{1}{T} - \frac{1}{T^{ref}}\right)\right] \quad (2.12)$$

Where T is the temperature of interest and T^{ref} is the reference temperature, both in Kelvin; R is the gas constant (8.314 J/(mol·K)); and E_a is the activation energy, considered here as 41.87 kJ/mol based on the conditions of the reservoir (mostly regime 2) (Plummer et al., 1978). Therefore, as we needed to omit the mineral reaction rate dependence on components activities, we considered calcite dissolution and precipitation as governed by equation (2.10). We then selected a rate constant representative of the mechanisms of the reservoir conditions studied here.

Although there are numerous calcite dissolution kinetics studies in the literature (see data compilations in (Palandri and Kharaka, 2004, Peng et al., 2015)), they present a high degree of variability on the conditions (reactor setup, transport and sample conditions, acid nature, ranges of salinity, pH, temperature, pressure, among other variables), making direct comparisons challenging. According to Peng et al. (2015), experimental calcite dissolution data in the (CO_2 + H_2O) system under reservoir-like conditions or surface-reaction-controlled regime (region 2) are scattered. The review by Morse et al. (2007) has indicated that fundamental knowledge is lacking regarding calcite reactions under these conditions, which is key when modelling reactive transport for CO_2 EOR and storage simulation, especially when advection is dominant.

Remarks on Reactive Surface Area

The reactive surface area of the dissolving minerals is difficult to estimate since it depends on the surface area in direct contact with the aqueous phase (André et al., 2015). According to White and Peterson (1990), *reactive* surface areas can be one to three orders of magnitude lower than *physical* surface areas measured using the BET (Brunauer–Emmett–Teller) method. Subhas et al. (2015) extensive experimental work found that N_2 and/or Argon BET measured surface areas were two to three orders of magnitude larger than calculated *geometric* surface areas. They also found inaccuracies in their BET data - they were strongly dependent on the sample size - leading the authors to normalize their dissolution rate data to geometric surface area. Morse et al. (2007), on the other hand, argue that geometric and reactive surface areas are merely an abstraction, doubting the latter is even measurable.

We believe the biggest trouble with using BET surface areas is that the measurement process involves grinding of the rock samples, which, by definition, changes the surface area in contact with the fluid and leads to overestimation. In the next chapter we will perform a 1D sensitivity analysis of the kinetic parameters k_β and A_β to evaluate their impact on our scale predictions.

2.4.3. Oilfield Scale Prevention

Scaling risk assessment starts at the exploration phase of the field, especially in an offshore context. Platform space is limited, and interventions are complex, so decisions regarding completion and production technologies need to be made well in advance. At these early stages, before production data are widely available, reservoir simulation models coupled with scale prediction models can be a powerful tool to forecast reactive multiphase flow in the near wellbore region, production wells, and surface facilities. Then, during the production phase of the field, engineers can have a better grasp of the scaling risk by monitoring produced water rates and chemistry, downhole pressures and gas production, history matching their models. These are essential for scale management, which involves designing preventive (and, if necessary, corrective) measures and reviewing any decisions made under higher uncertainty levels.

Scale inhibitor (SI) squeeze treatment is one of the main techniques applied to protect production wells from mineral scaling. The process consists of pumping the SI into the reservoir until it reaches a designed distance from the production wellbore. Three distinct slugs are injected: (1) the preflush, which acts as a buffer to condition the formation for the next key slug; (2) the main treatment, or the brine with the engineered concentration of SI; and (3) the overflush, which displaces the chemical deep into the formation, improving the longevity of the treatment. A subsequent shut-in period allows time for further retention of the SI onto the rock surface. The chemical is then gradually released as production is resumed. The near wellbore region remains protected until the concentration of the SI in the produced brine falls below a certain Minimum Inhibitor Concentration (MIC), determined through laboratory experiments (Vazquez et al., 2016). To avoid scale precipitation downstream of the wellbore, continuous SI injection can be applied through a chemical umbilical to the subsea flow line. It is also sometimes possible to deliver chemical continuously inside the wellbore via a dedicated capillary or through the gas lift mandrel; however, it is not possible to protect the completions below the packer by continuous

injection - hence the importance of squeeze treatments. In this study, we assessed scale tendency using reservoir simulation and scale prediction models to identify CO_2-WAG production strategies that minimised scaling risk. Then we used the forecasted data to design scale management strategies, specifically squeeze treatments with the lowest costs.

2.5. Conclusions

This chapter has demonstrated the necessity of investigations on the overall research question "how to *integrate* reservoir engineering calculations, cash flow projections, carbon accounting and production chemistry to support CCUS projects' operational decisions?"

While a number of studies have focused on the challenges of optimising CO_2-EOR operations when storage is also a priority, few painted a clear and comprehensive picture of the trade-offs intrinsic to the problem. And even fewer considered the implications of the operational strategies on the reservoir geochemistry and risk of scale in production systems. There is, therefore, room for developments on the integration of reactive transport and CCUS operational optimisation, which is the purpose of this work. We do not claim to have bridged the gaps in the knowledge, but we hope this study contributes to at least an 'infinitesimal' advancement of the cutting-edge of this topic.

The literature has revealed that the geochemistry plays an important role in the fate of oilfield production in the presence of CO_2, but that there are still many uncertainties regarding the kinetics of mineral reactions, especially under conditions around and far from equilibrium, so quantitative results should be treated with caution.

In this multiphase multispecies reactive heterogeneous system, the range of variables and their complex interaction make any modelling difficult. But the models, if appropriately designed, can give valuable insights for investments and operational decisions.

Chapter 3- Modelling and Optimisation of CCUS in Carbonate Reservoirs: What to Consider?

In this chapter, we describe a simulation-based reactive transport workflow to optimise Carbon Capture Utilization and Storage (CCUS) in offshore carbonate reservoirs. The analysis focuses on the economics, flow assurance and carbon footprint of CO_2 reinjection in the context of the Brazilian Pre-salt oilfields. We discuss what to include in models that integrate multiphase miscible displacement with geochemical reactions. We also address how uncertainties in the modelling assumptions and data can impact production performance, calcium carbonate scale and CO_2 retention in the reservoir. The complete data set of the models described in this chapter are available online (DOI: 10.17861/e267dcd5-3046-4a7f-9190-299764197bfd. Refer to 'CCUS_Optimisation.xlsm').

3.1. CCUS Operational Optimisation Workflow

Many factors influence the operational strategy of a coupled CO_2-EOR and storage project. The displacement alone can become intricate when gas is injected in the porous medium. Channelling can occur due to stratification, segregated flow because of buoyancy effects, crossflow between strata, viscous fingering, permeability changes due to dissolution/precipitation of rock, trapping of non-wetting phases, hysteresis of relative permeability and capillary pressure, wettability alterations, among other aspects (Stalkup, 1983).

Reservoir simulation models can be tailored to capture many of these phenomena, but the balance between accuracy and functionality is the 'holy grail' of reservoir development decisions. "All models are wrong, but some are useful" is a common aphorism in the area (Box, 1979). So how to build useful models for operational decision-making in CCUS applications?

A concise answer would be to customize the classical subsurface modelling workflow for the project's particularities. A longer answer is the main deliverable of this thesis: a detailed simulation-based methodology adapted to optimise operational strategies of CO_2-EOR and storage projects in carbonate reservoirs. We primarily developed it to the Brazilian Pre-salt offshore context (reservoir characteristics, supply chain, infrastructure, regulatory framework, and economic aspects) but the workflow can be generalized for other applications. Each step of the methodology we adopted throughout this thesis is

summarized in Figure 3.1. *Production forecast* is the 'beating heart' of the workflow, and it involves the creation of sub-models that reasonably capture the subsurface rock structures, the oil and gas components flowing, and the CO_2-brine-rock interactions, as follows:

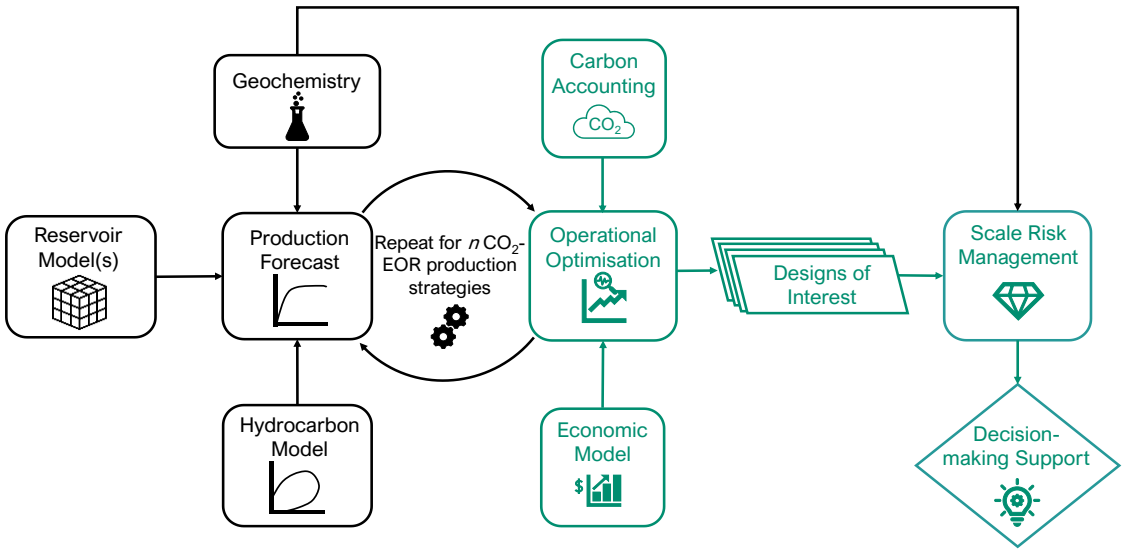

Figure 3.1 Workflow for CO_2-EOR and storage operational optimisation in carbonate reservoirs, integrating the subsurface (in black) and the surface systems (in green).

1. *Reservoir model(s):* select reservoir simulation models that fit the available field static and dynamic data and capture a wide range of geological uncertainties. Most investigations in this thesis were performed in single fictitious sector models, to demonstrate the methodology avoiding prohibitive simulation times. However, we acknowledge the necessity of addressing the uncertainties in reservoir characterization and believe a scenario-based approach with a few representative models could balance out robustness and computational cost (Bentley and Smith, 2008, Santos et al., 2020).
2. *Hydrocarbon model:* define an Equation of State (EOS) that adequately represents the phase behaviour of the system. For miscible CO_2-EOR applications with risk of carbonate scale, the use of a compositional model is essential. Lumping components will likely be necessary to reduce computational time.
3. *Geochemistry:* create a geochemical model with the pertinent chemical and mineral dissolution/precipitation reactions occurring as CO_2 dissolves and is released from the various phases. Depending on grid-size and flow rates (Damköhler number) (Ribeiro, 2017), and the capabilities of the software used, a kinetic model needs to be included.
4. *Operational optimisation:* first, identify variables that are optimisation candidates.

These are parameters that operators have control over in the field and may affect reservoir performance. Sensitivity analysis can narrow the list down to the most influential variables on the objectives. Then determine their respective domains based on the literature and field experience. The final crucial steps are the selection of a sampling method, optimisation algorithm and objective function(s).

5. *Economic model:* develop a fit-for-purpose economic model that will be integrated with the production forecasts to evaluate the impact of changing the operational inputs. We used this model as one of the main objective functions of all our optimisation studies.
6. *Scaling risk assessment/management:* for the designs of interest, evaluate the inorganic scaling tendency around the wellbores and in the production system (surface conditions). Use these results to draw a scale prevention plan optimised for costs and durability.
7. *Decision-making support:* rank the designs according to their economic performance, carbon footprint and scaling risk, to select the most promising overall operational strategies.

3.2. Hydrocarbon Model

The reservoir fluid used in this work has similar characteristics of a typical BPS (Santos basin) oil – 29 °API, high methane content, considerable CO_2 contaminant, and high Gas Oil Ratio (GOR) of about 221 sm^3/sm^3. The experimental data was from Moortgat et al. (2013) and test conditions were 44.1 MPa and 331.9 K. We used a commercial PVT package (CMG™ WinProp) to perform the EOS tuning and lumping as follows.

3.2.1. Equation of State (EOS) Tuning

The hydrocarbon phase properties were modelled using Peng-Robinson (PR) EOS (Peng and Robinson, 1976) with volume translation (Péneloux et al., 1982) to improve density predictions. PR-EOS is widely applied for CO_2 and hydrocarbon mixtures in a wide range of conditions, but it still gives inaccurate predictions especially close to the critical point. More reliable results can be achieved with regression of pertinent experimental data (de Medeiros et al., 2019).

Thus, we adjusted six regression parameters to match the bubble point pressure and PVT experiments (differential liberation, constant composition expansion and swelling test) of

Moortgat et al. (2013): volume shift, acentric factor, critical pressure and critical temperature of C_{20+}, as well as the binary interaction coefficients (BIC) amongst hydrocarbons and between CO_2-C_{20+}. We then tuned Pedersen's correlation viscosity parameters separately (Pedersen and Fredenslund, 1987). Bubble point pressure match (38.55 MPa) was in good agreement with the experimental value (38.58 MPa).

3.2.2. Component Lumping

Figure 3.2 shows how the originally 24 (pseudo-)components were lumped into six to reduce computational intensity. This pseudoisation scheme was based on the compositions and volatility ranges of the hydrocarbons. CO_2 was preserved as an individual component, as its phase behaviour is crucial in simulating miscible reactive transport through carbonate rocks. The composition and critical properties of each pseudo-component were estimated based on the mixing rules of Lee and Kesler (1975).

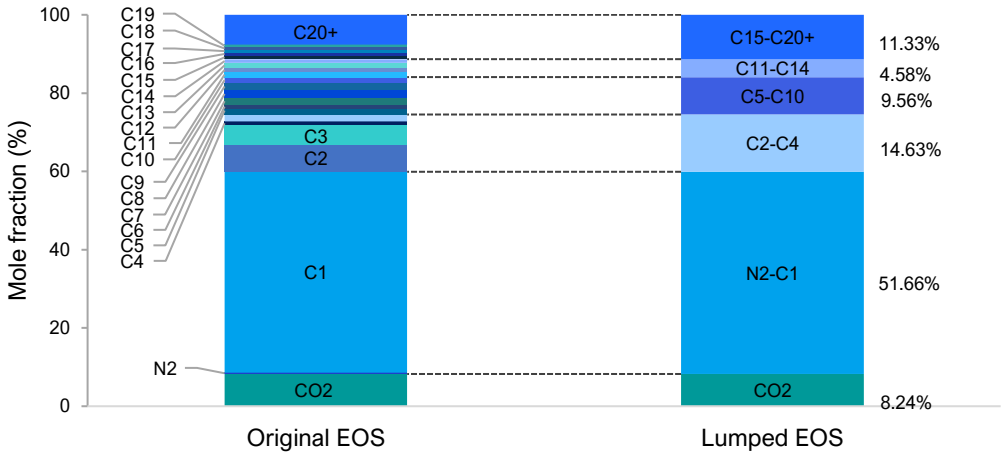

Figure 3.2 Original composition of the reservoir fluid from the PVT experiments of Moortgat et al. (2013) (left) and composition of reservoir fluid after pseudoisation (right).

We used a heuristic approach (rule of thumb), which is subjected to biases, but flow simulations suggested that, for our applications, the lumped model is an adequate proxy of the detailed reservoir fluid characterization (Figure 3.3), with relative average errors of 2.2% for oil recovery and -1.7% for gas oil ratio.

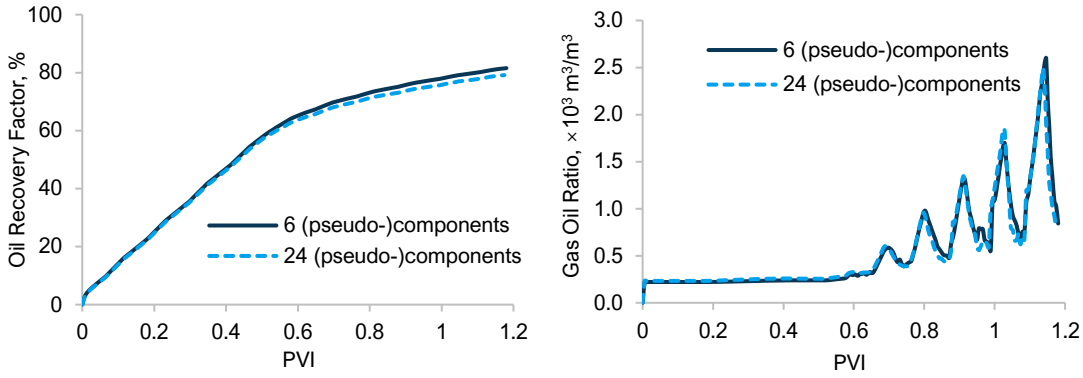

Figure 3.3 Oil recovery factor (left) and gas oil ratio (right) from compositional simulations with the original (dashed line) and lumped (solid line) EOS. Calculations performed with the '3D' box model of section 4.3.1.

3.2.3. CO_2 Solubility

CO_2 solubility in the aqueous phase is modelled in CMG's GEM™ compositional simulator by assuming thermodynamic equilibrium between the aqueous and gaseous phases (equality of fugacities). The fugacity of each component in the gas phase is calculated from an EOS, whilst the fugacity f_{iw} of a gaseous component i soluble in the aqueous phase is calculated using Henry's Law:

$$f_{iw} = y_{iw} \cdot H_i \tag{3.1}$$

Where y_{iw} is the mole fraction of component i in the aqueous phase. The Henry's constant H_i is calculated as a function of temperature and pressure (Harvey, 1996), then corrected for salinity using salting-out coefficients (Bakker, 2003).

In highly saline brines, the activity coefficients of aqueous species differ from unity and therefore should be calculated by an activity model. In GEM™ the activity coefficients can be calculated from the Debye-Hückel or the B-dot model (Bethke, 1996), which are only reasonably accurate in solutions up to 2 *M* NaCl. We used the latter in our calculations; however, as we are dealing with high salinity reservoirs (approximately 6 *M* NaCl), the estimated solubility of CO_2 in the formation water is most likely being underestimated (Jin et al., 2016). The Pitzer model would have been more appropriate in these conditions, but it was only recently implemented in GEM™.

When simulating gas dissolution in brine, a common issue is hydrocarbon disappearance from the grid-blocks close to injection points. We added a trace component to the EOS, with the same properties of CO_2 but insoluble in the aqueous phase, to improve stability of the model. We also made sure the irreducible water saturation of every relative

permeability curve used was non-zero to avoid convergence errors related to disappearance of water from the grid-cells.

3.2.4. Minimal Miscibility Pressure (MMP)

The MMP of CO_2 with the reservoir oil was estimated by simulation of a slim-tube test procedure. We created a 1D Cartesian model divided in 500×1×1 grid-cells, 24.38 m long and 0.423 cm wide and deep, to mimic a typical slim-tube test apparatus (Elsharkawy et al., 1992, Vulin et al., 2018). A porosity of 43.9% and a uniform permeability of 6 *darcies* were assigned, consistent with a coiled-tube packed with 160- to 200-mesh quartz sand. We chose this number of grid-cells after a sensitivity analysis had shown negligible changes in oil recovery with finer grids. Although physical dispersion is a reality in this kind of system, we applied a higher-order two-point fluxes method to control excessive numerical dispersion (CMG, 2020b). At various test pressures, we set an injection rate equivalent to 0.5 PV/day until a total of 1.2 PV of CO_2-rich fluid was injected. Temperature was constant at 331.9 K.

The process was repeated for different CO_2 injection concentrations since pure CO_2 utilization is unrealistic in the Brazilian pre-salt context due to two main reasons: (i) relatively low CO_2/CH_4 selectivity of the membrane separation process and (ii) unfitness of equipment for high CO_2 concentrations. The remainder of the injection gas was composed of methane (N_2-C_1). Oil recovery factors were plotted against operating pressure as shown in Figure 3.4.

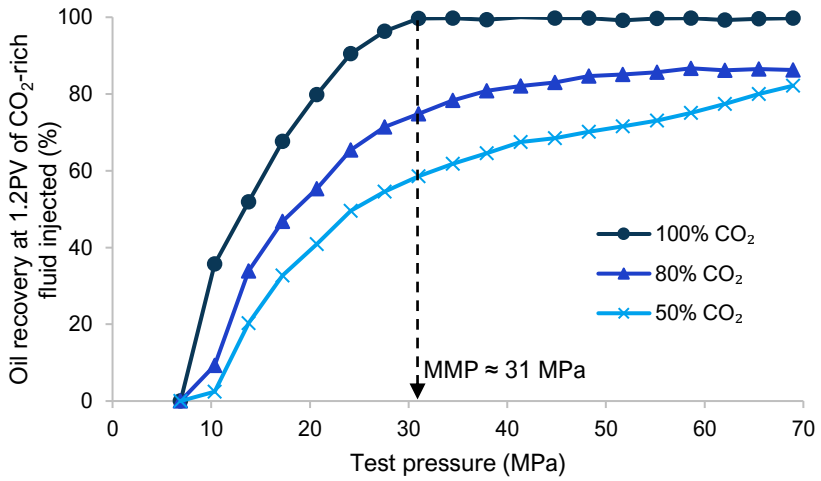

Figure 3.4 Slim-tube simulation for MMP determination between the reservoir oil (lumped EOS) and three different CO_2-rich fluid injection compositions. The dashed arrow indicates the point from which the recovery curves slopes are lower than 1.45%/MPa.

MMP is typically determined by an arbitrary breakover point in the recovery curve, signalling a change in displacement mechanism from immiscible to miscible. There is no consensus in the literature on how to define this "knee" point in a slim-tube plot, but most sources indicate that ultimate recoveries at pressures above the MMP are between 90 to 95% or higher (Stalkup, 1983). Under this criterion, only pure CO_2 achieves dynamic miscibility with the reservoir oil at attainable pressures, and the MMP is around 31.03 MPa.

On the other hand, Elsharkawy et al. (1992) suggests that, if the breakover is not sharp, MMP can be defined as the pressure from which oil recovery does not change by more than 1.45% per MPa pressure increase. By this definition, all three injection gas mixtures present MMP of approximately 31.03 MPa, although the sharpness of the break and level of recovery plateau reduced significantly as CO_2 concentration dropped. Lower recovery efficiencies were expected as methane content increased, since CO_2 can extract a broader range of hydrocarbons from oil than methane can.

Additional multiple contact miscibility calculations were performed using CMG's WinProp™ cell-to-cell, semi-analytical key tie lines and multiple mixing-cell methods. They yielded values for pure CO_2 MMP of 31.03; 31.89 and 17.77 MPa, respectively.

Maintaining reservoir pressure above an estimated MMP is a helpful guideline during CO_2-EOR, sufficient to create favourable conditions for an efficient displacement. There are many uncertainties associated with MMP determination, including the fact that the most used methods (slim-tube test, multiple mixing cell, rising bubble apparatus) do not embrace many aspects of displacement in reservoir rocks. However, high recoveries can be reached even if miscibility is not truly achieved, for instance at near miscible conditions, which gives flexibility to the project's operational design.

3.3. Geochemistry Model

3.3.1. Brine Chemistry

Seawater and formation water compositions used in this thesis were adapted from laboratory analysis of typical Brazilian Pre-salt field brines (Mackay and de Souza, 2014). Prior to the flow simulation, formation water was tuned to equilibrium (SR = 1) with calcite in the presence of the original reservoir oil. This was done by using the formation brine composition to run a calculation with no perturbation to the system for 1,000 years, at the initial reservoir pressure and temperature. The seawater composition was equilibrated

using PHREEQC code (Parkhurst and Appelo, 2013). The final seawater and formation brine compositions are shown in Table 3.1.

Table 3.1 Injection (low-sulphate seawater) and formation water compositions.

Species	Concentration (mol/kgw)	
	Low-sulphate Seawater (0.1 MPa, 298.15 K)	Formation Water (55.38 MPa, 331.9 K)
Na^+	5.52×10^{-1}	2.35
Ca^{2+}	1.00×10^{-2}	5.60×10^{-1}
CO_2	3.60×10^{-5}	4.30×10^{-2}
Cl^-	5.70×10^{-1}	3.50
HCO_3^-	2.00×10^{-3}	8.25×10^{-4}
OH^-	1.22×10^{-6}	2.20×10^{-9}
CO_3^{2-}	2.04×10^{-5}	5.68×10^{-9}
Salinity	1.13	6.41
pH	7.72	4.26

3.3.2. Assumptions for 1D Numerical Simulations

We ran several simulations changing one parameter at a time and maintaining the other variables constant with the objective of determining to what extent the geochemical outcomes were sensitive to changes in the inputs or assumptions. This approach works well on the determination of key uncertainties (Bratvold and Begg, 2010), although we are aware that, realistically, multiple input variables would change together.

The calculations you will see in this section were performed using a 1D model composed of 80% calcite, measuring 1,000 × 1,000 × 100 m, and subdivided in 100 grid-cells in the *x* direction. Injection occurs at the first grid-block (controlled by rate), while the producer is located at the last cell and is controlled by a minimum bottomhole pressure (BHP) of 39.3 MPa, just above the reservoir fluid bubble-point.

We assumed the relative permeability curves showed on Figure 3.5. The oil-water curve came from a BPS carbonate coquina reservoir analogue, whilst the gas-oil curve was extracted from a CMG™ GEM CO_2 study template. Capillary pressure and hysteresis were disregarded in this sensitivity analysis.

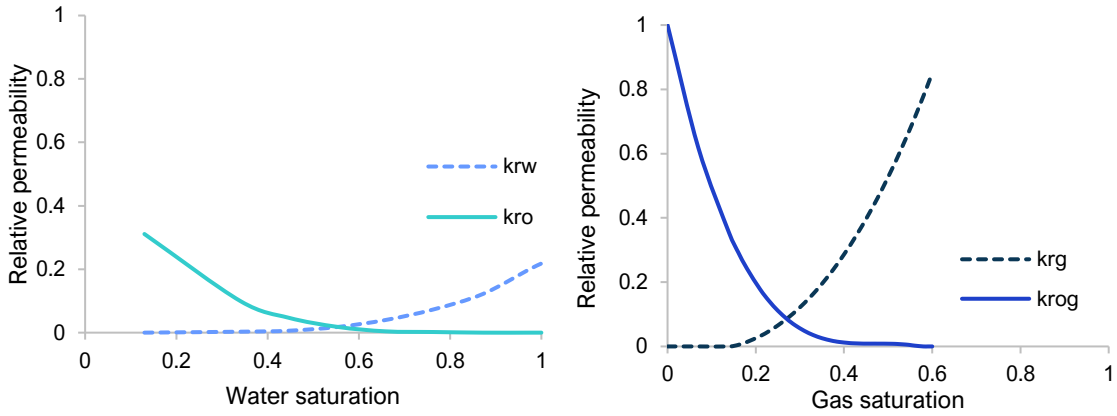

Figure 3.5 Oil-water (left) and gas-oil (right) relative permeability curves applied in the 1D simulations.

3.3.3. Kinetic Parameter Sensitivity Analysis

We simulated several combinations of the kinetic parameters k_β and A_β extracted from the literature to assess the impact of kinetics on our scale predictions. For a more simplified comparison, we described the cases in terms of the coefficient $\gamma = log(k_\beta \times A_\beta)$, which comes from the logarithmic form of the canonical rate equation (2.6). A summary of the cases is shown in Table 3.2, in ascending order of γ. Details of the source studies are listed. When A_β was not available from the study, we applied a specific surface area of 10 cm^2/g, which is often used in the literature for calcite, resulting in A_β = 2,710 m^2/m^3 (Xu et al., 2005).

Table 3.2 Calcite kinetic rate constants (k_β), reactive surface areas (A_β) and their corresponding γ investigated in this section.

Study	log k_β(T) ($mol/m^2/s$)	A_β (m^2/m^3)	$\gamma = log(k_\beta \times A_\beta)$ at 298.15 K ($mol/m^3/s$)	Observations
Nghiem et al. (2004), Kumar et al. (2004), Thibeau et al. (2007)	-8.80	88	-6.85	E_a = 41.7 kJ/mol; simulation studies of CCS in saline aquifers.
Plummer et al. (1978)	-8.92	2.71×10^3	-5.49	Correlation for T≥298 K.
Yasuda et al. (2013)	-	-	-4.41	Static test with core sample in carbonated water; T = 337.15 K; 31 to 62 MPa; γ obtained from reported mass loss rate [g/h].
Sazali et al. (2019)	-3.86	4.59×10^{-1}	-4.20	Limestone coreflood; SR = 0.24; 394.15 K; E_a = 41.7 kJ/mol.
Peng et al. (2015)	-6.43	2.71×10^3	-3.00	Far-from-equilibrium; T = 298.15 K; 1 atm.
Palandri and Kharaka (2004), André et al. (2015)	-5.81	2.71×10^3	-2.38	Neutral mechanism (eq. 3.11); E_a = 23.5 kJ/mol.
Subhas et al. (2015)	-5.42	2.43×10^5	-0.03	Low SR experiment; pH 5.5; $[Ca^{2+}]$ = 0.01 M; T = 294 K; E_a = 35.4 kJ/mol.
Walter and Morse (1984)	-5.68	1.22×10^6	0.41	pH-stat dissolution method; rhombic synthetic calcite; normal standard seawater; T = 298.15 K; $P_{CO2} = 10^{-2.5}$ atm.

We used the 1D model described previously to simulate the alternating slugs of CO_2-rich gas (50% concentration) and desulphated seawater, with a WAG ratio of 1, and solvent slug-size of 5% HCPV. The porosity changes due to mineral dissolution and precipitation in the injection and production grid-blocks for each case of Table 3.2 are shown in Figure 3.6. For

each curve, a *positive* slope means *dissolution* (increase in porosity) and a *negative* slope is a sign of *precipitation* (decrease in porosity).

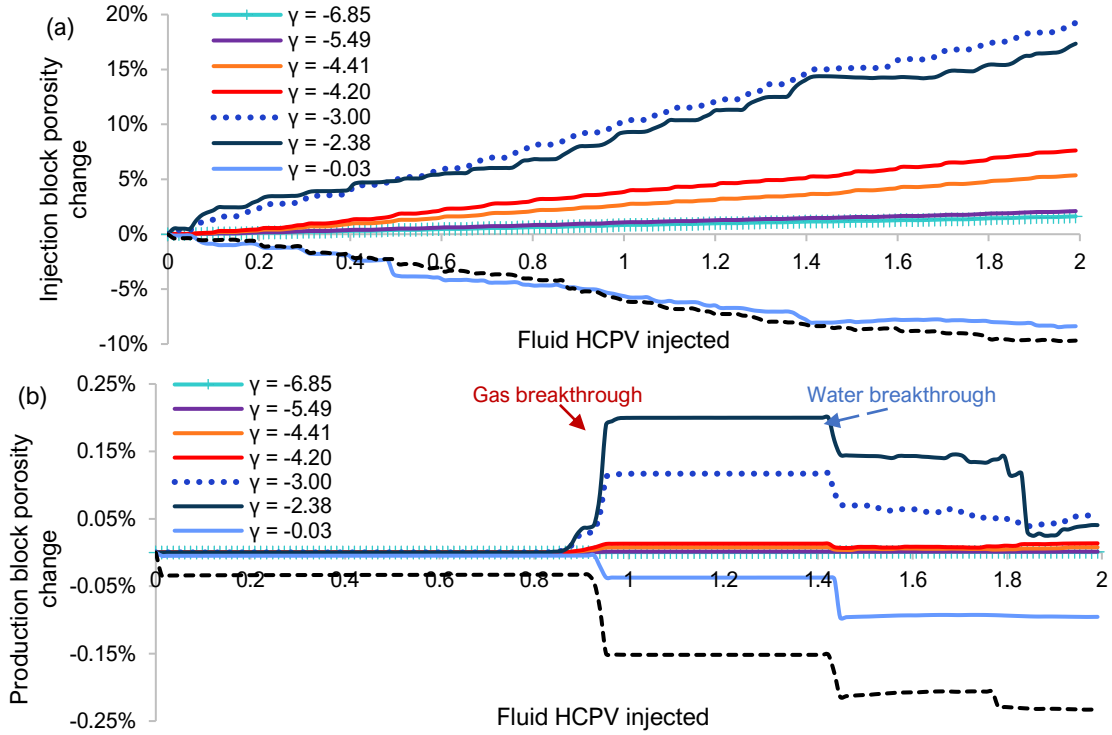

Figure 3.6 Porosity changes in the (a) injection and (b) production grid-blocks due to mineral reactions in 1D model for various kinetic coefficients *γ*.

The first six cases yielded calcite dissolution in both injection and production grid-cells. However, only the models with the first four lowest *γ* values (equivalent to slow kinetics) presented a consistent *qualitative* behaviour. In general, the dissolution intensity increased with *γ*, until the kinetics was so fast (last two cases) that the saturation state of the system flipped, resulting in calcite precipitation in both the injection and production blocks.

Cases with the highest *γ* values (*γ* = -0.03 and 0.41) essentially represented an instantaneous equilibrium, as their reaction rates were far higher than their flow rates. Their fast kinetics not only resulted in numerical instabilities, but they also did not reflect experimental and field observations, which have consistently pointed towards calcite dissolution near the injection point of CO_2-bearing fluids (Ribeiro, 2017). Interestingly, the third fastest kinetics analysed (*γ* = -2.38) is the one recommended by GEM's 'geochemistry wizard' for calcite modelling.

It is difficult to discuss the accuracy of these models without validation from pertinent field data. The results showed a high degree of variability amongst cases, which highlights the importance of the kinetic parameters on the predictions. Based on the general theory of

calcite reactions in the presence of CO_2, applying A_β from BET measurements or fast k_β from acid dissolution experiments on simulation studies seems to lead to unrealistic amounts of dissolution near the injection wellbore, and even a fundamental change in the reactions' mechanism. In case fast kinetic rates were a reality in the system modelled, a coarse grid would fail to give accurate predictions (grid-block length much larger than equilibrium length), and a simple equilibrium model would be more appropriate and efficient. However, this is not an option to date in CMG™ GEM and, as discussed, does not apply generally for carbonates, unless deep in the reservoir.

Yasuda et al. (2013) (γ =-4.41) and Sazali et al. (2019) (γ = -4.20) studies were the only ones performed in consolidated rock samples, which explains the comparatively small reactive surface area of the latter. The former study was the closest to our system's conditions, performed in travertine rocks composed of 86.5% calcite and conditions analogous to the BPS (62 MPa and 337.15 K). As Lasaga (1998) advises to consider the surface rates measured in the laboratory as the upper bounds to the overall rates, we used the calcite kinetic parameters of γ = -6.85 in our forthcoming simulations. This low γ was applied in several modelling studies of CO_2 storage in saline aquifers using GEM, as shown in Table 3.2.

In summary, mineral dissolution and precipitation reactions are largely influenced by the complex interplay between fluid chemistry, saturation state of fluid with respect to the mineral, hydrodynamics, and the physical-chemical properties of the reacting surface (Brantley, 2008). Application of kinetics to geochemical modelling is subject to several limitations due to the uncertainties in the experimental methods from which the rate parameters are derived, and from the models used for the simulations. Ideally, to derive a representative dissolution/precipitation rate law, one should acquire field or experimental data using *consolidated* rock samples in the ranges of temperature, pressure, fluids composition, and hydrodynamics of the reservoirs being studied, under conditions around and far from equilibrium.

3.3.4. Calcite pH Buffering: Waterflood Model Validation

To validate the geochemistry model, we first simulated the 1D limestone model described above under seawater injection only, with a constant Darcy velocity of 1 ft/D. We progressively incorporated the chemical and mineral equations to illustrate the role of calcite in buffering the system's pH. Figure 3.7 shows the pH in the injection and production grid-blocks for each scenario.

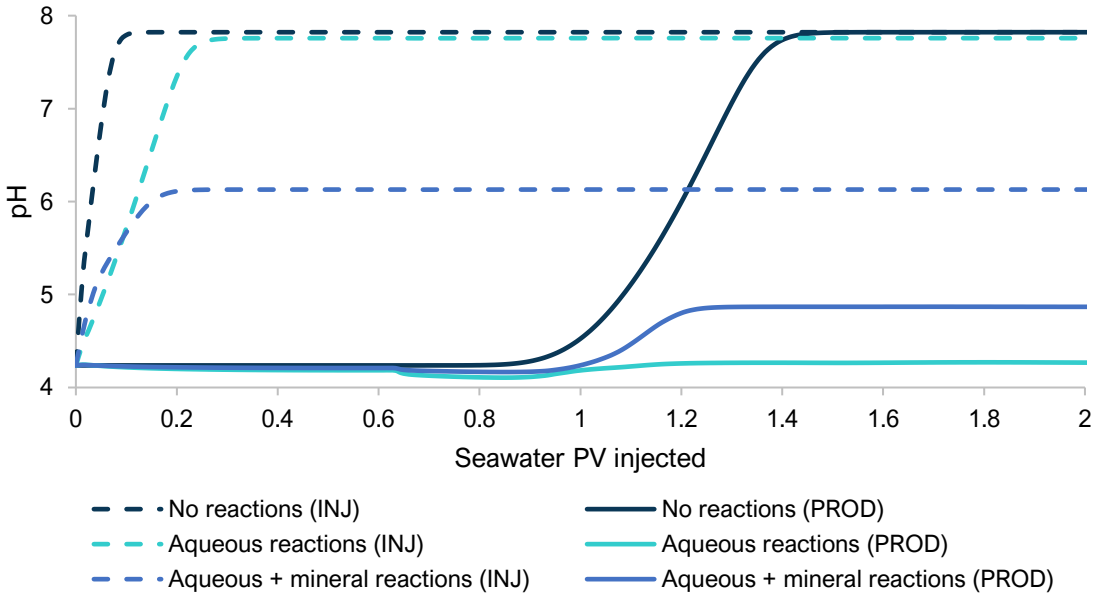

Figure 3.7 pH versus amount of seawater injected in a 1D reservoir for different geochemical modelling assumptions.

If no reactions are modelled, only the effect of mixing brines with different compositions is observed. The pH in the injection grid-block transits rapidly from a low pH formation water to a higher pH seawater. The production grid-block will also go through the same transition, although delayed because of residence time.

When we allow the CO_2 to dissolve in brine by modelling aqueous reactions (equations (2.1 to (2.3), the seawater arriving in the injection grid-block dissolves CO_2 from the oil phase, which results in a more gradual pH increase as the flood progresses. The pH plateau turned out to be slightly lower than the "no reactions" case because of the equilibration of seawater to the reservoir conditions. In the production block, when only aqueous reactions were considered, the brine pH first dropped slightly as injected brine broke through, but then did not rise to the original high pH of the seawater, because it is constantly stripping CO_2 out of the oil phase as it travels throughout the system. That is when the calcite makes a difference.

In the presence of calcite, the influx of seawater in the injection grid-block causes calcite dissolution initially, as CO_2 from the oil phase dissolved in the aqueous phase. After the CO_2 was washed out from the first grid-block (0.1 PVI), calcite precipitation started, removing carbonate ions from solution. In response, bicarbonate ions deprotonated, buffering the pH against the increase, reaching a plateau just above pH 6. Conversely, looking at the production grid-block, as water travels throughout the system more CO_2 dissolves into the aqueous phase, which leads to calcite dissolution and carbonate ions

release. The latter will combine with H^+ to form bicarbonate (which is more stable), therefore buffering the pH against the acid tendency, plateauing below pH 5.

3.3.5. Near-wellbore Calcite Dissolution and Precipitation

As previous studies have demonstrated that peak scale deposition occurs in the vicinity of the production wellbore rather than deep within the reservoir (Mackay, 2005), we present an analysis of calcite dissolution and precipitation around the injection and production wellbores i.e., in the grid cells to which the wells are connected. We examined the impact of the four operational parameters that operators normally have control over (see Table 3.3). The variables domains were defined based on literature review and field best practices (section 2.2).

Table 3.3 Ranges of WAG design parameters evaluated during this sensitivity analysis.

WAG design parameter	Range		Base-case
	Low	High	
WAG ratio	0.5	5	1
Solvent slug-size (%HCPV)	1%	10%	5%
CO_2 concentration in injection stream	20%	80%	50%
Darcy's velocity (ft/D)	0.5	2	1

For this sensitivity study, we assumed that the *total* amount of CO_2-rich gas available as EOR solvent was limited to one HCPV. Then, for each cycle, water was injected to match the WAG ratio and solvent slug-size designed. For example, for a design with WAG ratio of 3:1 and solvent slug-size of 5% HCPV, four reservoir HCPV were injected in total: one HCPV of gas, as fixed, and three HCPV of water, divided in 20 cycles composed of 5% HCPV of gas plus 15% HCPV of water. Waterflooding was also simulated for comparison.

The next plots will show porosity change in the injection and production grid-bocks due to mineral reactions. For each curve, a positive slope means dissolution (increase in porosity) and a negative slope is a sign of precipitation (decrease in porosity).

Figure 3.8 shows the system's response to different WAG ratios (WR). Independently of the WR, all WAG cases presented dissolution around the injection wellbore (Figure 3.8 (a)). The difference in degree of dissolution was down to which fluid was the mineral reaction limiting factor. For WR = 0.5 (i.e., 5% HCPV of CO_2-rich gas and 2.5% HCPV of water in each cycle), the water is the limiting factor: the CO_2 half-slugs are more than enough to saturate the water ones, but the water half-slugs are small, so the rock is not exposed to the reactive medium as much, resulting in intermediary levels of dissolution. The mineral dissolution then increases for WR = 1 and WR = 2, but they are almost indistinguishable, as the CO_2 is

still sufficient to fully saturate the increasing water half-slugs. This behaviour only flips at WR = 3, beyond which the CO_2 is the limiting factor: the higher the WR, the less acidic the water slugs are, the lower the dissolution levels. Recall that calcite dissolution occurs in the presence of CO_2-rich brine that has not yet equilibrated with calcite, a condition that happens mostly in the water/gas front (contact between half-slugs). Therefore, once the CO_2 is the limiting factor, higher WAG ratios will reduce calcite dissolution close to the injection zone. The extreme case is pure waterflooding, where dissolution happens at first, but once the CO_2 from the oil is washed away, precipitation takes place as seawater rapidly goes from surface to reservoir conditions - calcite is less soluble at higher temperatures. In reality though, the wellbore would be cooled down by the injected water, moving the precipitation away from the wellbore deeper into the reservoir. Our model did not capture this effect because of its isothermal assumption. The phenomena described persists for the production wellbore (Figure 3.8 (b)), culminating in precipitation for WR higher than 3.

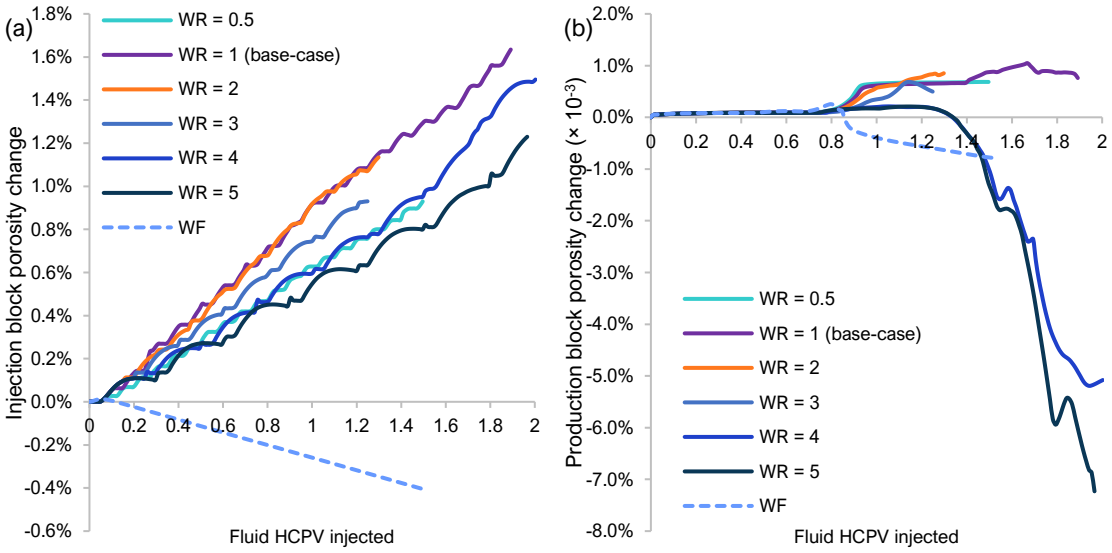

Figure 3.8 Porosity changes in the (a) injection and (b) production grid-blocks due to mineral reactions in 1D model for various WAG ratios (WR) and waterflooding.

The CO_2 injection concentration impact was conspicuous – the higher the CO_2 purity, the more CO_2 dissolved in the water slugs, the more calcite dissolution occurred (see Figure 3.9). As the WR was equal to 1 in these cases (water was the limiting fluid) and the producer BHP was kept above the bubble-point, CO_2 evolution from the aqueous phase was limited, keeping the pH low and still promoting dissolution at the production wellbore.

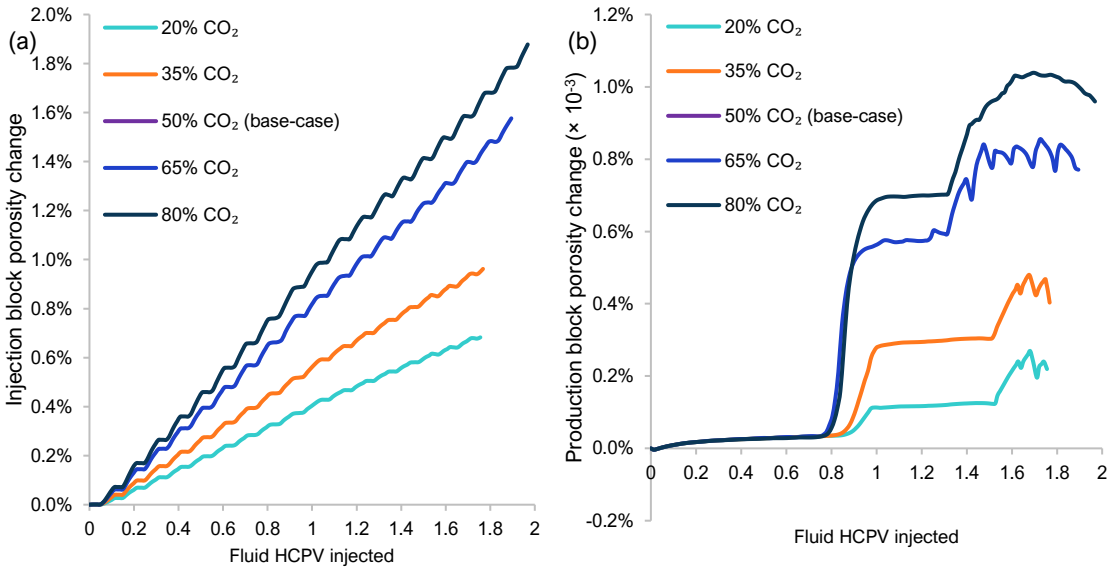

Figure 3.9 Porosity changes in the (a) injection and (b) production grid-blocks due to mineral reactions in 1D model for various CO_2 injection concentrations.

According to Figure 3.10, calcite dissolution was more severe in the injection block as the solvent half-slug sizes (SHSS) reduced since more mixing between seawater and CO_2 injected occurred. The alternating slugs' effect is smoothed out as SHSS reduces, culminating in almost a simultaneous WAG injection when SHSS = 1% HCPV. This is in line with the coreflood experiments and modelling performed by Snippe et al. (2020), which have shown that the *descending* order of dissolution severity in the vicinity of the injection wellbore is: simultaneous WAG at low rates (possible well integrity threat), carbonated water injection, WAG (possible well stimulation), and dry continuous CO_2 injection (little to no effect). Mineral change was practically insensitive to SHSS at the production grid-cell.

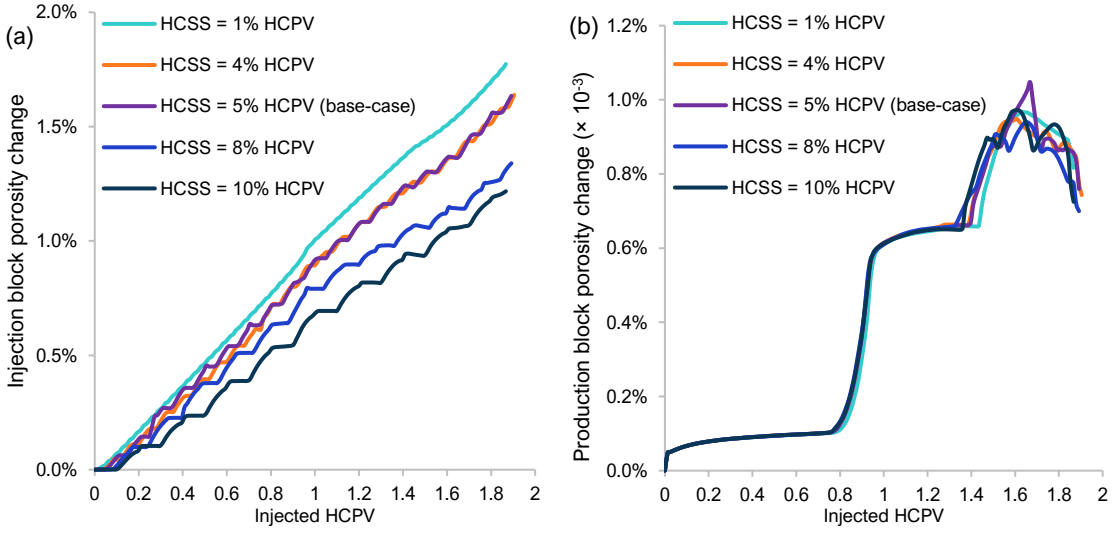

Figure 3.10 Porosity changes in the (a) injection and (b) production grid-blocks due to mineral reactions in 1D model for various WAG solvent half-slug sizes (SHSS).

Figure 3.11 (a) indicates that the calcite dissolution levels at the injection block increased when injection velocity went from 0.5 ft/D to 1 ft/D, but then dissolution reduced for faster injection rates, as the residence time became insufficient for the fluid to equilibrate before flowing to the next grid-block. In such cases, the kinetics controls the reaction pace and therefore must be modelled. We did not simulate injection velocities higher than 2 ft/D because the runs became numerically unstable. Because the x-axis is injected HCPV, it looks like the slower velocity cases had earlier gas breakthroughs, which would be counter intuitive (Figure 3.11 (b)). But the difference amongst these scenarios was the number of HCPV injected over time, so if porosity change were plotted against time, one would see that faster injection velocities resulted in earlier breakthrough of injected fluids, as expected.

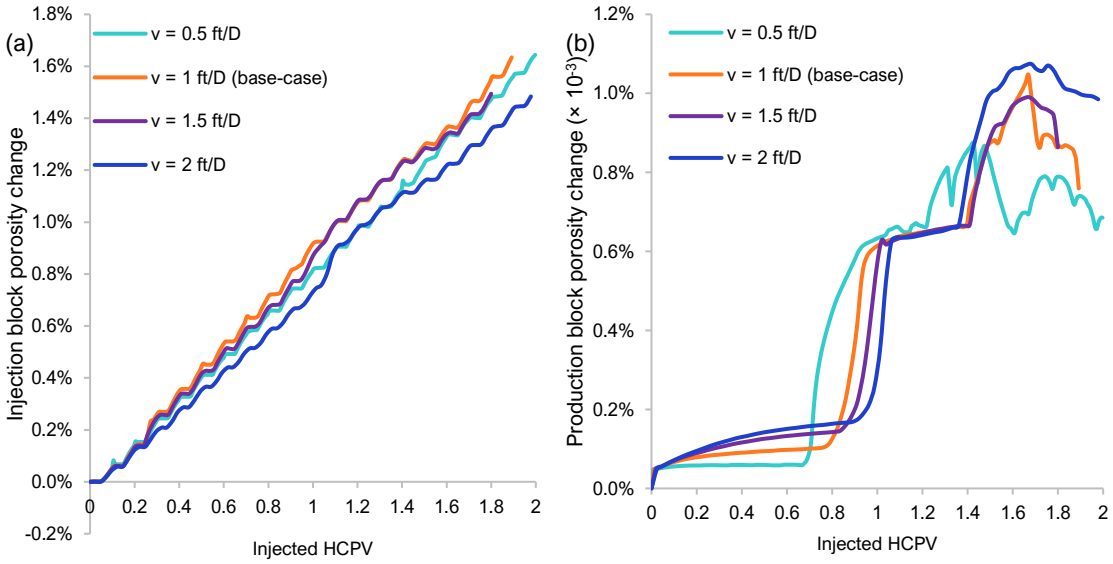

Figure 3.11 Porosity changes in the (a) injection and (b) production grid-blocks due to mineral reactions in 1D model for various Darcy's velocities (v).

Consistently, porosity changes in the production grid-blocks were around three orders of magnitude smaller than in the injection cells, because the injected fluids had time to equilibrate before reaching the production block. Additionally, as the producer BHP was above the bubble-point, the disruption in the equilibrium at the production wellbore was mild. This would not hold true as fluids reach surface conditions.

3.4. Calcite Scaling Risk beyond the Production Wellbore

Reactive transport calculations downstream to the production perforations are not available in any compositional reservoir simulator to date. For this reason, we extracted brine species compositions and flow rates at the production wellbore from our CMG™ GEM simulations and used them in our in-house scale prediction code, ScαleFAST (Silva, 2017).

There are several commercial scale prediction models that can be used to perform these flash calculations (USGS PHREEQC, Expro Petrotech™ MultiScale, OLI Systems™ ScaleChem), but none in the automated fashion ScαleFAST was designed for, being capable of calculating numerous timesteps at once. Additionally, ScαleFAST has been shown to have excellent prediction agreement with many of these software packages and with experimental data. However, discrepancies across codes are expected as each software uses different geochemical databases.

In GEM, the brine composition in the production well is calculated as the sum of individual component molar fluxes divided by the total molar flux (weighted average), meaning no equilibrium calculations are performed at the wellbore. ScαleFAST code accounts for that and performs a two-point calculation: (1) it equilibrates the total brine composition arriving at the wellbore, determining its saturation state at reservoir conditions, then (2) it calculates the total rate of calcite deposition, assuming all the CO_2 in the aqueous phase has evolved from solution once fluids have reached surface conditions. This deposition can potentially happen in various points of the production tubing, manifolds, riser, valves, and surface equipment, but here we are accounting for the entirety of calcite mass in the production system, which is a straightforward metric for designing a scale management plan. This ultimate calcite precipitation rate is expressed in kilograms of calcite per day, and it represents the *worst-case scenario* of calcite scale deposition of a given production strategy.

In the subsequent chapter, we will apply this method to the operational designs of interest from our optimisation studies to assess calcite scaling risk from the production wellbore to the surface facilities.

3.5. Long-term Scale Inhibitor Squeeze Treatment Optimisation

After understanding the risk of calcite precipitation, one can use the water production data forecasted on the reservoir simulations to design the squeeze treatments necessary to keep production wells safe from scale damage throughout production life. What would be the cost of scale prevention using squeeze treatments and can these costs be optimised? To answer that, we propose a methodology to design a series of squeeze treatments for the production life of a given strategy based on reservoir simulation data. The methodology is adapted from Vazquez et al. (2016) and it was applied in our pilot '3D' and field studies.

3.5.1. Assumptions

The cost of a squeeze treatment involves: (1) the cost of the scale inhibition chemical (SI); (2) the cost of deployment, which includes crew time and the hiring costs of pumps, tanks, and rig (Diving Support Vessel); and (3) the cost of deferred oil or postponed revenues from the shut-down period.

A conventional squeeze deployment time includes: (1) the SI injection; (2) a shut-in period to allow further SI retention, which we are assuming is 24 hours (Bezerra et al., 2013); (3) back-production of the liquid injected during the treatment; and (4) connection and disconnection of the deep-water intervention rig (considered as 48 hours (Graham et al., 2002)). We assumed a neat SI cost of 3,460 USD/m^3 and a deep-water rig hire cost of 11,000 USD/h (Vazquez et al., 2017b). Squeeze treatment injection and back-production rates were set to 1.06×10^{-2} m^3/s based on field experience.

The minimum Inhibitor Concentration (MIC) was fixed at 10 ppm for all scenarios, based on typical values used in the BPS carbonate systems (Bezerra et al., 2013). We acknowledge that MIC should vary with saturation ratio, but due to lack of experimental data on the correlation between these two parameters for calcium carbonate under the more general brine compositions and conditions of the BPS, we are assuming a fixed value, which can be interpreted as the MIC correspondent to the highest saturation ratio forecasted during the scaling risk assessment phase.

We considered the SI concentration as 150,000 ppm (15% concentration) for all scenarios, based on BPS field data from Bezerra et al. (2013) that showed SI concentrations varying from 10 to 15%. We have chosen the highest threshold based on the findings of Azari et al. (2020), which have revealed that optimal squeeze lifetimes can be achieved by injecting as much SI as early as possible during the treatment, although formation damage due to excessively high concentration needs to be considered. We used an instantaneous equilibrium Freundlich isotherm (Figure 3.12) to represent the SI retention, consistent with a phosphonate-based SI adsorbed in a carbonate rock.

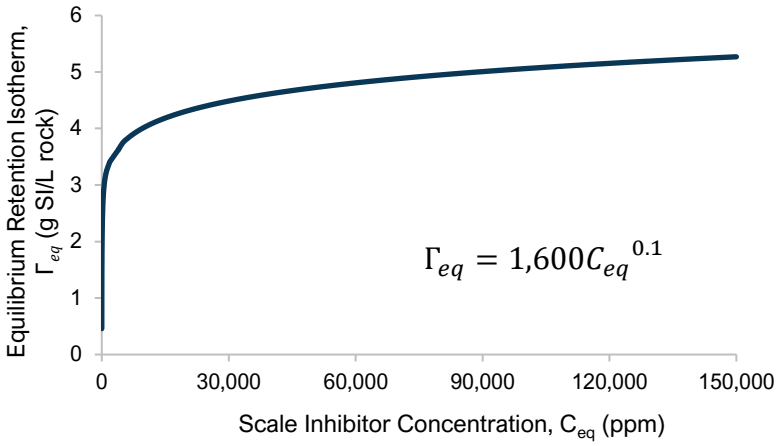

Figure 3.12 Generic scale inhibitor equilibrium retention isotherm for carbonate system.

3.5.2. Step-by-step: Squeeze Treatments Forecast

Step 1: choosing the squeeze lifetime targets.

We analysed the water production data per well of a representative simulation model (waterflooding case), then chose discrete levels of squeeze lifetime targets. This initial guess is based on field experience and can be revisited after the squeeze cost curve is generated (step 2).

Despite its name, squeeze 'lifetime' is often reported as the *cumulative water* produced that is protected against oilfield scale, i.e., water that has a SI concentration above the minimum inhibition concentration (MIC). The corresponding length of time will depend on the production rate.

Squeeze lifetimes often range from a few months to a few years, depending on the severity of the scale precipitation and the production water rates. Short squeeze lifetime targets may require more frequent well interventions, which can lead to higher costs. Conversely, long targets may involve injecting large volumes of aqueous solution, which can cause formation damage (e.g., changes in the near-wellbore wettability and/or increased water saturation in the near wellbore (Graham et al., 2002)) and delay oil production further. Additionally, the effectiveness of the scale inhibitor over long periods is uncertain.

Step 2: generating an optimised squeeze cost curve.

We used an in-house squeeze design code, SQUEEZE software (Vazquez et al., 2012) and applied the assumptions described previously – MIC, SI concentration, SI retention isotherm, and squeeze lifetime target. For each production well to be protected, we provided the petrophysical data (permeability and porosity) of the near wellbore layers.

The software uses a PSO algorithm to find several combinations of main treatment and over-flush volumes designed to achieve the squeeze target in question. The objective functions embedded in the code are to minimise the total design cost and the injected water volume, whilst achieving the squeeze lifetime target proposed by the user. The optimal squeeze design is identified as the one with the lowest cost to protect a unit of produced water for the duration of its respective squeeze lifetime. We repeated the same calculations for all squeeze lifetime targets.

These optimised squeeze designs for a specific well would look like Figure 3.13. In this example, the authors have chosen five levels of squeeze life targets. The plateau achieved indicates that higher targets would be counterproductive. Note the economy of scale - there is a clear cost advantage with progressively increased volumes of water targeted until the cost reduction levels off. The lifetime target of 2 million barrels is arguably the most advantageous in this example since it balances out a low unit cost with low volumes, reducing the risk of formation damage.

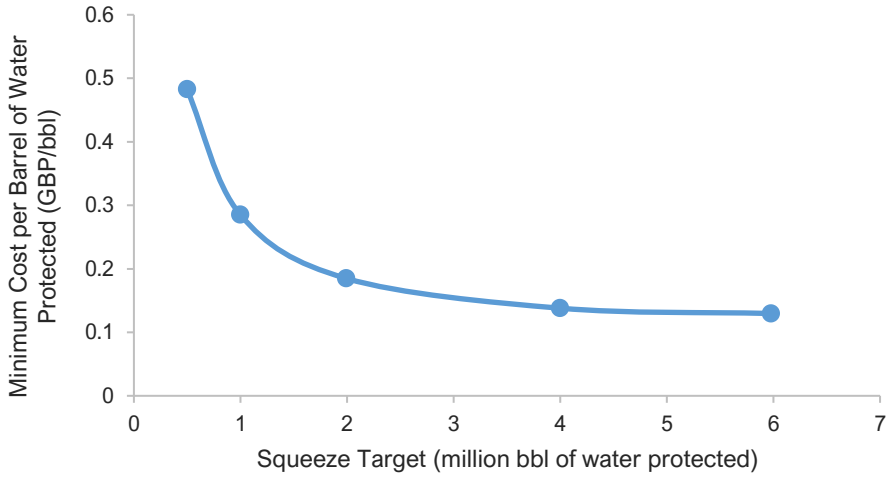

Figure 3.13 Cost curve for a production well generated through squeeze lifetime optimisation. Source: Azari et al. (2021).

Step 3: designing the pre-emptive squeeze treatment.

A pre-emptive squeeze is the first squeeze treatment of a production well, designed to cover the period before significant water breakthrough, when mostly formation water is produced at low rates. We design it through the procedure of step 2, but the squeeze lifetime target was the cumulative water produced prior to the injected water breakthrough.

As shown in the scaling risk assessment, in this carbonate system with CO_2 naturally present in the oil, the initial produced water may have a considerable scale tendency that should not be disregarded, even at low water cuts. A pre-emptive squeeze is also important for

data acquisition (value of information) as it is deployed at the time of well completion. The potential downside of pre-emptive squeeze treatments, however, is formation damage when the well is about to start its production life, so the volume of aqueous solution injected should be limited.

Step 4: progressive allocation of squeeze treatments.

The subsequent squeeze treatments should be designed to progressively target higher volumes of produced water, following the optimal unit cost curve generated in Step 2, until the best target is achieved, which we then maintained until the end of production. In other words, we aimed at small targets at first, then gradually built them up, as one would better understand the system and as oil production would diminish over time. In the above example, the squeeze targets plan would be: pre-emptive squeeze, protect 0.5 million barrels, 1 million barrels, then a series of 2 million barrel lifetimes thereafter.

Step 5: squeeze treatment cost calculation and inclusion in NPV.

Finally, we calculated the cost of each squeeze treatment and discounted them to include in the NPV calculations. The deferred oil cost was based on the oil that would have been produced during the squeeze deployment period. We determined the oil rates based on the reservoir simulation data of each strategy. The gas deferred cost was omitted for simplicity.

3.6. Relative Permeability Hysteresis

Relative permeability hysteresis plays an important role in flow reversal processes such as WAG, where simultaneous flow of all three phases, and a sequence of drainage and imbibition cycles occur i.e., decreasing and increasing of wetting phase saturation, respectively. Field data suggest conventional two-phase relative permeability curves without hysteresis modelling may not be adequate for describing WAG processes (Rogers and Grigg, 2000). Hence, more rigorous models are required to capture the relative permeability dependence on the saturation history of not only its own phase.

A three-phase relative permeability hysteresis model was included in our models to allow both water and gas relative permeability reductions due to repeated WAG injection cycles. The three-phase hysteresis model implemented in GEM™ is based on the work of Larsen and Skauge (1998). The non-wetting phase (gas) relative permeability hysteresis behaviour follows Land (1968) trapping function and Carlson (1981) two-phase hysteresis model. This

entails that the gas relative permeability is coupled with both the historical water and gas saturations, accounting for reduced mobility and irreversible hysteresis loops during three-phase flow. We assumed a maximum trapped gas saturation of 0.4.

The wetting phase (water) relative permeability hysteresis is modelled through interpolations between two- and three-phase relative permeability curves using the Killough (1976) method. We assumed the three-phase relative permeability curve for the water phase as being the two-phase curve multiplied by 0.5. This means that the water mobility following a gas cycle is reduced by half compared to its mobility in the original oil-water system. Any subsequent drainage is calculated by interpolating between the imbibition curve and either the three- or the two-phase curve, depending on the gas saturation. Finally, the inclusion of normalized Stone's first model made it possible to account for process-dependency in three-phase flow oil relative permeability as well (Aziz, 1979).

To evaluate the impact of relative permeability hysteresis modelling in our WAG systems, we simulated a general WAG scenario on the 2D reservoir model described in section 4.1, with and without hysteresis modelling. We assumed a WAG ratio of 1:1, half-slug size of 5%HCPV and CO_2 concentration in the injection gas of 50%. The first half-cycle is a gas slug followed by water and so on.

Since the injection well operates at a fixed injection rate, its BHP is an indicator of injectivity status. Figure 3.14 shows bottom-hole pressure values for the case where hysteresis is modelled and the one where its effect is disregarded.

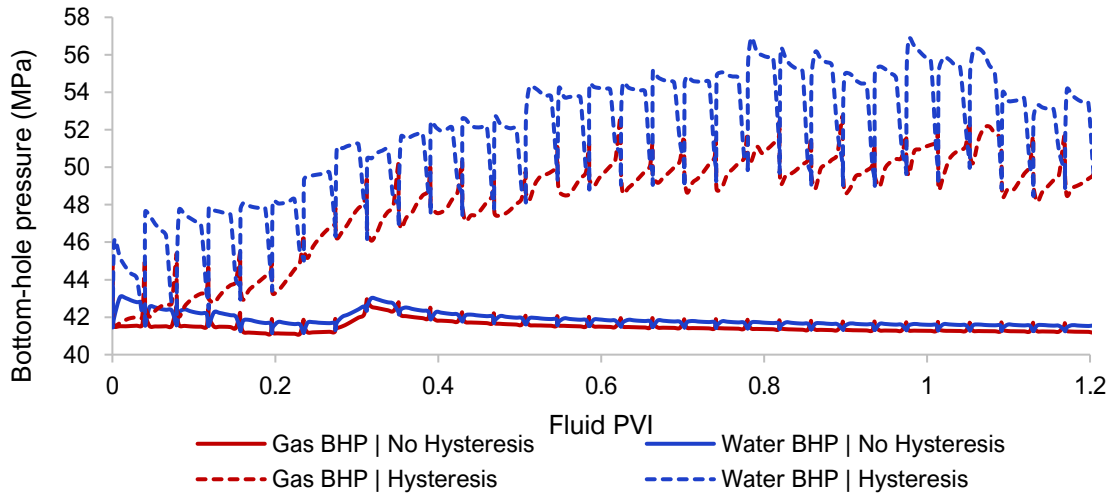

Figure 3.14 Bottom-hole pressure of injection well during WAG cycles for cases with and without relative permeability hysteresis modelling.

In the case where hysteresis is modelled, higher BHPs are required to inject the same volume of fluid than in the case without hysteresis, implying injectivity reduction. The gap between the two cases gets wider as cycles progress, reaching a plateau when the maximum trapped gas saturation is reached. Note that this gap is less expressive in gas cycles compared to the water ones, when more gas trapping by the wetting phase occurs.

The changes in gas and water mobility values caused by hysteresis also affect the breakthrough of injected fluids (Figure 3.15). The gas breakthrough is delayed due to mobility reduction. Because of larger volumes of gas being trapped as an immobile phase, a much smaller cumulative volume of gas is produced in the case with hysteresis.

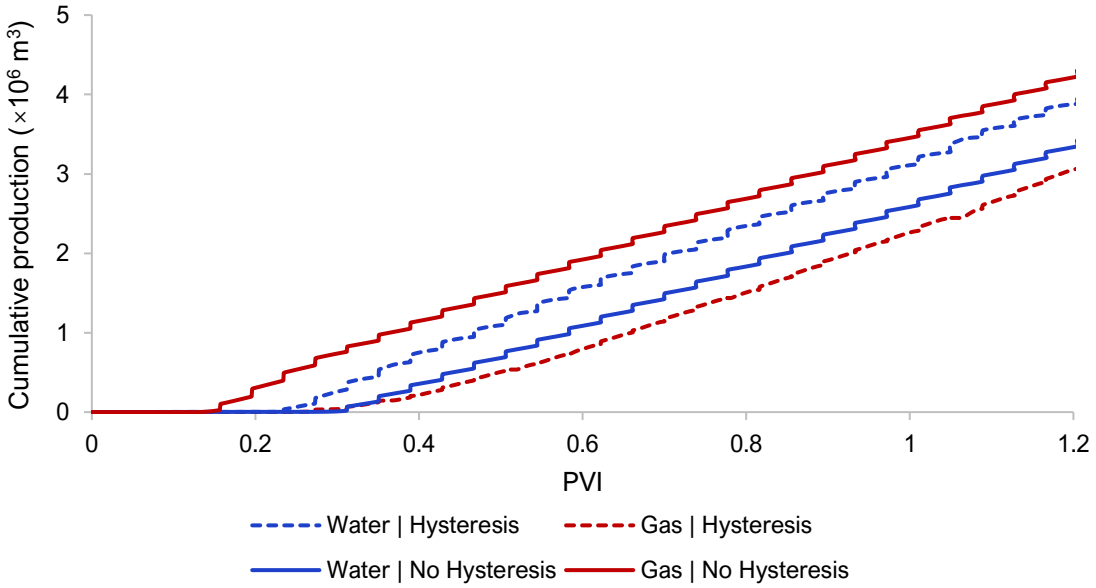

Figure 3.15 Gas and water breakthrough for cases with and without relative permeability hysteresis modelling.

Furthermore, as more of the pore space is occupied by trapped gas, less water stays in the reservoir, and its breakthrough in the production well happens earlier than predicted by the model without hysteresis. Although both gas and water phases had their relative permeabilities reduced, the non-wetting phase presents a much more pronounced effect. Since both phases are injected at the same injection rate, the significant reduction in gas mobility generates a net increase in water fractional flow, resulting in earlier water breakthrough.

Simulation results also showed that gas trapping correspondingly reduced residual oil saturation, which resulted in a recovery factor 23% higher compared to the model that omitted hysteresis. Additionally, by applying hysteresis, the predictions for CO_2 storage were almost 60% higher than in the case without it. The relative permeability hysteresis

impact in our simulations was in accordance with previous simulations studies (Ghomian et al., 2008, Laboissiere et al., 2013).

3.7. Economic Model

Net Present Value (NPV) analysis is widely applied to evaluate the economic feasibility of CO_2-EOR projects. In the optimisation studies to follow, we used NPV calculations as an objective function to drive the algorithm's search for operational strategies that yielded better economics:

$$NPV = \sum_{j=1}^{Nt} \frac{NCF_j}{(1+r)^{tj}} \tag{3.2}$$

where *j* is the time increment, *Tn* is the total number of periods, *to* is the time elapsed in years during period *j* from the reference date, and *r* is the annual discount rate. To estimate the net cash flows, NCF_j, we first identified the main sources of revenue and operational costs of a typical Brazilian pre-salt FPSO unit (Figure 3.16).

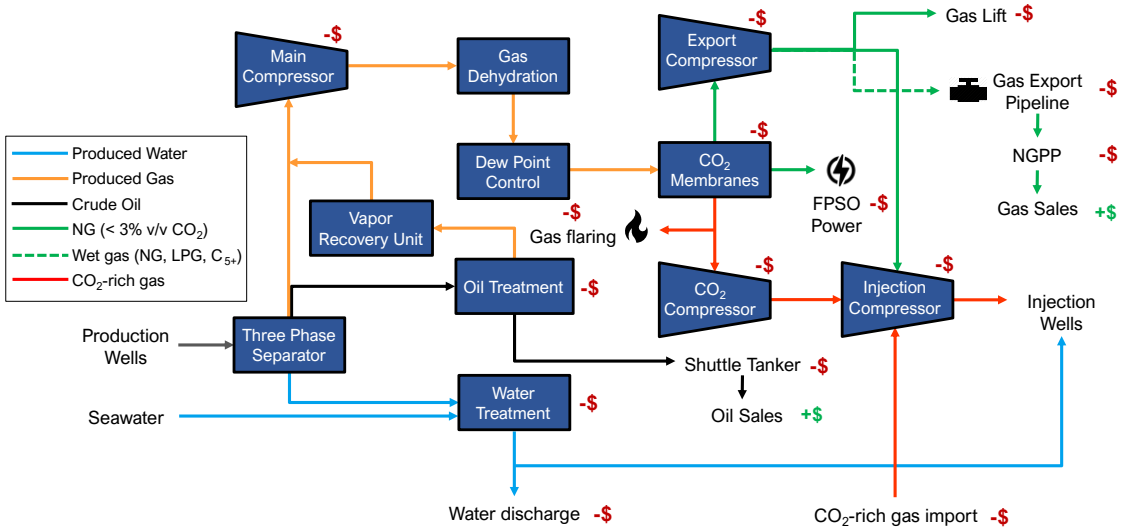

Figure 3.16 Pre-salt FPSO topside operations and its sources of income and costs. Adapted from de Andrade et al. (2015).

The net cash flows can thus be calculated as follows:

$$NCF_j = [Rev_j(1 - Roy - SocTax) - OPEX_j - D\&C_j - Dp_j](1 - CorpTax) + Dp_j - CO_2Tax_j - CAPEX_j - ABEX_j \tag{3.3}$$

Refer to Table 3.5 for more details on the economic parameters. $D\&C_j$ denotes well drilling and completion costs, which are considered intangible since they essentially have no salvage value: rig hire, mud, cement, well-platform connections, etc. Dp_j is the depreciation of facilities and is only considered in the field studies of Chapter 5, modelled linearly

throughout a 27-year period from the moment each equipment is installed. CO_2Tax_j is the carbon emission penalty imposed by the local government in case of flaring in period *j*. The next section details how the flaring emissions were calculated.

The gross revenues (Rev_j) from oil and gas sales are, respectively:

$$Rev_j|_{oil} = \left(P_o . q^S_{o,j}\right) \tag{3.4}$$

$$Rev_j|_{gas} = \left(P_{NG} . q^S_{NG,j}\right) + \varepsilon . \left(P_{LPG} . q^S_{LPG,j} + P_{C5+} . q^S_{C5+,j}\right) \tag{3.5}$$

P_i refers to the price of commodity *i*, ε is the NGPP liquid removal efficient, and $q^S_{i,j}$ refers to the cumulative quantity (mass, volume, or moles) of *i* sent to sales during *j*, where *i* can be crude oil, natural gas, liquefied petroleum gas (LPG) or C_{5+} fraction. These quantities are in surface conditions and the appropriate conversion factors were applied for unit consistency (see Table 3.4). We assumed the injected water goes through a Sulphate Removal Unit (SRU) prior to injection to reduce sulphate scaling risk. The operational costs ($OPEX_j$) of oil and gas production can be calculated as, respectively:

$$\begin{aligned} OPEX_j|_{oil} = {} & [FPSO\ oil\ processing\ cost] + [Tanker\ oil\ transport\ cost] + \\ & [Gas\ injection\ compression\ cost] + [Gas\ injection\ import\ cost] + \\ & [Water\ injection\ cost] + [Water\ desulphation\ cost] + [Water\ production\ cost] \quad \Rightarrow \end{aligned}$$

$$\begin{aligned} OPEX_j|_{oil} = {} & \left(C_o^{FPSO} + C_o^{trp}\right) q^S_{o,j} + C^{comp}_{inj,CO2} . q^{inj}_{CO2,j} + C^{comp}_{inj,NG} . q^{inj}_{NG,j} + C_g^{imp}\left(q^{imp}_{NG,j} + q^{imp}_{CO2,j}\right) \\ & + \left(C_w^{inj} + C_w^{SRU}\right) q^{inj}_{w,j} + C_w^{pr} . q^{pr}_{w,j} \end{aligned} \tag{3.6}$$

$$\begin{aligned} OPEX_j|_{gas} = {} & [CO_2\ capture\ cost] + [Gas\ export\ compression\ cost] + \\ & [Pipeline\ gas\ transport\ cost] + [NGPP\ gas\ treatment\ cost\ ] \quad \Rightarrow \end{aligned}$$

$$OPEX_j|_{gas} = C^{Cap}_{CO2} . q^{pr}_{CO2,j} + \left(C^{comp}_{exp} + C_g^{pip} + C_g^{NGPP}\right)\left(q^S_{NG,j} + q^S_{LPG,j} + q^S_{C5+,j}\right) \tag{3.7}$$

Table 3.4 Constants used in the cash flow calculations for unit conversion.

Gas fraction type	Hydrocarbon component	Calorific value (J/kg)	Molar weight (g/mol)
Liquefied Natural gas (LNG)	CO_2 + N_2-C_1	5.17E+07	16.13
Liquefied Petroleum Gas (LPG)	C_2-C_4	4.92E+07	39.90
C_{5+}	iC_5-C_{10}	4.69E+07	104.20

The economic parameters used in this thesis are summarized on Table 3.5. Any outdated cost was adjusted to the base-date using the Upstream Capital Costs Index (UCCI) (IHS Markit, 2020). The platform operates 365 days per year.

As remarked in the last two columns, all terms of the economic model are applied in the field studies in Chapter 5, whilst a simplified version is used on the pilot studies (Chapter 4). In Chapter 4, we are considering each pilot as part of an *already developed platform*.

Therefore, capital costs ($CAPEX_j$) and consequently depreciation costs (Dp_j), as well as $D\&C_j$ and abandonment costs ($ABEX_j$) are disregarded.

Note that we eliminated the capture OPEX, C_{CO2}^{Cap}, from the field study to avoid quantifying the same cost twice. Araújo et al. (2017) argued that the main OPEX component of a FPSO membrane permeation unit is the combustion of NG for power generation, which we are accounting for in the field study by diverting 10% of the treated NG to fuel the FPSO gas turbines. The actual percentage used is 14% to account for leaks and gas-lifting. This value was based on average fuel gas consumption of typical Brazilian pre-salt FPSOs (MME, 2020, ANP et al., 2020, EPE and MME, 2014).

Table 3.5 Parameters used in the economic model.

Description	Oil	Gas	Unit	Parameter	Pilot studies	Field studies
Oil price	314.50	-	USD/sm^3	P_o	✔	✔
NG (N_2-C_1) price (EPE, 2014)	-	13.20	USD/MMBtu	P_{NG}	✔	✔
LPG (C_2-C_4) price (EPE and MME, 2014)	-	0.40	USD/kg	P_{LPG}	✔ ('3D')	✔
C_{5+} price (EPE and MME, 2014)	-	0.47	USD/kg	P_{C5+}		✔
CAPEX exploration (EPE, 2019)	58.32	4.29	million USD	$CAPEX_j$		✔
CAPEX D&C per well (EPE, 2019)	137.73	10.69	million USD	$CAPEX_j$		✔
CAPEX submarine infrastructure (EPE, 2019)	1,025.82	81.24	million USD	$CAPEX_j$		✔
CAPEX FPSO infrastructure (EPE, 2019)	974.16	78.99	million USD	$CAPEX_j$		✔
CAPEX CO_2 membranes (Araújo et al., 2017, EPE, 2019)	-	232.71	million USD	$CAPEX_j$		✔
CAPEX gas subsea pipeline[1]	-	36.00	million USD	$CAPEX_j$		✔
CAPEX compressors[2]	289.00	274.05	million USD	$CAPEX_j$		✔
CAPEX SRU (Hardy and Simm, 1996)	655.58	-	USD/(m^3/d)	$CAPEX_j$		✔
CAPEX connection well-platform (Correia et al., 2015)	13.33	-	million USD	$CAPEX_j$		✔
Depreciation rate (EPE and MME, 2014)	4.00	4.00	% CAPEX a.a.	Dp_j		✔
Abandonment (EPE, 2019)	7.00	7.00	% CAPEX a.a	$ABEX_j$		✔
OPEX oil transport[3]	0.40	-	USD/sm^3	C_o^{trp}	✔	✔
OPEX gas pipeline export (EPE, 2019, Rochedo et al., 2016)	-	1.40	USD/MMBtu	C_g^{pip}	✔	✔
OPEX oil processing at FPSO (Correia et al., 2015)	68.80	-	USD/sm^3	C_o^{FPSO}	✔	✔
OPEX CO_2 capture cost[4]	-	9.96	USD/tCO_2	C_{CO2}^{Cap}	✔	

[1] Cost to build a 15 km pipeline with 18 in. diameter from the FPSO to the main pipeline of 300 km that links a few platforms to the NGPP onshore (EPE, 2019).

[2] Compressors for oil are 2×18 MW CO_2 injection compressors and 2×11 MW NG injection compressors. Compressors for gas are 3×11 MW main compressors and 2×11 MW export pipeline compressors (Gallo et al., 2017). We assumed unit CAPEX for compressors as 4.98 USD/W (EPE and MME, 2014).

[3] Assuming round-trip in a Suezmax oil tanker with 160,000 sm^3 oil capacity, travelling at average velocity of 24 km/h, with connection/disconnection time of 20 hours and freight cost of 1,417 USD/h (Meza et al., 2015).

[4] The unitary capture cost was calculated assuming the OPEX is 5% a.a. of the membrane modules CAPEX (EPE, 2019), capture capacity of 6 × 10^6 sm^3/d, average CO_2 feed concentration of 29% throughout field life (from our reservoir simulation forecasts), and CO_2 density of 1.84 kg/m^3 at standard conditions.

OPEX FPSO gas consumption	-	14.00	% of NG produced			✔
OPEX CO_2-rich gas import (Torrez Camacho, 2017)	0.02	-	USD/sm^3	C_g^{imp}	✔	✔
OPEX compressors[5] - CO_2 injection	1.78	-	USD/tCO_2	$C_{inj,CO2}^{comp}$	✔	✔
OPEX compressors – NG injection	2.99	-	USD/tonne NG	$C_{inj,NG}^{comp}$	✔	✔
OPEX compressors – NG export	-	1.91	USD/tonne NG	C_{exp}^{comp}	✔	✔
Water injection (Correia et al., 2015)	6.88	-	USD/m^3	C_w^{inj}	✔	✔
Water production (Correia et al., 2015)	6.88	-	USD/m^3	C_w^{pr}	✔	✔
Water desulphation (Hardy and Simm, 1996)	0.55	-	USD/m^3	C_w^{SRU}	✔	✔
NGPP gas processing (EPE, 2014, EPE, 2019)	-	0.70	USD/MMBtu	C_g^{NGPP}	✔	✔
Flaring penalty (Galp, 2018)	-	40.00	USD/tCO_2	C_{CO2}	✔	✔
Royalties rate (Correia et al., 2015)	10.00	10.00	%	Roy	✔	✔
Social taxes rate (Correia et al., 2015)	9.25	9.25	%	$SocTax$	✔	✔
Corporate tax rate (Correia et al., 2015)	34.00	34.00	%	$CorpTax$	✔	✔
Annual discount rate (EPE, 2019)	10.00	10.00	% a.a.	r	✔	✔

3.8. Carbon Emissions Quantification

We have created a simple model to estimate CO_2 emissions of commercializing hydrocarbon for energy consumption. For each scenario simulated in the field studies (Chapter 5), we quantified the carbon emissions of a barrel of oil equivalent considering the following sub-systems: (1) the E&P offshore operations, which comprised power generation in the platform and gas flaring, (2) the hydrocarbons refining, and (3) the combustion of the oil and gas fuel products. We called the total emissions - from extraction to the final consumer – wells-to-wheels (WTW) carbon emissions, also known as gate-to-grave boundary emissions or scope 3 emissions.

Our assessment does not consider emissions associated with leakages nor the transport of the hydrocarbons through pipelines or cargo, but these should be considered if suitable data are available. Cavanagh and Ringrose (2014) estimate that transportation would conservatively increase the carbon footprint by around 10%. In the Brazilian context, where road freight dominates long-distance transportation, the share of total emissions attributed to transport of the final products can be as high as 30% (Petrobras, 2020). CO_2 permanently stored in the oil reservoir is accounted as *negative* emissions. Figure 3.17 summarizes the factors considered in our carbon footprint analysis.

[5] The unitary compression cost was calculated assuming the OPEX is 4% a.a. of the compressors' CAPEX (McCollum and Ogden, 2006), compression capacity of 6 × 10^6 sm^3/d, and densities of N_2-C_1 and export NG gas at standard conditions of 0.67 and 1.05 kg/m^3, respectively.

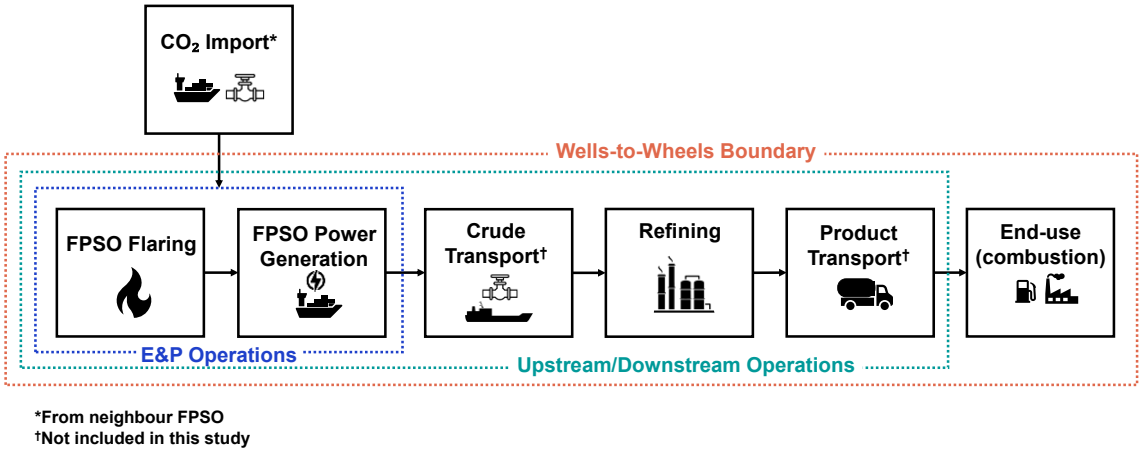

Figure 3.17 Carbon-accounting components adapted to the BPS oil and gas value chain.

The carbon *balance* is calculated as the total emissions minus the total CO_2 stored during the CCUS project. The carbon *intensity* of a produced barrel was then estimated as the total CO_2 emissions balance of the production strategy divided by the total barrels of oil equivalent (BOE), which included both oil and gas produced.

Considering each hydrocarbon component in the oil and gas phases as alkanes of the form C_nH_{2n+2}, we calculated CO_2 emissions from complete combustion of the gas in the FPSO for power and flaring (E&P emissions), as well as from combustion of the oil and gas for fuel by the end-consumer, according to the simplified equations:

$$\textit{Complete combustion:} \quad C_nH_{2n+2} + \left(\frac{3n+1}{2}\right)O_2 \rightarrow nCO_2 + (n+1)H_2O \tag{3.8}$$

The carbon taxation can then be calculated based on the mass of CO_2 equivalent emitted during combustion in the FPSO flare:

$$CO_2\ emissions_j = \sum_n m^C_{n,j}.\bar{n}.\left(\frac{MM_{CO2}}{MM_n}\right) \tag{3.9}$$

Where $m^C_{n,j}$ is the mass of component *n* combusted during *j*, and *n* can be CO_2 or a hydrocarbon component C_nH_{2n+2}; MM_n is the molecular weight of component *n*, obtained during the EOS pseudoisation (refer to section 3.2). We calculated $\bar{n}$ for each pseudo-component of the EOS as the weighted average of the original component fractions before pseudoisation. The values of $\bar{n}$ and MM_n are shown in Table 3.6. As CO_2 is not a combustible hydrocarbon, equation (3.9) considers the mass of CO_2 combusted as direct emissions ($\bar{n}$ = 1).

Table 3.6 Average coefficient $\bar{n}$ of the reservoir fluid's pseudo-components.

Pseudo-component	$\bar{n}$	MM_n (g/mol)
CO_2	1	44.0
N_2+C_1	1	16.1
C_2-C_4	2.7	39.9
iC_5-C_{10}	7.6	104.2
C_{11}-C_{14}	12.4	167.0
C_{15}-C_{20}	18.9	470.3

For end-use consumption emissions, we assumed that 80% of each oil barrel produced was burnt for fuel (Cavanagh and Ringrose, 2014), the rest being used as feedstock for petrochemicals, asphalt, and the like. Finally, to address the emissions from refining the oil, we used the average carbon intensity of refinery operations in Brazil in 2017 and 2018, which was approximately 35.9 kgCO_2 per barrel of oil equivalent processed (Petrobras, 2020).

3.9. Conclusions

In this chapter, we detailed this thesis' research methodology. Below we summarize some of the lessons learnt and best practices when modelling a reactive multiphase miscible transport in porous media. They apply particularly to the simulator used in this work (CMG^{TM} GEM) but may also be pertinent to other commercial packages.

We highlighted the importance of describing the hydrocarbons' behaviour through a compositional model based on pertinent PVT experimental data. Lumping of components will likely be necessary to reduce computational intensity, but CO_2 should be preserved as an individual component as its phase behaviour is crucial in simulating CO_2-EOR and storage in reactive carbonate rocks.

When CO_2 solubility in brine is modelled, it is likely that the PVT model will need a trace component to avoid hydrocarbon disappearance from the grid-blocks close to injection points. This trace component should have the same properties of CO_2 but be insoluble in the aqueous phase. To avoid convergence errors related to disappearance of water from the grid-cells, one may need to set the irreducible water saturation of the relative permeability curves as different from zero.

Regarding the geochemistry model, it is important that formation water and injection water compositions are equilibrated prior to the flow simulation. Our sensitivity analysis on the mineral kinetics models showed that values of calcite rate constant and reactive surface area assigned in numerical simulations can greatly impact mineral change forecasts,

especially close to the injection wellbore. In general, fast kinetic rates were not representative of the calcite behaviour in the presence of CO_2 under reservoir conditions.

The kinetics model is subject to uncertainties in the experimental methods from which the rate parameters were derived, and from the models implemented on the simulator. Ideally, to derive a representative dissolution/precipitation rate law, one should acquire field or experimental data using consolidated rock samples in the ranges of temperature, pressure, fluids composition, and hydrodynamics of the reservoirs being studied, under conditions around and far from equilibrium. Then, further investigations on near wellbore zones with finer grids should be performed.

We described the use of two in-house software for a more complete scale assessment and management. The first, ScαleFAST, was our scale prediction code of choice to calculate reactive transport downstream to the production perforations. Its input was the reservoir simulation output – the brine compositions and water production rates, which are dependent on the history of the fluids path through the reservoir. The second, SQUEEZE 12, optimises the cost of applying squeeze treatments as a scaling prevention method.

Our economic model for CO_2-EOR was outlined, including a full breakdown of CAPEX, OPEX, taxes, and other assumptions. We also showed how we are quantifying the carbon footprint of the CO_2-EOR oil in our models. These models were tailored to the BPS applications, but they can be straightforwardly adapted to other frameworks. We recognize the drawbacks of many of the simplifications we have made, for example, assigning a constant oil price and constant unit costs over time, but we believe they do not reduce the value of the comparative analysis. We recognise that these assumptions are limiting, and completely different solutions could be obtain if they were relaxed. For instance, a dynamic oil price forecast could accelerate, delay or halt all together investments in EOR infrastructure.

In the next two chapters, we apply the methodology to sector and full-field reservoir models, discussing its outcomes, capabilities, and limitations.

Chapter 4- CCUS Operational Optimisation: Pilot Studies

In this chapter, we applied the methodology proposed in Chapter 3, performing a series of optimisation studies to investigate the impact of nuances in the workflow, namely:

- *Objective functions:* economically focused *(*Net Present Value, unit profit) or environmentally focused (Carbon Storage Efficiency, Carbon Storage Mass).
- *CO_2-EOR strategy type:* uniform WAG or tapered WAG, also compared to waterflooding and continuous CO_2 injection.
- *Optimisation variables:* CO_2 injection concentration, injection rate, production BHP, switching time from secondary to tertiary recovery, and WAG variables (WAG ratio and solvent slug size).

The calculations were performed in fictitious two-well box models to demonstrate the methodology avoiding prohibitive simulation times. When dealing with real applications, we acknowledge the necessity of creating reservoir simulation models that fit the available field static and dynamic data and capture a wide range of geological uncertainties.

4.1. Rock-fluid Properties

The following rock-fluid data were used in all studies in this chapter. To obtain relative permeability curves, we applied the generalized correlation of Corey (1954) for a two-phase water-oil system (equations (4.1) and (4.2)) and gas-oil system (equations (4.3) and (4.4)), with water-wet rock input parameters from Table 4.1. Figure 4.1 shows the resulting curves.

$$k_{rw} = k_{rwro}\left(\frac{S_w - S_{wirr}}{1 - S_{wirr} - S_{orw}}\right)^{n_w} \tag{4.1}$$

$$k_{row} = k_{rocw}\left(\frac{1 - S_w - S_{orw}}{1 - S_{wirr} - S_{orw}}\right)^{n_{ow}} \tag{4.2}$$

$$k_{rg} = k_{rgro}\left(\frac{S_g - S_{gc}}{1 - S_{gc} - S_{wirr} - S_{org}}\right)^{n_g} \tag{4.3}$$

$$k_{rog} = k_{rocw}\left(\frac{1 - S_g - S_{wirr} - S_{org}}{1 - S_{wirr} - S_{org}}\right)^{n_{og}} \tag{4.4}$$

Table 4.1 Relative permeability input parameters for Corey's correlation.

Parameter	Value	Description
k_{rwro}	0.41	Water relative permeability at residual oil saturation.
k_{rocw}	1.00	Oil relative permeability at irreducible water saturation.
k_{rgro}	1.00	Gas relative permeability at residual oil saturation.
S_{wirr}	0.20	Irreducible water saturation.
S_{orw}	0.30	Residual oil saturation in a two-phase oil-water system.
S_{gc}	0.05	Critical gas saturation.
S_{org}	0.00	Residual oil saturation in a two-phase gas-oil system.
n_w	2.90	Corey's water exponent in a two-phase oil-water system.
n_{ow}	2.00	Corey's oil exponent in a two-phase oil-water system.
n_g	3.50	Corey's gas exponent in a two-phase gas-oil system.
n_{og}	3.00	Corey's oil exponent in a two-phase gas-oil system.

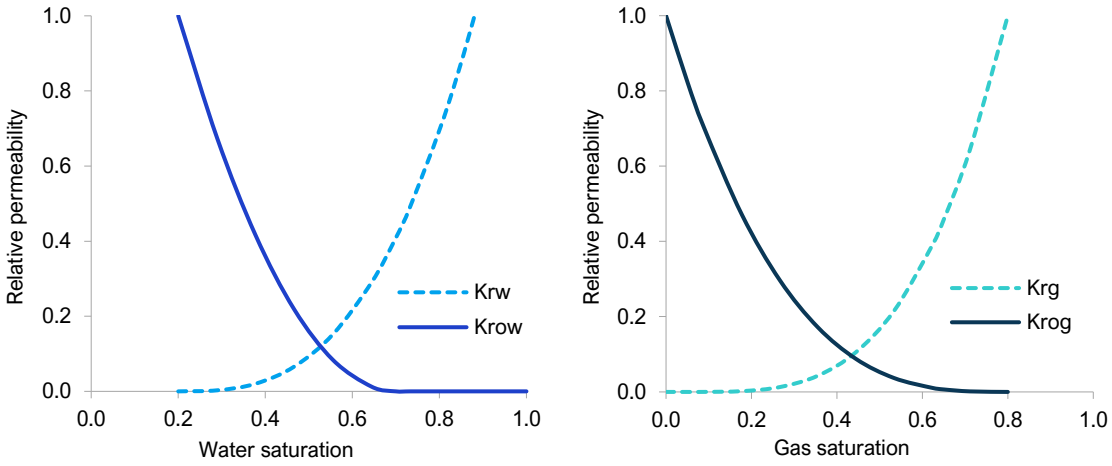

Figure 4.1 Water-oil (left) and gas-oil (right) two-phase relative permeability curves used in the 2D model.

4.2. Pilot Study '2D': Uniform WAG

In this section, we performed single-objective optimisation studies with various objective functions and WAG operational variables to evaluate their impact on the economic reservoir performance, CO_2 storage, and calcite scale (the latter being addressed after the optimization of the first two aspects). All designs investigated were uniform, i. e. for each simulation, the WAG design was maintained throughout field production life.

4.2.1. Reservoir Model Description

A synthetic two-dimensional cross-sectional reservoir model was built to represent a pilot study with one WAG injector and one producer. Layers with high contrast horizontal permeability were created to illustrate heterogeneity as shown in Figure 4.2, where additional details on the model are listed.

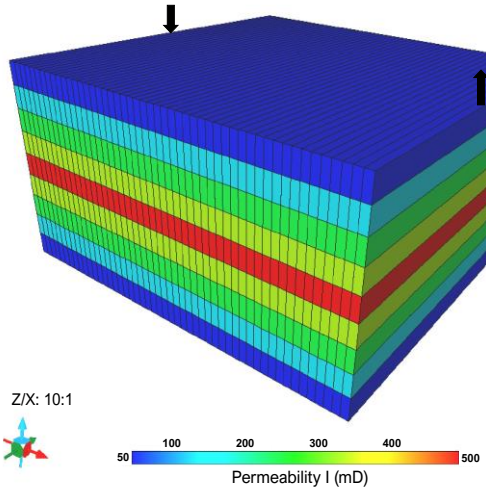

Property	Value
Model dimensions (m)	1,000 × 1,000 × 50
Number of grid-cells	50 × 1 × 9
Porosity	8%
kv/kh ratio	0.1
Initial water saturation	25%
Rock mineralogy	80% calcite
Initial reservoir pressure (MPa)	55.38
Initial reservoir temperature (K)	331.9
Maximum production lifetime (years)	30
Maximum water-cut	95%
Maximum GOR (sm^3/sm^3)	8,900

Figure 4.2 2D reservoir model horizontal permeability distribution (left) and characteristics (right).

The injection BHP was not allowed to surpass the reservoir's fracture pressure (68.95 MPa). We also set well controls to cease production when water-cut or Gas Oil Ratio (GOR) exceeded the thresholds listed in Figure 4.2 (Ghomian et al., 2008). No previous waterflood was performed, and the WAG schemes always started with a gas slug, as a first contact miscible gasflood can yield lower residual oil saturations.

As for injection fluids supply, we consider seawater to be widely available, although limited platform processing capacity or maintenance of membranes equipment can lead to desulphated seawater shortage. Besides recycling CO_2 from the production well for reinjection, neighbour wells can supply CO_2-rich gas for reinjection in this pilot. As the field is significantly larger than the pilot itself, a steady gas supply is maintained.

4.2.2. Sensitivity Analysis prior to Optimisation

We first conducted a sensitivity study to evaluate the effect of four key parameters in the outcomes of interest: (1) WAG ratio, (2) CO_2 injection concentration (CIC), (3) injection rates (the same for gas and water but different across scenarios), and (4) gas (solvent) slug size. Table 4.2 shows their ranges and discretization.

Table 4.2 Pilot study '2D' optimisation design variables, their respective domains, and discrete increments.

Parameter	Range		Increments
	Low	High	
WAG ratio	0.2	6	0.1
Solvent slug-size (%HCPV)	0.431%	10.49%	1%
Injection CO_2 concentration	10%	90%	10%
Injection rate (ft/D)	0.2	1.5	0.1
(rm^3/d)	344.8	2,586.3	172.4
Producer BHP (MPa)	13.8	48.3	3.45

We adapted the half-slug sizes according to operational restrictions to avoid impracticable well switches: designs with half-cycles lower than 30 days were discarded, as frequent injection fluid changes can become an operational challenge. We do not have information on the WAG injectors' technology in the BPS, but the time to change a well from water to gas injection and vice-versa is reported to be three days offshore North Sea (Muggeridge et al., 2014). This is due to the necessity of physically removing the injection line for one fluid and replacing it with the other phase line.

We used Response Surface Methodology (RSM), mentioned in section 2.2 of this thesis, where the variables' domains are sampled using experimental design to explore the relationships between inputs and responses using a minimal number of simulations. A set of 62 designed experiments was necessary to build the proxy model.

We were mostly interested in the following outcomes: (1) the project's NPV, (2) the unit NPV i.e., NPV per barrel of oil equivalent (BOE) produced, (3) the total mass of CO_2 stored in the reservoir (CSM), and (4) the CO_2 storage efficiency (CSE), which is the percentage of CO_2 injected that stays in the subsurface after production is ceased.

Figure 4.3 shows Sobol method results, a variance-based sensitivity analysis that quantifies how each input parameter influences the variance of the outputs (Sobol, 1993). For instance, the first bar means that the NPV variance would reduce by 77% on average if the CIC were kept constant.

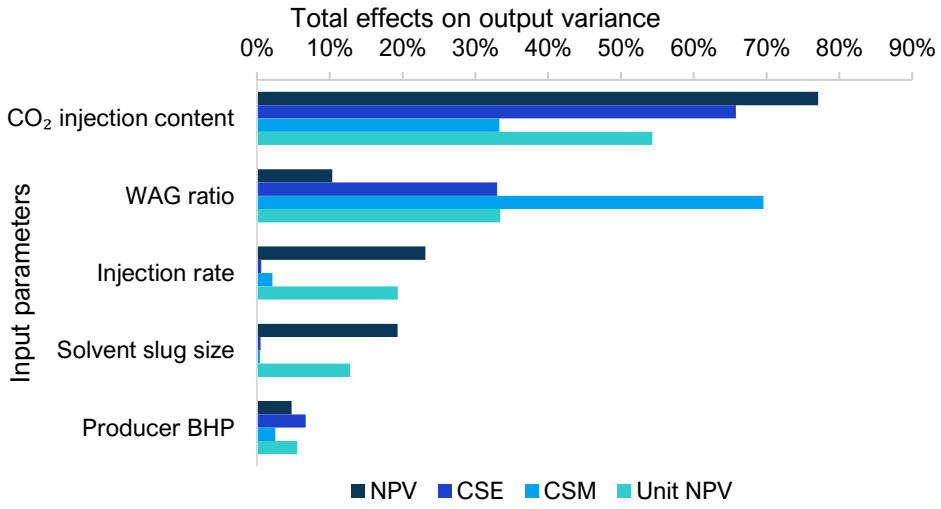

Figure 4.3 Sobol analysis for key parameters affecting CO_2-EOR and storage outcomes of pilot study 2D: net present value (NPV), CO_2 storage efficiency (CSE), CO_2 storage mass (CSM) and profit (USD/BOE).

The CIC plays a major role in all outcomes, chiefly on NPV, CSE and unit NPV. CSM was mostly influenced by the WAG ratio. Interestingly, the injection rate and solvent slug size seem to have little effect on storage, both absolute (CSM) and in terms of efficiency (CSE). In the next section, we will expand on the interplays amongst these objectives and operational variables, except for the producer BHP and injection rates, which will be optimised in the pilot study '3D'.

4.2.3. Single-Objective Optimisation Studies

In a coupled CO_2-EOR and storage context, the goal is to balance both economic and environmental outcomes. To identify trade-offs and synergies amongst objectives, we performed independent single-objective optimisation studies, subdivided in 'case A' and 'case B', and evaluated the impact of assigning environment-driven objectives over prioritizing profitability and vice-versa.

For both cases A and B, the economically oriented target was to maximise the project's NPV, and their common storage objective was to maximise CSE. In case B we expanded the single-objective functions to examine the impact of maximising the unit NPV and the CSM. Three operational variables - WAG ratio, gas slug-size and CO_2 injection concentration - were optimised in case A, whilst only the first two were considered in case B. We maintained the input ranges of the previous section sensitivity analysis. A summary of the optimisation assumptions can be seen in Figure 4.4. We fixed the CIC to 50% in case B to study the impact of having no control over this parameter. According to operators in the BPS, the CO_2 content is uncertain and strongly dependent on the recycled gas

availability within the field, membranes separation efficiency and natural CO_2 concentration in the solution gas.

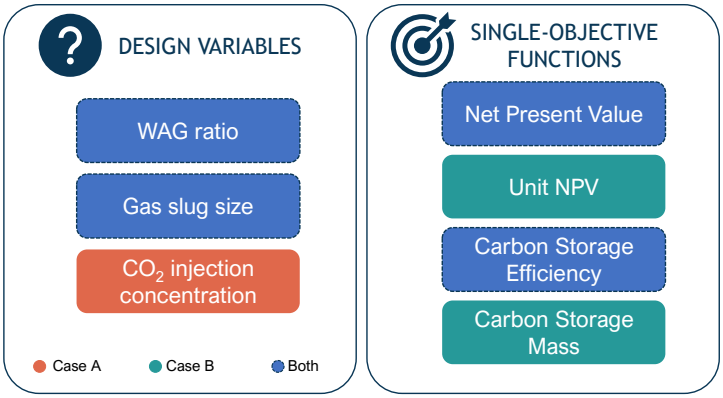

Figure 4.4 Pilot '2D' cases A and B optimisation assumptions: design variables and objective functions.

In both cases, the injection well was controlled by a constant injection rate of 862.2 rm^3/d, corresponding to a Darcy velocity of 0.5 ft/D. The producer BHP was kept constant at 39.3 MPa, just above the reservoir fluid bubble-point. A waterflood (WF) case with these specifications was simulated for reference.

The optimisation algorithm used was the Designed Exploration and Controlled Evolution (DECE) method implemented in CMG™ CMOST AI, explained in Chapter 2.

Case A: Variable CO_2 Injection Concentration

Table 4.3 summarizes the inputs and outcomes of the optimal designs selected by the optimisation algorithm. To put this into perspective, we reported NPV as a percentage change relative to the WF base-case. A continuous gas injection (CGI) scenario, with the optimised CO_2 concentration, was included for comparison. Both optimal designs are quite similar when it comes to the final oil recovery factor, but largely different regarding the other results, including the oil recovery path (Figure 4.5).

Table 4.3 Optimal designs and continuous gas injection (CGI) description of pilot '2D' studies with variable CO_2 injection concentration (case A).

	Single-objective functions →	Maximise NPV	Maximise CSE	CGI
Outcomes	NPV change to WF (%)	65.82	50.72	55.31
	CSM ($MMtCO_2$)	1.34	0.98	1.65
	CSE (%)	67.62	85.48	58.01
	Oil recovery factor (%)	95.69	95.10	86.27
	GUR ($kgCO_2$/incSTB)	388.56	228.24	724.6
	Project life (years)	20.06	27.04	21.75
Design variables	WAG ratio	0.5	1.7	-
	Gas slug size (days)	292	282	-
	(%HCPV)	8.39	8.10	-
	CO_2 injection concentration (%)	90	90	90

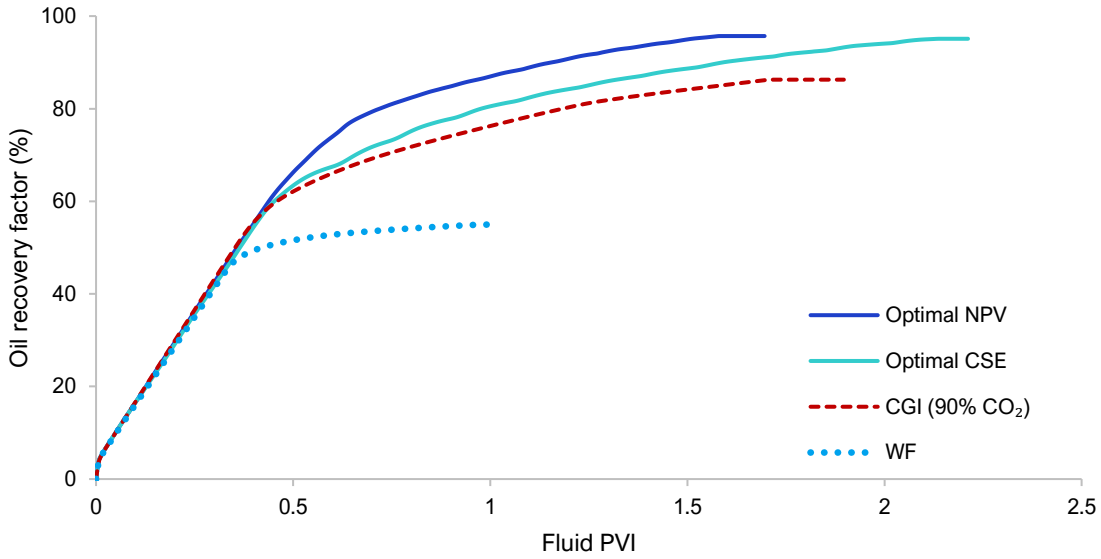

Figure 4.5 Pilot '2D' (case A) optimal designs oil recovery factors. Continuous CO_2 injection and waterflood are included for comparison.

The water-cut and GOR production restrictions led to distinct simulation durations, hence the differences in total volume of seawater and/or gas injected. The simplicity and grid coarseness of the model resulted in recovery factor overestimation, reaching values that are not realistic for most field applications. It is reported in the literature that coarse areal grid-cells tend to give over-optimistic recoveries and delayed breakthrough of injected fluids (Meddaugh, 2006, Meddaugh et al., 2011). However, this does not take away the value of the analysis, as its significance is on the relative changes and methods rather than the absolute values.

The optimal NPV design promoted anticipation of revenues with faster oil recovery rates (greater slope). Its project life was cut short due to high production GOR, but this also contributed to a higher *present* value (less discounting over time). Under the optimal CSE

design, production would have continued for seven more years, until the high water-cut would have deemed the production well uneconomical.

In terms of the CO_2 storage, applying the optimal CSE design would evidently result in a higher storage efficiency compared to the optimal NPV case. However, counterintuitively, the optimal NPV design stored a total CO2 mass 37% larger than the optimal CSE design (1.34 $MMtCO_2$ *versus* 0.98 $MMtCO_2$, respectively). The lower CO_2 storage efficiency in the optimal NPV design was due to a higher cyclicity of the CO_2 reinjected, while its larger absolute storage was a result of a greater gas utilization. Because of its high WAG ratio, the optimal CSE design was able to keep most of the CO_2 injected underground by delaying early gas breakthrough, but at the expense of the CSM, filling up the available pore space with water and limiting the amount of CO_2 stored.

In the CGI scenario, since the mobility control fluid (seawater) was not injected, its CSE was lower – approximately 42% of the CO_2 injected was produced again. However, from all cases simulated, this production strategy was the most advantageous regarding total carbon mass stored, with the downside of a less efficient flood and reduced economic returns compared to the optimal NPV case.

As there was a production well operating, the overall optimal design was dependent on how efficiently the mobility control fluid can hold back the CO_2 front and avoid over-production of gas, especially in high permeability zones (middle layer) and reservoir top strata (due to buoyance effects). Accordingly, the optimal CSE involved injecting 1.7 times more water than gas to reduce the high CO_2 mobility. However, its actual CO_2 usage per incremental barrel (see the GUR) was lower than 59% of the optimal NPV design, which limited absolute storage.

Therefore, optimising for CSE alone did not appear sufficiently advantageous from an environmental perspective, as it failed to embrace the whole picture. Plotting the main objectives against each other for all scenarios simulated (Figure 4.6 (a)) revealed a trade-off between NPV and CSE along the edge of the solutions domain – to achieve higher storage efficiency, some NPV gains would have to be sacrificed, and vice-versa. For CSE values below the 50% threshold, the economic performance of the pilot would likely be inferior to waterflooding. The three domed levels observed at the top right represent clusters of higher CIC as the NPV is improved: 80%, 85% and 90% CIC. The top of the curve was highly sampled since higher CIC greatly improved both objective functions.

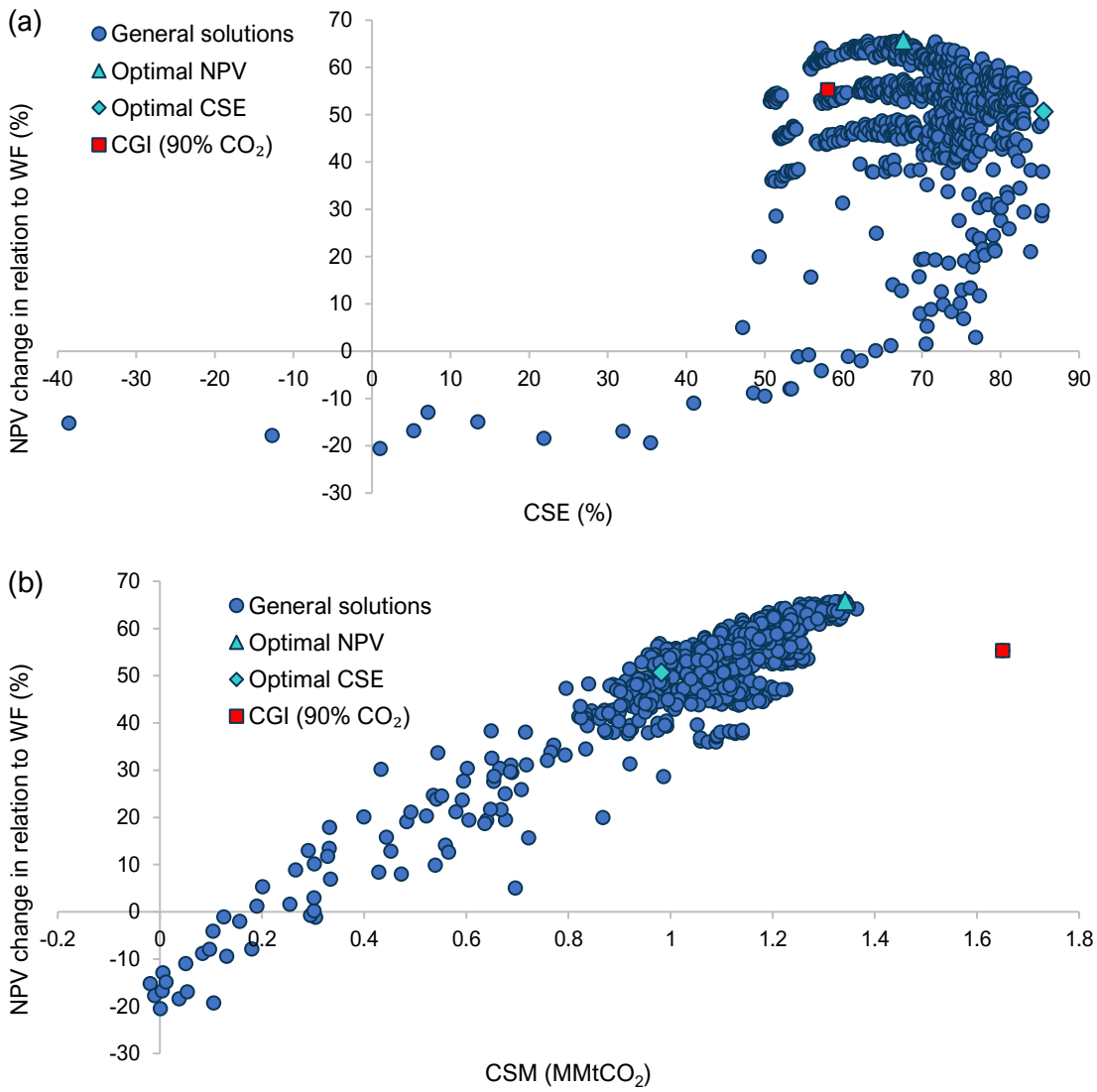

Figure 4.6 All cases simulated in the pilot study '2D' case A (all objective functions tested). On the y axis is NPV change in relation to the waterflood base case vs (a) carbon storage efficiency (%) and (b) carbon storage mass ($MMtCO_2$).

In addition, a surprisingly positive correlation between NPV and CSM was observed (Figure 4.6 (b)), which implies that the environmentally driven objectives (CSE and CSM) are not necessarily aligned in this context. In fact, the most profitable designs presented more mass of CO_2 trapped underground, even when their CSEs were poorer. The question that remains is: which outcome – CSE or CSM – is more representative of the environmental goal of this CCUS pilot? Arguably, it is CSM, since CSE, although an important metric, measures the *cyclicity* of the CO_2 in the subsurface-surface system, rather than the final storage at the end of the EOR endeavour. Aiming to optimise efficiency of storage (CSE) can lead to sub-optimal solutions, where a small amount of CO_2 is injected in the reservoir with large slugs of water solely to avoid CO_2 breakthrough in the production well. In such cases, the

efficiency would be high, but the CO_2 re-utilization and actual volume stored would be restricted.

Finally, how did the variables influence the main outcomes? Figure 4.7 shows their relationships. Note how essentially all results linearly increased with CO_2 injection concentration; only CSE had a more gradual rise followed by a plateau.

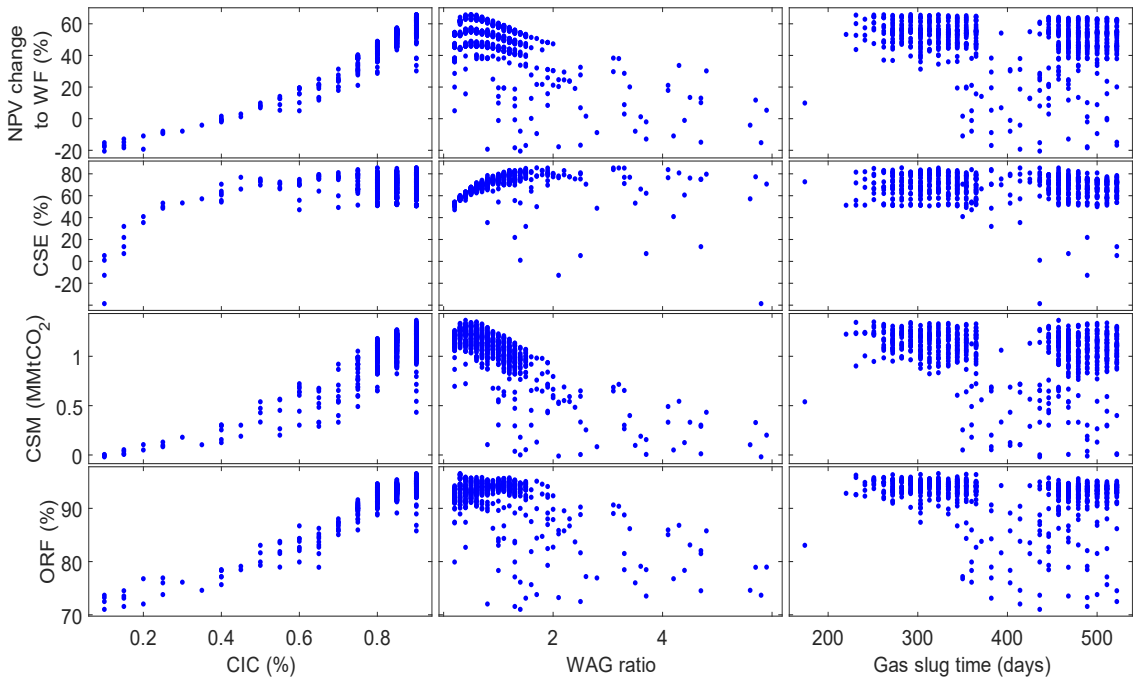

Figure 4.7 Pilot '2D' (case A) objective functions – NPV change to the waterflood base-case and carbon storage efficiency – and other outcomes – carbon storage mass and oil recovery factor- *versus* the operational variables – CO_2 injection concentration, WAG ratio, and gas slug time.

The models suggest that maintaining the highest CO_2 purity in the injection gas stream would be beneficial both financially and environmentally. However, considering the high variability in CO_2 concentrations in the solution gas across reservoirs and limited pipeline connection amongst fields, operators in the BPS cannot guarantee a highly pure CO_2 supply, but they can aim for the highest CO_2 concentration possible under their circumstances. Should they compromise on the total *rate* of gas injection to keep CO_2 purity elevated, or should they "dilute" their CO_2-rich stream with sales natural gas to increase the injection volume? We will shed more light on this question with the experiments of Section 4.3.3.

Figure 4.7 also indicates that all outcomes were insensitive to changes in the gas slug time, which can be an advantage in the BPS context, where the CO_2-rich gas supply can be restricted and intermittent, depending on produced gas availability and composition. Low

WAG ratios yielded the best NPV and CSM outcomes and were only detrimental to the CSE, for reasons argued earlier in this section.

In summary, the results of these optimisation studies suggested that a high CO_2 injection purity would improve the profitability and CO_2 storage of this pilot. Flexibility was seen regarding the amount of gas injected in every cycle and, if low WAG ratios were maintained, improved NPV and CSM outcomes would be achieved, to the detriment of a low CSE. Ultimately, the choice of design will depend on the operator's priority and operational constraints - gas injection supply and produced gas handling capacity.

Case B: 50% CO_2 Concentration

In case B, we investigated the maximisation of four objective functions separately (NPV, CSE, CSM, and unit NPV), but reduced the level of complexity on each study by considering two operational variables only (WAG ratio and gas slug size). As argued before, it is more likely that the CIC will be an uncertain parameter rather than an optimisable one. All cases simulated were plotted in Figure 4.8 to show the relationships between the four objective functions. The limited number of scenarios in the last row and column is because unit NPV was only calculated during its own optimisation study. Note how the NPV gains, CSE and CSM were restricted by the fixed CIC compared to 'case A'.

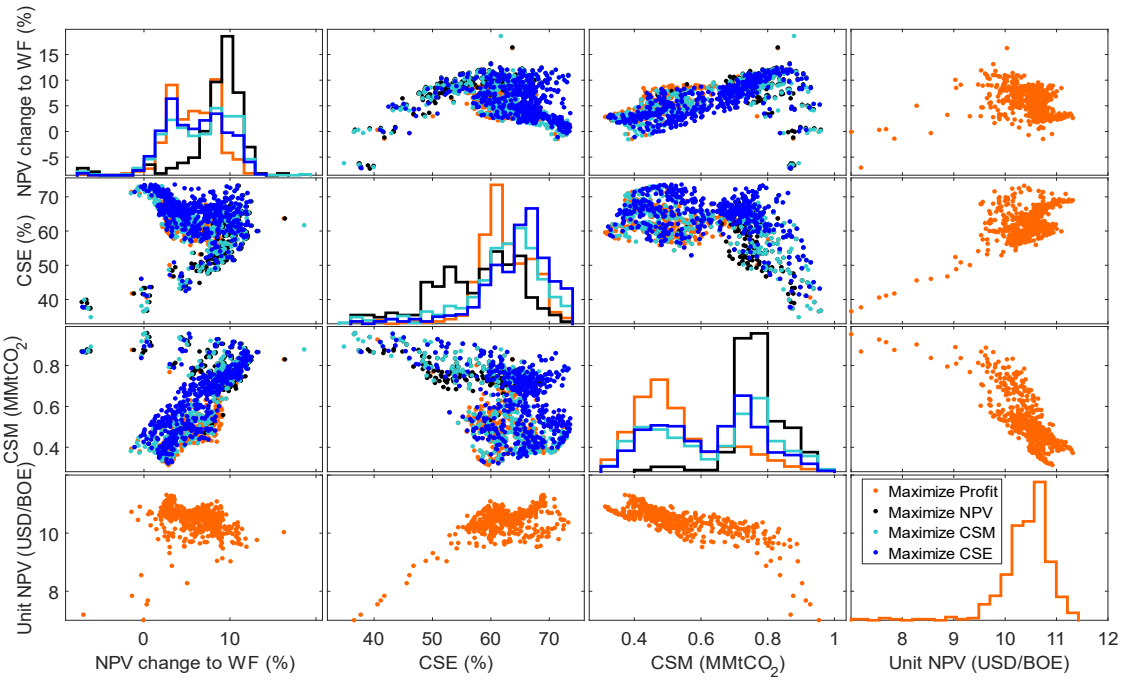

Figure 4.8 Scatter matrix for all objective functions investigated in case B: Net Present Value (NPV) change relative to the waterflood (WF) base-case, carbon storage efficiency (CSE, %), carbon mass storage (CSM, million tonnes of CO_2 stored), and unit NPV (USD/BOE).

The relationship between NPV and CSE was slightly different from 'case A': with a constant CIC, the efficiency of CO_2 storage was positively correlated to NPV growth at first, peaking for CSE values between 60 and 70%; the optimal NPV design was an outlier of the general trend. Recall that, to optimise CSE, WAG strategies tended to minimise overproduction of gas to guarantee that most of the CO_2 injected stayed in the reservoir. A high WAG ratio was selected to accomplish that, but it also prevented NG from being produced - a valuable commodity that would boost the NPV. Additionally, as in 'case A', the optimal CSE stored nearly 44% less CO_2 than the best scenarios (optimal CSM and CGI) because of its low GUR.

Another trade-off can be observed between absolute NPV (normalized to WF) and unit NPV (per BOE). In fact, the highest unit NPV (14.65 USD/BOE) of all scenarios was the WF base-case, as it produced the lowest volumes of oil and gas and it had almost no costs related to gas handling. For these reasons, high WAG ratios (closer to waterflooding), favoured unit NPV (Figure 4.9), but they harmed both absolute NPV and total mass of CO_2 stored, demonstrating that maximising unit NPV was not an overall advantageous approach for this pilot operations optimisation.

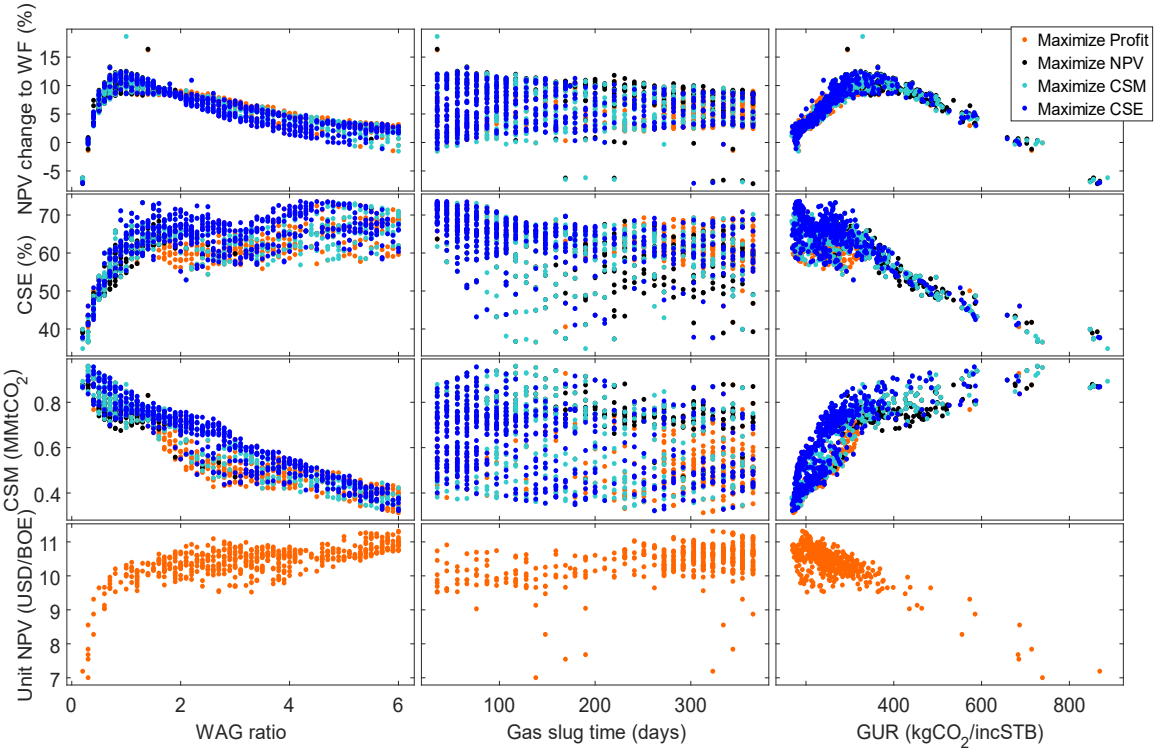

Figure 4.9 Objective functions *versus* operational variables and the consequential gross utilization ratio for the pilot '2D' (case B).

Still regarding Figure 4.8, the positive correlation between NPV and CSM observed in 'case A' persisted, but only until a CSM of about 0.8 $MMtCO_2$. From that point onwards, the designs that achieved larger CSM would also yield a wider range of NPV changes, mostly

lower than the trend. The reason for this is that the variables' region that yielded the best NPV and CSM were close – both objectives benefited from low WAG ratios and were fairly insensitive to solvent slug size - but did not coincide. According to Figure 4.9, high NPV outcomes were achieved when a WAG ratio of around 1 was applied, combined with a small gas slug size, whilst a lower WAG ratio (0.3 to 0.4) with intermediate gas half-slugs would have benefited the CSM objective the most. Ultimately, designs with a gross utilization ratio of around 300 kilograms of CO_2 per incremental STB (like the optimal NPV strategy) appeared to have balanced out most objectives positively overall. To put this into perspective, GURs in CO_2-EOR projects in the United States range between 300 to 600 kilograms of CO_2 per incremental STB (IEA, 2018).

A closer look at the optimal design recovery paths (Figure 4.10) shows how oil recovery factor and NPV were not necessarily correlated, which demonstrates that oil recovery is not a direct proxy for reservoir performance. Prioritizing NPV is a more suitable way of comprising hydrocarbons recovery and costs simultaneously. The faster production response of the optimal NPV design attenuated income depreciation and reduced the overall operational cost of the project (less total injection fluids needed), resulting in the highest NPV value.

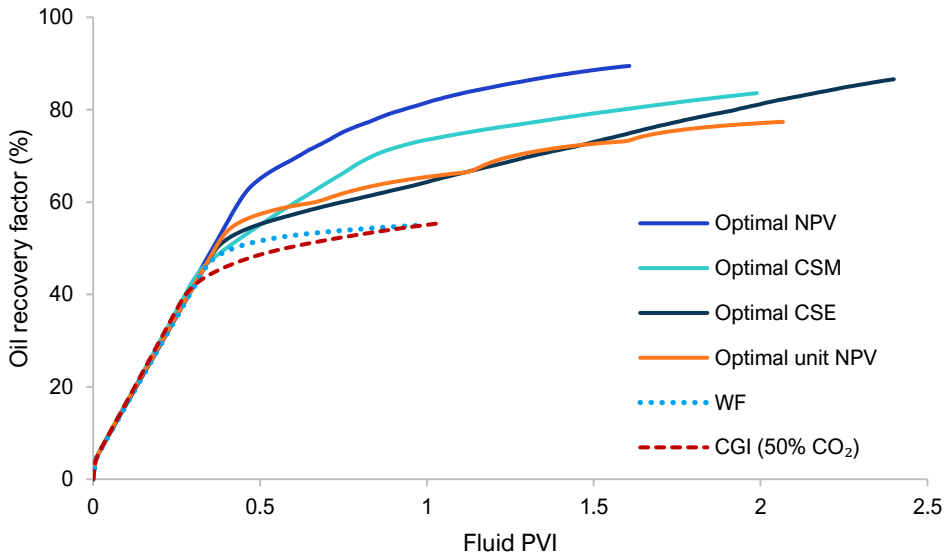

Figure 4.10 Pilot '2D' (case B) optimal designs oil recovery factors. Continuous CO_2 injection and waterflood are included for comparison.

Pure waterflood and gasflood injection schemes resulted in poorer sweeps, but the WF economic feasibility was higher than the CGI scenario (see Table 4.4). This was mainly due to the lower costs associated with injecting only seawater and because of the earlier response of the system to the waterflood stimulus compared to the gasflood one. The

quicker initial response to WF was a result of the more favourable mobility ratio of water in relation to oil in comparison to the gas/oil mobility ratio. The former creates a more piston-like displacement in the streaks, even with a high permeability contrast. The recovery factor of the CGI scheme was already surpassing the WF one, due to miscibility effects that reduce residual oil saturation, but the production GOR constraint stopped the simulation early. The CGI performance in case B was much inferior to case A due to its lower CO_2 injection purity, which limited the miscibility effects.

Table 4.4 Optimal designs description of pilot '2D' studies with a 50% CO_2 injection concentration (case B).

	Single-objective functions →	Maximise NPV	Maximise CSE	Maximise CSM	Maximise unit NPV	CGI
Outcomes	NPV change to WF (%)	18.62	3.58	0.12	2.62	-29.77
	CSM ($MMtCO_2$)	0.88	0.54	0.96	0.37	0.96
	CSE (%)	61.71	73.59	36.72	69.01	50.49
	Unit NPV (USD/BOE)	8.38	9.22	5.15	11.31	5.24
	Oil recovery factor (%)	89.47	86.59	83.59	77.36	55.49
	GUR ($kgCO_2$/incSTB)	329.10	185.59	727.28	191.98	28,640.38
	Project life (years)	20.25	30.03	25.20	25.70	13.34
Variables	WAG ratio	1	4.2	0.3	6	-
	Gas slug size (days)	35	35	117	323	-
	(%HCPV)	1.01	1.01	3.36	9.28	-

To sum up, the results of this section showed how the NPV gains, CSE and CSM can be restricted by a limited CO_2 injection content. As in case A, high CSE did not mean that more molecules of CO_2 stayed trapped in the subsurface – it simply indicated that majority of the CO_2 injected was not produced again. Neither CSE, CSM, oil recovery nor unit NPV appeared as appropriate single objective functions for this CCUS operations optimisation. Prioritizing NPV turned out to be a more suitable way of balancing both the economic performance and the storage objectives.

4.2.4. Calcite Scaling Risk Assessment

The inorganic scaling risk associated with a CO_2-EOR design is crucial to the decision-making process of selecting the project's operations. Having a geochemistry model embedded in the reservoir simulation calculations is a powerful tool to understand the complex interactions between the injected fluids and the porous medium, encountering formation water, reactive rock, gas, and oil phases. We used the output of these simulations, more specifically ionic compositions, and the phase flow rates for each production well, to predict how much calcite deposition may occur in the production system, so a scale management plan can be developed.

At the time of writing, there is no scale prediction software fully coupled with commercial reservoir simulators to perform flash calculations beyond the production perforations. The path from the production wellbore to the surface facilities is critical in carbonate scale forecasts, since it is where produced fluids suffer the most significant pressure drops, causing CO_2 evolution that may result in deposition.

Near Wellbore (Case A)

We analysed the impact of the optimal CO_2-WAG designs of 'case A' on the near-wellbore calcite dissolution and precipitation. According to Figure 4.11, for both optimal NPV (a) and CSE (b) designs, the simulation results revealed continuous dissolution of calcite in the grid blocks around the injection well. The rate of dissolution was proportional to the permeability of the layers and it was more significant when the optimal CSE design was applied, because the larger water slugs (higher WAG ratio) exposed the rock to the acidic aqueous phase for longer.

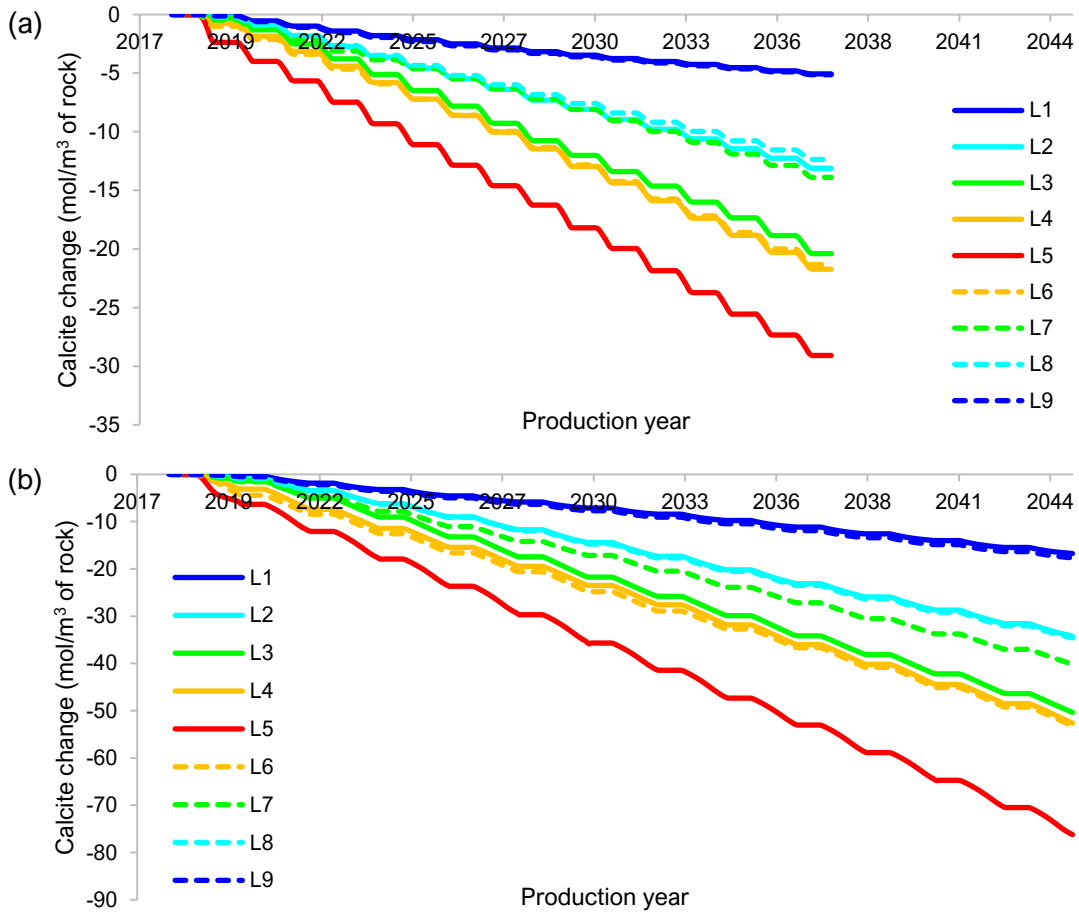

Figure 4.11 Calcite change in grid-cells adjacent to the injection well for 'case A' (a) optimal NPV design and (b) optimal CSE design. 'L' stands for layer and the numbers are increasing from the top to the bottom layers. Equal colours represent equal permeability values (refer to Figure 4.2 for permeability distribution).

The WAG cycles are noticeable: dissolution sharply occurs during water half-cycles (sloped part of each cycle), whilst a plateau develops during each CO_2 slug. This behaviour indicates that the gasflood half-slugs do not trigger calcite dissolution near the injection block, as the water saturation nearly reaches zero during these slugs. Due to the high-pressure profile close to the injection block, the amount of CO_2 dissolved in the water phase is maintained at high levels, which contributes to the high dissolution rates. Depending on the magnitude, this dissolution can stimulate the wellbore, improving injectivity or, in the other extreme, jeopardizing the well integrity.

Regarding calcite change around the production perforations, the difference in magnitude from one optimal design to the other persisted (Figure 4.12).

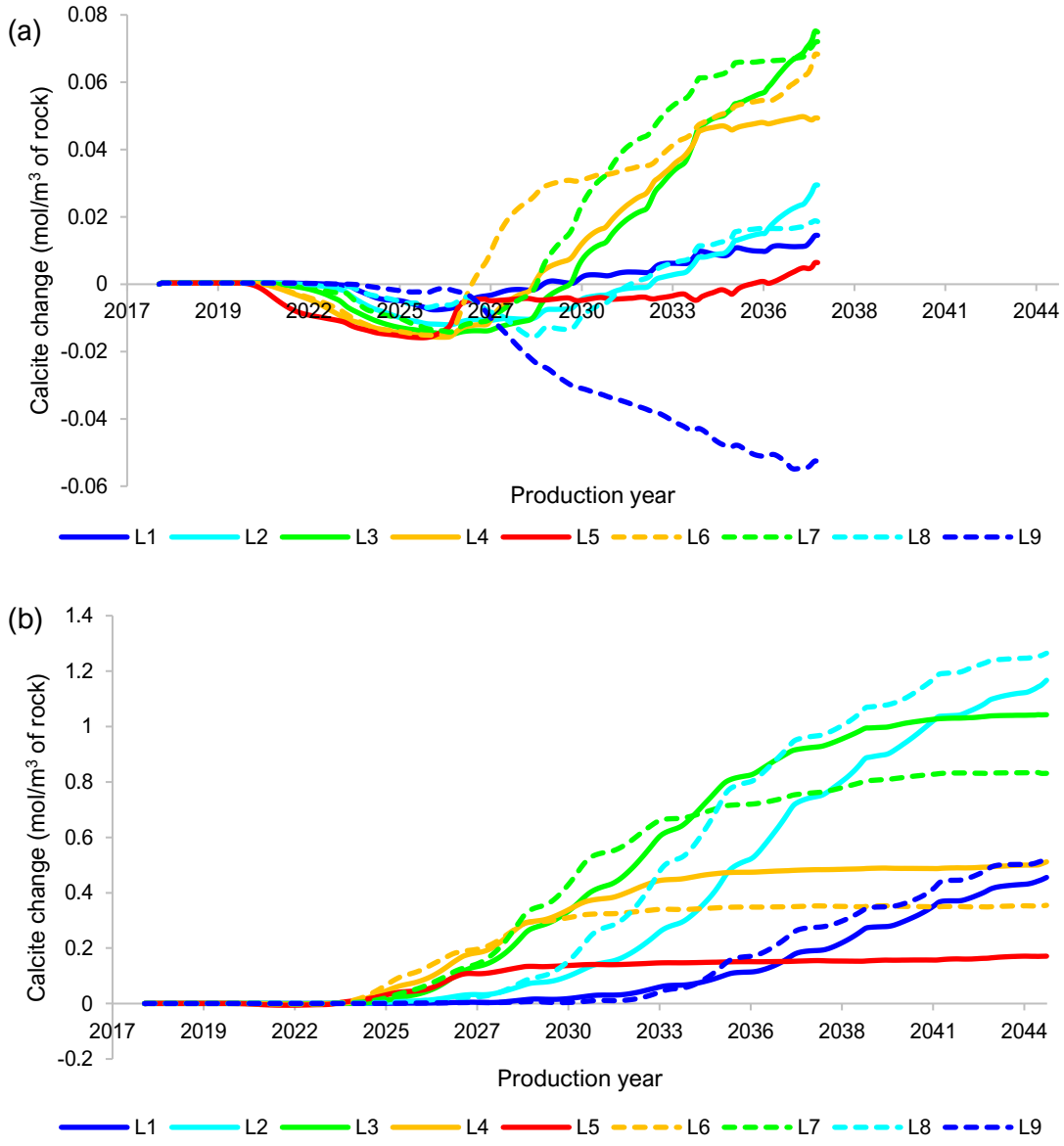

Figure 4.12 Calcite change in grid-cells adjacent to the production well for the (a) optimal NPV design and (b) optimal CSE design.

For the optimal NPV case (Figure 4.12a), dissolution was first observed as the low pH aqueous phase that has been dissolving calcite arrived at the production grid-blocks. Then, precipitation started to take place as the CO_2 free-gas phase broke through, except for layer L9 due to gravity segregation - more of the denser fluid, water, flowed to the bottom of the model, and its low pH continued the calcite dissolution. Layer L6 would be the first to show signs of formation damage, whilst layer L5 would be the least affected, with net precipitation only towards the end of production life. L5 is the highest permeability layer and the quickest to produce the high Ca^{2+} formation water, which limits the calcite precipitation rate in the middle region.

Mostly precipitation occurred around the production wellbore of the optimal CSE case as soon as CO_2 started to evolve from aqueous solution (Figure 4.12b). Its larger water slugs (WAG ratio 1.7) promoted more severe dissolution within the reservoir, and when this brine, fully saturated with bicarbonate ions mixed with the high Ca^{2+} formation water around the production well, precipitation happened. Additionally, the lower pressures closer to the producer cause CO_2 to evolve from the aqueous phase, increasing the pH and boosting calcite deposition. After all formation water has been produced, a plateau in precipitation rate is observed in the high permeability middle layers (L4, L5 and L6).

So, which design presented the highest scaling risk? Mineral precipitation near production perforations was more predominant in the optimal CSE case. The consequences are formation damage and productivity loss, depending on the amount of precipitation with respect to the pore volume around the well. To prevent permeability reduction, squeeze treatments need to be applied, which are costly and operationally challenging in the BPS environment.

On the other hand, when dissolution is still taking place once the injected fluids reach the production wellbore (as in the optimal NPV case), it means that the brine is more saturated with respect to calcite than it would be if precipitation were happening instead, leading to a higher potential of mass precipitation when CO_2 evolves from solution downstream of the perforations. Although more mass of scale could form in such a scenario, its prevention method is more straightforward: continuously injecting scale inhibitor in the production wellbore. Therefore, *where* the precipitation takes place, as well as its severity, need to be considered when deciding which design produces the highest scaling risk and how to tackle its management.

From Wellbore to Surface Conditions (Case B)

We applied the methods described in section 3.4 to evaluate calcite scale risk beyond the production wellbore. Figure 4.13 shows the calcite scale rate for the key CO_2-EOR designs investigated in 'case B'. The variability in the optimal strategies is due to the WAG cycles and coarseness of the grid-cells.

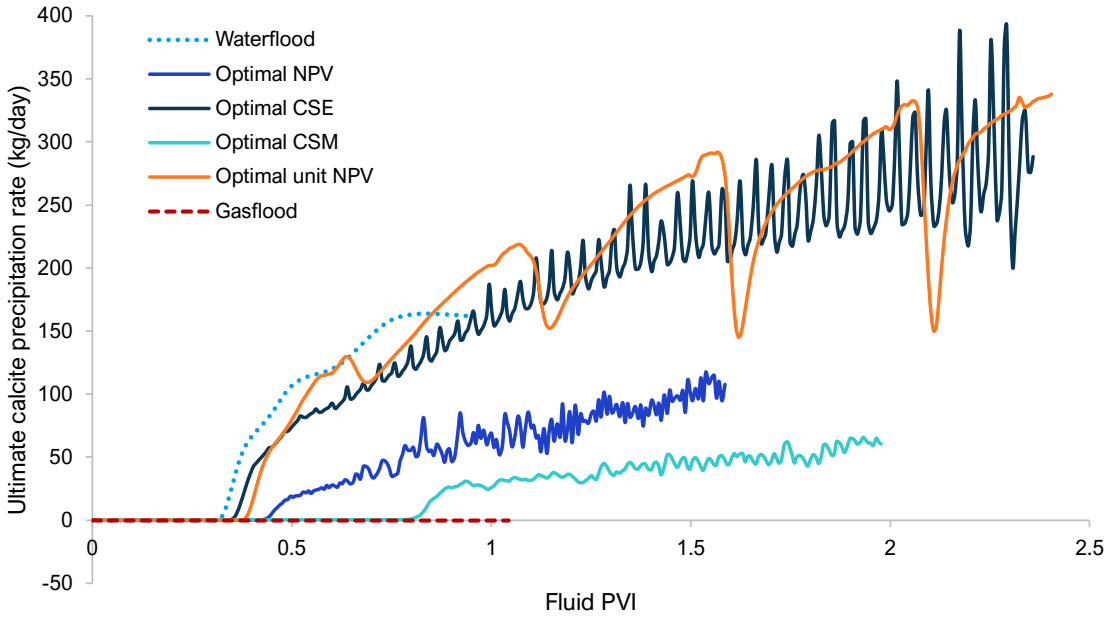

Figure 4.13 Rate of calcite ($CaCO_{3(s)}$) precipitate when produced fluids are flashed from wellbore (55.38 MPa, 331.9 K) to surface conditions (0.1 MPa, 298.15 K) for different operational designs of 2D case B (50% CO_2 injection concentration).

Calcite precipitation in the gasflood strategy was negligible compared to any other option that involves seawater injection. The only scale risk during gasflooding would be due to CO_2 evolving from formation water since there is no acidification of injection brine nor significant dissolution of rock. On the other hand, waterflood presented the most severe scaling risk at the start of the project's lifetime due to earlier water breakthrough, mixing of injected and formation brines, and CO_2 speciation from the original oil. After around 0.7 PVI, all the CO_2 present in the oil phase was stripped out by the seawater influx, so calcite precipitation reached a plateau then started to decline due to a lack of CO_2 in the system. The simulation reached the water-cut limit before a more significant drop in deposition rate occurred.

Comparing the WAG designs, calcite scale risk increased as WAG ratio increased, since more seawater (the reactions' medium) is put through the system, with enough CO_2 to maintain the saturation ratio high at surface conditions. When CO_2 is added into the reservoir as part of a WAG injection scheme, every water slug will have direct contact with CO_2 in the

transition zone, either from the oil or from the gas injected. This will promote calcite dissolution in high pressure zones and precipitation when CO_2 evolves from solution, but not limited by the original CO_2 content in the oil – therefore, more severe than pure WF (see the optimal CSE and optimal unit NPV curves).

The optimal CSM case achieved the lowest precipitation rate and a delayed water breakthrough by applying the lowest WAG ratio (0.3) of all optimal designs and a moderate gas slug size (117 days). However, this case had only a marginal NPV improvement (0.12%) in relation to WF. To make a sound decision, one would need to estimate the scale prevention cost savings that the optimal CSM design would bring, considering that this case had only a marginal NPV improvement (0.12%) in relation to WF. On the pilot study '3D' (section 4.3) we will include the squeeze treatment costs in the NPV calculations for an integrated approach.

Lastly, we evaluated the influence of the CO_2 injection concentration in the calcite scale tendency using the optimal NPV design as base-case. Ultimate calcite precipitation rates for three levels of CIC are shown in Figure 4.14.

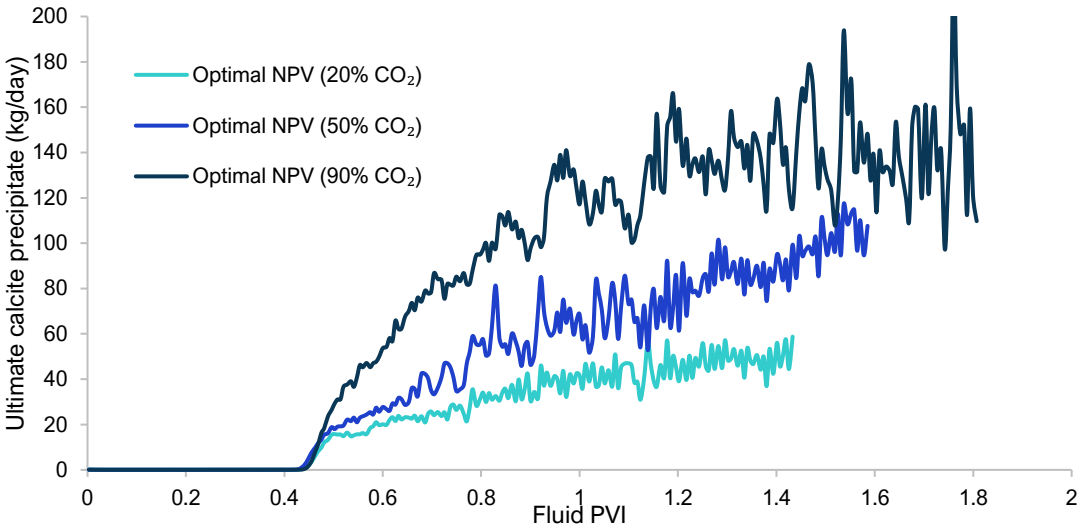

Figure 4.14 Calcite ($CaCO_{3(s)}$) precipitation rates for 'case B' optimal NPV design with different CO_2 injection purity levels.

Calcite scale risk significantly rose with greater CIC. Increasing CO_2 partial pressure made the system more acidic under reservoir conditions, which induced more rock dissolution and yielded a different equilibrium brine/gas/rock, in which the aqueous phase had retained more calcium and bicarbonate ions as it flowed through the reservoir. Consequently, even though the availability of water was the same in the three cases, the brine arriving in the

production wellbore was more saturated with respect to calcite for higher CIC, thus the greater calcite precipitation experienced in these cases.

Note that cases with higher CIC had longer production periods because they did not violate the maximum production GOR threshold we set (8,900 sm^3/sm^3). This can be explained by the *retardation* effect CO_2 experiences as it flows through the reservoir and dissolves in both oil and water (Ghanbari et al., 2020). Methane, on the other hand, is immiscible in water and its concentration in the oil phase is either constant (for CIC equals 20%) or diminishes as CIC increases. Therefore, cases with higher methane content had higher and more unstable gas production rates, hitting the GOR operational constraint earlier. To a lesser extent, higher CIC promoted higher oil rates, which contributed to smaller GOR values.

Interestingly, although the gas injection rates in *reservoir conditions* were kept the same for the three cases, more gas was injected in surface conditions as CO_2 content increased, since CO_2 was more compressible (see Figure 4.15). One may think that gas production in surface conditions would also be higher as CIC increased. However, a more controlled GOR was observed for higher CICs, and the cumulative gas production in surface conditions was similar across cases.

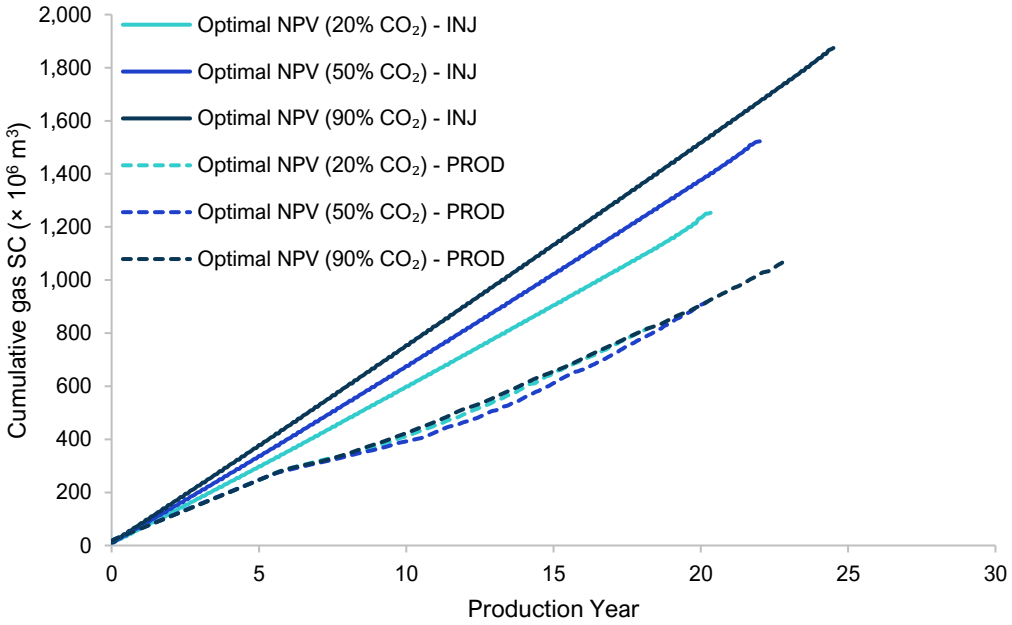

Figure 4.15 Cumulative gas injected and produced at surface conditions for 'case B' optimal NPV design with different CO_2 injection purity levels.

4.2.5. Conclusions: Pilot Study '2D'

Results of this pilot study '2D' showed the impact of optimising WAG designs when distinctive single-objective functions were modelled. We showed to which extent such designs influence CO_2 mobility control, recovery, and calcite scale risk. The following conclusions were drawn:

1. *Impact of CO_2 injection concentration:* according to the sensitivity analysis, CIC had the biggest impact on the outcomes. The optimisation results (case A) confirmed that higher CICs were beneficial to all objectives analysed, although the scaling risk assessment (case B) reveals that purer CO_2 injection streams resulted in more severe calcite scale in the production facilities. In the BPS context, CIC is mostly dependent on factors operators can hardly control, thus it can be considered as an uncertain parameter rather than a design variable. If there is flexibility regarding the CIC, higher values should be prioritized (for a constant injection rate).

2. *Storage objective functions:* both cases A and B (with and without CIC as a design variable) show that selecting CSM as the optimisation objective function can be more representative of environmental-driven goals, although its low storage efficiency would bring the onus of large amounts of produced gas to be handled in the topside. Aiming to improve CSE can lead to sub-optimal solutions, where a small amount of CO_2 is injected in the reservoir with large slugs of water (the mobility control fluid) solely to avoid CO_2 breakthrough in the production well.

3. *Economically focused objective functions:* results of case B suggested that loftier unit NPV outcomes would be accompanied by loses in total NPV and CSM. Waterflooding the reservoir would in fact bring the highest profitability per BOE produced.

4. *Oil recovery factor and NPV relationship:* they were not always directly correlated but closely related – the highest oil recoveries did not result in the highest NPVs, but faster oil recovery rates (steeper positive slopes) benefited NPV greatly through revenue anticipation. This reinforces that CO_2-EOR optimisation analysis that prioritizes NPV is more likely to achieve a more cost-effective reservoir performance than studies that simply attempt to maximise oil recovery, since, in the former case, production and costs are being considered simultaneously.

5. *Holistically beneficial WAG design:* the domain where NPV and CSM were maximised had a fortunate overlap - low WAG ratio and low to intermediate gas slug size. The right

combination of these variables promoted a more uniform macroscopic sweep, higher NPV and above average CSM, balancing out the environmental and economic driven objectives but with the consequence of poorer CSEs for this pilot.

6. *Most apt single-objective function:* neither CSE, CSM, oil recovery nor unit NPV appeared as appropriate single-objective functions for this CCUS operations optimisation. Prioritizing NPV yielded solutions that balanced both the economic performance and the storage objectives. A multi-objective optimisation approach may be necessary to find compromised designs.

7. *Higher WAG ratios increased scaling risk:* low WAG ratio designs (such as the optimal NPV) had less calcite dissolution around the injection perforations, although some dissolution persisted until injected fluids reached the production wellbore, which may result in higher precipitation rates within surface facilities compared to high WAG ratio scenarios (optimal CSE and optimal unit NPV). However, after calculating the worst-case calcite precipitation rate at surface conditions, it was clear that calcite scale tendency increased with water availability (higher WAG ratios), as a lower salinity water encounters CO_2 that is naturally present and/or periodically injected through WAG, keeping both water production and saturation ratios high.

8. *Full storage capacity hard to fulfil:* in the context of coupled CO_2-EOR and storage, no design could fulfil the full storage capacity of this reservoir during the production period, which was around 3.7 $MMtCO_2$ (pore volume for an average reservoir pressure of 7,000 psi). This is because production wells are operating, so gas breakthrough will occur. Moreover, delaying this breakthrough would mean occupying pore space with mobility control fluid (seawater) rather than with CO_2 itself. A subsequent stage of continuous CO_2 injection for CCS purposes after the EOR period may be necessary for complete re-utilization of the CO_2 produced from elsewhere in the field.

4.3. Pilot Study '3D': Tapered WAG

In this section, we investigated the impact of varying the WAG design *over time* (tapered WAG) on economic reservoir performance, CO_2 storage, and calcite scale. We also evaluated additional decision variables (injection rates and producer BHP) and laid the foundation for optimising a long-term scale prevention plan.

4.3.1. Study Description

We expanded the layered synthetic model of the previous section into the 3D grid shown in Figure 4.16, with one WAG injector and one producer in opposite corners. As in the pilot study '2D', the injection BHP was not allowed to surpass the fracture pressure of 68.95 MPa, the WAG cycles always started with a gas slug and the rock-fluid properties were maintained.

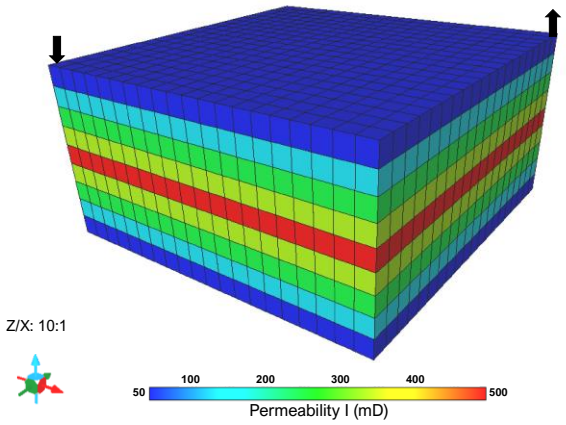

Property	*Value*
Model dimensions (m)	1,000 × 1,000 × 50
Number of grid-cells	20 × 20 × 9
Porosity	10%
kv/kh ratio	0.1
Initial water saturation	25%
Rock mineralogy	80% calcite
Solution GOR (sm^3/sm^3)	221
Production lifetime (years)	20
Initial reservoir pressure (MPa)	55.38
Initial reservoir temperature (K)	331.9

Figure 4.16 Synthetic reservoir 3D model horizontal permeability distribution (left) and characteristics (right).

The three main optimisation assumptions that distinguish this section from the previous are:

1. we allowed and optimised a waterflooding period prior to the tertiary recovery;
2. the CO_2-EOR period was subdivided into three optimisable stages (tapered WAG) and;
3. injection rate and production BHP were considered as variables (case B).

Additionally, all scenarios had 20 years of production life, and the injection gas concentration was fixed at 80% CO_2 purity, the remainder being the pseudo-component N_2-C_1. Table 4.5 shows the ranges and discretization of the design variables for this '3D' study. They were similar to the pilot '2D' but some of the boundaries were narrowed based on previous results and to reduce the number of possibilities. Once again, any combination of parameters that yielded a half-slug duration shorter than 30 days was excluded from the study to avoid impracticable well switches.

Table 4.5 Pilot '3D' optimisation design variables, their respective domains, and discrete increments.

	Parameter	Range		Increments
		Low	High	
Cases A & B	WAG ratio	0.2	5	0.25
	Solvent slug-size (%HCPV)	0.55%	10%	0.55%
	Waterflood duration (days)	0	1825	90
	Number of full cycles per stage	1	30	1
Case B	Gas or water injection rate (%PV/year)	2.5%	10%	1.25%
	Producer Bottom-hole pressure (MPa)	13.8	48.3	3.45

The choice of these WAG parameters as optimisation variables was made to embrace most of the key WAG operational controllers with the least number of variables. However, different combinations can also be applied. The other important WAG controllers were then indirectly calculated as follows:

$$Water\ half\ slug\ size|_i = (Gas\ half\ slug\ size|_i)(WAGratio_i) \tag{4.5}$$

$$Gas\ half\ cycle\ time|_i = \frac{Gas\ half\ slug\ size|_i}{Gas\ injection\ rate|_i} \tag{4.6}$$

$$Water\ half\ cycle\ time|_i = \frac{Water\ half\ slug\ size|_i}{Water\ injection\ rate|_i} \tag{4.7}$$

4.3.2. Case A: Tapered versus Uniform WAG

As in the pilot study '2D', the production BHP was kept above the reservoir fluid bubble-point, at 39.3 MPa, but the injection well was controlled by a constant injection rate of 0.05 PV/year (to result in 1 PVI in 20 years), which was equivalent to a volumetric injection rate of 685.17 rm^3/d. We simulated a waterflood and a continuous gas injection with these specifications as comparison cases.

The tapered WAG study nine decision variables: the switching time from secondary to tertiary recovery, as well as the WAG ratio, gas half-cycle size, and number of cycles for three distinct WAG stages. One could optimize each individual cycle, but the number of possibilities would be enormous. We decided to allow the WAG designs to change in two occasions throughout production life (resulting in three WAG stages), as if the operator were adapting the design based on injection fluids' breakthrough.

We used CMG™ CMOST DECE optimisation algorithm and performed over 300 simulations to find the WAG operational design that maximised the NPV of the project. For comparison, we performed the same calculations for a *uniform* WAG framework (nearly 1,000 simulations) with three optimisation variables: switching time from secondary to tertiary recovery, WAG ratio, and gas half-cycle size. Figure 4.17 shows the NPV improvement

relative to waterflooding *versus* both the environmental outcomes, CSE and CSM. The familiar trade-off between NPV and CSE appeared again in both set of results, as well as the direct correlation between NPV and CSM.

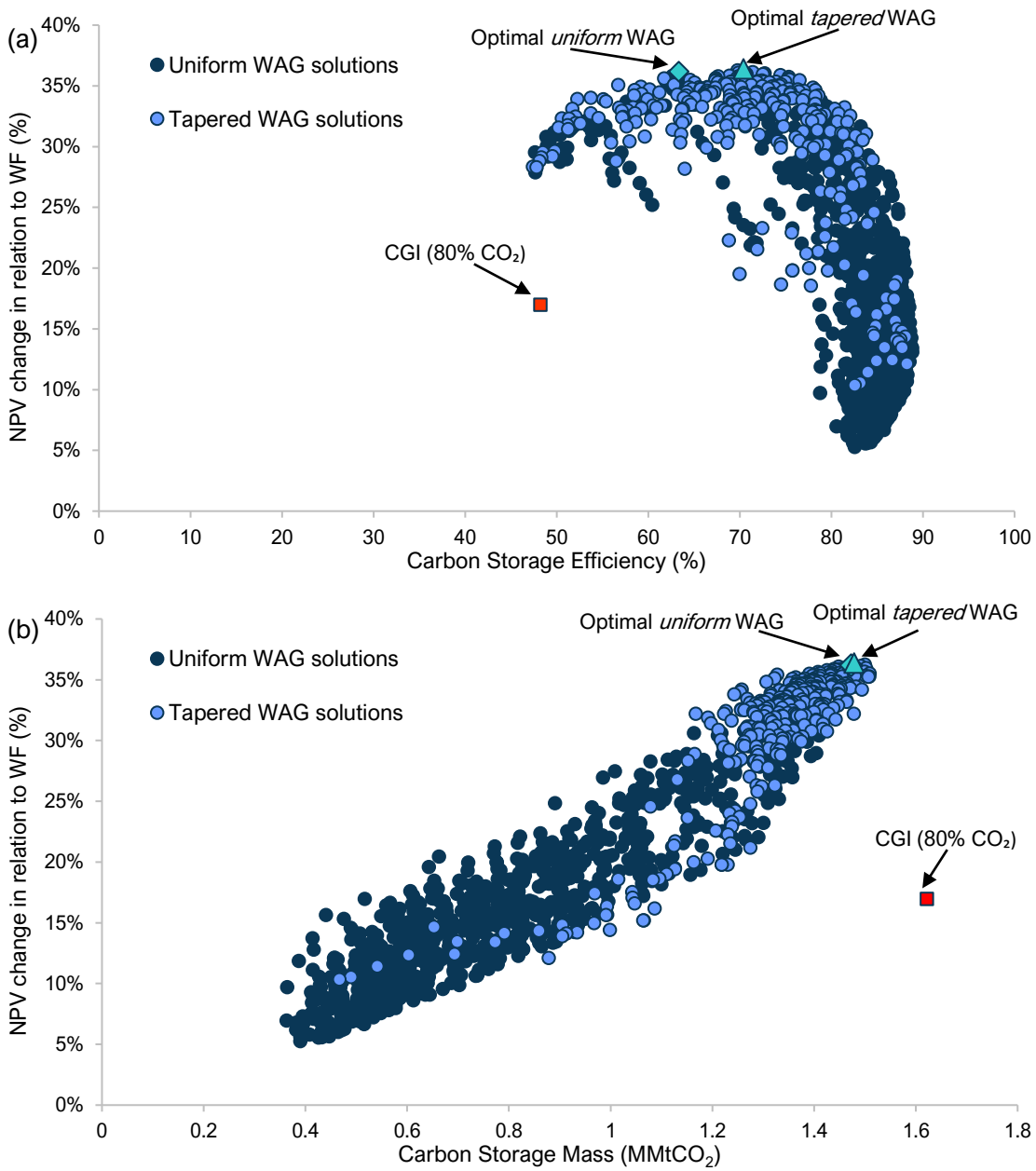

Figure 4.17 Pilot study '3D' optimisation solutions – tapered and uniform WAG.

Under the restrictions imposed and for the variables optimised, it was possible to find versions of both types of WAG that achieved similar results, as the optimisation algorithm scrutinised the search space with hundreds of combinations. There were several scenarios on the edge of the solution space worth considering when choosing the most suitable WAG design, which gives flexibility to the decision-making process, and it is especially important when CO_2-rich gas supply is uncertain and intermittent.

As the uniform and tapered WAG designs lay practically on the same solution domain for the outcomes of interest, it seems as if there is no clear advantage to applying one type of WAG over the other. The optimal uniform and tapered designs had essentially the same NPV and CSM – as well as oil recovery factors. Surely, applying the optimal tapered design would require more operational adjustments than the uniform one (see their design description in Table 4.6 and injection well switches in Figure 4.18), which makes a stronger case for using the latter.

Table 4.6 Pilot '3D' case A operational design of optimal uniform WAG and optimal tapered WAG.

Parameter	Optimal uniform WAG	Optimal tapered WAG		
		Stage 1	Stage 2	Stage 3
WAG ratio	0.5	0.5	1	0.75
Solvent slug-size (%HCPV)	7.0	4.7	0.5	4.7
(days)	385.8	256.4	30	256.4
Secondary recovery duration (days)	91.25		0	
Number of full cycles per stage	-	3	13	Rest of production time

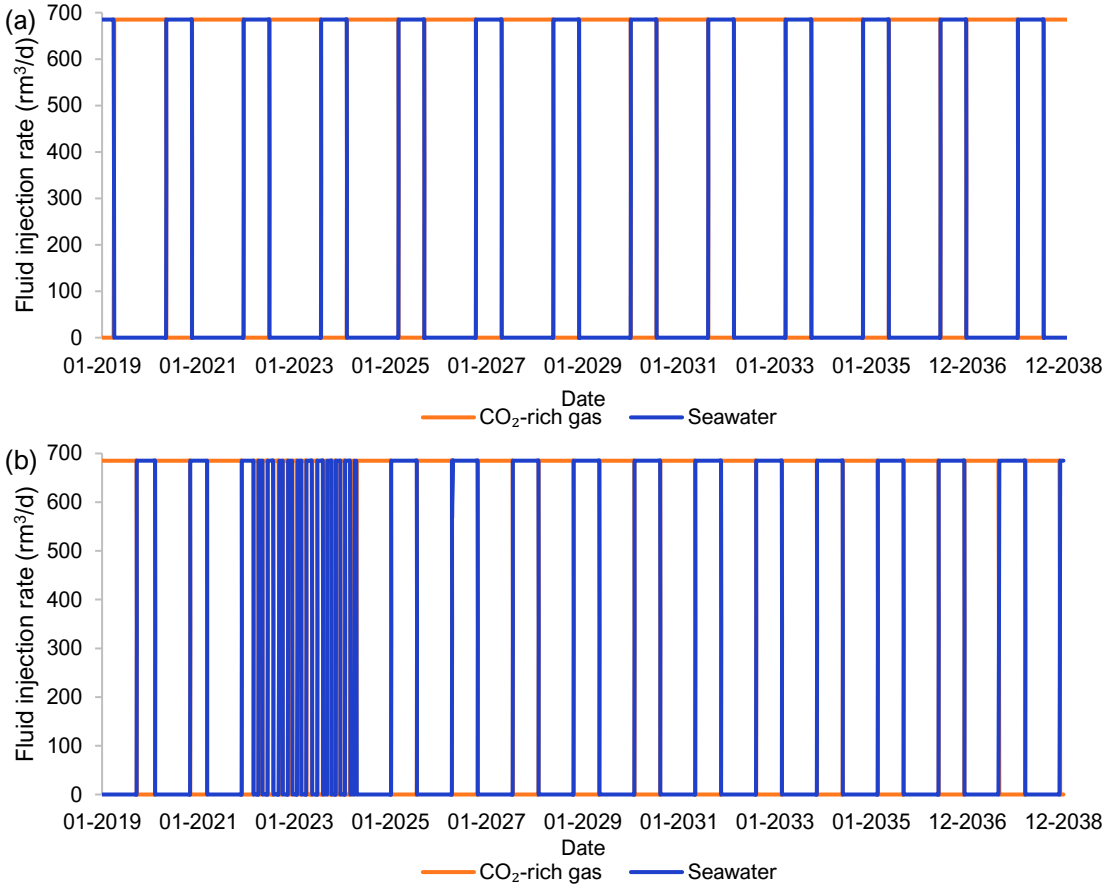

Figure 4.18 Fluid injection rate in reservoir conditions for the optimal NPV (a) uniform and (b) tapered WAG designs.

However, the optimal tapered WAG utilized the CO_2-rich gas more efficiently, even though the injection rates were kept constant in all scenarios. The optimal tapered WAG needed 10.5% less CO_2 to produce an incremental barrel of oil and it had a CSE 11.2% higher than

the optimal uniform WAG (70.4% *versus* 63.3%). Note how both optimal scenarios had little to no secondary recovery prior to the WAG period, suggesting that this system would benefit from an early CO_2-EOR start.

Additionally, according to Figure 4.19, the optimal tapered WAG design showed improved gas mobility control compared to the optimal uniform WAG, with lower CO_2 rates and smaller cycle oscillations. The downside was an earlier water breakthrough and higher water rates than the uniform design, which can increase calcite scale risk, as we shall analyse soon.

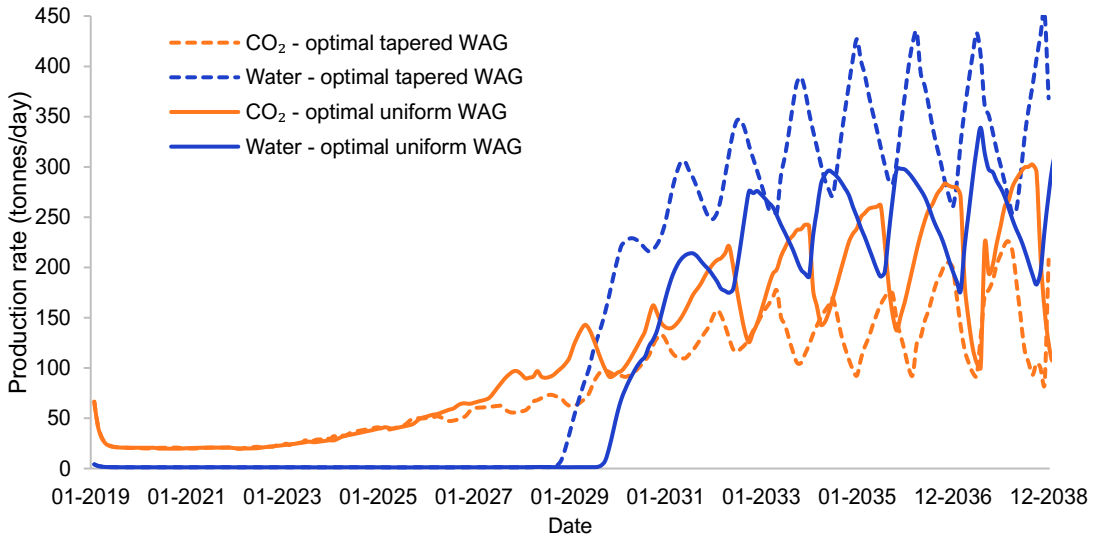

Figure 4.19 Water and CO_2 gas production rates for the optimal uniform and tapered WAG scenarios.

4.3.3. Case B: Variable Injection Rates and Production BHP

Including injection rates and producer BHP as decision variables is essentially the main difference between the optimisation process of the present case and that of 'Case A'. This may appear as a minor change, but it greatly increased the number of candidate solutions, and therefore the complexity of the search for the optimal design. To give the reader an idea, considering only one injection and one production well, the number of variables went from nine to 20 and the search-space broadened from 14 orders of magnitude to 30.

Figure 4.20 shows NPV change in relation to the waterflooding case for all WAG designs simulated in cases A and B to put into perspective. We plotted it against total CO_2 stored in the reservoir to address the trade-off between financial and environmental objectives.

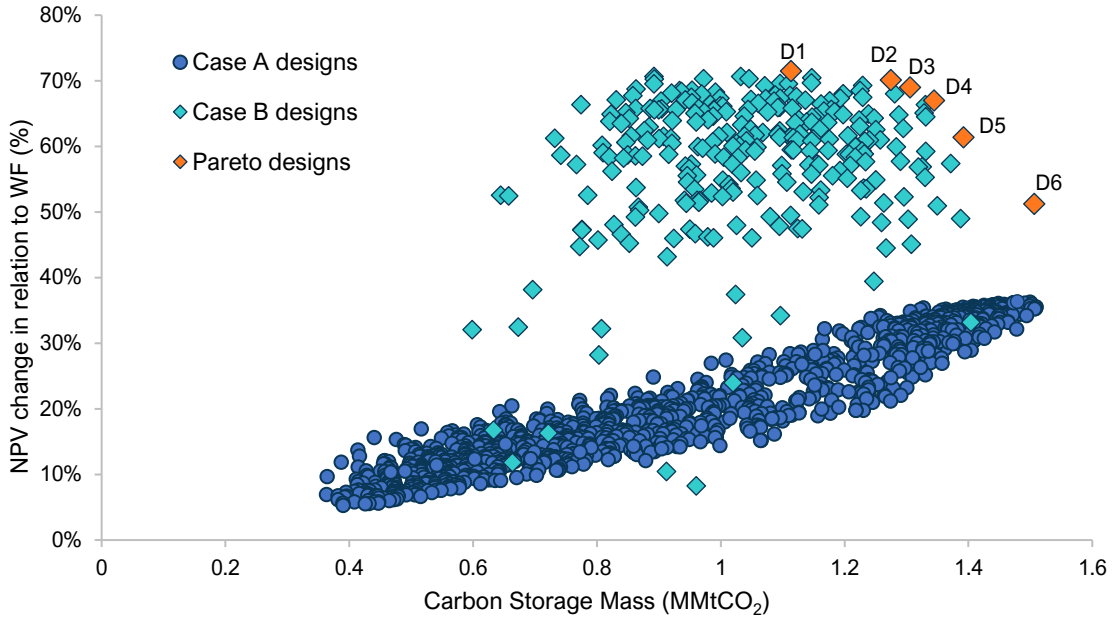

Figure 4.20 NPV change in relation to waterflood versus total CO_2 stored in the reservoir during production lifetime for tapered WAG designs in cases A and B (variable injection rates and producer BHP).

Note how including injection rates and producer BHP as decision variables unlocked the potential for maximising NPV. Additionally, because the search space was less restricted, a trade-off between NPV and CSM appeared, rather than the direct correlation observed in previous sections of this thesis.

The highest NPV identified by the DECE algorithm was design D1, but we identified designs on the edge of the search space as cases of interest (Pareto front). Depending on the operator's priority, a middle-ground strategy like D3 could be a strong candidate for best overall design, as it showed a small reduction in NPV for a significant gain in CO_2 storage compared to the optimal D1.

The oil recovery paths of all strategies simulated in case B (Figure 4.21) demonstrated the non-direct relationship between NPV and oil recovery, as the highest NPV design did not produce the most oil (nor gas). Often solutions with the highest oil recovery factors do not necessarily yield the maximum cash flow projections (Pariani et al., 1992), as we saw in previous sections. Design D1 allowed most of the oil to be produced in the early stages of the field lifetime, which was advantageous for NPV, but it also had reduced injection and production costs compared to the other designs, showing an all-round more efficient flood.

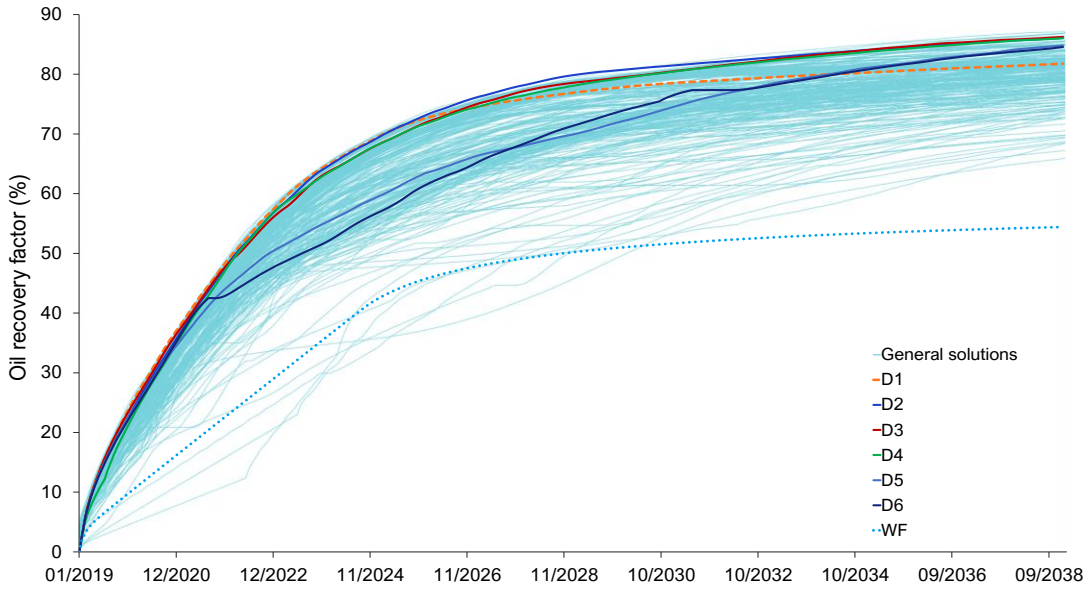

Figure 4.21 Oil recovery factor for all 'case B' designs.

Optimisation Variables Behaviour

Which WAG design considered in Case B resulted in the best outcomes? As WAG half-cycle durations are a consequence of most WAG operational parameters considered here (gas slug size, WAG ratio and injection rates), we show them for the Pareto designs in Figure 4.22, as well as the corresponding WAG ratios. The producer bottomhole pressure is plotted in Figure 4.23. Although these designs were found through heuristic methods using the DECE algorithm, they all followed consistent trends and one can draw general conclusions from the results.

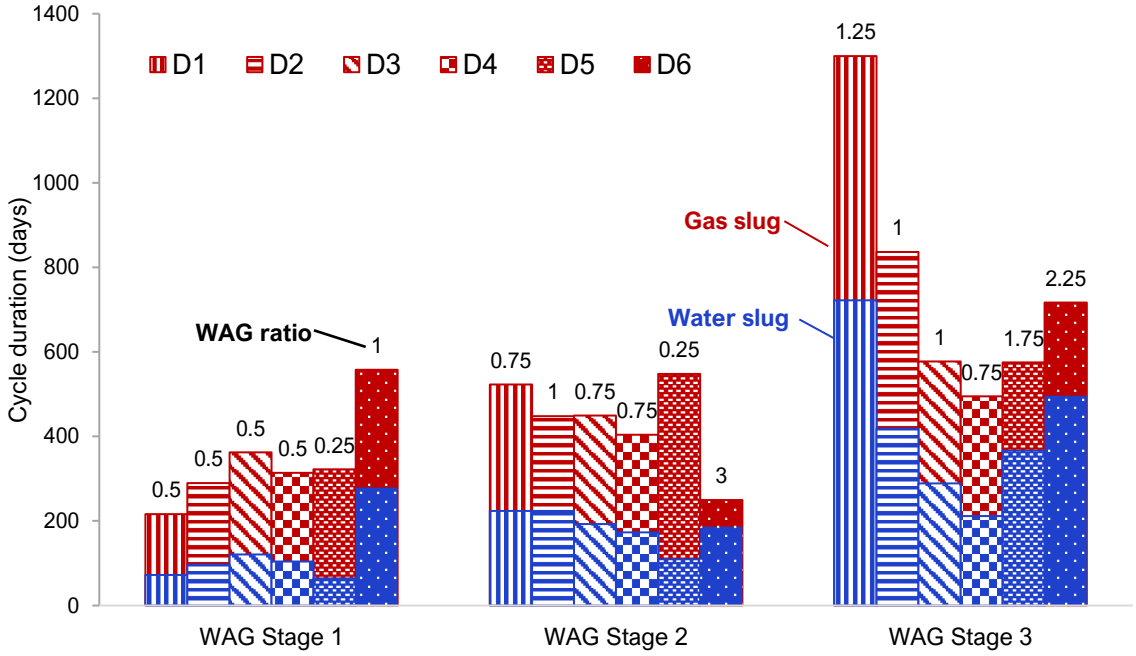

Figure 4.22 Tapered WAG half-cycle durations for the Pareto designs of case B.

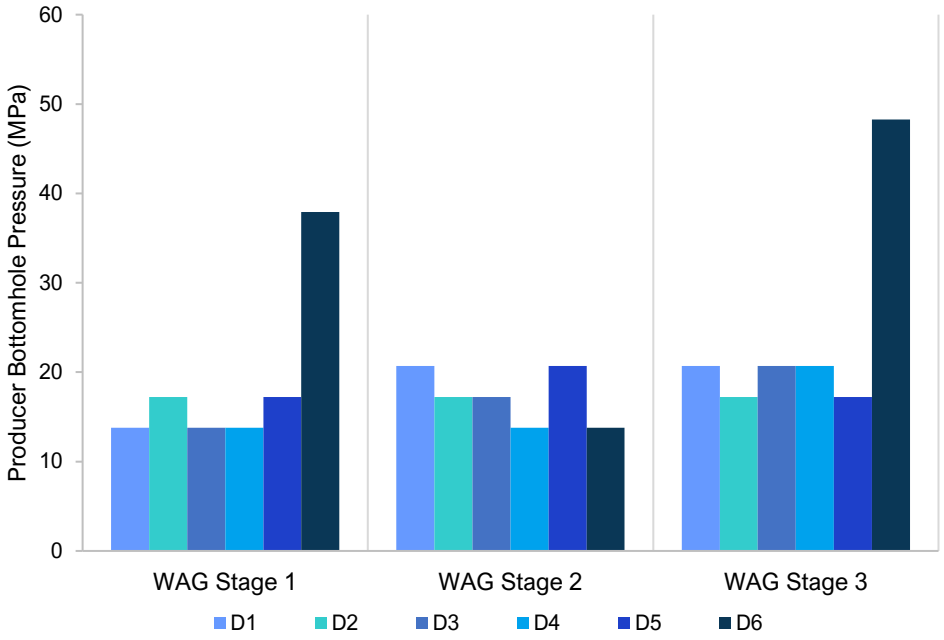

Figure 4.23 Producer bottomhole pressure for each WAG stage of the Pareto designs (case B).

During the first WAG stage of the scenarios with best NPV (D1 to D3), both water and gas injection rates were set to their maximum levels, while BHP in the producer was set to its minimum. This combination created a large drawdown in the reservoir, significantly increasing oil recovery earlier in the flood. Additionally, the WAG ratio was kept low during stage one in all scenarios but D6, which agrees with the classic tapered WAG concept of injecting more gas in the beginning of a tertiary flood to improve microscopic displacement efficiency (Pariani et al., 1992, Khan et al., 2016).

During stage two, the WAG cycle times were longer for all cases except D6. This was a result of a reduction in both gas and water injection rates for most cases, with a more consistent and significant drop in the gas to control the high CO_2 mobility. For designs D1 to D5, the WAG ratio was kept below 1:1, favouring more gas injection in relation to water.

During the final WAG stage, cases D1 to D3 had their water and gas injection rates reduced to similarly lower levels, whilst the WAG ratios were equal or above 1:1 towards the end of the reservoir life. This boost in injected water in relation to gas caused a better macroscopic displacement and pressure maintenance, as well as a constant produced gas profile.

The waterflood period prior to EOR was also an optimisation variable and it was set to zero in all Pareto designs (except D4 and D6), demonstrating the benefit of starting the CO_2-EOR as early as possible in the field production life.

Design D6 was a clear outlier regarding the operational parameters assigned, hence its lower NPV and higher CSM. This strategy also had the highest CSE amongst the Pareto designs (65.8%). This was achieved through maintaining the producer BHP elevated, to control the drawdown and avoid appearance of a gas phase in the reservoir that could increase gas production, with the downside of an undesirable abandonment pressure that was higher than the initial reservoir pressure (see Figure 4.24).

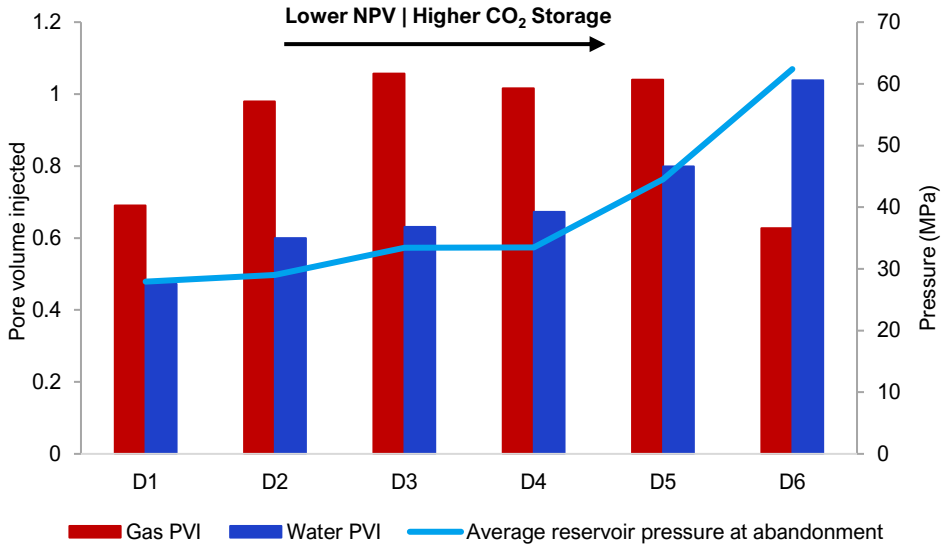

Figure 4.24 Pareto designs total gas (80% CO_2) and total water pore volumes injected during field life, and the resulting average reservoir pressure at the time of abandonment.

Additionally, an average WAG ratio higher than 1:1 was kept in design D6 – around 65% more water was injected in relation to CO_2. This may be counterintuitive, from a pure CO_2 storage perspective, since the large volumes of water injected will occupy pore space that would otherwise be filled with CO_2, limiting the storage capacity of the reservoir. However, as also demonstrated in previous sections, higher than 1:1 WAG ratios (for the well distance examined of around 1.4 km) helped control the high CO_2 to water mobility ratio.

Figure 4.24 also shows that the most economically successful designs were the ones that used the energy of the reservoir more efficiently, i.e., ended up with a low reservoir pressure at abandonment. In general, higher NPV values were achieved with low average WAG ratios (between 0.6 and 0.7) and a combination of low production BHPs and injection rates that kept the reservoir pressure close to the MMP of 31 MPa.

Injection Rate and CO_2 Injection Concentration Relationship

Finally, in section 4.2.3 case A, we asked: should operators compromise on the total *rate* of gas injected to keep CO_2 purity elevated, or should they "dilute" their CO_2-rich stream with

sales natural gas to increase injection volume? Previous results pointed out to high CO_2 injection concentrations for improved NPV and storage objectives. Results of this section suggested that high gas injection rates are crucial in the start of the flood when gas availability within the reservoir may be limited.

To deploy high CO_2 concentrations, one needs to limit the volume of gas injected and vice versa. So which compromise would be the most advantageous? To answer that, we simulated three versions of the optimal NPV case D1: (1) same injection rates with inversely proportional CO_2 injection concentrations; (2) the lowest injection rate of the optimal case with its highest CIC; and (3) the highest injection rate of the optimal case with its lowest CIC. The optimal producer BHPs were maintained across scenarios. A summary of the design assumptions is shown in Table 4.7.

Table 4.7 Assumptions for sensitivity analysis on injection rate and CO_2 injection concentration.

Scenario	WAG Stage	Injection rate (IR) – PVI/year	CO_2 injection concentration (CIC)
D1 (optimal NPV)	1	10%	80%
	2	4%	80%
	3	2%	80%
D1 – correlated IR & CIC	1	10%	20%
	2	4%	50%
	3	2%	80%
Low IR | High CIC	-	2%	80%
High IR | Low CIC	-	10%	20%

The correlation between injection rate and CO_2 injection concentration was heuristically chosen based on the ranges used in our optimisation studies. A more rigorous approach would involve determining their relationship using the CO_2 feed concentration and membrane separation efficiency, then making the CIC a variable that is dependent on the injection rate in the optimisation process.

All design variants tested were a downgrade in terms of oil recovery compared to design D1 (see Figure 4.25), especially the version with low injection rate and high CIC. Maintaining the injection rate high throughout production life to the detriment of CO_2 injection purity seemed to be the best compromise in terms of oil recovery, but, according to Figure 4.26, this design had the second worst NPV performance, with an 11% improvement in relation to the WF base-case (recall that D1 showed a 71.5% NPV change relative to WF).

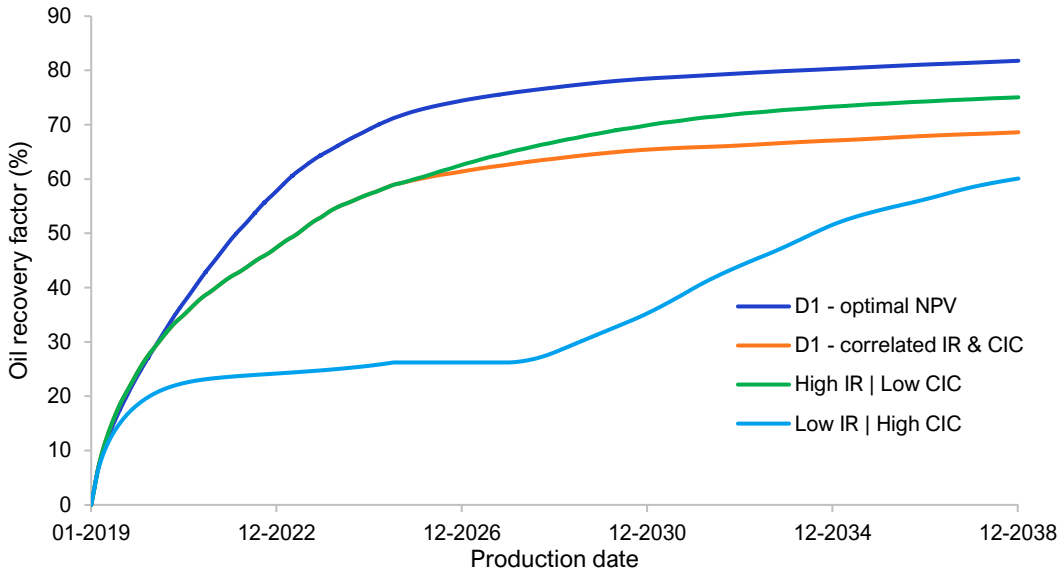

Figure 4.25 Oil recovery factors for sensitivity analysis cases on injection rate and CO_2 injection concentration.

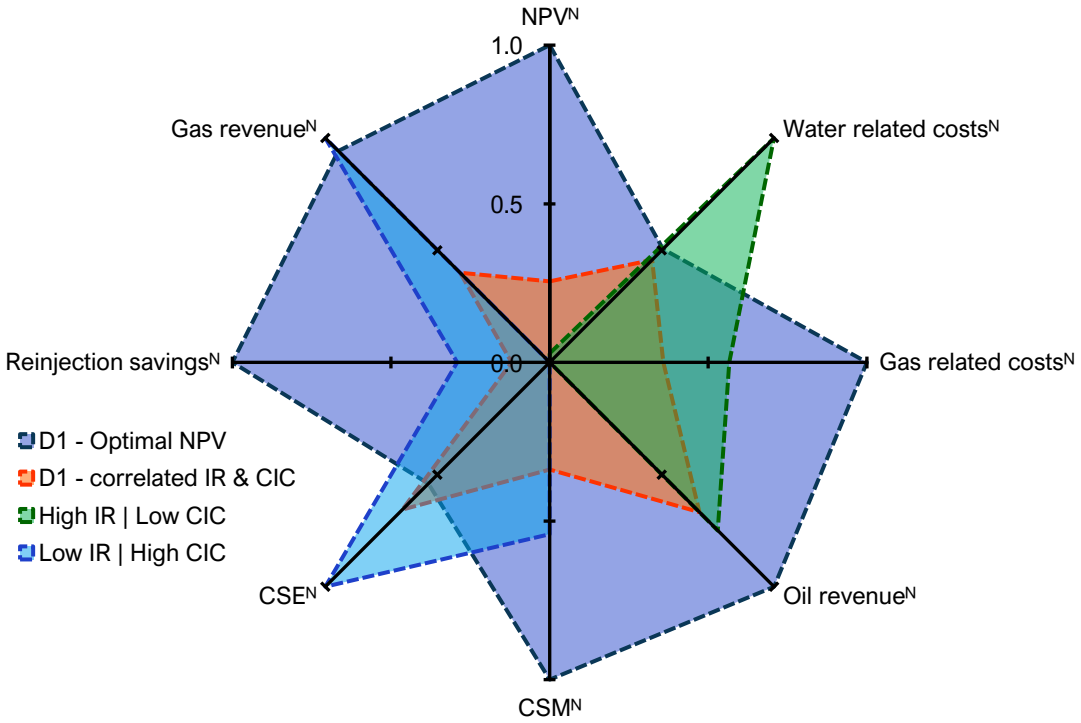

Figure 4.26 Radar chart for main outcomes of sensitivity analysis on injection rate (IR) and CO_2 injection concentration (CIC).

A combination of high injection rate with low CIC meant that large volumes of methane were diverted for injection instead of immediately sold, reducing the NG present revenues. Additionally, the water costs of the 'high IR | low CIC' case were almost as high as its gas costs (USD 13.4 million and USD 15.3 million, respectively), and its CO_2 tax avoidance (reinjection savings) was the lowest of all because of its poor CO_2 storage performance.

Therefore, the version of D1 with inversely correlated IR and CIC was not only more representative of the operational conditions in the BPS, but it also appeared as the best overall alternative if the optimal design could not be maintained. It had a higher CSM and NPV with a lower oil recovery factor compared to the 'high IR | low CIC' case, which makes it a more economically and environmentally advantageous compromise.

4.3.4. Calcite Scaling Risk Assessment

We quantified how the different CO_2-WAG operational strategies examined in this section impacted scaling risk and management. We used the water production rates predicted in our reservoir simulation calculations (shown in Figure 4.27 (a)) with their respective ionic compositions to calculate calcite scale risk at wellbore and surface conditions, following the methodology described in section 3.4. Figure 4.27 (b) shows the calcite saturation ratio at wellbore conditions calculated through ScαleFAST using GEM's resulting wellbore calcium and carbonate molalities.

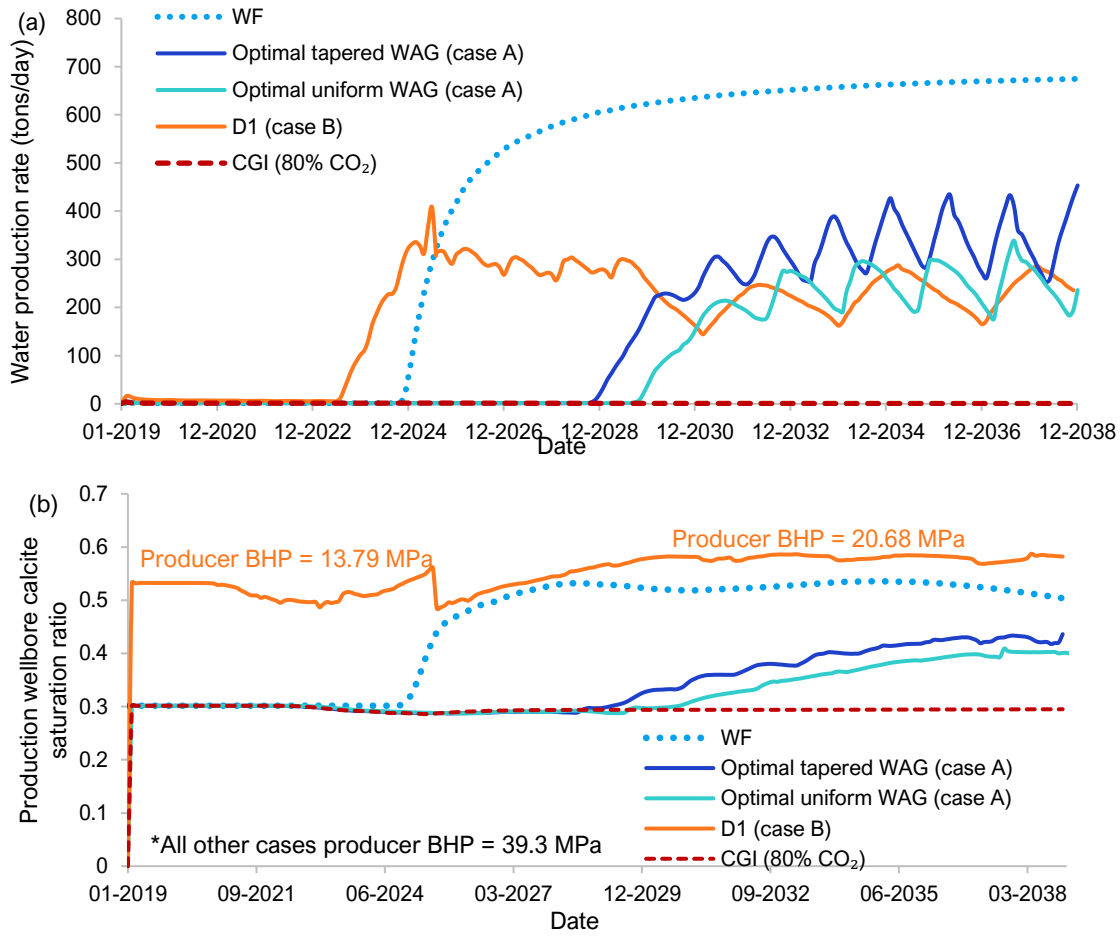

Figure 4.27 Pilot study '3D' optimal designs, waterflood (WF) and continuous CO_2-rich gas injection (CGI) (a) water production rates and (b) production wellbore calcite saturation ratio.

Note that the formation water arriving at the production wellbore is undersaturated in all cases (Figure 4.27 (b)). However, except for case D1, they are in equilibrium with the rock within the grid-blocks adjacent to the production well, as the pressure is above the bubble-point. The only perturbation to the system was a slight pressure drop from the near wellbore grid-blocks to the wellbore itself (at the breakthrough of injection fluids), which would result in a slightly over-saturated brine at wellbore conditions. We believe the discrepancy (initial SR equal to 0.3 instead of 1 for most cases) is due to two factors: (1) GEM's brine molalities are not equilibrated at wellbore conditions, i.e., further speciation from the adjacent grid-blocks to the wellbore was not allowed, and (2) ScαleFAST then calculates the saturation state based on those molalities using a different database. The result was a base level of formation water SR around 0.3, which we can interpreted as being the equilibrium point of the system. SR above that would indicate supersaturation. The relative differences between the cases (qualitative) are robust, but the absolute SR values at wellbore conditions need to be considered with care.

As case D1 was the only strategy with a variable producer BHP below the reservoir fluid's bubble-point, it presented the highest SR and, therefore, the highest calcite scale risk per unit volume of water at the wellbore. Its lower bottom-hole pressure allowed more CO_2 to evolve from the aqueous solution, reducing the solubility of calcite. In the second WAG stage, case D1's producer BHP increased slightly, leading to a decrease in wellbore SR, demonstrating the inverse relationship between pressure and SR in these CO_2 systems. At breakthrough of injected fluids, the SR increased sharply for the WF and gradually for the WAG cases.

Additionally, case D1's low production BHP triggered an earlier water breakthrough, which would lead to premature concerns with scale management. However, its water production rate reached a lower plateau than the other designs (Figure 4.27 (a)), leaving the waterflooding as the strategy with the most severe overall calcite scale risk, as shown below in Figure 4.28.

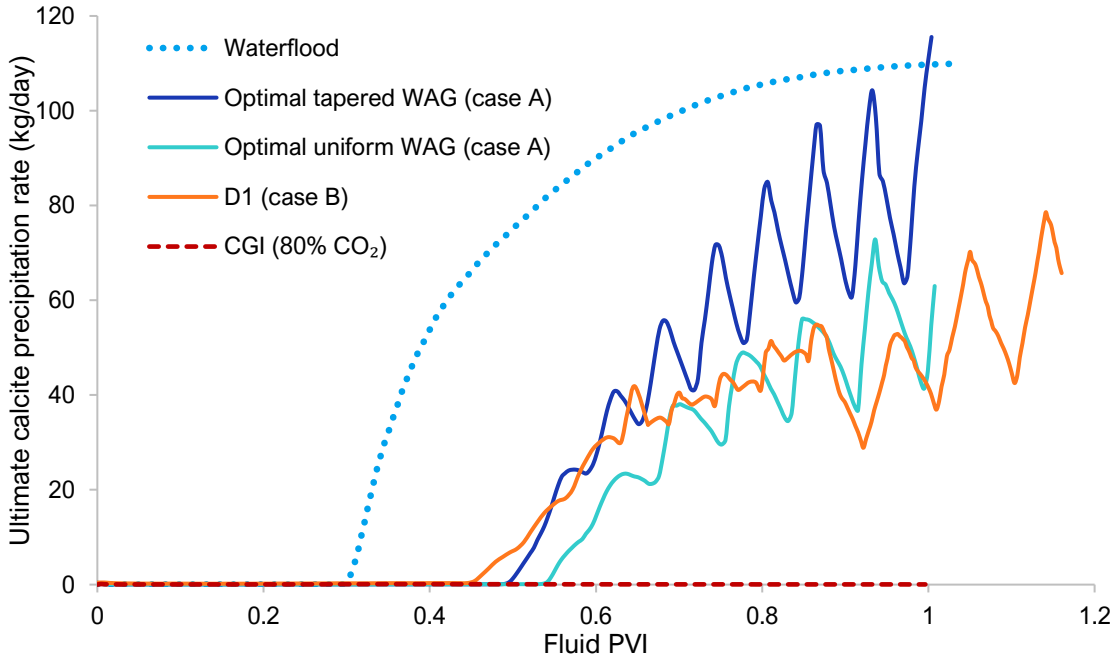

Figure 4.28 Total calcite precipitation rate when produced fluids are flashed from wellbore to surface conditions for the optimal designs of pilot study '3D', waterflood (WF) and continuous CO_2-rich gas injection (CGI).

Interestingly, the uniform optimal WAG of case A showed the lowest overall calcite scale risk, which is another benefit of this design compared to the optimal tapered WAG, as expected from their water production profiles. In general, the water production curves were appropriate predictors of the total calcite precipitation risk behaviour (compare (Figure 4.27 (a) and Figure 4.28). Dry CO_2 injection, for example, as in previous assessments, presented little to no threat of scale precipitation on surface facilities compared to all other designs due to its limited water availability.

4.3.5. Squeeze Treatment Designs

Following the methodology described in section 3.4, we designed squeeze treatment plans for the Pareto designs of 'case B' and the waterflood base-case, since they presented the best performance – environmentally and economically – of all the strategies simulated for pilot '3D'. We estimated the cost of squeeze treatments for each strategy and updated the NPV calculations to include these prevention costs.

According to the water production data of our simulations, we selected four squeeze lifetime targets, as shown in Figure 4.29. Each point of those curves represents a combination of main treatment and over-flush volumes designed to protect the cumulative water volume in question (squeeze target). We used the values of the dashed curve as they

result in the lowest cost to protect a unit of produced water for the duration of its respective squeeze lifetime.

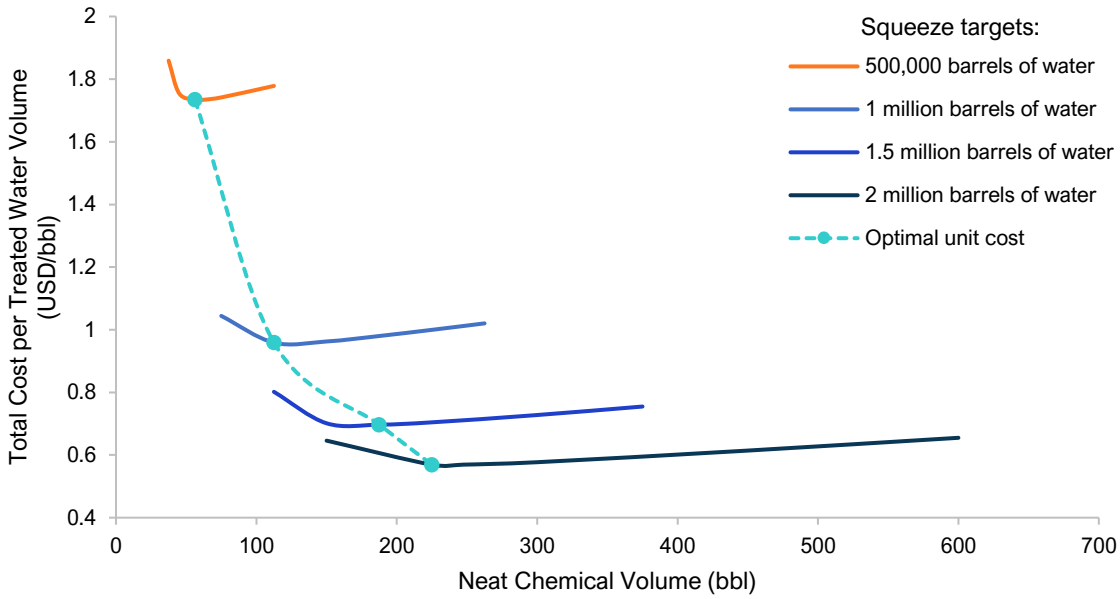

Figure 4.29 Total cost per treated water volume *versus* neat chemical volume for different squeeze life targets (cumulative water protected) calculated using SQUEEZE 12.

Each WAG strategy had an ad hoc pre-emptive squeeze with a target lifetime of 100,000 barrels of water produced. The treatments following the pre-emptive squeeze were designed to progressively target higher volumes of produced water, following the optimal unit cost curve of Figure 4.29.

The distribution of squeeze interventions for the Pareto designs of 'case B' and the waterflood base-case would look like Figure 4.30. A summary of the results can be seen in Table 4.8. The design most densely populated with squeeze treatments was D6 since it had the highest cumulative water production, although its PVI was practically the same as the WF (1.06 PVI *versus* 1.03 PVI respectively). Conversely, the optimal NPV design D1 would need the least number of interventions – seven squeeze treatments were predicted to adequately protect the production well throughout its 20 years lifetime. When WAG was applied, the water fractional flow reduced as production of injected CO_2 limited the total amount of water that came out of the production well. Design D1 promoted this most effectively, resulting in the lowest scale risk of all cases tested.

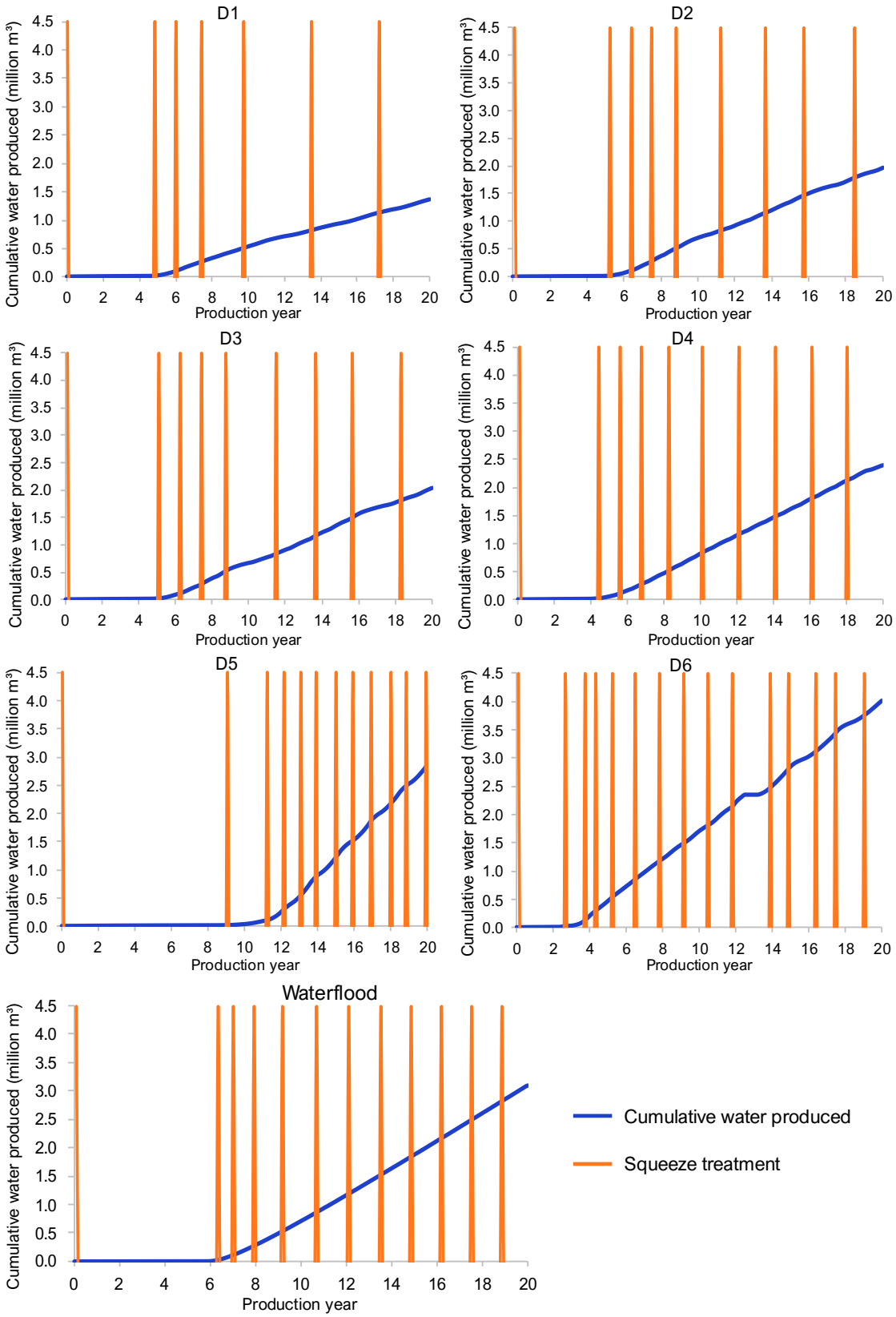

Figure 4.30 Cumulative water produced (blue) and squeeze treatment deployment moment in time (orange) for the production well of all Pareto designs and waterflood base-case.

Table 4.8 Summary of squeeze costs throughout field lifetime for all Pareto designs and waterflooding.

Design	Number of Squeeze Treatments	Total Unit Squeeze Cost (USD/bbl water)	Percentage of Project's NPV spent on Squeeze
D1	7	1.69	0.90%
D2	9	1.46	1.12%
D3	9	1.43	1.14%
D4	10	1.43	1.37%
D5	12	0.89	1.05%
D6	15	1.54	2.72%
Waterflood	12	1.09	2.23%

Note that the fractions of the total NPVs that would be spent on squeeze treatments were small, especially compared to the advantages of preventing scale from happening in the first place. Strategy D1 yielded the lowest absolute cost of squeeze prevention (USD 2.32 million), representing less than 1% of its total NPV. However, design D5 would result in the lowest cost per barrel of water protected, mostly because of its ability to delay the water breakthrough (squeeze costs started later in the production life).

Although the reduction in water production due to the WAG application reduced the number of squeeze treatments necessary, the higher CO_2 concentration in the reservoir will increase the levels of saturation of the produced brine, as demonstrated in the scaling risk assessment. This in turn may require a higher MIC to inhibit deposition, which could increase the scale prevention costs, so it is important to calculate the mass of calcite that could deposit in the system, then use this information to design the squeeze campaign. Here we used the water production as a proxy for scaling risk and kept the MIC constant at what we assumed to be the highest level to cover these variations. This is a robust approach when there is little to no data correlating SI MIC and saturation ratio or calcite deposition mass, and when it is difficult to calculate the latter (water production forecast is more readily available from reservoir simulations).

4.3.6. Conclusions: Pilot Study '3D'

WAG Design Optimisation

1. Including injection rates and producer BHP as decision variables unlocked the potential for optimising NPV. The optimal WAG design found through the methodology increased NPV by 71.5% compared to the base-case waterflooding scenario.
2. The direct correlation between NPV and CSM observed in the pilot study '2D' was also true for the pilot study '3D' case A. However, when the problem was expanded

to allow for optimisation of the injection rates and producer BHP in case B, then a trade-off appeared, and a Pareto front was identified.

3. As also demonstrated in the pilot study '2D', solutions with the highest oil recovery factors do not necessarily yield the maximum cash flow projections.
4. In case A, when only the WAG variables were optimised (WAG ratio and solvent slug-size), uniform and tapered WAG designs lay on the same solution domain for the outcomes of interest (NPV and CSM), appearing to be interchangeable. However, the optimal tapered WAG utilized the CO_2-rich gas more efficiently and showed improved gas mobility control compared to the optimal uniform WAG, which is consistent with the literature and field experience (Zhou et al., 2012). The downside of applying a tapered WAG design over an equivalent uniform one is the former's higher frequency of well switches.
5. In case B, the operational strategy D1 accelerated hydrocarbons production in the early stages of the field lifetime, which greatly benefited NPV, and it also reduced injection and production costs compared to the other designs. However, design D3 represents a strong candidate for best overall design, as it balanced out the economic and storage aspects of the project – there was only a small drop in NPV for a significant gain in CO_2 storage.
6. According to case B results, higher NPV values were generally achieved with low average WAG ratios (between 0.6 and 0.7) and a combination of low production BHPs and injection rates that kept the reservoir pressure close to the MMP of 31 MPa. More specifically, the best performing strategies in terms of NPV presented designs with the following characteristics:
    - No waterflooding period prior to EOR – WAG injection started as soon as possible, as in case A.
    - First WAG stage: maximum values of water and gas injection rates, minimum value of producer BHP and low WAG ratio. This combination promoted a large drawdown in the reservoir and improved microscopic displacement efficiency.
    - Second WAG stage: reduction of both gas and water injection rates, but with a more significant reduction in the former to control the high CO_2 mobility. WAG ratio was kept below 1:1, still favouring more gas injection in relation to water.

- Third WAG stage: water and gas injection rates reached similarly lower levels, combined with a higher WAG ratio. The boost in injected water in relation to gas promoted better macroscopic displacement and pressure maintenance, as well as a constant produced gas profile.
- Efficient use of the reservoir energy: injection of large total CO_2 volumes (allowing for improved miscible displacement), limited total volume of water and low producer BHP, resulting in a low reservoir pressure at abandonment.

7. Applying a lower BHP would likely result in higher costs related to gas lifting, which were not considered in the calculations. Traditionally, BHP is kept higher than the bubble-point at the start of the flood to maintain a two-phase flow and favour the production of the higher fractional flow fluid, oil. Towards the end of production life, after gas breakthrough, a lower BHP will benefit the fluid with lower fractional flow, again oil. The rational of the optimal NPV case, D1, was simply to maintain the reservoir pressure above and close to the MMP.
8. If it is not possible to maintain the optimal design for operational reasons, the best compromise would be to follow the injection rate pattern of the optimal design (in this case, high initial injection gas rate), even if it jeopardized the CO_2 injection purity. The version of case B optimal design D1 with inversely correlated injection rate and CO_2 injection concentration was not only more representative of the operational conditions in the BPS, but it was also more economically and environmentally advantageous compared to the other compromised designs.

Calcite Scale Management

1. In general, the water production curves were appropriate proxies for the behaviour of calcite precipitation rates from wellbore to surface conditions. However, it is important to quantify the saturation levels for the design of scale prevention plans, specifically the MIC of squeeze treatments and continuous injection of scale inhibitor.
2. Dry CO_2 injection, as in previous assessments, presented little to no threat of scale precipitation on surface facilities compared to all other designs due to its limited water availability.
3. Waterflooding a carbonate reservoir that has high CO_2 content in the oil will result

in more severe calcite scale risk than adding more CO_2 into the system, i.e., by applying equivalent CO_2-WAG injection schemes. In waterflooding, the CO_2 in the original oil will supersaturate the injected seawater and the premature water breakthrough will require earlier and more frequent squeeze treatments.

4. Applying a below bubble-point producer BHP allowed more CO_2 to evolve from the aqueous solution, reducing the solubility of calcite and increasing the brine's saturation ratio (scale risk) at the wellbore. However, because part of the CO_2 evolved further downhole, the calcite scale precipitation within the surface facilities was milder than it would have been if the producer BHP were kept above the bubble-point.
5. The low production BHP of design D1 triggered an earlier water breakthrough, which would lead to premature concerns with scale management. However, its water production rate reached a lower plateau than the other designs, reducing its relative risk.
6. A below bubble-point producer BHP can lead to precipitation *before* the perforations, in the near wellbore zone, resulting in productivity loss. Cases with a producer BHP above the reservoir fluid's bubble-point only presented calcite scale risk at the wellbore after breakthrough of injected fluids.
7. The total discounted cost of squeeze treatments was only a fraction of the NPV for each scenario, reinforcing the advantages of scale prevention.
8. WAG schemes reduced water production and, therefore, the number of squeeze treatments necessary during production life. However, the higher CO_2 concentration in the reservoir will increase the levels of saturation of the produced brine, as demonstrate in the scaling risk assessment. This in turn may require a higher MIC to inhibit deposition, which could increase the scale prevention costs. We considered MIC constant in this work, but we acknowledge that it may be appropriate to use the mass of calcite that could deposit in the system to design the squeeze interventions, integrating the workflow even further.

Chapter 5– Field-scale CCUS Multi-Objective Operational Optimisation Studies

Real-world problems often have multiple conflicting interests that need to be considered in decision-making to meet the demands of key players – shareholders, consumers, the company itself, the government. In operational optimisation, there is hardly a single solution that can satisfy the technical constraints and all parties involved. A multi-objective optimization approach may help decision makers to find a set of solutions that fulfil multiple conflicting objectives simultaneously and provide more options to choose from.

Each business has different priorities but, in this work, we conceptualised the field optimisation problem below as dual-objective, aiming at maximizing the economic returns for the oil producer and minimizing the emissions impact of the final product, satisfying flaring regulations and aligning the project with the energy transition. The set of solutions will reflect the interconnected nature of the economic and environmental objectives, which have synergies and trade-offs. For example, as flaring penalties represent a cost, maximizing NPV may also indirectly reduce operational emissions. When injected CO_2 substitutes oil in the porous medium, oil recovery may improve with CO_2 storage, but the cost of transporting, separating, and compressing that CO_2 may drive the value down.

5.1. UNISIM-II Description: Brazilian Pre-salt Benchmark Model

The field-scale optimisation study was performed using the synthetic open-source static model UNISIM-II-D, combined with the production strategy (well placement and well opening schedule) of UNISIM-II-H, which consists of nine horizontal injectors and 11 vertical producers (Correia et al., 2015). The benchmark is a dual-medium model of a fractured carbonate reservoir Type III of microbial origin, partially dolomitized, 3,658 m deep, and geological features that mimics the BPS and Ghawar fields. Further details are shown in Figure 5.1.

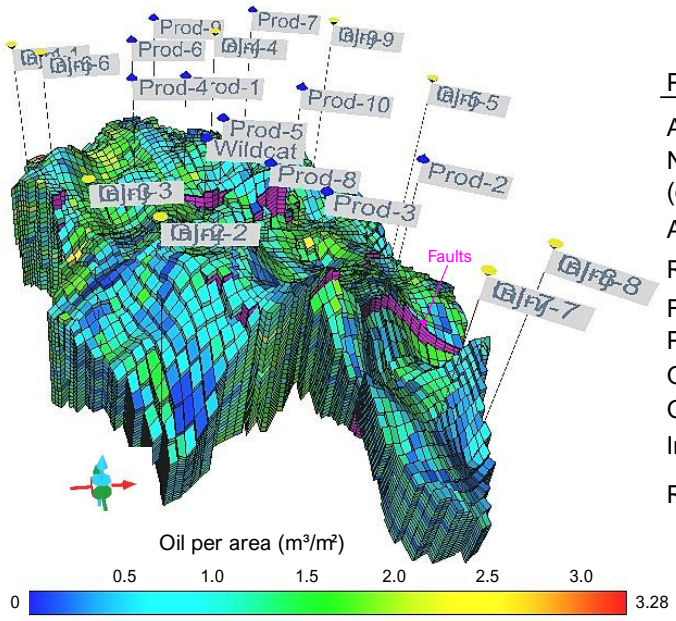

Property	Value
Average grid-cell size, m	100×100×8
Number of active blocks (corner-point)	65,000
Average kv/kh ratio	0.05
Rock mineralogy	80% calcite
Fractures, %PV	12%
Pore volume, rm ³	4.35×10^{8}
OOIP, sm³	2.31×10^{8}
OGIP, sm³	5.12×10^{10}
Initial pressure, MPa	44.13
Reservoir temperature, K	331.9

Figure 5.1 UNISIM-II oil per unit area (m^3/m^2) and well placement (left), and relevant model characteristics (right).

The model has 16 faults, high vertical permeability heterogeneity, and is composed of four facies: (1) grainstone (high energy), (2) packstone (medium energy), both with medium to good reservoir properties, (3) non-reservoir (low energy), with zero net-to-gross and comprising 10% of the reservoir volume, and (4) super-k (5% of reservoir volume), composed of thin high permeability and high porosity layers that are the main flow drivers. Table 5.1 describes their petrophysical characterization.

Table 5.1 Matrix petrophysical characterization of the UNISIM-II reference case (Correia et al., 2015).

	Porosity, fraction (normal distribution)		**Permeability, mD (log-normal distribution)**	
Reservoir facies	Mean	Standard deviation	Mean	Standard deviation
Grainstone	0.2	0.05	200	100
Packstone	0.15	0.05	50	50
Super-k	0.25	0.05	7,000	1,000

The relative permeability curves used are shown in Figure 5.2. The matrix rock is intermediate-wet, and there is so little capillary pressure between the fluids when they flow through the super-k and fractures that their relative permeability curves are almost straight lines between the end points (c and d).

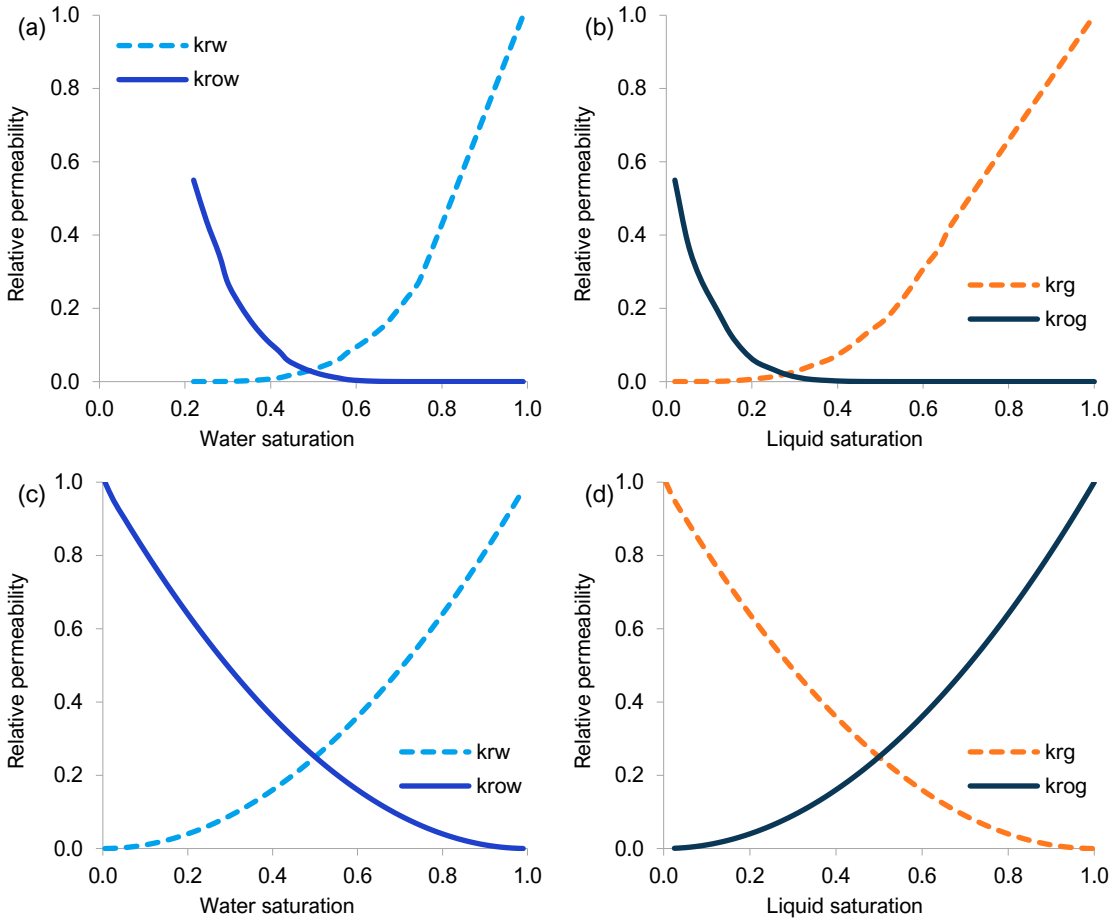

Figure 5.2 UNISIM-II water-oil and gas-oil relative permeability curves for matrix rock (a and b) and super-k and fractures (c and d).

For comparison, we calculated a waterflood (WF) base-case, where voidage replacement was applied. The injection wells were set to not surpass a maximum surface rate of 6,000 sm^3/d and a maximum bottom-hole pressure (BHP) of 68.95 MPa, just below the fracture pressure. The BHPs of all producers were fixed at 31.03 MPa, which is the estimated minimal miscibility pressure of CO_2 in relation to the reservoir oil. We assumed that the platform operates 365 days per year, and it is limited by the operational restrictions of a standard BPS FPSO (de Andrade et al., 2015), according to Table 5.2. A schematic view of the hypothetical system modelled is shown in Figure 5.3.

Table 5.2 Standard BPS FPSO operational constraints.

Platform restrictions	Oil (STB/day)	Gas (sm^3/day)	Water (STB/day)
Production	150,000	6,000,000	120,000
Injection/compression	-	6,000,000	180,000
Export pipeline	-	6,000,000	-

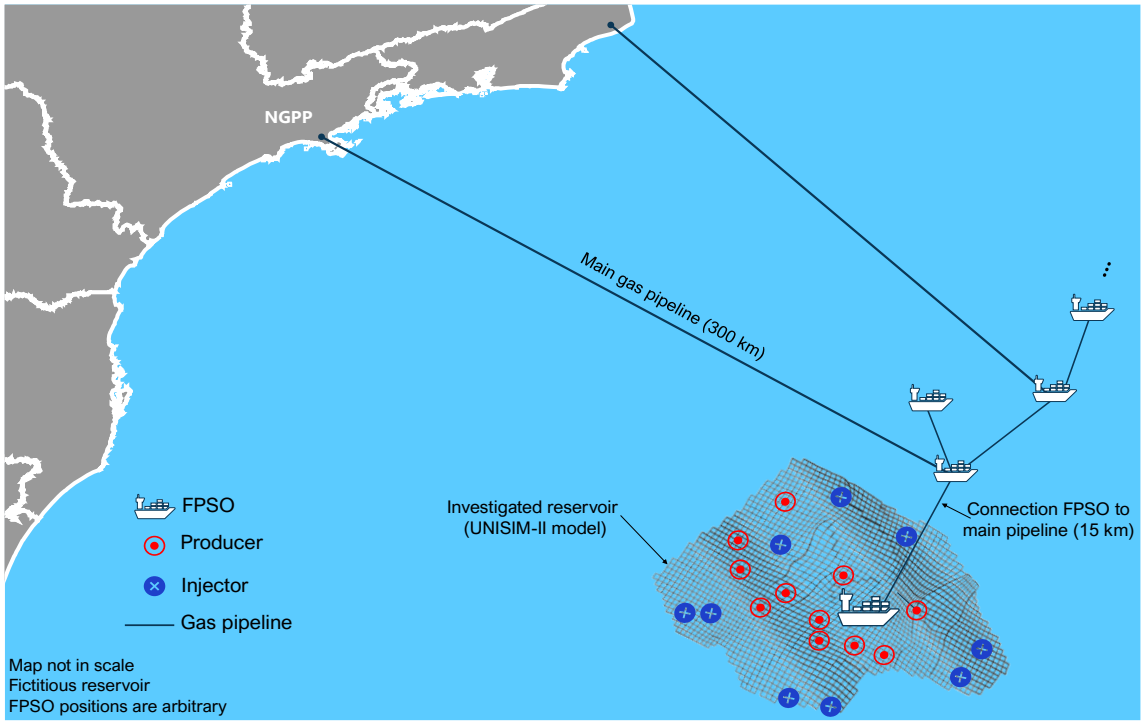

Figure 5.3 Hypothetical CCUS project modelled in this chapter based on the Brazilian Pre-salt fields. The main gas pipelines to shore are rigid and the connections between FPSOs are flexible. Flexible lines can be installed for natural gas and CO_2-rich gas transport.

All assumptions described in Chapter 3 remain (PVT, geochemical model, economic model, etc.), except for the water three-phase relative permeability curve, which here we are considering as being the water two-phase curve multiplied by 0.8 (in the pilot studies it was multiplied by 0.5). Additionally, even though we acknowledge this may affect the optimisation results, we are including the geochemistry in specific cases as a post-optimisation step, due to the prohibitive computational times involved in modelling reactions in this large, fractured model.

From 30-Sep-2016, UNISIM-II-D has 516 days of 'historical' production data of one vertical producer – Wildcat – as part of an EWT. Field development – drilling, completion, well opening, installation of facilities – lasted until 30-Sep-2021, when forecast commenced, until production ceased in 30-Sep-2045 (30 years of field life). For accurate allocation of cash flow terms in time, we detail in Table 5.3 the field development and production timeline.

Table 5.3 Field timeline description (adapted from Santos and Schiozer (2018)).

Time (days)	Date	Field Timeline - events description	Duration (months)
0	2015-09-30	Exploration begins. Present day (for NPV calculation).	12
366	2016-09-30	Wildcat starts production (EWT). Start oil export.	6
547	2017-03-30	D&C Prod-5.	3
578	2017-04-30	D&C Prod-2.	3
639	2017-06-30	D&C Prod-8. Pre-emptive Squeeze Prod-5.	3
669	2017-07-30	D&C Prod-9. Pre-emptive Squeeze Prod-2.	3
731	2017-09-30	D&C Prod-10. Pre-emptive Squeeze Prod-8.	3
761	2017-10-30	D&C Prod-4. Pre-emptive Squeeze Prod-9.	3
822	2017-12-30	D&C Prod-6. Pre-emptive Squeeze Prod-10.	3
853	2018-01-30	D&C Prod-3. Pre-emptive Squeeze Prod-4.	3
882	2018-02-28	Drilling vessel disconnection. End Wildcat history.	1
912	2018-03-30	D&C Prod-1. Pre-emptive Squeeze Prod-6.	3
943	2018-04-30	D&C Inj-5. Pre-emptive Squeeze Prod-3.	3
1004	2018-06-30	D&C Prod-7. Pre-emptive Squeeze Prod-1.	3
1034	2018-07-30	D&C Inj-9.	3
1096	2018-09-30	D&C Inj-4.	3
1126	2018-10-30	D&C Inj-6.	3
1187	2018-12-30	D&C Inj-2.	3
1218	2019-01-30	D&C Inj7.	3
1247	2019-02-28	Submarine infrastructure installation. FPSO anchoring.	4
1277	2019-03-30	D&C Inj-8.	3
1308	2019-04-30	D&C Inj-3. Gas pipeline installation (15 km).	3 + 4
1338	2019-05-30	CO_2 membranes and SRU installation.	
1369	2019-06-30	D&C Inj-1.	3
1399	2019-07-30	Prod-5 to FPSO connection. Compressors' installation.	1
1430	2019-08-30	Prod-8 connection to FPSO. Open Prod-5.	1
1461	2019-09-30	Prod-9 to FPSO connection. Open Prod-8.	1
1491	2019-10-30	Prod-4 to FPSO connection. Open Prod-9.	1
1522	2019-11-30	Prod-10 to FPSO connection. Open Prod-4.	1
1552	2019-12-30	Wildcat to FPSO connection. Pre-emptive Squeeze Wildcat. Open Prod-10.	1
1583	2020-01-30	Prod-6 to FPSO connection. Open Wildcat.	1
1613	2020-02-29	Inj-9 to FPSO connection. Open Prod-6.	1
1643	2020-03-30	Inj-3 to FPSO connection. Open Inj-9 (injection starts).	1
1674	2020-04-30	Inj-5 to FPSO connection. Open Inj-3.	1
1704	2020-05-30	Prod-7 to FPSO connection. Open Inj-5.	1
1735	2020-06-30	Inj-1 to FPSO connection. Open Prod-7.	1
1765	2020-07-30	Inj-4 to FPSO connection. Open Inj-1.	1
1796	2020-08-30	Inj-6 to FPSO connection. Open Inj-4.	1
1827	2020-09-30	Prod-2 to FPSO connection. Open Inj-6.	1
1857	2020-10-30	Inj-7 to FPSO connection. Open Prod-2.	1
1888	2020-11-30	Inj-8 to FPSO connection. Open Inj-7.	1
1918	2020-12-30	Prod-3 to FPSO connection. Open Inj-8.	1
1949	2021-01-30	Inj-2 to FPSO connection. Open Prod-3.	1
1978	2021-02-28	Prod-1 to FPSO connection. Open Inj-2.	1
2008	2021-03-30	Open Prod-1.	
2192	2021-09-30	Production forecast starts (EOR).	
10958	2045-09-30	Abandonment. Final simulation time.	

In this chapter, we investigate two major scenarios:

1. *CO_2 recycle scenario*: the CO_2-rich gas, a by-product of the membrane separation system, is reinjected into the reservoir for EOR. We would like to know which injection wells should receive the CO_2 and how (WAG design).
2. *CO_2 import scenario*: the reinjection gas consists of the recycled gas from the field itself plus the CO_2 concentrated stream of a neighbour field. We would like to know what volume of gas should be imported, which fraction of the produced gas should be reinjected, which wells should receive the injection gas and how (WAG design).

A third scenario where the *hydrocarbon gas* is recycled could be investigated and we suggest it for future work.

Calcite Scale Management

For flow assurance purposes, we implemented the workflow described in section 3.4 of this thesis to estimate the number and cost of scale inhibitor squeeze treatments necessary to protect each production well from calcium carbonate scale damage.

We started by finding optimised squeeze designs for several target squeeze lifetimes that were representative of the water production levels of this field. Table 5.4 shows the volumes of main scale inhibitor treatment and overflush that yielded the lowest cost per volume of brine treated, for each production well (columns) and each squeeze lifetime target (rows).

Table 5.4 Optimised volumes ($\times 10^3$ m^3) of main treatment (V_{MT}) and overflush (V_{OF}) for different squeeze lifetimes or cumulative water protected ($\times 10^3$ m^3) for each production well.

Squeeze	Prod-1	Prod-2	Prod-3	Prod-4	Prod-5	Prod-6	Prod-7	Prod-8	Prod-9	Prod-10	Wildcat
life target	V_{MT} V_{OF}	V_{MT} V_{OF}	V_{MT} V_{OF}	V_{MT} V_{OF}	V_{MT} V_{OF}	V_{MT} V_{OF}	V_{MT} V_{OF}	V_{MT} V_{OF}	V_{MT} V_{OF}	V_{MT} V_{OF}	V_{MT} V_{OF}
50	0.04 0.16	0.04 0.14	0.08 0.11	0.04 0.14	0.06 0.11	0.06 0.15	0.06 0.10	0.06 0.14	0.06 0.12	0.06 0.08	0.04 0.14
150	0.14 0.57	0.14 0.46	0.14 0.66	0.14 0.50	0.14 0.60	0.14 0.72	0.14 0.52	0.14 0.65	0.14 0.61	0.21 0.35	0.14 0.49
300	0.28 1.28	0.32 0.93	0.32 1.35	0.28 1.12	0.28 1.32	0.28 1.58	0.41 0.90	0.28 1.47	0.28 1.31	0.28 1.05	0.28 1.05
500	0.56 2.02	0.56 1.52	0.56 2.22	0.56 1.74	0.56 2.12	0.56 2.51	0.56 1.82	0.56 2.25	0.56 2.08	0.56 1.64	0.49 1.81
700	0.78 2.97	0.78 2.23	0.81 3.17	0.78 2.59	0.78 3.10	0.78 3.63	0.78 2.64	0.85 3.12	0.78 3.09	0.78 2.47	0.70 2.67

Next, we coupled this look-up table with the reservoir simulation forecasts, to calculate the minimum number of squeeze treatments per well and their costs, which changes as we optimise the production strategies. Since scale management cost is included in the NPV calculations, we indirectly optimised the calcite scale risk: to a certain extent, the search algorithm prioritized strategies that reduced the scale management costs and boosted the NPV. The reader will find results from the application of this method in the next field studies.

5.2. 'CO_2 Recycle' Scenario

In this scenario, our objective is to find the most cost-effective way to mitigate (ideally eliminate) gas flaring on the platform during the forecast period, by capturing the CO_2 from the produced gas and reinjecting it into the reservoir. We applied a multi-objective optimisation approach, with *Net Present Value (NPV) and well-to-wheels (WTW) emissions as objective functions*. This means the algorithm (Particle Swarm Optimisation) searched for CO_2 reinjection strategies that yielded better economics and lower carbon footprint simultaneously. We considered *total* emissions to capture the trade-offs between producing more oil and gas for revenue purposes, and limiting it for environmental reasons. Considering direct operational emissions or CO_2 storage alone would be insufficient to represent this balance. WTW emissions were estimated according to the methodology described in section 3.8 of this thesis.

5.2.1. Assumptions

In this 'CO_2 recycle' study, the CO_2 utilized for injection comes from the production wells within the platform and is continuously recycled in a closed-loop process. As detailed in Chapter 2, the CO_2 is captured by membrane permeation on the FPSO topside, designed to yield a purified natural gas (mostly composed of N_2-C_1, with no more than 3% v/v of CO_2) that can be both commercialized and/or used in the platform's gas turbines to generate power. Our economic model assumes that the wet sales gas sent to the shore is further treated at a Natural Gas Processing Plant (NGPP) onshore, where the heavier ends (pseudo-components C_2-C_4 and C_{5+}) are recovered with a 95% efficiency (ε).

Average fuel gas consumption of a typical BPS FPSO is reported to be around 10 to 11% of the produced gas (MME, 2020, ANP et al., 2020, EPE and MME, 2014). We increased the value to 14% to include leaks and gas-lift usage. From the remaining gas, 80% is sent to sales through a subsea gas pipeline, the rest being reinjected for EOR (17.2% of the total gas produced). The production gas breakdown applied is compatible with the gas destination of a typical BPS field with 10% CO_2 content in the associated gas (Capeleiro Pinto et al., 2014).

As there is around 10% m/m CO_2 concentration in the separator, the CO_2-rich gas captured is only enough for one out of the nine injectors. As the FPSO has no gas storage capacity and all the recycled gas must be reinjected, the WAG design includes two injectors to ensure

no flaring during any water half-cycle. The pair has mirrored WAG ratios - when one well injects water, the other injects gas and vice-versa. Gas reinjection rates were constrained to a maximum of 2×10^6 sm^3/d per well, which was equivalent to the injection water rates at reservoir conditions (gas is injected in a super-critical state). The WAG pairing approach was also adopted by Torrez Camacho (2017), although the author tested pairs of injectors with a fixed WAG design (36 possibilities), then optimised the WAG variables.

We investigated three types of CO_2-EOR methods: (1) continuous CO_2-rich gas injection (CGI); (2) uniform WAG, where CO_2 and brine are injected in an alternating manner, with the same design (water and gas half-cycle lengths) throughout the forecast period; and (3) tapered WAG, where the WAG design can change over time, responding to the reservoir performance.

For the CGI study, the only optimisation variable was which injection well should receive the recycled CO_2, therefore, only nine cases were simulated. For the WAG studies, the optimisation variables were the reinjection well pair, and the gas and water half-cycle durations. Additionally, in the tapered WAG cases, we allowed the gas and water half-cycle durations to change on two occasions, meaning each simulation could have three distinct WAG stages in the same well pair. The number of full WAG cycles per stage was also a variable in the tapered study. The resulting WAG ratio was considered a secondary resulting parameter rather than a variable because the gas injection rates were dependent on the production rates, making the WAG ratio hard to fix. Table 5.5 shows the variable domains, for the WAG studies.

Table 5.5 'CO_2 recycle' optimisation design variables, their respective domains, and discrete increments.

WAG design parameter	Low	High	Increments
Gas and water half-slug, days	90	360	30
Number of full cycles per stage (tapered only)	2	20	2
Injection WAG pair	Combination of any two distinct wells from the nine candidates		

5.2.2. Results and Discussion

First, it is worth mentioning that the extreme case of complete flaring (not monetizing the gas and focusing on the oil production exclusively) would not financially make sense in this field. According to our calculations, flaring all the associated gas and selling only the oil would yield a negative NPV, despite the investment cost savings (simpler platforms with no gas separation nor transport infrastructure). Additionally, the operational emissions of such

a scenario would be enormous: 6.8 times higher than the waterflood base-case with commercialization of the gas and flaring of only the CO_2-rich gas.

Figure 5.4 shows all cases simulated according to the two objective functions, both in relation to the waterflooding base-case. The NPV response to the variations in recycling designs was far more prominent than the emissions changes. Ideally, the best results would be in quadrant II (improved NPV and reduced WTW emissions), but the optimisation results showed a direct correlation between the two objectives: the higher the efficiency of the EOR strategy, the more hydrocarbons were produced, the higher the revenues *and* total emissions. As this was a multi-objective optimisation procedure, a Pareto frontier was identified, but it showed solely a trade-off between the objectives. This direct relationship reinforces the idea that additional emissions from the extra hydrocarbons produced due to EOR will overshadow the emissions abatement from the flaring avoidance. In fact, the WAG case with the highest NPV (called 'max NPV) reduced its E&P emissions by 43.5% with its CCUS strategy, but the 9% increase in its end-use emissions was enough to increase total WTW emissions balance by 5% compared to the WF base-case (see Figure 5.5).

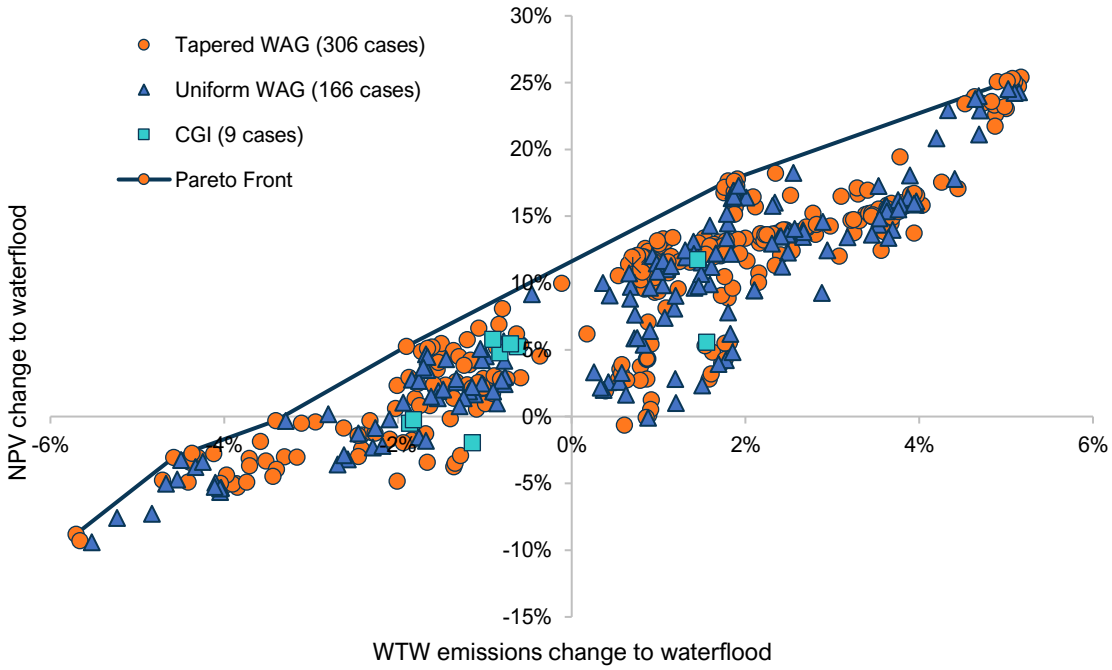

Figure 5.4 Change in relation to the waterflood base-case of Net Present Value and well-to-wheels emissions for all CCUS operational strategies simulated in the field 'CO_2 recycle' optimisation study.

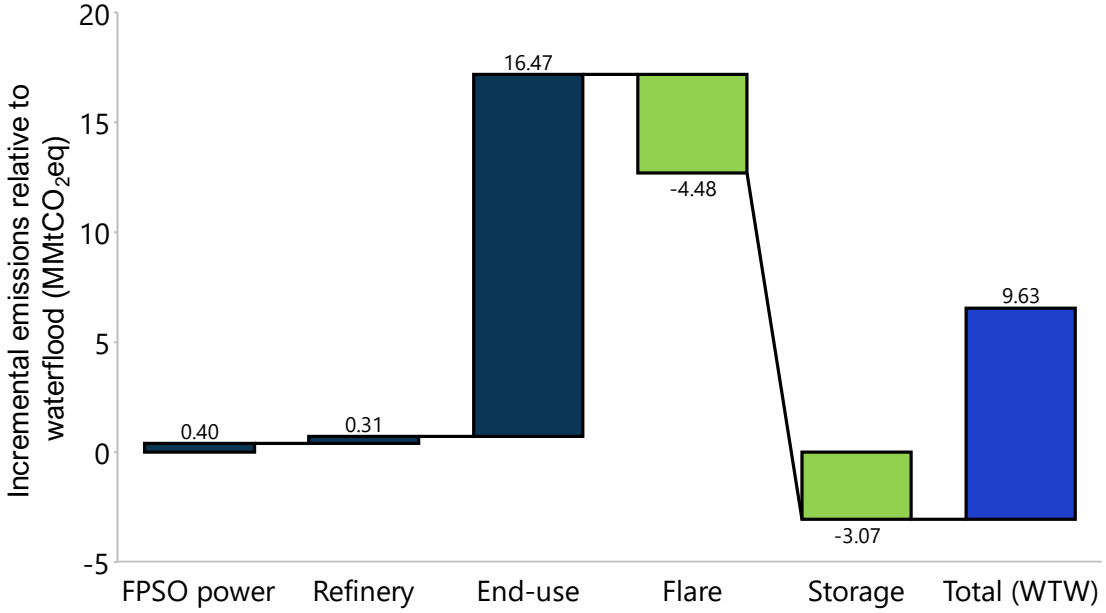

Figure 5.5. 'Max NPV' tapered WAG incremental emissions balance in relation to the waterflood base-case by sector.

Nevertheless, all 'CO_2 recycle' CCUS scenarios, regardless of their total emissions, yielded a *less carbon-intensive* BOE compared to the WF base-case – a 3.4% average reduction. If this lower carbon footprint oil is simply meeting an existing demand – i.e., not increasing overall consumption by reducing the oil price - but rather displacing market share from a more carbon-intensive oil, total emissions could potentially reduce.

Because of the sheer trade-off between the objectives and uniform carbon intensity amongst designs, it makes sense to differentiate them in economic terms. There were a few scenarios close to the maximum NPV of the search space, but we will take a closer look at the highest overall NPV ('max NPV'). It was a tapered WAG, and its design is summarized in Table 5.6. Figure 5.6 shows the breakdown of the methane and CO_2 destination if this operational design were applied. The achieved CO_2 injection concentrations can be seen in Figure 5.7.

Table 5.6 'Max NPV' recycle WAG design parameters generated by the PSO algorithm.

	Injector 1			Injector 6		
WAG stage →	**S1**	**S2**	**S3**	**S1**	**S2**	**S3**
Water half-cycle (days)	90	90	240	90	90	90
Gas half-cycle (days)	90	90	90	90	90	240
Number of cycles	2	2	Rest of the time	2	2	Rest of the time
Average WAG ratio (rm^3 water/rm^3 gas)	3.72	2.75	4.10	3.94	4.07	2.51

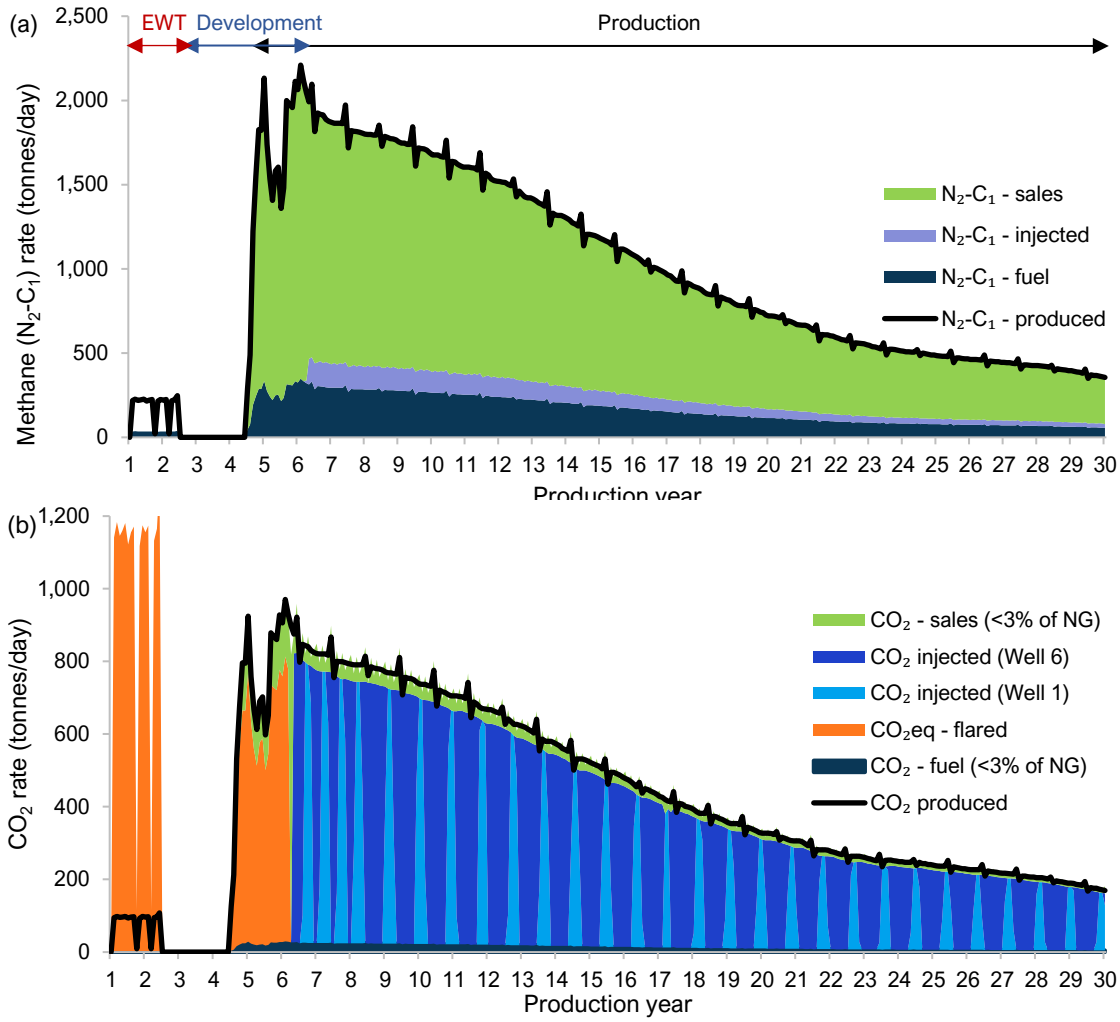

Figure 5.6. 'Max NPV' tapered WAG design gas production destination (monthly rates) for (a) N_2-C_1 component and (b) CO_2.

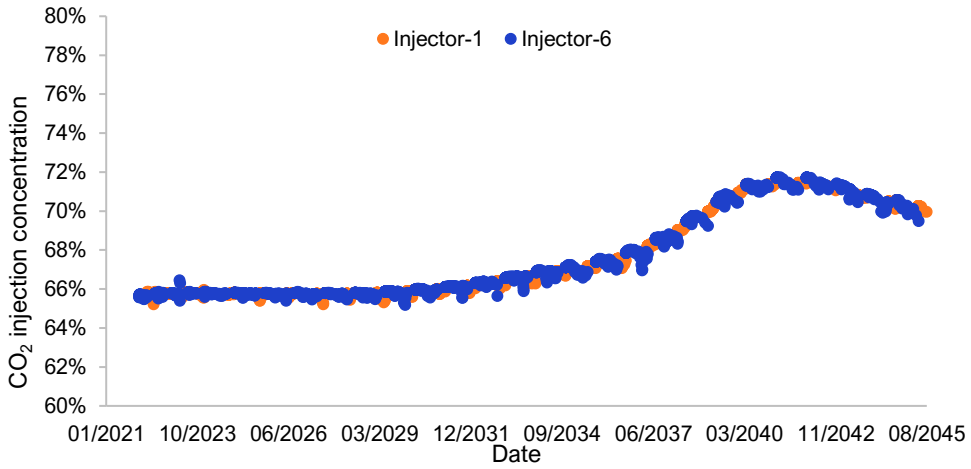

Figure 5.7 Recycled CO_2 injection concentration achieved during the 'max NPV' tapered WAG.

According to Figure 5.6, the period with highest emissions was during the EWT, before the gas separation and export capabilities were installed, and before CO_2 reinjection commenced. During the forecasted period, however, most of the methane was sold or

used for fuel and most of the CO_2 would be re-recycled for EOR. The 'max NPV' tapered WAG design was able to reinject 90.7% w/w of all the CO_2 produced during the forecasted period in a closed loop into injection wells '1' and '6' (total CO_2 injected was equivalent to 1.86% HCPV). The amount of CO_2 that the operator would avoid flaring (4.48 $MMtCO_2eq$) was comparable to removing 32,452 passenger cars from the roads (EPA, 2018).

Injector 1 lost injectivity during its WAG cycles, with water injection rates around 1,500 sm^3/d (rather than the 6,000 sm^3/d it was meant to inject), possibly due to relative permeability hysteresis effects. This explains the differences in average WAG ratio between the two injectors during stages S1 and S2, when the slug durations were the same (see Table 5.6). Injector 1 did not achieve maximum injectivity in the WF case either, operating at rates of around 4,000 m^3/d. However, all cases simulated injected the same cumulative volumes of water (equivalent to 59.4% PV or 73.2% HCPV), because we assumed water voidage replacement in the simulations. The overall average WAG ratio achieved in both injection wells was equal to 3.5.

The savings in flaring penalties reached almost 91% - around 179 million USD reduction. We also estimated that the abatement cost of this CCUS strategy would be *negative* 94.8 USD/tCO_2 abated over the lifetime of the asset. Abatement cost is the incremental cost of a lower-emission technology (in this case, the 'CO_2 recycle' WAG) compared to the case without it (waterflooding), including the extra investment costs, operating costs, and possible revenues or savings generated by use of the lower-carbon alternative (Nauclér and Enkvist, 2009). Thus, a negative abatement cost suggests financial benefit from the flaring avoidance and from the extra hydrocarbon recovery, even with the additional capital intensity of USD 45 per tonne of CO_2 avoided.

The injected CO_2 necessary to produce one incremental barrel of oil was 56 $kgCO_2/incBOE$ for the 'max NPV' case, which is a relatively low CO_2 gross utilization ratio (Núñez-López et al., 2019), but this is because the CO_2 supply was limited to the field itself. To put this into perspective, each incremental barrel would emit 201 $kgCO_2/incBOE$ from 'wells to wheels' - still a long way to carbon neutrality. However, there is a vast potential to scale-up the CO_2 stored - e.g., in fields with higher initial CO_2 content or with CO_2 importation, either from neighbour platforms or from anthropogenic sources onshore, if a pipeline infrastructure is put in place.

Care should be taken on the CO_2 storage quantification. If we assume the CO_2 material balance in the reservoir is a simple account of what enters and leaves the system (IPCC, 2005), disregarding the CO_2 initially in the reservoir, CO_2 storage would be *negative* since some of the CO_2 produced will end up in the oil and gas sold and there are no CO_2 external sources. The best-case scenario would yield zero CO_2 storage, meaning all the CO_2 produced was reinjected. Thus, the negative CO_2 storage of the 'CO_2 recycle' designs meant some of the CO_2 produced did not make its way back to the reservoir, ending up on a flare or combustion engine. These emissions are already included in our calculations, so negative storage values were disregarded to avoid double counting.

The 'max NPV' design was the best performing CCUS strategy in our calculations, but it appeared vulnerable to oil price fluctuations (see Figure 5.8). Additionally, the marginal cost of this design (or incremental cost to produce one extra barrel of oil equivalent) was 5 USD/BOE, but with an 8.4% higher return per BOE in relation to the WF reference case. Its break-even oil price - around 39 USD/STB - was still in alignment with deep-water projects.

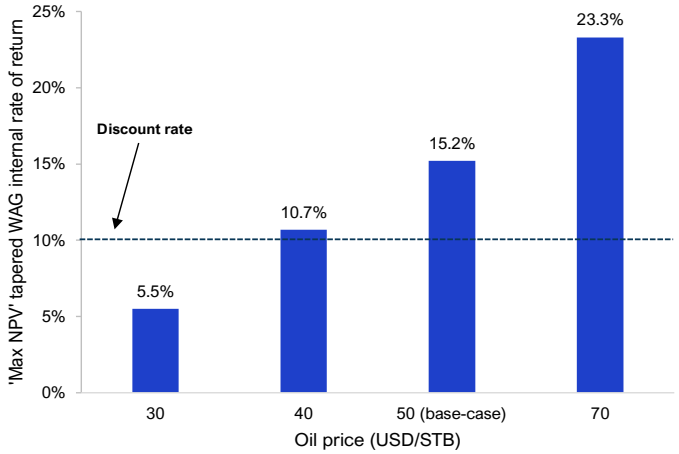

Figure 5.8. 'Max NPV' tapered WAG internal rate of return per long-term oil price assumption.

Finally, in terms of calcite scale management, Figure 5.9 shows the incremental number of squeeze treatments that each producer would need under the 'max NPV' WAG scheme as opposed to WF. A negative number represents a reduction in number of interventions. The plot also displays the NPV change that each well would experience (disregarding gas production, for simplicity) if the 'max NPV' WAG design were applied. Note how most wells substantially improve their productivity, especially 'Prod-6', the closest to the WAG injection pair. Under WF, this well required numerous interventions - roughly every 3 months- but with the WAG scheme, oil production was favoured over water. Although some wells had their water production increased and needed more interventions, the total number of

squeeze treatments was lower in the optimal tapered WAG (182 against 187 interventions for the WF), with a drop of 13% in total squeeze costs and of 8% in the cost to protect a barrel of water produced.

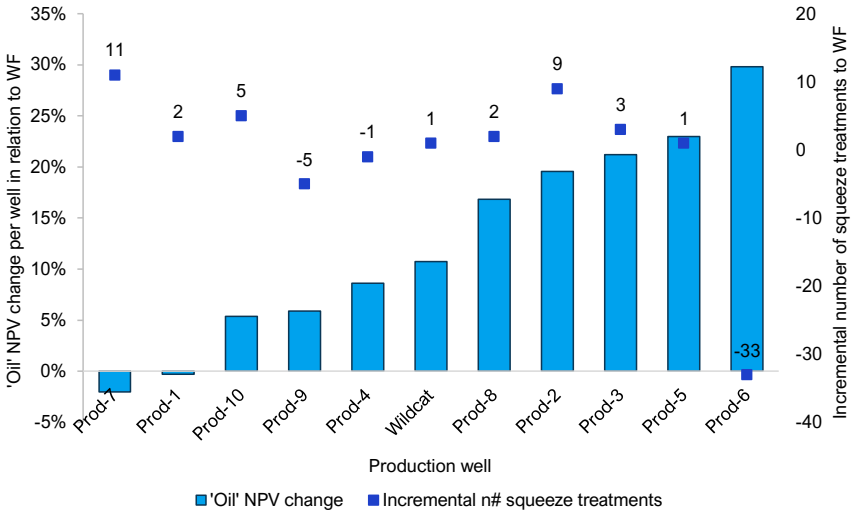

Figure 5.9 Net Present Value (considering oil only) change per production well and incremental number of squeeze treatments in relation to the waterflood base-case.

5.2.3. Conclusions: 'CO₂ Recycle' Scenario

In this section, we applied the research methodology to investigate the consequences of recycling the natural CO_2 of an offshore carbonate reservoir for EOR and storage. The objective was to find operational strategies that achieved high economic returns, utilized the CO_2 produced sustainably (avoiding flaring) and prevented calcite scale hazards.

Our results demonstrated that the total carbon intensity when CO_2-EOR is applied can be lower than the usual waterflood, due to the reduction in flaring emissions and increased efficiency of hydrocarbon recovery. We have seen that complete flaring of the produced gas is both financially and environmentally harmful, yielding negative NPV and enormous operational emissions. Investing in gas export infrastructure is essential in this context.

All simulated CCUS 'CO_2 recycle' scenarios yielded a 3.4% lower carbon footprint oil, with 43.5% decrease in E&P emissions and, in the best scenarios, a 25% increase in NPV, even if the WTW emissions did not reduce. Absolute WTW emissions varied slightly across WAG scenarios (±6% around the waterflood base-case), but carbon intensity was practically the same. This limitation on carbon intensity reduction was due to the restricted volumes of CO_2 available for reinjection. In the next section we will explore a scenario with higher CO_2 availability.

Results on the internal rate of return for the WAG design with highest NPV suggested that large upfront capital investments and a prospect of low oil prices as climate change concerns grow may represent significant hurdles to offshore CCUS in the BPS. Finally, the tapered WAG design also resulted in fewer squeeze interventions and a lower cost of calcite scale management.

In summary, this study showed how recycling the produced CO_2-rich gas and designing the WAG slugs can significantly improve the economics, CO_2 storage and scale management of CCUS operations using the CO_2 from the associated gas. It also provided valuable insights into the simulation and co-optimisation of these projects when multiple objectives are at stake.

5.3. 'CO_2 Import' Scenario

In this section, we consider the possibility of connecting the FPSO under investigation to a neighbouring one, so that the CO_2-rich gas supply of the former is boosted. To the best of our knowledge, this scenario has not been applied in the BPS to date. However, it is technically feasible given many platforms are connected to each other through flexible natural gas pipelines that gather the sales gas to the sparse main pipelines.

5.3.1. Assumptions

Given the high variability in CO_2 concentrations in the solution gas across the BPS reservoirs, the amount of recyclable gas available is not sufficient to effectively gasflood all fields. Additionally, not every reservoir in the cluster will be suitable for miscible gas displacement. Sections with high potential for success should be screened and a hub-and-spoke system put in place to deliver CO_2 to these hotspots. In that way, only a few platforms need to be equipped with compressors and other resources necessary to perform CO_2-WAG, although platforms that will act as CO_2 providers will still need CO_2 separation facilities and a pipeline connection to the CO_2 receivers.

We assumed that, alongside the NG flexible line that connects the FPSO to the main export pipeline, the operator would install an additional flexible line to import the CO_2-rich gas of a neighbour field with higher CO_2 content (15 km away). The maximum capacity of this CO_2 flexible line was considered as 6×10^6 sm^3/d, the same as the natural gas line. As the CO_2 supply is dependent on the production profile, CO_2 availability will likely reach a peak and then decline over time. Assuming the initial CO_2 concentration in the solution gas of this

neighbour field is 40% m/m, the CO_2-rich gas imported for injection would have a CO_2 concentration of 69%, the rest being methane (ANP et al., 2020). This is not a highly pure CO_2 stream, so there are implications around the non-trivial amount of methane imported. In the following, we discuss the adaptations we have made in the economic model to account for them.

Since the gas is brought from outside the system's boundary, it is important to put a 'price' on the gas imported, so as the algorithm is not biased towards importing methane (a valuable commodity) and considers all the financial benefits of storing the extra CO_2. If both fields were operated by the same company, the financial benefit of the endeavour would be: (1) the incremental oil recovered and (2) the *avoided* flaring penalties. As our model focuses on the CO_2-receiving field only, benefit (1) is already embedded, but benefit (2) should be included as if the CO_2-receiving field is providing a *service* to the CO_2-donating field – storing the CO_2-rich gas that would otherwise be a burden. Therefore, we assumed that imported CO_2 volumes have a *positive* value on the NPV of the CO_2-receiving field (positive 40 USD/tCO_2) and imported methane needs to be paid for, to account for the opportunity cost of the gas-donating field. This cost was considered as the market price of natural gas (*negative* 13 USD/MMBtu or 647 USD per tonne of methane), but this was a conservative assumption, given the methane imported is not ready for sales. It is worth mentioning that importing the CO_2 does not guarantee its storage, but if the CO_2-receiving field fails to safely store the CO_2, an emission penalty is paid to the government.

Finally, the separation cost of the CO_2-rich stream in the neighbour platform is borne by the CO_2 provider, but the operational cost of importing the CO_2 through the flexible line is paid by the CO_2-receiving field (review economic model in section 3.7).

We again applied a multi-objective optimisation approach, with Net Present Value (NPV) as the financial-driven objective, but with well-to-wheels (WTW) carbon *intensity* as the environmentally focused goal. As the total CO_2 stored can vary more in this scenario than in the 'CO_2 recycle' study, we expected that the impact on carbon intensity would be more pronounced.

We only investigated uniform WAG possibilities. The operational variables were similar to the previous 'CO_2 recycle' study, with the following additional ones: the fraction of the produced gas diverted for reinjection and the number of injection well pairs that would become WAG injectors. The imported CO_2-rich gas served as a make-up gas, maintaining

the rates of the chosen WAG injectors (up to the maximum limit of the import pipeline). The injection wells that were not converted into WAG injectors remained as water injectors. A summary of the design variables is shown in Table 5.7.

Table 5.7 'CO_2 import' optimisation design variables, their respective domains, and discrete increments.

WAG design parameter	Low	High	Increments
Gas and water half-slug, days	90	360	30
Number of injection well pairs	1	4	1
Fraction of produced gas (discounting the fuel) diverted for reinjection after separation, v/v	0.2	1	0.3
Injection WAG pairs	Combination of any two distinct injectors from the nine candidates		

We recognize that the injection rates and production BHP were not optimised in the field cases, but they could be included as variables, as demonstrated in the pilot '3D' study. At first, we attempted to optimise the rates and bottomhole pressure, but the platform restrictions left little room for improvement. Alternatively, we decided to set the simulator to seek voidage replacement, respecting the fracture pressures and maximum rates technically feasible. If one were to optimise the rates and BHPs in this study, only the water injection rates could be effectively optimised, as the CO_2 rates are restricted by the CO_2 availability (recycled and/or imported). Moreover, the additional number of variables would require a larger sample of designs to simulate, increasing the computational cost.

5.3.2. Results and Discussion

Figure 5.18 shows the objective functions of all cases simulated in relation to the waterflooding base-case. For comparison, we included the 'CO_2 recycle' designs of the previous section.

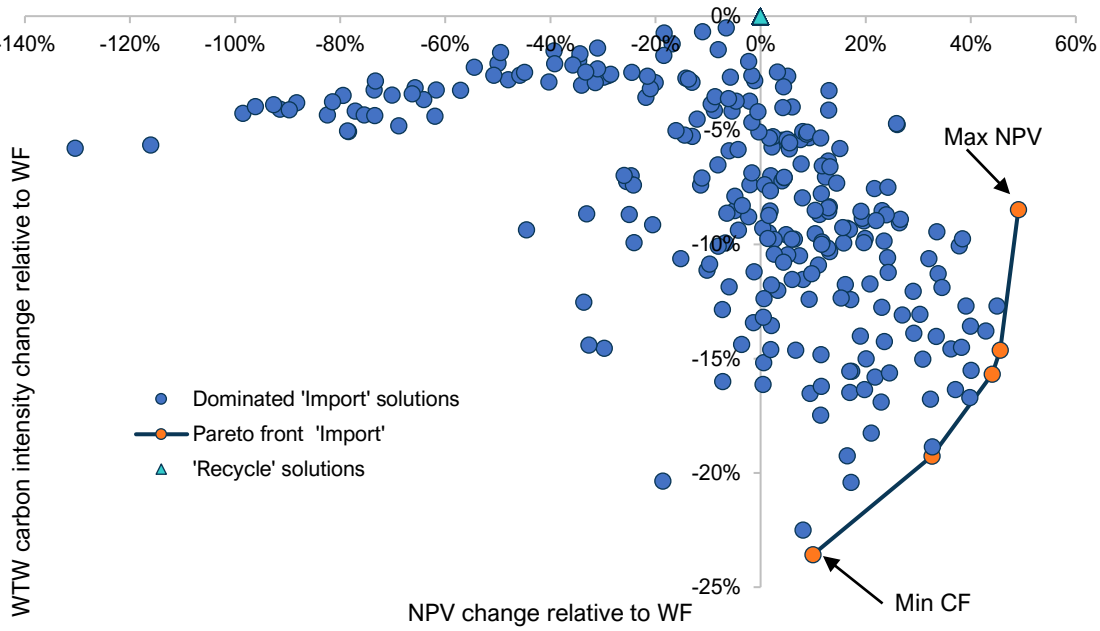

Figure 5.10 Well-to-wheels carbon intensity and Net Present Value (relative to waterflooding) for all CCUS operational strategies simulated in the field 'CO_2 import' and 'CO_2 recycle' optimisation studies.

The pareto front comprises the designs that balanced out both objective functions. Note how the 'CO_2 recycle' scenarios had a limited range of outcomes due to their gas recycling restrictions. Importing CO_2-rich gas greatly expanded the potential to reduce the carbon footprint of the hydrocarbons produced and to boost the NPV. Many designs had worse performing NPV compared to WF, because of the high cost of importing large volumes of CO_2-rich gas from a neighbour FPSO (especially the opportunity cost of selling the methane immediately).

We ran a total of 204 'CO_2 import' cases, but we are aware that better solutions exist, inside and outside of the constrained boundary of the design space. It is at the discretion of the reservoir engineer to continue running scenarios or to stop, and then analyse the designs with the best outcomes to gain insights on the field operations. The bottle neck at this point is computation time – each of these scenarios took from 10 to 23 hours to run using one CPU per simulation. We also used two cores per simulation at times, but further parallelization slowed the runs down. As the scenarios were run in batches using 10 to 30 cores on a remote cluster, it took almost six days to simulate all the 'CO_2 import' cases. The software optimisation provider suggests the number of simultaneous simulations should not be above 10, especially in the first generations, because this would jeopardize the optimiser's ability to learn from the outcomes before designing the next experiments to move towards an optimum solution (CMG, 2020a).

Scrutinising each strategy is also a time-consuming task, even when one focuses on the Pareto designs only. For the sake of this discussion, we picked the extremes Pareto cases, the ones that achieved the highest NPV (called 'max NPV') and lowest carbon footprint per barrel (called 'min CF') to analyse further. Table 5.8 and Table 5.9 detail their designs.

Table 5.8 'Max NPV' import WAG design parameters generated by the PSO algorithm.

	WAG pair 1		**WAG pair 2**	
Well number →	**Inj-1**	**Inj-4**	**Inj-2**	**Inj-6**
Water half-cycle (days)	90	90	270	90
Gas half-cycle (days)	90	90	90	270
Reinjection gas fraction	50% v/v of available gas produced			
Resulting CO_2 injection concentration	40% to 73% m/m (median of 62%)			

Table 5.9 'Min CF' import WAG design parameters generated by the PSO algorithm.

	WAG pair 1		**WAG pair 2**		**WAG pair 3**		**WAG pair 4**	
Well number →	**Inj-1**	**Inj-4**	**Inj-2**	**Inj-8**	**Inj-3**	**Inj-9**	**Inj-5**	**Inj-7**
Water half-cycle (days)	180	360	180	180	360	360	90	120
Gas half-cycle (days)	360	180	180	180	360	360	120	90
Reinjection gas fraction	20% v/v of available gas produced							
Resulting CO_2 injection concentration	69% to 78% m/m (median of 72%)							

Environmental Performance

The 'min CF' design involved converting the maximum number of injection wells to WAG injectors (eight out of nine candidates), which required a larger volume of gas imported to maintain the injection rates. The design also used the minimum fraction of associated gas for recycling, which meant only the CO_2-rich gas was reinjected and the CO_2 purity was kept high. These measures boosted the CO_2 storage and minimised the overall carbon footprint. The 'min CF' case was able to store 2.66 times more CO_2 than the 'max NPV' design. A comparison of the *operational* carbon footprint of the key designs simulated demonstrates the potential of using CCUS to offset carbon emissions (see Figure 5.11 (a) below). We also included the *total* carbon intensity for comparison (Figure 5.11 (b)).

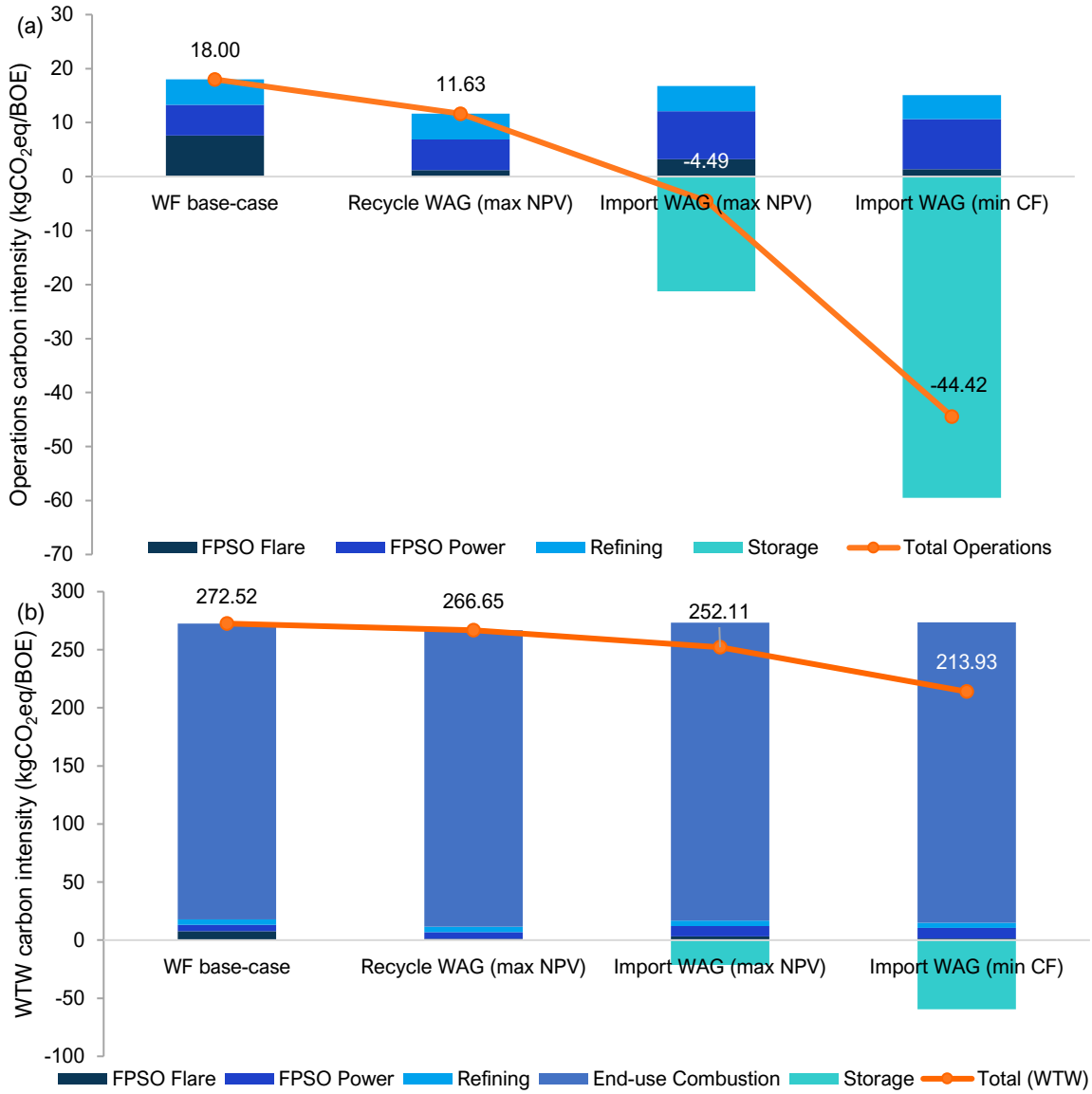

Figure 5.11 Carbon intensity of the key field strategies at the (a) operational (scope 1) and (b) well-to-wheels (scopes 1 and 3) levels.

When WTW emissions intensity are quantified (b), the end-use emissions dictate the overall footprint, although it is still possible to see the positive impact of applying CCUS. On the other hand, when the focus is on the *operational* emissions of a BOE produced (a), the substantial impact of the CO_2 storage and the flaring avoidance on the carbon intensity was clearer, even achieving negative operational carbon balances in the 'CO_2 import' cases. Although environmentally beneficial, this does not mean these CO_2-EOR scenarios would provide carbon-negative oil, after all, the term only applies when the *total* emissions are negative, i.e., when CO_2 is drawn from the atmosphere. Additionally, the hydrocarbons produced in the CO_2-providing oilfield would not have their emissions reduced. As the analysis was restricted to the CO_2-receiving field, a negative carbon footprint means that more CO_2 was stored in the reservoir (diverted from flaring) than was emitted during the

extraction and refining of a BOE. If the system of study included both fields (CO_2 receiver and provider), the overall emissions offsetting would have been milder. Moreover, for CO_2-EOR to truly reduce the accumulation of CO_2 in the atmosphere, the source of injected CO_2 would need to come from biomass conversion or direct air capture (IEA, 2019a).

Economic Performance

The 'max NPV' design utilized four out of the nine injection wells as WAG injectors and diverted more of its produced gas toward reinjection, reducing the volumes of CO_2-rich gas imported. The main driver for this limited gas importation was the cost of bringing methane in, which far outweighed the CO_2 tax savings. Interestingly, the recycling of a greater fraction of the produced gas was financially beneficial despite the dilution of CO_2 purity and the delay of revenues from selling the NG diverted to reinjection.

Although 'max NPV' design did not store as much CO_2, it *recovered* gas more efficiently than the 'min CF' case, which improved the sales gas revenues (see Figure 5.12). Additionally, it achieved a higher oil recovery factor, enhancing even further the financial gains.

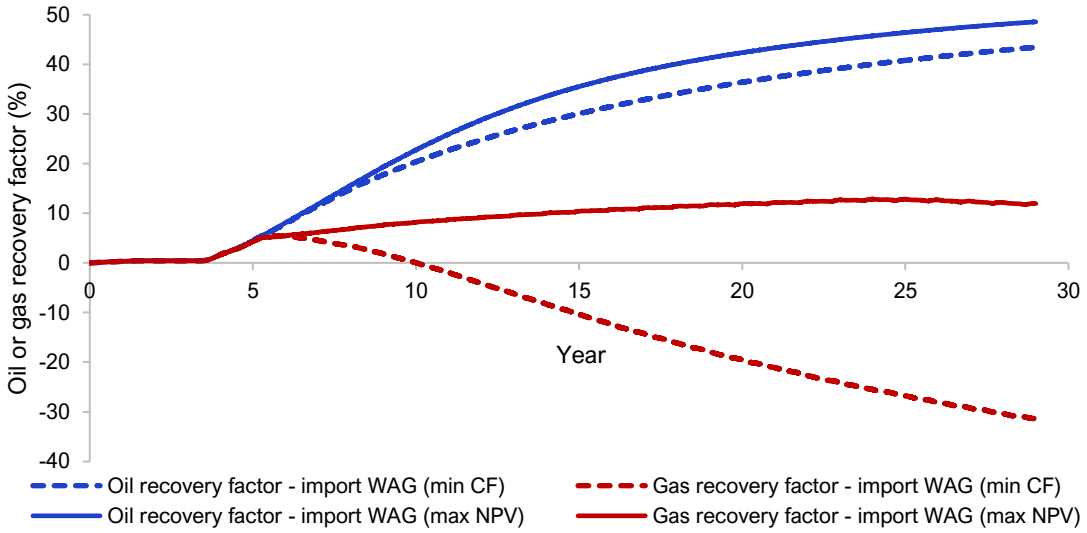

Figure 5.12 Oil and gas recovery factors for the two extreme Pareto front designs – highest Net Present Value (max NPV) and lowest carbon footprint (min CF).

Looking at how the cash flows behaved over time for the 'max NPV' case on Figure 5.13, it is clear that even with a positive NPV, the multibillion initial investment is substantial and break-even point occurs late into the project, which should be considered when making investments decisions. Still, these attributes (high capital investments and long payback periods) are characteristic of offshore CCUS projects and, in this case, highly competitive with the most likely production alternative – waterflooding.

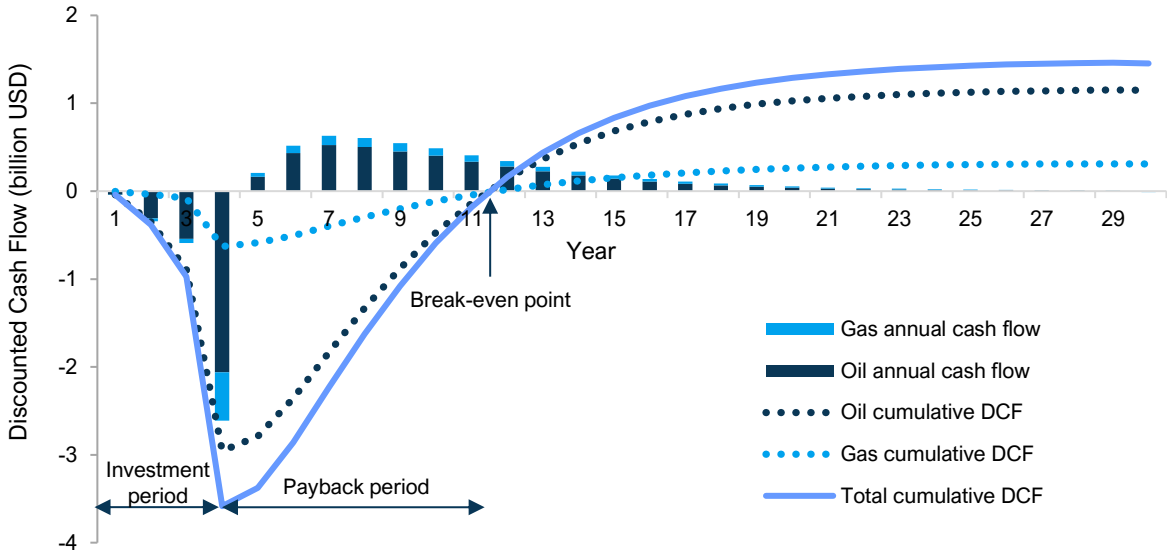

Figure 5.13 'Max NPV' import WAG design discounted cash flows (annual and cumulative).

We also calculated the NPV for the individual wells to evaluate the extend of CO_2-EOR benefits. With these metrics we could identify the wells with highest productivity and if any would need to be shut at some point of its production life - if its NPV were ever negative. We only considered the revenues and costs from oil production, for simplicity. Figure 5.14 shows the results for the key 'CO_2 import' designs compared to the waterflooding reference-case. All production wells were better off with the CCUS schemes, with the most significant improvements seen in the 'max NPV' design.

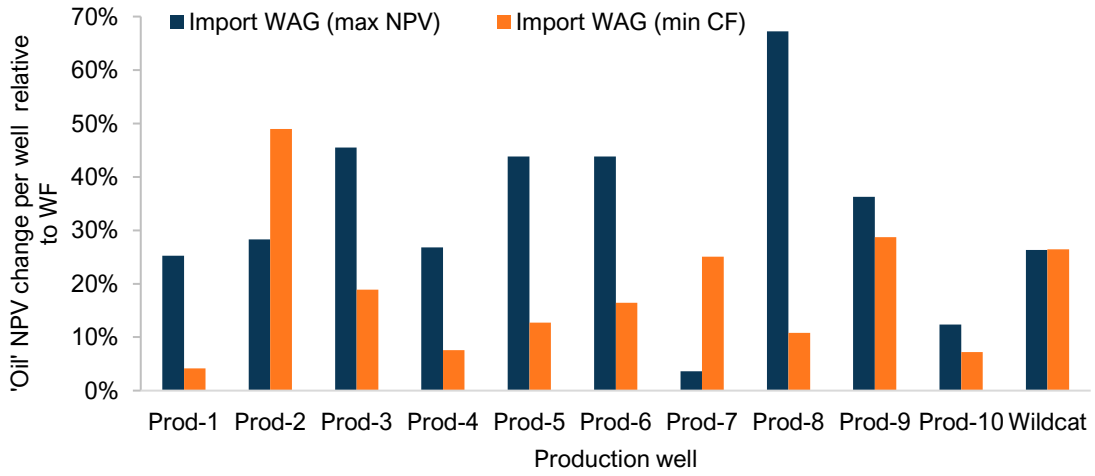

Figure 5.14 Net Present Value (considering oil only) per production well in relation to the waterflooding base-case for the key 'CO_2 import' CCUS designs.

WAG Injectivity

Regarding injectivity, we observed significant losses, particularly when the WAG half-slugs were short. The water half-cycles were affected the most, as they suffer more from hysteresis effects. For example, injectors 7 and 8 reached zero injection rates towards the

end of production life. However, be aware that these wells' injection rates were far lower than the maximum of 6,000 sm^3/d assigned to them even during waterflooding (4% and 18% of the maximum rate, respectively) because they are connected to lower permeability and porosity grid-cells. On the other hand, during the gas cycles the recurrent issue was violation of the maximum injection BHP constraint (fracture pressure), which capped the gas injection rates of some wells by up to 25%.

Calcite Scale Risk

For the scale risk analysis, we compare the waterflooding base-case with the 'CO_2 import' WAG Pareto scenario that yielded the lowest scale risk, which was the 'min CF' mainly because its water injection was partially substituted by gas injection. However, introducing more CO_2 into this carbonate reservoir alongside seawater through WAG triggered more dissolution overall within the reservoir (Figure 5.15).

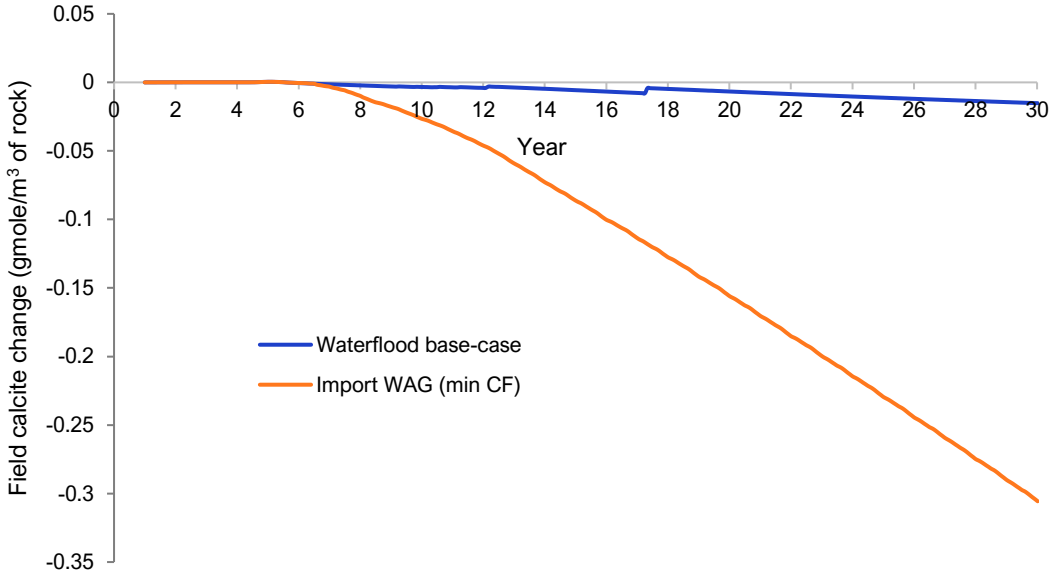

Figure 5.15 Field calcite ($CaCO_{3(s)}$) mineral change for waterflood base-case and 'CO_2 import' WAG with the lowest carbon footprint (min CF).

A thorough analysis of each well's scaling risk would be required for real life applications, but for conciseness and clarity, we chose the injection and production wells with highest volume throughput, 'Inj-3' and 'Prod-6' respectively, to do a deeper analysis in the near wellbore regions. We examined the porosity change around these wells' perforations for our cases of interest. A positive slope in the curve means dissolution (increased porosity), while a negative slope depicts precipitation (decreased porosity).

In both scenarios, as soon as seawater flows through Inj-3 grid-blocks (see Figure 5.16), dissolution takes place because the CO_2 present in the oil dissolves in brine at high pressure, reducing the pH. In the WAG scenario this dissolution continues to escalate, since CO_2 is injected periodically alongside seawater. However, in the waterflood case, this behaviour flips once the CO_2 in the oil is washed out by the injected brine, causing precipitation around the injection wellbore.

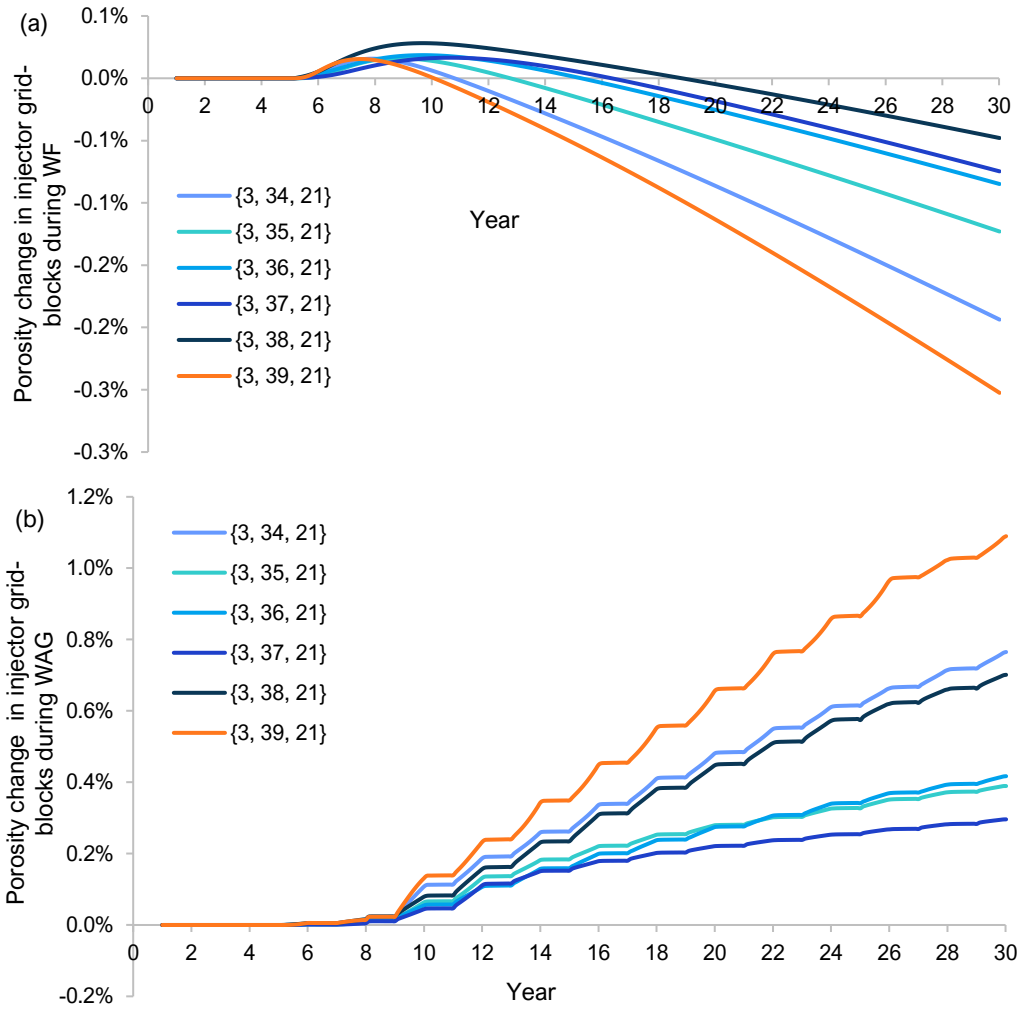

Figure 5.16 Porosity change due to mineral reactions in the grid-blocks of Inj-3 for (a) waterflood base-case and (b) 'CO_2 import' WAG with the lowest carbon footprint.

Around Prod-6 perforations, on the other hand, the effect of mineral reactions is more prominent in the layers with highest permeability (in orange and red respectively in Figure 5.17). Note how these layers mainly experienced precipitation in the first years of waterflooding, as the HCO_3^- rich injection brine mixes with the high calcium formation brine. However, this behaviour switches to dissolution in layer 14 once that formation water is gone. Interestingly, dissolution prevails in layer 14 in the WAG case. This may bring a higher precipitation risk to the well and production facilities, since this more saturated brine will

experience higher pressure drops, eventually precipitating the ions dissolved from the rock matrix upstream.

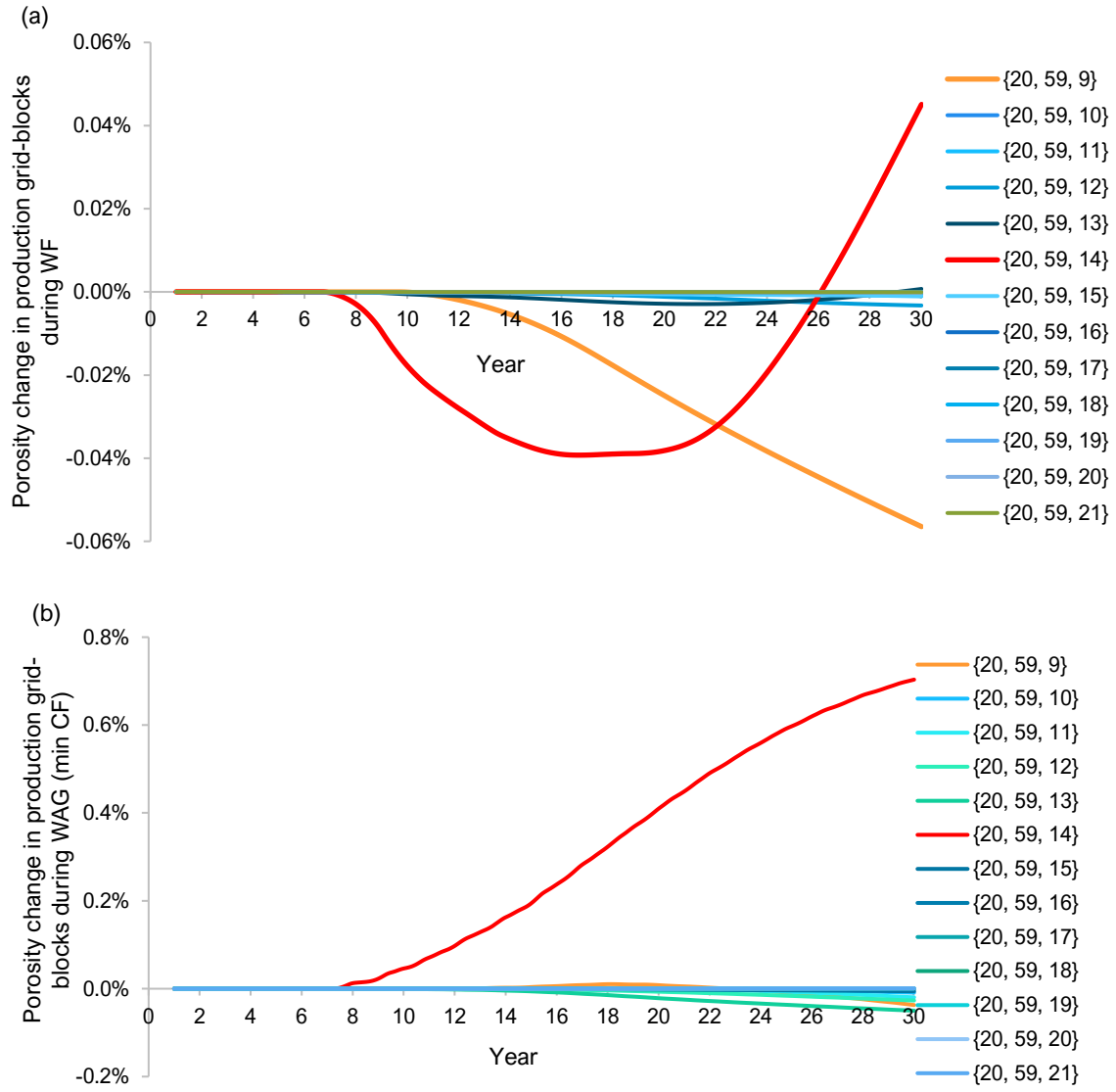

Figure 5.17 Porosity change due to mineral reactions in the grid-blocks of Prod-6 for (a) waterflood base-case and (b) 'CO_2 import' WAG with the lowest carbon footprint (min CF).

Lastly, we should mention the computational cost of running these scenarios including geochemical reactions. Recall that the geochemistry was only added in specific cases as a post-optimisation step of the field cases. Even after numerical tuning, the WAG model with reactive transport took 3.7 times longer than the version without geochemical reactions (CPU elapsed time).

Calcite Scale Management

We applied our methodology for squeeze treatments design optimisation for the key 'CO_2 import' designs. Figure 5.18 shows the incremental number of squeeze treatments that

each producer would need under these scenarios as opposed to WF. A negative number represents a reduction in number of interventions.

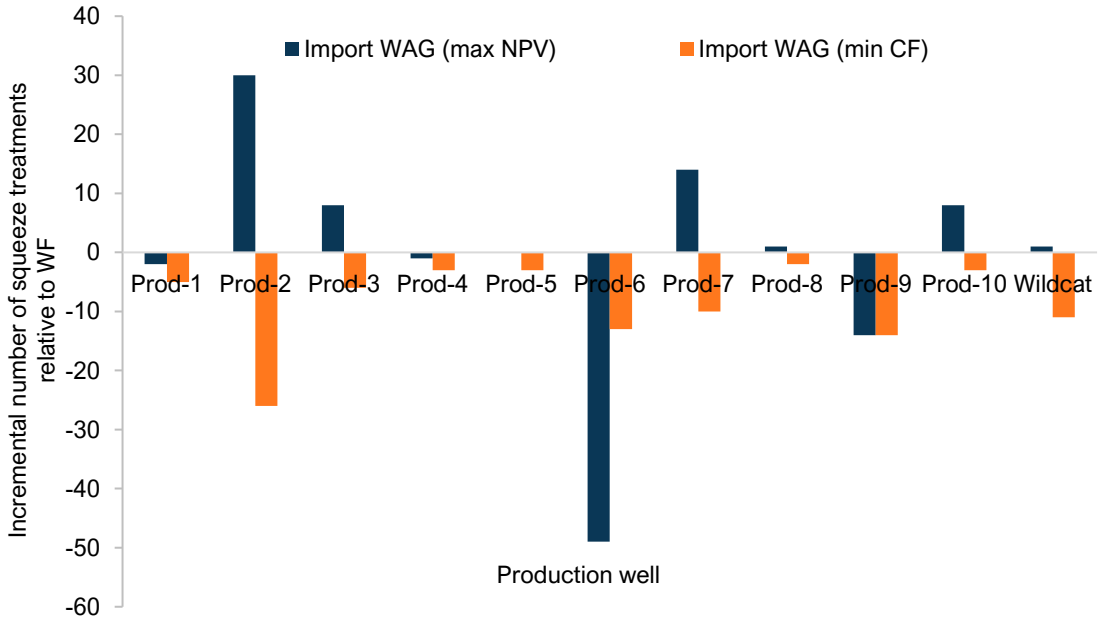

Figure 5.18 Incremental number of squeeze treatments per production well in relation to the waterflood base-case for the key 'CO_2 import' CCUS designs.

The increased availability of gas in the 'CO_2 import' designs greatly reduced the water cut of production wells and therefore the need for squeeze interventions, particularly in the 'min CF' case. In the 'max NPV' case, six out of the eleven wells had their water production increased and needed more squeeze interventions, but *total* number of squeeze treatments of this design was lower than in the WF. Figure 5.19 below illustrates the drop in total number of squeeze interventions as more gas is introduced into the system.

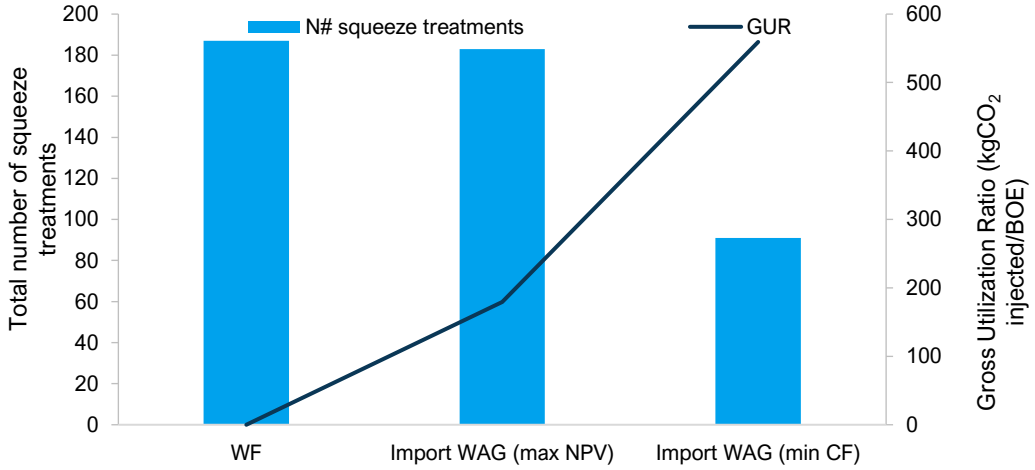

Figure 5.19 Total number of squeeze treatments and gas utilization ratio (GUR) per field operational design.

By applying higher GURs it was possible to shrink the overall water production, and therefore the number of interventions needed. Nonetheless, it is important to consider the

risk of deposition in the production system since the greater reservoir dissolution will increase the levels of saturation of the produced brine.

Finally, a synopsis of the cost results for the main designs is shown in Figure 5.20. We included the 'CO_2 recycle' highest NPV case for comparison. Total squeeze programme costs dropped as optimised WAG strategies were applied. The unit squeeze cost was higher in the 'min CF' case simply because the total water production was significantly diminished.

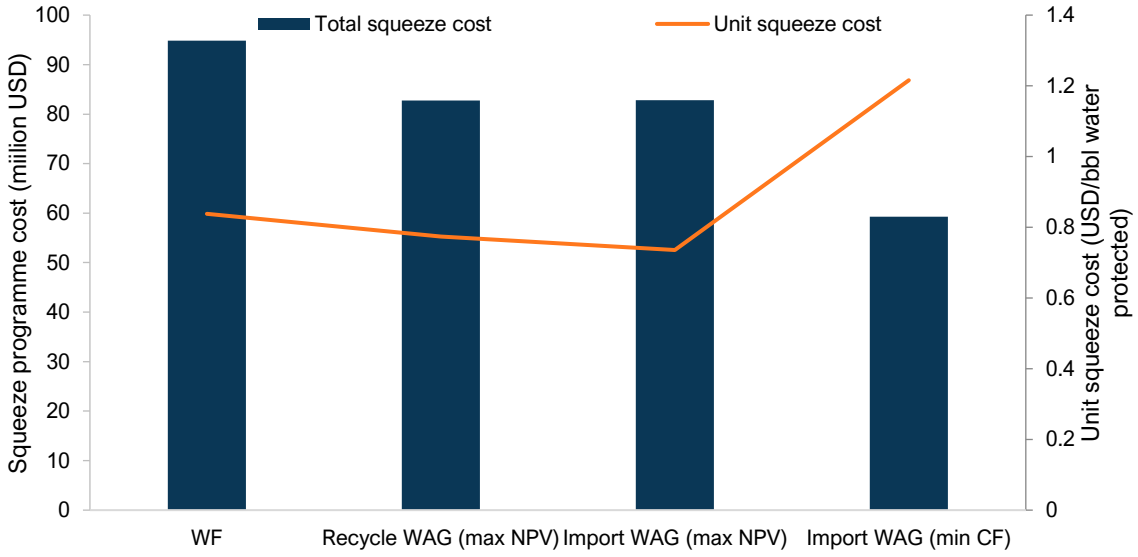

Figure 5.20 Total squeeze costs and unit squeeze costs per field operational design.

5.3.3. Impact of Geological Uncertainties

Reservoir simulation calculations are valuable tools for evaluating the performance of CO_2-EOR and storage. However, uncertainties on static properties (e.g., porosity, permeability, faults, fractures) and dynamic parameters (e.g., relative permeability, capillary pressure curves, PVT) strongly affect the results (Ampomah et al., 2017). The traditional approach of anchoring on a deterministic base-case reservoir model does not account for these uncertainties, whist the probabilistic approach of using multiple stochastic realizations (equiprobable spatial distributions of petrophysical properties) can be computationally demanding and equally anchored, if the suite of realizations were generated through perturbations of a single concept (Bentley, 2016).

We have seen in this chapter that production optimisation is a challenging and computationally demanding task even using a single best-guess model, especially for fractured carbonate reservoirs under WAG injection using a compositional hydrocarbon

model. The problem can involve many decision variables and, combined with a multi-objective optimisation approach, can result in an exceedingly large search space.

A middle ground in dealing with subsurface uncertainties in a timely manner is the use of representative models (RM) that capture the uncertainty range of hundreds or thousands of realizations with a handful of models (Schiozer et al., 2004). The validity of this method requires that these RMs are robust throughout the optimisation process, even when the production strategy changes. A great deal of effort has been put elsewhere into developing a methodology using a metaheuristic optimisation algorithm that ensures the consistency of RMs in long-term optimisation (Meira et al., 2020). This methodology was applied by Santos et al. (2020) to obtain a set of RMs for the UNISIM-II-D benchmark, accounting for geological uncertainties (porosity, permeability, fracture spacing, net-to-gross, rock type, relative permeability, rock compressibility) and operational uncertainties (well index multiplier and availability of groups, platforms and wells). The authors assumed a simplified WAG injection strategy (6-month half-cycles and WAG ratio 1:1), full reservoir coverage with 28 injectors and 28 producers, and no restrictions from production facilities. Based on NPV, recovery factor and cumulative production curves (oil, water, and gas), they selected nine RMs from an ensemble of 199 uncertain scenarios, as depicted in Figure 5.21. Note that the nominal base-case used in our field studies, which is the base-case of the UNISIM-II-D benchmark, was not the most likely geological scenario (P50), but rather a more optimistic one.

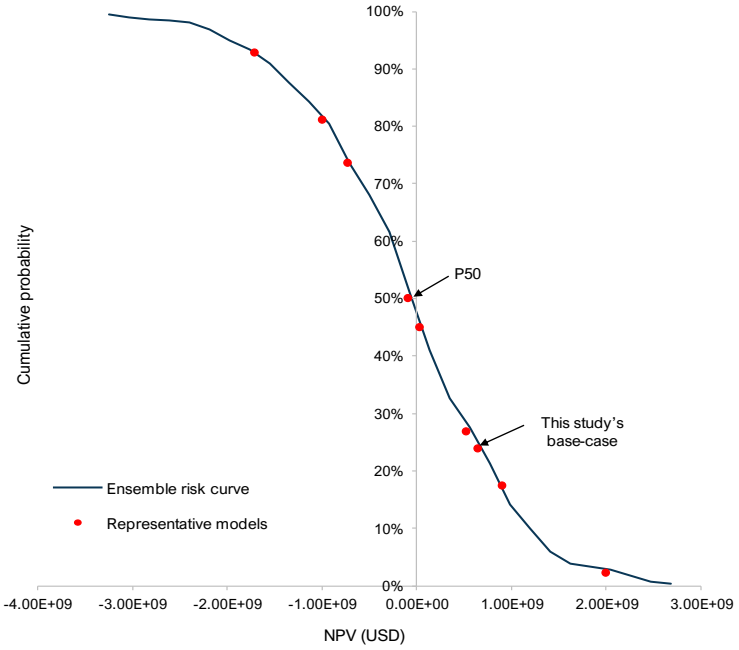

Figure 5.21 Risk curve (complementary cumulative distribution function) for the 199 uncertain scenarios and the

nine representative models selected from it. Data from Santos et al. (2020).

We used these nine RM to re-run the highest NPV 'CO_2 import' scenario, with the goal of demonstrating the impact, if any, of the subsurface uncertainties in our outcomes of interest, namely NPV, WTW absolute emissions and squeeze treatment costs (see Figure 5.22 below).

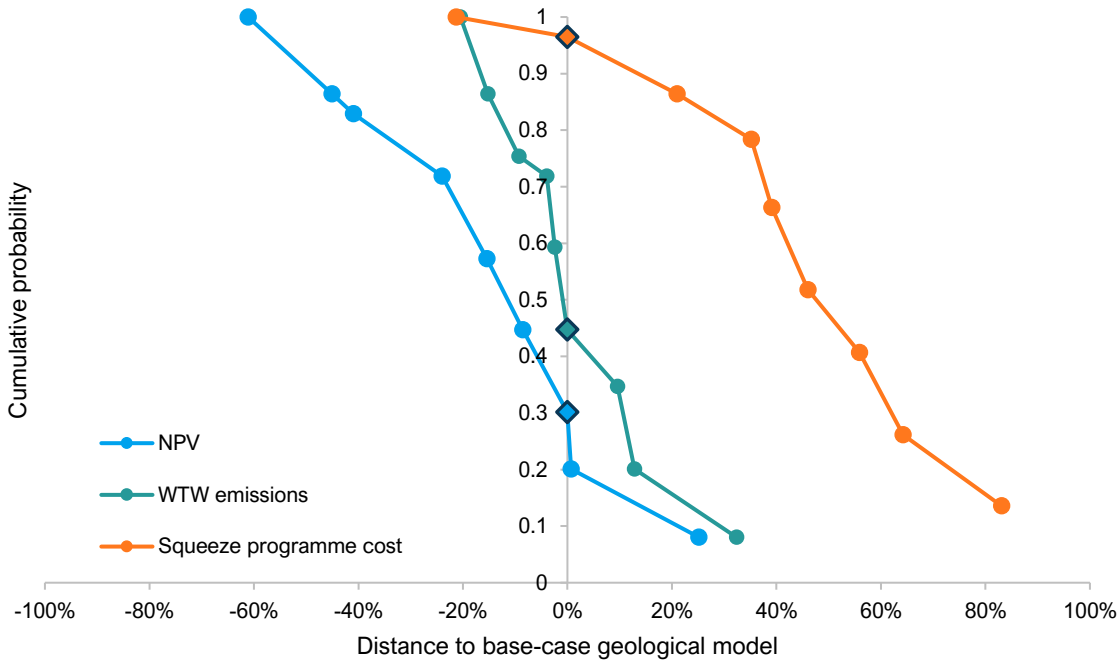

Figure 5.22 Risk curves for the 'max NPV' production strategy of the 'CO_2 import' field study. Each point is a representative geological model under this design. The models circled in black are the base-case outcomes.

As we wanted to see the variability in the outcomes caused by the subsurface uncertainties, we plotted the percentage change of each RM outcome in relation to the base-case geological model output. The base-case used gave optimistic results in terms of NPV and squeeze costs. The WTW emissions response was less sensitive to the geological uncertainty covered, but also more balanced, with most scenarios yielding lower total emissions. As the uncertainties in the geological characterization would affect the outcomes, one should ideally carry out a robust optimisation process using these RMs simultaneously to find a production strategy that is on average optimal for the set of RMs. We suggest this as future work following on from this thesis.

5.3.4. Conclusions: 'CO_2 Import' Scenario

In this section, we deepened our investigations on CCUS in BPS oilfields by extending the availability of CO_2 through connection with a nearby platform. The goal was to find operational strategies that improved the project's NPV, reduced the carbon intensity of the oil produced and prevented calcite scaling. The following conclusions were drawn:

- Despite the high upfront investments and long payback periods, the optimal CCUS design in NPV terms was highly competitive compared to the most likely production alternative – waterflooding. Importing CO_2-rich gas greatly expanded the potential to reduce the carbon footprint of the hydrocarbons produced and to boost the NPV, but there was a trade-off. Whilst the highest NPV design simulated (called 'max NPV') had 49% higher NPV and 8% lower carbon intensity compared to the WF base-case, the lowest total carbon footprint design (called 'min CF') achieved 10% NPV improvement and 24% carbon intensity reduction.
- The 'min CF' design involved the importation of 50.6 $MMtCO_2$ from a neighbour field and the recycling of most of the CO_2 produced, guaranteeing the storage of 98% of the CO_2 available. Our highest NPV design achieved a 93% carbon storage efficiency, but it utilized a lower volume of external CO_2 (20.5 $MMtCO_2$). The downside of importing large volumes of CO_2-rich gas was the methane associated with it. A great portion of this valuable gas remained in the subsurface in the 'min CF' case, which hurt its economic performance.
- We observed significant injectivity losses, particularly when the WAG half-slugs were short. The water half-cycles were affected the most, as they suffer more from hysteresis effects.
- The design with the highest gas utilization ('min CF') showed the lowest scale risk amongst the cases simulated, mainly due to reduction of water production due to the higher gas injection. Although the number of squeeze treatments substantially dropped, the introduction of more CO_2 into this carbonate reservoir alongside seawater through WAG triggered more dissolution overall within the reservoir. This may bring a higher precipitation risk to the well and production facilities, since this more saturated brine will experience higher pressure drops, eventually precipitating the ions dissolved from the rock matrix upstream.
- The assessment of geological uncertainties revealed that the base-case used in this field study gave optimistic results in terms of NPV and squeeze costs. The WTW emissions response was less sensitive to the geological uncertainty covered, but also more balanced, with most scenarios yielding lower total emissions. The variability in the key outcomes was significant, so a robust optimisation approach should be considered.

5.4. Conclusions: Field-Scale Studies

In the field optimisation studies, the impact of CO_2 availability in the CO_2-EOR and storage performance was explored. Figure 5.23 below compares the key outcomes of the two cases analysed: 'CO_2 recycle' and 'CO_2 import'. The three optimised strategies are fundamentally different in their designs - WAG pairs, WAG ratios, slug sizes, recycle ratio, CO_2 injection concentration, and total CO_2-rich gas slug-size injected (TGSS) throughout production life. However, we highlighted the latter as one of the most influential parameters and one that summarizes the strategies best.

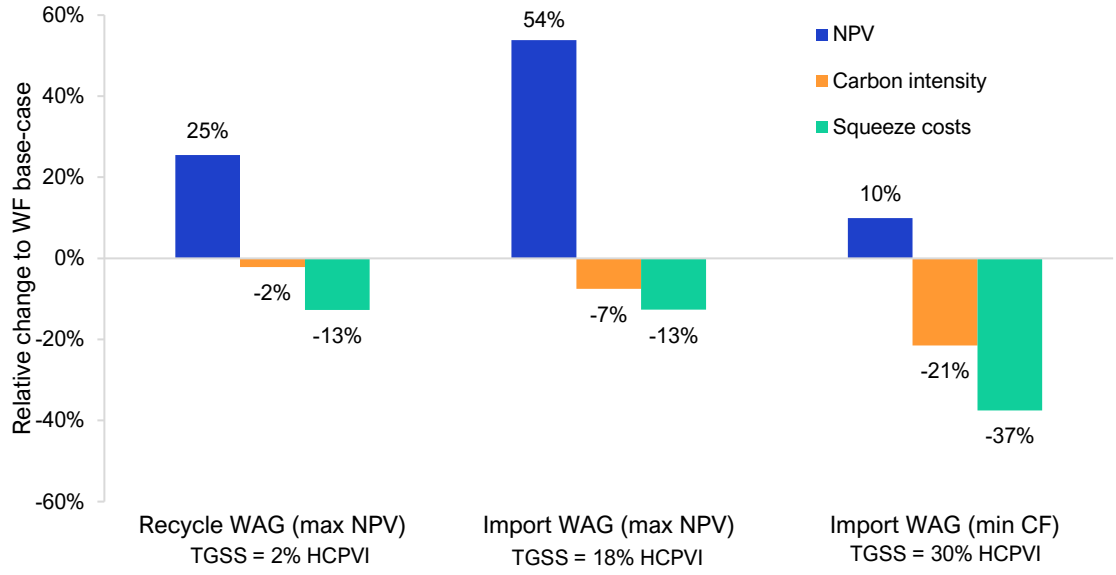

Figure 5.23 Summary of the outcomes of the main field operational strategies achieved in the field optimisation.

Although we observed NPV improvements for the three optimised CCUS strategies, the best NPV outcome simulated was achieved with an increase in CO_2 supply, resulting in a total of 18% HCPVI. However, there is a point where the gas injection volumes can be excessive and hurt the profits, as demonstrated by the lower economic performance of 'min CF' case (30% HCPVI).

In terms of the environmental impact, all CCUS scenarios yielded a lower carbon footprint oil compared to the WF base-case – up to -21% in the 'CO_2 import' lowest carbon footprint case (min CF), due to the high CO_2 storage achieved. It is important to remember that the additional emissions from the incremental EOR hydrocarbons overshadowed the emissions abatement from the carbon capture and storage, especially when the CO_2 available was restricted ('CO_2 recycle' scenario).

Finally, according to our estimates, WAG schemes with high gas utilisation ratios significantly reduced water production, resulting in lower scale risk and costs with squeeze

treatments. However, the higher CO_2 concentration in the reservoir compared to the initial content will increase the levels of rock dissolution overall and the levels of saturation of the produced brine, which may require higher inhibition concentrations resulting in higher chemical cost.

In summary, the key message from the field studies was that optimized CO_2-WAG operational designs showed potential to improve reservoir performance and scale management, whilst reducing total carbon intensity of the hydrocarbons produced.

Chapter 6- Conclusions and Recommendations

In this work, we applied reservoir modelling and simulation tools to investigate the operational performance of offshore CCUS projects in carbonate reservoirs with natural CO_2 content. The Brazilian Pre-salt (BPS) CCUS operations captures and reinjects CO_2 from the associated gas that would otherwise be released into the atmosphere through venting/flaring. In this context, we focused on three key challenges: i) the economics, ii) carbon footprint and iii) inorganic scale, the latter being crucial when CO_2-WAG is performed in reactive carbonate rocks. Our research methodology involved the *integration* of reservoir engineering calculations, cash flow projections, carbon accounting and production chemistry to support field operational decisions. Although the analysis was made for the BPS framework, the methodology can be straightforwardly adapted to any coupled CO_2-EOR and carbon storage projects where mineral scale poses a considerable risk.

This thesis contributes to the development of an integrated approach that not only considers the traditional techno-economic feasibility of O&G projects, but also their potential to align with the energy transition. The holistic proposed methodology demonstrated that the optimisation of operational designs can not only improve economic and environmental performance, but also reduce the production damage caused by CO_2 speciation.

We performed a series of optimisation studies to investigate the impact of different assumptions in the workflow. While optimisation studies are fundamentally focused on how success can be achieved, we also considered what would cause failure and how to manage it. Applying the stoic 'inversion principle' or 'negative visualization', instead of only asking "what operational design would yield the best outcomes?" we also wondered "what could really hurt the outcomes of interest?" and discussed how to avoid them. Fortunately, the studies performed gave us insights on both questions. Table 6.1 presents a summary of the operational variables and objective functions considered. Some of the questions addressed in this thesis are outlined as follows.

Table 6.1 Operational variables and objective functions considered in each study.

	Study →	Pilot '2D' A	Pilot '2D' B	Pilot '3D' A	Pilot '3D' B	Field: CO_2 Recycle	Field: CO_2 Import
Operational Variables	WAG ratio	✔	✔	✔	✔	✔*	✔*
	Gas slug size	✔	✔	✔	✔	✔	✔
	Water slug size					✔	✔
	Injection CO_2 concentration	✔					✔*
	Water injection rate				✔		
	Gas injection rate				✔	✔*	✔*
	Producer BHP				✔		
	WF duration prior to EOR			✔	✔		
	Uniform WAG	✔	✔			✔	✔
	Tapered WAG			✔	✔	✔	
	Injection wells conversion to WAG					✔	✔
	Recycle ratio						✔
Objectives	Maximise NPV	✔	✔	✔	✔	✔	✔
	Maximise CSE	✔	✔				
	Maximise CSM	✔	✔				
	Maximise Profit		✔				
	Minimise WTW Emissions					✔	
	Minimise carbon intensity						✔

* Indirectly optimised.

What are some of the 'best practices' applied in this methodology that one should consider when modelling reactive multiphase miscible transport in porous media?

- It is important to describe the hydrocarbons' behaviour through a compositional model based on pertinent PVT experimental data. Lumping of components may be necessary to reduce computational intensity, but CO_2 should be preserved as an individual component.
- When CO_2 solubility in brine is modelled, it is likely that the PVT model will need a trace component to avoid hydrocarbon disappearance from the grid-blocks close to injection points. This trace component should have the same properties of CO_2 but be insoluble in the aqueous phase.
- To avoid convergence errors related to disappearance of water from the grid-cells, one may need to set the irreducible water saturation of the relative permeability curves as different from zero.
- Formation water and injection water compositions should be equilibrated prior to the flow simulation.
- The mineral kinetics model (calcite rate constant and reactive surface area) can greatly impact mineral change forecasts, especially close to the injection wellbore. In general,

fast kinetic rates are not representative of the calcite behaviour in the presence of CO_2 under reservoir conditions.

- Ideally, to derive a representative dissolution/precipitation rate law, one should acquire field or experimental data using consolidated rock samples in the ranges of temperature, pressure, fluid compositions, and hydrodynamics of the reservoirs being studied, under conditions around and far from equilibrium. Then, further investigations on near wellbore zones with finer grids should be performed.
- Highly heterogeneous fractured models with many grid-blocks will struggle to converge when the geochemical reactions are included. High CO_2 concentrations (above 90%) will also affect numerical stability and slow the simulations down. Under these circumstances, we recommend modelling the reactive transport in the key designs only as a post-optimisation step. Reservoir simulators and computational power are in continuous improvement and this may not represent a problem soon.

What was the impact of the operational designs in the CCUS projects' performance?

- According to our models, higher CO_2 injection concentrations were beneficial to the economic and environmental objectives, although purer CO_2 injection streams resulted in more severe calcite scale in the production facilities. For a constant injection rate, higher CO_2 injection concentrations should be maintained. From the sensitivity studies in sub-section 4.3.3, if one were to choose between maintaining a high gas injection rate or a high CO_2 concentration (typical of the BPS context), the best compromise in terms of NPV was to keep the high injection gas rate at the start of the flood, even if it jeopardised the CO_2 injection purity.
- According to the pilot studies, low WAG ratio and low to intermediate gas slug size are likely to yield enhanced NPV and CSM. Additionally, better performance was achieved by applying low production BHPs and maintaining the reservoir pressure close to the MMP. Higher injection rates should be the target at the beginning of the flood and higher WAG ratios at the end. If possible, WAG should start at the early stages of field production.
- Including injection rates and producer BHP as decision variables unlocked the potential for optimising NPV and CSM in the pilot studies. In the full-field studies, these parameters were not optimised due to platform capacity restrictions and substantial increase of the optimisation search space. However, the gas injection rates and

concentrations were indirectly optimised.

- There was a direct correlation between NPV and CSM for scenarios with constant injection rates and producer BHP. A trade-off appeared when these assumptions were relaxed.
- There were marginal performance benefits of applying tapered WAG designs over uniform ones, in both the field and pilot studies. Tapered WAG cases seemed to utilize the CO_2-rich gas more efficiently and showed improved gas mobility control, which is consistent with the literature and field experience (Zhou et al., 2012). The downside of applying a tapered WAG design over an equivalent uniform one is the former's higher frequency of well switches, which can be operationally demanding.

How would variations in the CO_2 (penalty) price affect the results?

- *Economics were generally attractive* when CCUS designs were optimised but they will vary case by case. According to our calculations, the financial incentives of deploying CO_2 recycling in these deep-water fields far surpassed the hurdles of the process, even when the CO_2 supply is limited to the boundaries of the FPSO. In that sense, the models were not sensitive to the carbon penalty charged by the government in the case of flaring. In fact, the higher the carbon tax the more rewarding, since the operator would avoid higher taxes by performing CO_2 reinjection, with the additional advantages of greater hydrocarbon recoveries. The downsides to consider are the high upfront costs and long payback periods characteristic of these projects.

What implications did different objective functions have in the key outcomes?

- Selecting absolute mass of CO_2 stored (CSM) as optimisation objective function was more representative of environmental-driven goals in the pilot studies, although its low storage *efficiency* (CSE) would bring the consequence of large amounts of produced gas in the topside. Aiming to improve CSE can lead to sub-optimal solutions, where a small amount of CO_2 is injected in the reservoir with large slugs of water solely to avoid CO_2 breakthrough in the production wells.
- In the field studies, the restricted CO_2 volumes of the 'CO_2 recycle' scenario meant that the carbon *intensity* was insensitive to changes in the production design, so using *absolute* emissions as objective function was the most appropriate approach. There was an inverse correlation between NPV and total emissions, meaning a single-

objective optimisation would have sufficed. When the CO_2 availability was expanded in the 'CO_2 import' scenario, then trade-off between the financial and environmental objectives appeared and the multi-objective optimisation approach was essential.

- CO_2-EOR optimisation analysis that prioritizes NPV is more likely to achieve a more cost-effective reservoir performance than studies that simply attempt to maximise oil recovery. Oil recovery factor and NPV were not always directly correlated but closely related – the highest oil recoveries did not result in the highest NPVs, but *faster* oil recovery rates (steeper positive slopes) benefited NPV greatly through revenue anticipation. In contrast, aiming at maximising *unit* NPV appeared sub-optimal, with waterflooding presenting the highest profitability per BOE produced.

What were the lessons learnt regarding calcite scale assessment and management in carbonate reservoirs under CO_2-EOR?

- The CO_2 behaviour in these systems was consistent with the literature: it mobilized the oil improving recovery and it dissolved in brine causing dissolution of calcite. As brine flows through the porous medium away from the injectors, the dissolution continues until the brine becomes saturated. The lower pressures closer to production points will then result in supersaturation and mineral precipitation. The kinetics of these processes under a wide range of reservoir conditions requires further investigations.
- In general, the water production curves were appropriate proxies for the behaviour of calcite precipitation rates from wellbore to surface conditions. However, it is still important to quantify the saturation levels for the design of scale prevention plans, specifically the MIC of squeeze treatments and continuous injection of scale inhibitor.
- The total discounted cost of squeeze treatments was only a fraction of the NPV for each scenario, reinforcing the advantages of scale prevention.
- The simulated scenarios demonstrated the high mineral reactivity of the near-well region and the implications for production facilities. The overall reservoir properties were mildly affected by the injection of slugs of CO_2 and water.

How did the operational designs affect calcite scale risk?

- Dry CO_2 injection presented little to no threat of scale precipitation on surface facilities compared to other production strategies due to its limited water availability.
- Waterflooding a carbonate reservoir that has a considerable CO_2 content in the oil will

result in more severe calcite scale risk than adding more CO_2 into the system, i.e., by applying equivalent CO_2-WAG injection schemes. In waterflooding, the CO_2 in the original oil will supersaturate the injected seawater and the premature water breakthrough will require earlier and more frequent squeeze treatments.

- Applying a below bubble-point producer BHP allowed more CO_2 to evolve from the aqueous solution, reducing the solubility of calcite and increasing the brine's saturation ratio (scale risk) in the wellbore. However, the same effect reduced calcite scale risk within the surface facilities, as the low BHP promoted mineral precipitation *within* the reservoir, before reaching the production well. In such a scenario, productivity loss due to deposition in the near wellbore should be monitored.
- Cases with a producer BHP *above* the reservoir fluid's bubble-point only presented calcite scale risk at the wellbore after breakthrough of injected fluids.
- WAG schemes with high gas utilization ratios reduced water production and, therefore, the number of squeeze treatments necessary during production life. However, the higher CO_2 concentration in the reservoir will increase the levels of saturation of the produced brine. This in turn may require a higher MIC to inhibit deposition, which could increase the scale prevention costs.
- Higher WAG ratios increased scaling risk, in general. Even with the lower degree of mixing, the CO_2 from both the oil and the WAG scheme was enough to saturate the lower salinity seawater injected in most of our scenarios. Applying high WAG ratios will keep both water production and saturation ratios high.

What was the carbon intensity of CO_2-EOR oil produced in the BPS hypothetical model?

All CCUS scenarios simulated, regardless of their total emissions, yielded a *less carbon-intensive* BOE compared to the WF base-case – a 3.4% average reduction for the 'CO_2 recycle' and up to 24% in the 'CO_2 import' scenario (best case in carbon emissions terms). If this lower carbon footprint oil simply meets an existing demand and does not increase overall consumption, but rather displaces market share from a more carbon-intensive oil, total emissions could potentially reduce.

When the CO_2 source is limited to the boundaries of the field, additional emissions from the incremental EOR hydrocarbons will overshadow the emissions abatement from the

flaring avoidance, especially when the initial CO_2 concentration in the reservoir is moderate (10% m/m in our studies).

In short, the oil and gas produced in these remote fields can be especially energy-intense due to the non-conventional nature of its offshore operations, the application of EOR, and the need for artificial lift. Yet our results demonstrated that the total carbon intensity when CO_2-EOR is applied can be significantly lower than the usual waterflood, due to the reduction in flaring emissions and increased efficiency of hydrocarbon recovery. Carbon intensity could reduce further by using more than the available recycled CO_2, sourced from anthropogenic sources onshore via a pipeline. Investigations of these alternative scenarios would shed more light on the topic.

What can be said about the limitations of the research approach?

There are *significant uncertainties* associated with applying a reservoir-simulation-based workflow, especially at the start of the venture when limited production data are available for model validation. However, calculations of this nature can improve our qualitative understanding of the complex subsurface phenomena and its implication to the surface systems (facilities, economics, and emissions models). Although the actual quantitative impact is still difficult to model, these results can pinpoint the overall tendencies of the system and, combined with other methodologies, aid the decision-making process, provided the uncertainties and limitations are considered.

6.1. Future work

There are several lines of research that could be pursued based on the work performed for this thesis. We explore a few, subdivided in two main areas, as follows.

6.1.1. CCUS Project Optimisation

1. Robust optimisation considering geological uncertainties

In chapter 5, we acknowledged the importance of assessing geological uncertainties in production optimisation. However, a robust optimisation under uncertainties is still required to truly incorporate their impact in the decision-making process and reduce risks (Schiozer et al., 2019).

2. Alternative CO_2 sources

One of the keys to EOR success is the availability of suitable injection fluids. Alternative sources of CO_2 for injection in the oil leg could be evaluated. For example, one could consider the impact of different initial CO_2 concentrations in the solution gas within the reservoir, or the utilization of anthropogenic CO_2 for EOR.

In the Brazilian context, a prospective source of CO_2 is the fermentation from the various sugarcane ethanol distilleries near the coast (Rochedo et al., 2016). The gas stream is highly concentrated in CO_2, which lowers capture costs, and there is a potential to achieve net negative emissions, as the biomass feedstock also captures CO_2 from the atmosphere through photosynthesis (Global CCS Institute, 2019). Feasibility studies have been conducted for applications in post-salt oilfields (closer to the shore) (Rockett et al., 2013, Rochedo et al., 2016), but they could be extended to the pre-salt basins.

3. CO_2-EOR and Subsequent CCS

All calculations in this thesis ended at cessation of production. Consideration could be given in continuing CO_2 injection for storage purposes (CCS) after cessation of production, using CO_2 from anthropogenic sources or from neighbour fields still under production. Natural gas pipelines could be repurposed for transport of the anthropogenic CO_2 to the depleted oil reservoir. Such a system would be sensitive to CO_2 price, capture costs, and tax incentives, so sensitivity analysis should be carried out.

4. Hybrid CO_2-EOR methods

Other CO_2-EOR methods could be considered to give a safe destination to the CO_2 produced whilst improving oil recovery. For instance:

- CO_2 low-salinity water alternating gas (CO_2-LSWAG): using low-salinity water in the WAG slugs may promote wettability alterations, which may in turn improve oil recovery. It can also be effective to prevent $BaSO_4$ scale deposition and enhance injectivity. The lower salinity will reduce the interfacial tension between the CO_2 and the brine, lowering their gravity differences and flow resistance, which may increase injectivity (Awolayo et al., 2019). However, it should be considered that a low-salinity brine combined with CO_2 leads to higher CO_2 solubility and diffusion, which can increase brine acidity and carbonate dissolution.
- Polymer water alternating with CO_2 gas (CO_2-PAG): the addition of a polymer to the

water slugs can reduce mobility differences and increase sweep efficiency. Nevertheless, polymer introduction may bring other flow assurance concerns, such as precipitation and fouling from back-produced polymer in the production facilities (Vazquez et al., 2017a), which should be investigated.

5. *Additional optimisation variables*

Many parameters that were kept constant in this study could be considered as optimisation candidates: the number, types and location of wells, the drilling and shut-in schedule of wells, the platform processing capacities, to name a few. The choice of optimisation parameters will depend on the project's phase and the balance between number of variables and computational cost, as well as the efficiency of the optimisation method in dealing with numerous variables.

6. *Oil price volatility*

Low oil prices may represent the new reality of the oil and gas industry. An analysis of how oil price uncertainties would impact decision making in these large-scale investment intensive CCUS projects is essential.

7. *Reduction of assumptions*

There were assumptions made in this work for simplicity purposes or because of lack of data that could be explored. A few examples are:

- A more rigorous approach would involve determining the relationship between injection gas rate and its CO_2 concentration, based on the initial CO_2 in the solution gas and the membrane separation efficiency. Then, CO_2 injection concentration can be a variable dependent on the injection rate, and they both could be optimised simultaneously.
- We did not adapt the gridblock sizes to the WAG slug sizes. If the half-slugs are small, a fine grid may be needed to avoid mixing of several slugs in the first cells
- We considered constant the fraction of the gas produced in the FPSO that is consumed as fuel, when it should vary with the operational design, especially with the gas compression power.
- More granular details of the oil and gas value chain may be added in the WTW carbon emissions quantification, such as transportation and trading of the products.

6.1.2. Geochemistry

1. Thermal effects

Carbonate reactivity can be highly sensitive to temperature (André et al., 2010). It would be of interest to investigate the impact of thermal processes in scale prediction, especially in the near-well injection zone, where there can be a significant temperature gradient between the injected fluids and the reservoir.

2. Water vaporization

It has been reported that complete vaporization of water could occur during CO_2 injection, which would form a dry zone near the injector and decrease gas injectivity (Tang et al., 2018). Water vaporization could also cause salt precipitation with rapid loss of formation porosity and permeability (salting-out effect). It may be important to model these phenomena, especially during long CO_2 injection cycles. However, this would require inclusion of halite (NaCl) reactions and H_2O as a component in the hydrocarbon model, which may in turn make the simulations more numerically demanding.

3. Different rock types

Another line of investigation is the understanding of how CO_2-WAG schemes may alter porosity, permeability, and wettability of heterogeneous rocks at the pore scale and the implications to larger full-field reservoir model applications.

4. Other flow assurance and scale hazards

Other important flow assurance issues have been observed during CO_2-WAG operations in carbonate reservoirs: asphaltene precipitation, hydrate formation, corrosion, and scale deposition of other minerals such as anhydrite ($CaSO_4$) and dolomite ($CaMg(CO_3)$), which may compete for the same ions as calcite and impact its thermodynamic equilibrium (Ribeiro, 2017). Many studies have been performed on those individual themes with valuable insights, but more holistic investigations are still lacking on: how to forecast and manage these operational hazards; how they influence each other; and how they impact the effectiveness of prevention chemicals (e.g., scale and hydrate inhibitors).

5. Interplay between geomechanics and geochemistry

Seal and well integrity are crucial safety concerns during CO_2 utilization and storage operations in geological formations. They are both influenced by rock dissolution and changes in mechanical stresses driven by pressure changes. A coupled reactive flow and

geomechanical modelling approach can be used to assess their long-term implications to reservoir and caprock in the presence of CO_2.

6. Model validation with observed data

History matching using field and laboratory data would strengthen the reliability of the methodology proposed, qualitatively and quantitatively. For example, field data on injectivity and productivity of wells, production brine composition, and rock composition through core sampling would be particularly valuable. In addition to numerical models, a reliable laboratory scale physical model would be helpful for mechanistic study and understating of the behaviour of scale inhibitor retention on the rock surface (to design squeeze treatments).

REFERENCES

Abraham, A. & Goldberg, R. 2005. *Evolutionary Multiobjective Optimization: Theoretical Advances and Applications*, Springer doi: 10.1007/1-84628-137-7.

Ampomah, W., Balch, R. S., Cather, M., Will, R., Gunda, D., Dai, Z. & Soltanian, M. R. 2017. Optimum Design of CO_2 Storage and Oil Recovery under Geological Uncertainty. *Applied Energy,* 195, 80-92. doi: https://doi.org/10.1016/j.apenergy.2017.03.017.

Anabaraonye, B. U., Crawshaw, J. P. & Trusler, J. P. M. 2019. Brine Chemistry Effects in Calcite Dissolution Kinetics at Reservoir Conditions. *Chemical Geology,* 509, 92-102. doi: https://doi.org/10.1016/j.chemgeo.2019.01.014.

André, L., Azaroual, M., Bernstone, C. & Wittek, A. 2015. Modeling the Geochemical Impact of an Injection of CO_2 and Associated Reactive Impurities (SO_2 and O_2) into a Saline Reservoir. *Transport in Porous Media,* 108, 185-205. doi: 10.1007/s11242-014-0359-7.

André, L., Azaroual, M. & Menjoz, A. 2010. Numerical Simulations of the Thermal Impact of Supercritical CO_2 Injection on Chemical Reactivity in a Carbonate Saline Reservoir. *Transport in Porous Media,* 82, 247-274. doi: 10.1007/s11242-009-9474-2.

ANP 2000. Portaria Nº 249 - Regulamento Técnico de Queimas e Perdas de Petróleo e Gás Natural.

ANP, MME, EPE, PPSA & BNDES 2020. Estudo Sobre o Aproveitamento do Gás Natural do Pré Sal. [Accessed 21 June 2020]; Available: http://www.anp.gov.br/arquivos/estudos/aproveitamento-gn-pre-sal.pdf.

Appelo, C. A. J. & Postma, D. 2004. *Geochemistry, Groundwater and Pollution*, CRC press.

Araújo, O. d. Q. F., Reis, A. d. C., de Medeiros, J. L., Nascimento, J. F. d., Grava, W. M. & Musse, A. P. S. 2017. Comparative Analysis of Separation Technologies for Processing Carbon Dioxide Rich Natural Gas in Ultra-Deepwater Oil Fields. *Journal of Cleaner Production,* 155, 12-22. doi: 10.1016/j.jclepro.2016.06.073.

Awolayo, A. N., Sarma, H. K. & Nghiem, L. X. Numerical Modeling of Fluid-Rock Interactions During Low-Salinity-Brine-CO_2 Flooding in Carbonate Reservoirs. SPE Reservoir Simulation Conference, 2019. D021S016R004.

Azari, V., Rodrigues, H., Suieshova, A., Vazquez, O. & Mackay, E. 2021. Long-Term Strategy Optimization of Scale Squeeze Treatment in a Carbonate Reservoir under CO_2-WAG (Water-Alternating-Gas) Injection. *SPE International Oilfield Chemistry Conference.* Texas, USA: SPE.

Azari, V., Vazquez, O., Mackay, E., Sorbie, K., Jordan, M. & Sutherland, L. Squeeze Design Optimization by Considering Operational Constraints, Numerical Simulation and Mathematical Modelling. SPE International Oilfield Scale Conference and Exhibition, 2020. D022S009R006.

Aziz, K. 1979. Petroleum Reservoir Simulation. *Applied Science Publishers,* 476.

Bakker, R. J. 2003. Package Fluids 1. Computer Programs for Analysis of Fluid Inclusion Data and for Modelling Bulk Fluid Properties. *Chemical Geology,* 194, 3-23.

Belazreg, L., Mahmood, S. M. & Aulia, A. 2019. Novel Approach for Predicting Water Alternating Gas Injection Recovery Factor. *Journal of Petroleum Exploration and Production Technology,* 9, 2893-2910. doi: 10.1007/s13202-019-0673-2.

Bentley, M. 2016. Modelling for Comfort? *Petroleum Geoscience,* 22, 3-10. doi: 10.1144/petgeo2014-089.

Bentley, M. & Smith, S. 2008. Scenario-Based Reservoir Modelling: The Need for More Determinism and Less Anchoring. *Geological Society, London, Special Publications,* 309, 145-159. doi: 10.1144/sp309.11.

Bethke, C. 1996. *Geochemical Reaction Modeling: Concepts and Applications*, Oxford University Press on Demand.

Bezerra, M. C. M., Rosario, F. F. & Rosa, K. R. S. A. Scale Management in Deep and Ultradeep Water Fields. OTC Brasil, 2013. OTC-24508-MS.

Box, G. E. P. 1979. Robustness in the Strategy of Scientific Model Building. *In:* Launer, R. L. & Wilkinson, G. N. (eds.) *Robustness in Statistics.* Academic Press.

bp 2020. bp Energy Outlook: 2020 Edition. [Accessed 3 November 2020]; Available: https://www.bp.com/en/global/corporate/energy-economics/energy-outlook.html.

Brantley, S. L. 2008. Kinetics of Mineral Dissolution. *In:* Brantley, S. L., Kubicki, J. D. & White, A. F. (eds.) *Kinetics of Water-Rock Interaction.* New York, NY: Springer New York.

Bratvold, R. B. & Begg, S. 2010. *Making Good Decisions*, Society of Petroleum Engineers Richardson, Texas.

Capeleiro Pinto, A. C., Martins Vaz, C. E., Moreira Branco, C. C. & Ribeiro, J. An Evaluation of Large Capacity Processing Units for Ultra Deep Water and High Gor Oil Fields. Offshore Technology Conference, 2014. D011S005R007.

Carlson, F. M. Simulation of Relative Permeability Hysteresis to the Nonwetting Phase. SPE annual technical conference and exhibition, 1981. Society of Petroleum Engineers.

Carman, P. C. 1956. *Flow of Gases through Porous Media,* New York, Academic Press.

Cavanagh, A. & Ringrose, P. 2014. Improving Oil Recovery and Enabling CCS: A Comparison of Offshore Gas-Recycling in Europe to CCUS in North America. *Energy Procedia,* 63, 7677-7684. doi: 10.1016/j.egypro.2014.11.801.

Chen, S.-M., Allard, D. R. & Anli, J. 1984. Factors Affecting Solvent Slug Size Requirements in Hydrocarbon Miscible Flooding. *SPE Enhanced Oil Recovery Symposium.* Society of Petroleum Engineers.

Chen, S. 2012. *Integrated Optimization of Carbon Dioxide Enhanced Oil Recovery and Storage under Uncertainty.* Doctor of Philosophy, University of Regina.

CMG 2020a. CMOST AI User Manual. *Intelligent Optimization & Analysis Tool.* Calgary, Canada: Computer Modelling Group Ltd.

CMG 2020b. GEM User Manual. *Compositional & Unconventional Simulator.* Calgary, Canada: Computer Modelling Group Ltd.

Corey, A. T. 1954. The Interrelation between Gas and Oil Relative Permeabilities. *Producers monthly,* 19, 38-41.

Correia, M., Hohendorff, J., Gaspar, A. T. & Schiozer, D. UNISIM-II-D: Benchmark Case Proposal Based on a Carbonate Reservoir. SPE Latin American and Caribbean Petroleum Engineering Conference, 2015. D031S020R004.

d'Almeida, K. S., Vilela, P. C., Cardoso, R. A., Fernandes, R. F. & Souza, M. F. F. 2018. Ocorrência de CO_2 em Campos Petrolíferos na Margem Leste Brasileira. Rio de Janeiro: Empresa de Pesquisa Energética [Accessed 7 of September 2019]; Available: https://www.epe.gov.br/sites-pt/publicacoes-dados-abertos/publicacoes/PublicacoesArquivos/publicacao-322/.

da Costa Fraga, C. T., Capeleiro Pinto, A. C., Branco, C. C. M., de Sant´Anna Pizarro, J. O. & da Silva Paulo, C. A. 2015. Brazilian Pre-Salt: An Impressive Journey from Plans and Challenges to Concrete Results. Offshore Technology Conference.

de Andrade, A. M. T., Vaz, C. E. M., Ribeiro, J., Lopreato, L. G. R. & do Nascimento, R. F. S. Offshore Production Units for Pre-Salt Projects. Offshore Technology Conference, 2015. OTC-25691-MS.

de Medeiros, J. L., de Oliveira, L., Mendonça, A. & de Queiroz, O. 2019. *Offshore Processing of CO_2-Rich Natural Gas with Supersonic Separator*, Springer.

Delfani, S., Mortezapour, A., Firouz, A. R. Q. & Shadizade, S. R. Evaluation of Miscible and Immiscible Gas Injection in One of the Iranian Oilfield. Abu Dhabi International Petroleum Exhibition and Conference, 2008. SPE-117305-MS.

Eberhart, R. & Kennedy, J. Particle Swarm Optimization. Proceedings of the IEEE international conference on neural networks, 1995. Citeseer, 1942-1948.

Elsharkawy, A. M., Poettmann, F. H. & Christiansen, R. L. 1992. Measuring Minimum Miscibility Pressure: Slim-Tube or Rising-Bubble Method? *SPE/DOE Enhanced Oil Recovery Symposium.* Tulsa, Oklahoma: Society of Petroleum Engineers; Available: https://doi.org/10.2118/24114-MS.

EPA 2018. Greenhouse Gas Emissions from a Typical Passenger Vehicle. *In:* Quality, O. o. T. a. A. (ed.). United States Environmental Protection Agency, [Accessed 20 November]; Available: https://www.epa.gov/greenvehicles/greenhouse-gas-emissions-typical-passenger-vehicle.

EPA. 2020. *Understanding Global Warming Potentials* [Online]. United States Environmental Protection Agency. Available: https://www.epa.gov/ghgemissions/understanding-global-warming-potentials [Accessed 7 November 2020].

EPE 2014. Provocação de Terceiros: GUAPIMIRIM-COMPERJ II. [Accessed 8 October 2020]; Available: http://filesrodadas.anp.gov.br/arquivos/Edital_TG/Gasoduto_de_Referencia_Guapimirim_COMPERJII.PDF.

EPE 2019. Informe - Custos de Gás Natural no Pré-Sal Brasileiro. [Accessed 29 June 2020]; Available: https://www.epe.gov.br/pt/publicacoes-dados-abertos/publicacoes/informe-custos-de-gas-natural-no-pre-sal-brasileiro.

EPE & MME 2014. Plano Decenal de Expansão da Malha de Transporte Dutoviário–PEMAT 2022. [Accessed 29 June 2020]; Available: https://www.epe.gov.br/sites-pt/publicacoes-dados-abertos/publicacoes/PublicacoesArquivos/publicacao-166/Relat%C3%B3rio%20final%20PEMAT.pdf.

Ettehadtavakkol, A. 2013. *CO_2 EOR-Storage Design Optimization under Uncertainty*. Doctor of Philosophy PhD, The University of Texas at Austin.

Ettehadtavakkol, A., Lake, L. W. & Bryant, S. L. 2014. CO_2-EOR and Storage Design Optimization. *International Journal of Greenhouse Gas Control,* 25, 79-92. doi: 10.1016/j.ijggc.2014.04.006.

Friedmann, S. J., Fan, Z. & Tang, K. 2019. Low-Carbon Heat Solutions for Heavy Industry: Sources, Options, and Costs Today. *In:* York, N. (ed.). School of International and Public Affairs, Columbia University; Available: https://www.energypolicy.columbia.edu/sites/default/files/file-uploads/LowCarbonHeat-CGEP_Report_100219-2_0.pdf.

Gallo, W. L. R., Gallego, A. G., Acevedo, V. L., Dias, R., Ortiz, H. Y. & Valente, B. A. 2017. Exergy Analysis of the Compression Systems and Its Prime Movers for a FPSO Unit. *Journal of Natural Gas Science and Engineering,* 44, 287-298. doi: https://doi.org/10.1016/j.jngse.2017.04.023.

Galp. 2018. *Capital Markets Day Presentation* [Online]. Available: https://www.galp.com/Portals/0/Recursos/Investidores/SharedResources/Apresentacoes/EN/CMD2018.pdf [Accessed 23 August 2018].

Ghanbari, S., Mackay, E. J., Heinemann, N., Alcalde, J., James, A. & Allen, M. J. 2020. Impact of CO2 Mixing with Trapped Hydrocarbons on CO2 Storage Capacity and Security: A Case Study from the Captain Aquifer (North Sea). *Applied Energy,* 278, 115634. doi: https://doi.org/10.1016/j.apenergy.2020.115634.

Ghomian, Y. 2008. *Reservoir Simulation Studies for Coupled Carbon Dioxide Sequestration and Enhanced Oil Recovery*. 3311475 Ph.D., The University of Texas at Austin.

Ghomian, Y., Pope, G. A. & Sepehrnoori, K. 2008. Hysteresis and Field-Scale Optimization of WAG Injection for Coupled CO2-EOR and Sequestration. Society of Petroleum Engineers.

Global CCS Institute 2019. Bioenergy and Carbon Capture and Storage. *In:* Consoli, C. (ed.) *2019 Perspective*. Available: https://www.globalccsinstitute.com/wp-content/uploads/2019/03/BECCS-Perspective_FINAL_18-March.pdf.

Graham, G. M., Mackay, E. J., Dyer, S. J. & Bourne, H. The Challenges for Scale Control in Deepwater Production Systems: Chemical Inhibition and Placement. CORROSION 2002, 2002. OnePetro.

Green, D. W. & Willhite, G. P. 1998. *Enhanced Oil Recovery*, Henry L. Doherty Memorial Fund of AIME, Society of Petroleum Engineers ….

Grond, M. O. W., Luong, N. H., Morren, J. & Slootweg, J. G. Multi-Objective Optimization Techniques and Applications in Electric Power Systems. 2012 47th International Universities Power Engineering Conference (UPEC), 4-7 Sept. 2012 2012. 1-6.

Gundogan, O. 2011. *Geochemical Modelling of CO_2 Storage*. Doctor of Philosophy, Heriot-Watt University.

Hadlow, R. E. Update of Industry Experience with CO_2 Injection. SPE Annual Technical Conference and Exhibition, 1992. SPE-24928-MS.

Hardy, J. & Simm, I. 1996. Low Sulfate Seawater Mitigates Barite Scale. *Oil and Gas Journal,* 94, 64-67.

Harvey, A. H. 1996. Semiempirical Correlation for Henry's Constants over Large Temperature Ranges. *AIChE Journal,* 42, 1491-1494. doi: https://doi.org/10.1002/aic.690420531.

Huang, E. T. S. & Holm, L. W. 1988. Effect of WAG Injection and Rock Wettability on Oil Recovery During CO_2 Flooding. *SPE Reservoir Engineering,* 3, 119-129. doi: 10.2118/15491-pa.

IEA 2018. World Energy Outlook 2018. Paris: International Energy Agency; Available: https://www.iea.org/reports/world-energy-outlook-2018.

IEA 2019a. Can CO_2-EOR Really Provide Carbon-Negative Oil? *In:* McGlade, C. (ed.). Paris; Available: https://www.iea.org/commentaries/can-co2-eor-really-provide-carbon-negative-oil.

IEA 2019b. Number of EOR Projects in Operation Globally, 1971-2017. Paris; Available: https://www.iea.org/data-and-statistics/charts/number-of-eor-projects-in-operation-globally-1971-2017.

IEA 2020a. CCUS in Clean Energy Transitions. Paris: [Accessed 8 Nov 2020]; Available: https://www.iea.org/reports/ccus-in-clean-energy-transitions.

IEA 2020b. Flaring Emissions. Paris: International Energy Agency; Available: https://www.iea.org/reports/flaring-emissions.

IHS Markit. 2020. *Upstream Capital Costs Index (UCCI)* [Online]. Available: https://ihsmarkit.com/Info/cera/ihsindexes/index.html [Accessed 15 June 2020].

IPCC 2005. *Carbon Dioxide Capture and Storage: Special Report of the Intergovernmental Panel on Climate Change*, Cambridge University Press; Available from: https://www.ipcc.ch/site/assets/uploads/2018/03/srccs_wholereport-1.pdf, https://www.ipcc.ch/site/assets/uploads/2018/03/srccs_wholereport-1.pdf.

Janga Reddy, M. & Nagesh Kumar, D. 2020. Evolutionary Algorithms, Swarm Intelligence Methods, and Their Applications in Water Resources Engineering: A State-of-the-Art Review. *H2Open Journal,* 3, 135-188. doi: 10.2166/h2oj.2020.128.

Jin, M., Ribeiro, A., Mackay, E., Guimarães, L. & Bagudu, U. 2016. Geochemical Modelling of Formation Damage Risk during CO_2 Injection in Saline Aquifers. *Journal of Natural Gas Science and Engineering,* 35, 703-719. doi: https://doi.org/10.1016/j.jngse.2016.08.030.

Kah, M. 2020. Columbia Global Energy Dialogue: Natural Gas Flaring Workshop Summary. [Accessed 14 September 2020]; Available: https://www.energypolicy.columbia.edu/research/global-energy-dialogue/columbia-global-energy-dialogue-natural-gas-flaring-workshop-summary.

Khan, M. Y., Kohata, A., Patel, H., Syed, F. I. & Al Sowaidi, A. K. Water Alternating Gas WAG Optimization Using Tapered WAG Technique for a Giant Offshore Middle East Oil Field. Abu Dhabi International Petroleum Exhibition & Conference, 2016. D041S096R001.

Killough, J. 1976. Reservoir Simulation with History-Dependent Saturation Functions. *Society of Petroleum Engineers Journal,* 16, 37-48.

Kumar, A., Noh, M., Pope, G. A., Sepehrnoori, K., Bryant, S. & Lake, L. W. Reservoir Simulation of CO_2 Storage in Deep Saline Aquifers. SPE/DOE Symposium on Improved Oil Recovery, 2004. SPE-89343-MS.

Laboissiere, P., Mello, S. F., Trevisan, O. V. & Schiozer, D. J. 2013. Relative Permeability Effects on the Miscible CO_2 WAG Injection Schemes Trough Compositional Simulations of Brazilian Small Scale Water-Wet Synthetic Pre-Salt Reservoir. Offshore Technology Conference.

Lake, L. W., Johns, R., Rossen, B. & Pope, G. A. 2014. *Fundamentals of Enhanced Oil Recovery*.

Land, C. S. 1968. Calculation of Imbibition Relative Permeability for Two-and Three-Phase Flow from Rock Properties. *Society of Petroleum Engineers Journal,* 8, 149-156.

Larsen, J. & Skauge, A. 1998. Methodology for Numerical Simulation with Cycle-Dependent Relative Permeabilities. *SPE Journal,* 3, 163-173.

Lasaga, A. C. 1998. *Kinetic Theory in the Earth Sciences,* Princeton, N.J., Princeton University Press.

Lee, B. I. & Kesler, M. G. 1975. A Generalized Thermodynamic Correlation Based on Three-Parameter Corresponding States. *AIChE Journal,* 21, 510-527.

Li, X., Wang, S., Yuan, B. & Chen, S. 2018. Optimal Design and Uncertainty Assessment of CO_2 WAG Operations: A Field Case Study. *SPE Improved Oil Recovery Conference*. Tulsa, Oklahoma, USA: Society of Petroleum Engineers; Available: https://doi.org/10.2118/190157-MS.

Mackay, E. & de Souza, A. P. M. 2014. Modelling of CO_2 and Seawater Injection in Carbonate Reservoirs to Evaluate Inorganic Scaling Risk. *SPE International Oilfield Scale Conference and Exhibition*. Aberdeen, Scotland: Society of Petroleum Engineers; Available: https://doi.org/10.2118/169766-MS.

Mackay, E. J. 2003. Modeling in-Situ Scale Deposition: The Impact of Reservoir and Well Geometries and Kinetic Reaction Rates. *SPE Production & Facilities,* 18, 45-56. doi: 10.2118/81830-pa.

Mackay, E. J. 2005. *The Application of Reservoir Simulation Calculations to Oilfield Scale Management*. http://hdl.handle.net/10399/224, Heriot-Watt University.

McCollum, D. L. & Ogden, J. M. 2006. Techno-Economic Models for Carbon Dioxide Compression, Transport, and Storage & Correlations for Estimating Carbon Dioxide Density and Viscosity.

McCoy, S. T. 2008. *The Economics of CO_2, Transport by Pipeline and Storage in Saline Aquifers and Oil Reservoirs*. Sean T. McCoy.

McKinsey 2020. The Future Is Now: How Oil and Gas Companies Can Decarbonize. *In:* Beck, C., Rashidbeigi, S., Roelofsen, O. & Speelman, E. (eds.). McKinsey Insights [Accessed 3 August 2020]; Available: https://www.mckinsey.com/industries/oil-and-gas/our-insights/the-future-is-now-how-oil-and-gas-companies-can-decarbonize.

Meddaugh, W. S. 2006. Reservoir Modeling for Mature Fields - Impact of Workflow and up-Scaling on Fluid Flow Response. *SPE Europec/EAGE Annual Conference and Exhibition*. Vienna, Austria: Society of Petroleum Engineers; Available: https://doi.org/10.2118/99833-MS.

Meddaugh, W. S., Champenoy, N., Osterloh, W. T. & Tang, H. 2011. Reservoir Forecast Optimism - Impact of Geostatistics, Reservoir Modeling, Heterogeneity, and Uncertainty. *SPE Annual Technical Conference and Exhibition*. Denver, Colorado, USA: Society of Petroleum Engineers; Available: https://doi.org/10.2118/145721-MS.

Meira, L. A. A., Coelho, G. P., da Silva, C. G., Abreu, J. L. A., Santos, A. A. S. & Schiozer, D. J. 2020. Improving Representativeness in a Scenario Reduction Process to Aid Decision Making in Petroleum Fields. *Journal of Petroleum Science and Engineering,* 184, 106398. doi: https://doi.org/10.1016/j.petrol.2019.106398.

Meza, E. B. M., Vianna, D. S., De Macedo, A. A. & Vianna, M. d. F. D. 2015. Um Modelo Matemático para o Roteamento de Navios Aliviadores no Escoamento da Produção de Petroléo. *Revista Eletrônica Gestão e Saúde*, 955-970.

MME 2020. Boletim Mensal De Acompanhamento Da Indústria De Gás Natural. *Destaques de janeiro de 2020*. Ministério de Minas e Energia [Accessed 12 March 2019]; Available: http://www.mme.gov.br/documents/1138769/0/Boletim_Gas_Natural_nr_155_JAN_20.pdf.

Moortgat, J. B., Firoozabadi, A., Li, Z. & Espósito, R. O. 2013. CO_2 Injection in Vertical and Horizontal Cores: Measurements and Numerical Simulation. *SPE Journal,* 18, 331-344. doi: 10.2118/135563-PA.

Morse, J. W. & Arvidson, R. S. 2002. The Dissolution Kinetics of Major Sedimentary Carbonate Minerals. *Earth-Science Reviews,* 58, 51-84. doi: https://doi.org/10.1016/S0012-8252(01)00083-6.

Morse, J. W., Arvidson, R. S. & Lüttge, A. 2007. Calcium Carbonate Formation and Dissolution. *Chemical Reviews,* 107, 342-381. doi: 10.1021/cr050358j.

Muggeridge, A., Cockin, A., Webb, K., Frampton, H., Collins, I., Moulds, T. & Salino, P. 2014. Recovery Rates, Enhanced Oil Recovery and Technological Limits. *Philos Trans A Math Phys Eng Sci,* 372, 20120320. doi: 10.1098/rsta.2012.0320.

Nauclér, T. & Enkvist, P.-A. 2009. Pathways to a Low-Carbon Economy: Version 2 of the Global Greenhouse Gas Abatement Cost Curve. *McKinsey & Company,* 192.

Nghiem, L., Sammon, P., Grabenstetter, J. & Ohkuma, H. Modeling CO_2 Storage in Aquifers with a Fully-Coupled Geochemical Eos Compositional Simulator. SPE/DOE Symposium on Improved Oil Recovery, 2004. SPE-89474-MS.

Núñez-López, V., Gil-Egui, R. & Hosseini, S. A. 2019. Environmental and Operational Performance of CO_2-EOR as a CCUS Technology: A Cranfield Example with Dynamic LCA Considerations. *Energies,* 12, 448. https://www.mdpi.com/1996-1073/12/3/448.

Palandri, J. L. & Kharaka, Y. K. 2004. A Compilation of Rate Parameters of Water-Mineral Interaction Kinetics for Application to Geochemical Modeling. Geological Survey Menlo Park CA; Available: https://pubs.usgs.gov/of/2004/1068/.

Pariani, G. J., McColloch, K. A., Warden, S. L. & Edens, D. R. 1992. An Approach to Optimize Economics in a West Texas CO_2 Flood. *Journal of Petroleum Technology,* 44, 984-1025. doi: 10.2118/22022-pa.

Parkhurst, D. L. & Appelo, C. 2013. Description of Input and Examples for Phreeqc Version 3: A Computer Program for Speciation, Batch-Reaction, One-Dimensional Transport, and Inverse Geochemical Calculations. US Geological Survey.

Pedersen, K. S. & Fredenslund, A. 1987. An Improved Corresponding States Model for the Prediction of Oil and Gas Viscosities and Thermal Conductivities. *Chemical Engineering Science,* 42, 182-186. doi: https://doi.org/10.1016/0009-2509(87)80225-7.

Péneloux, A., Rauzy, E. & Fréze, R. 1982. A Consistent Correction for Redlich-Kwong-Soave Volumes. *Fluid Phase Equilibria,* 8, 7-23. doi: https://doi.org/10.1016/0378-3812(82)80002-2.

Peng, C., Crawshaw, J. P., Maitland, G. C. & Trusler, J. P. M. 2015. Kinetics of Calcite Dissolution in CO_2-Saturated Water at Temperatures between (323 and 373)K and Pressures up to 13.8mpa. *Chemical Geology,* 403, 74-85. doi: https://doi.org/10.1016/j.chemgeo.2015.03.012.

Peng, D.-Y. & Robinson, D. B. 1976. A New Two-Constant Equation of State. *Industrial & Engineering Chemistry Fundamentals,* 15, 59-64. doi: 10.1021/i160057a011.

Petrobras 2020. Caderno de Mudança do Clima. [Accessed 02 Nov 2020]; Available: https://issuu.com/estantepetrobras/docs/petrobras_caderno_clima_pt.

Pizarro, J. O. D. S. & Branco, C. C. M. 2012. Challenges in Implementing an EOR Project in the Pre-Salt Province in Deep Offshore Brasil. *SPE EOR Conference at Oil and Gas West Asia.* Muscat, Oman: Society of Petroleum Engineers; Available: https://doi.org/10.2118/155665-MS.

Plummer, L., Wigley, T. & Parkhurst, D. 1978. The Kinetics of Calcite Dissolution in CO_2-Water Systems at 5 Degrees to 60 Degrees C and 0.0 to 1.0 Atm CO_2. *American journal of science,* 278, 179-216.

Ribeiro, A. S. 2017. *Modelling of Geochemical Reactions during CO_2 WAG Injection in Carbonate Reservoirs.* Doctor of Philosophy in Petroleum Engineering, Heriot-Watt University, Universidade Federal de Pernambuco.

Ringrose, P. 2020. *How to Store CO_2 Underground: Insights from Early-Mover CCS Projects*, Springer.

Rochedo, P. R. R., Costa, I. V. L., Império, M., Hoffmann, B. S., Merschmann, P. R. d. C., Oliveira, C. C. N., Szklo, A. & Schaeffer, R. 2016. Carbon Capture Potential and Costs in Brazil. *Journal of Cleaner Production,* 131, 280-295. doi: 10.1016/j.jclepro.2016.05.033.

Rockett, G. C., Ketzer, J. M. M., Ramírez, A. & van den Broek, M. 2013. CO_2 Storage Capacity of Campos Basin's Oil Fields, Brazil. *Energy Procedia,* 37, 5124-5133. doi: https://doi.org/10.1016/j.egypro.2013.06.427.

Rogers, J. D. & Grigg, R. B. A Literature Analysis of the WAG Injectivity Abnormalities in the CO_2 Process. SPE/DOE Improved Oil Recovery Symposium, 2000. SPE-59329-MS.

Salomão, M. C., Marçon, D. R., Rosa, M. B., de Salles Pessoa, T. C. & Capeleiro Pinto, A. C. Broad Strategy to Face with Complex Reservoirs: Expressive Results of Production in Pre-Salt Area, Offshore Brasil. Offshore Technology Conference, 2015. OTC-25712-MS.

Santos, S. & Schiozer, D. 2018. Case Study for Field Development and Management– Selection of Production Strategy Based on UNISIM-II. Center for Petroleum Studies University of Campinas [Accessed 12 June 2020]; Available: https://www.unisim.cepetro.unicamp.br/benchmarks/br/unisim-ii/unisim-ii-h.

Santos, S. M. G., Santos, A. A. S. & Schiozer, D. J. 2020. Selecting Representative Models for Ensemble-Based Production Optimization in Carbonate Reservoirs with Intelligent Wells and WAG Injection. 2020, 1-28. doi: https://doi.org/10.3997/2214-4609.202035041.

Sazali, Y. A., Sazali, W. M. L., Ibrahim, J. M., Dindi, M., Graham, G. & Gödeke, S. 2019. Investigation of High Temperature, High Pressure, Scaling and Dissolution Effects for Carbon Capture and Storage at a High CO2 Content Carbonate Gas Field Offshore Malaysia. *Journal of Petroleum Science and Engineering,* 174, 599-606. doi: https://doi.org/10.1016/j.petrol.2018.11.060.

Schiozer, D. J., de Souza dos Santos, A. A., de Graça Santos, S. M. & von Hohendorff Filho, J. C. 2019. Model-Based Decision Analysis Applied to Petroleum Field Development and Management. *Oil & Gas Science and Technology - Revue d'IFP Energies nouvelles,* 74, 46. doi: 10.2516/ogst/2019019.

Schiozer, D. J., Ligero, E. L., Suslick, S. B., Costa, A. P. A. & Santos, J. A. M. 2004. Use of Representative Models in the Integration of Risk Analysis and Production Strategy Definition. *Journal of Petroleum Science and Engineering,* 44, 131-141. doi: https://doi.org/10.1016/j.petrol.2004.02.010.

Silva, D. J. A. d. C. 2017. *Mineral Scale Prediction Modelling: Precipitation of $CaCO_3$ Scale in CO_2-Water Alternating Gas Production Systems*. http://hdl.handle.net/10399/3301, Heriot-Watt University.

Snippe, J., Berg, S., Ganga, K., Brussee, N. & Gdanski, R. 2020. Experimental and Numerical Investigation of Wormholing during CO_2 Storage and Water Alternating Gas Injection. *International Journal of Greenhouse Gas Control,* 94, 102901. doi: https://doi.org/10.1016/j.ijggc.2019.102901.

Sobol, I. 1993. Sensitivity Estimates for Nonlinear Models. *Mathematical modeling and computational experiment,* 1, 407-414.

Stalkup, F. I. 1983. *Miscible Displacement,* New York, Henry L. Doherty Memorial Fund of AIME, Society of Petroleum Engineers of AIME.

Subhas, A. V., Rollins, N. E., Berelson, W. M., Dong, S., Erez, J. & Adkins, J. F. 2015. A Novel Determination of Calcite Dissolution Kinetics in Seawater. *Geochimica et cosmochimica acta,* 170, 51-68. doi: 10.1016/j.gca.2015.08.011.

Talbi, E.-G. 2009. *Metaheuristics: From Design to Implementation*, John Wiley & Sons.

Tang, Y., Yang, R. & Kang, X. 2018. Modeling the Effect of Water Vaporization and Salt Precipitation on Reservoir Properties Due to Carbon Dioxide Sequestration in a Depleted Gas Reservoir. *Petroleum,* 4, 385-397. doi: https://doi.org/10.1016/j.petlm.2017.12.003.

Thibeau, S., Nghiem, L. X. & Ohkuma, H. A Modelling Study of the Role of Selected Minerals in Enhancing CO_2 Mineralization During CO_2 Aquifer Storage. SPE Annual Technical Conference and Exhibition, 2007. SPE-109739-MS.

Torrez Camacho, L. D. 2017. *Methodology for the Development of Carbonate Reservoirs with CO_2-WAG.* Master of Science, Universidade Estadual de Campinas.

Vazquez, O., Fursov, I., Beteta, A. & Mackay, E. 2017a. Optimization of Alkaline-Surfactant-Polymer (Asp) Flooding Minimizing Risk of Scale Deposition. 2017, 1-20. doi: https://doi.org/10.3997/2214-4609.201700325.

Vazquez, O., Fursov, I. & Mackay, E. 2016. Automatic Optimization of Oilfield Scale Inhibitor Squeeze Treatment Designs. *Journal of Petroleum Science and Engineering,* 147, 302-307. doi: https://doi.org/10.1016/j.petrol.2016.06.025.

Vazquez, O., Mackay, E. & Sorbie, K. 2012. A Two-Phase near-Wellbore Simulator to Model Non-Aqueous Scale Inhibitor Squeeze Treatments. *Journal of Petroleum Science and Engineering,* 82-83, 90-99. doi: https://doi.org/10.1016/j.petrol.2011.12.030.

Vazquez, O., Ross, G., Jordan, M., Baskoro, D. A., Mackay, E., Johnson, C. & Strachan, A. Automatic Optimisation of Oilfield Scale Inhibitor Squeeze Treatments Delivered by Dsv. SPE International Conference on Oilfield Chemistry, 2017b. D021S005R004.

Venkatraman, A., Dindoruk, B., Elshahawi, H., Lake, L. W. & Johns, R. T. 2017. Modeling Effect of Geochemical Reactions on Real-Reservoir-Fluid Mixture During Carbon Dioxide Enhanced Oil Recovery. *SPE Journal,* 22, 1519-1529. doi: 10.2118/175030-PA.

Venter, G. 2010. Review of Optimization Techniques. *Encyclopedia of aerospace engineering*.

Vulin, D., Gaćina, M. & Biličić, V. 2018. Slim-Tube Simulation Model for CO_2 Injection EOR. *Rudarsko-geološko-naftni zbornik,* 33, 37-48. doi: 10.17794/rgn.2018.2.4.

Walter, L. M. & Morse, J. W. 1984. Reactive Surface Area of Skeletal Carbonates during Dissolution; Effect of Grain Size. *Journal of Sedimentary Research,* 54, 1081-1090. doi: 10.1306/212f8562-2b24-11d7-8648000102c1865d.

White, A. F. & Peterson, M. L. 1990. Role of Reactive-Surface-Area Characterization in Geochemical Kinetic Models. *Chemical Modeling of Aqueous Systems II.* American Chemical Society.

World Bank 2017. Carbon Tax Guide: A Handbook for Policy Makers. License: Creative Commons Attribution CC BY 3.0 IGO ed.: Partnership for Market Readiness; Available: http://documents1.worldbank.org/curated/en/728421535605566659/pdf/129668-V1-WP-PUBLIC-Carbon-Tax-Guide-Main-Report.pdf.

WRI & WBCSD. 2021. *A Corporate Accounting and Reporting Standard Revised Edition* [Online]. World Resources Institute & World Business Council for Sustainable Development. Available: https://ghgprotocol.org/ [Accessed 05 March 2020].

Xu, T., Apps, J. A. & Pruess, K. 2005. Mineral Sequestration of Carbon Dioxide in a Sandstone–Shale System. *Chemical Geology,* 217, 295-318. doi: https://doi.org/10.1016/j.chemgeo.2004.12.015.

Yasuda, E. Y., Santos, R. G. d. & Vidal Trevisan, O. 2013. Kinetics of Carbonate Dissolution and Its Effects on the Porosity and Permeability of Consolidated Porous Media. *Journal of Petroleum Science and Engineering,* 112, 284-289. doi: https://doi.org/10.1016/j.petrol.2013.11.015.

Zhou, D., Yan, M. & Calvin, W. M. Optimization of a Mature CO_2 Flood — from Continuous Injection to WAG. SPE Improved Oil Recovery Symposium, 2012. SPE-154181-MS.